Molecular, biochemical and pharmacological characterisation of *Mycobacterium tuberculosis* cytochrome *bd*-I oxidase: a putative therapeutic target

Taghreed Abdulaziz Hafiz

Ph.D. 2013

Molecular, biochemical and pharmacological characterisation of *Mycobacterium tuberculosis* cytochrome *bd*-I oxidase: a putative therapeutic target

Thesis is submitted in accordance with the requirements of the University of Liverpool for the degree of Doctor of Philosophy

By

Taghreed Abdulaziz Hafiz

M.Sc (University of Liverpool)

June 2013

Declaration

This thesis is the result of my own work. The material contained in the thesis has not been presented, nor is currently being presented, either wholly or as a part, for any other degree or other qualification.

The research work was carried out in the Liverpool School of Tropical Medicine, University of Liverpool, United Kingdom.

……..

Taghreed Abdulaziz Hafiz (2013)

Dedication

First and foremost, I would like to dedicate this work to my lovely parents, my husband and to my son Adel and my daughter Danah

Acknowledgements

I am profoundly indebted to the grace of Allah for giving me the ability, insights, ideas and strength to make this thesis possible. Thank you Allah for your blessing on my family and me.

I would like to acknowledge my supervisor Dr Giancarlo Biagini for his support, encouragement, stimulating suggestions and constructive criticism throughout the time of research and writing of this thesis. I also wish to thank my co-supervisor Professor Steve Ward for his helpful suggestions and comments on my work.

I would like to express my gratitude and appreciation to Dr Ashley Warman for all of the guidance and support in helping me with various aspects of my work; your advice was immeasurable and I am extremely thankful. Additionally, special thanks go to Dr Nicholas Fisher for all of his advice and help on my work.

The Steve Ward group, especially Mrs Alison Ardrey, Dr Gavin Laing, Dr Darren Moss, Dr Gemma Nixon, Dr Alison Shone, Angela Travis and Mary Creegan, are all acknowledged for their support, help and ability to make the working environment very comfortable and conducive to research.

I am equally grateful to my colleagues, Dr Roslaini Abd Majid, Dr Teresa Ratio and Dr Thomas Antoine for their support and help. You have all been wonderful and it was great getting to know you and working with you.

My deepest gratitude to my lovely mother Rajaa Obaid and to my father Abdulaziz Hafiz; you are simply the best parents in the whole world. Without your prayers to Allah, resolute encouragement, patience and help with taking care of my kids and myself, this thesis would not have been possible. A special big thank you goes to my lovely sisters, Kholoud, Nehad, Hanan, Tahani and Deema, and to my beloved brother Mohammed for all of your prayers and support. Thank you for making my adored daughter Danah laugh and helping her to enjoy her time with you and for committing to sending me pictures of her every day. I love you all very much.

My sincerest love and apology go to my son Adel (2 years and 5 months) and to my baby daughter Danah (1 year) for being busy and away from you. I am sorry. Thank you for your patience with me. I adore you. Thank you Danah for being my pretty princess; every night away from you was a big challenge and burden to bear.

Finally, I wish to express my heart-felt thankfulness to my dear husband Murad Mubaraki for his love, support and help throughout my lab work and during my pregnancies of Adel and Danah. Thank you for teaching me the techniques used in my metabolomics work. Thank you for lifting the burden off my shoulders throughout my PhD and thank you for being so supportive during the hardest nights, when I had to leave Danah back in Saudi Arabia. I love you.

Publications and presentations

Work in this thesis is in preparation for publication and has been presented at meetings in the following forms:

Publication in preparation:

Mycobacterium tuberculosis* cytochrome *bd* oxidase; Initial characterisation of a putative therapeutic target

Taghreed A. Hafiz[1*], Ashley J. Warman[1*], Nicholas E. Fisher[1], Gemma L. Nixon[1], Neil G. Berry[2], Paul M. O'Neill[2], Stephen A. Ward[1], and Giancarlo A. Biagini[1]

*Running title: Characterisation of Mtb cytochrome *bd* oxidase

[*] Joint first author

Presentations:

***Mycobacterium tuberculosis* cytochrome *bd* oxidase: a terminal solution?**

Taghreed A. Hafiz[1], Ashley J. Warman[1], Nicholas E. Fisher[1], Gemma L. Nixon[1], Neil G. Berry[2], Paul M. O'Neill[2], Stephen A. Ward[1], and Giancarlo A. Biagini[1]

Has been presented at the Tuberculosis 2012 Conference held, September 11-15, 2012 at the Institut Pasteur, Paris, France.

Table of content

List of Figures

Chapter 1:

Chapter 2:

Chapter 3:

Chapter 4:

Chapter 5:

List of Tables

Chapter 1:

Chapter 2:

Chapter 3:

Chapter 4:

Chapter 5:

List of appendixes

Abbreviations

ACDP	Advisory Committee on Dangerous Pathogens
ADP	Adenosine diphosphate
AIDS	Acquired immune deficiency syndrome
Ala	Alanine
AMB44	Aerobically grown MB44 competent cells
AML16	Aerobically grown ML16 competent cells
AMP	Adenosine monophosphate
AnMB44	O_2-limited grown MB44 competent cells
AnML16	O_2-limited grown ML16 competent cells
AOX	Alternative oxidase
APS	Ammonium persulphate
Arg	Arginine
ARV	Antiretroviral
Asn	Asparagine
Asp	Aspartic acid
ATMB44	Transformed cells grown in aerobic growth condition
ATP	Adenosine triphosphate
BCG	Bacillus Calmette-Guérin
BN-PAGE	Blue-Native polyacrylamide gel electrophoresis
Bp	Base pair
BSA	bovine serum albumin
CCM	Central carbon metabolic
CcO	aa_3-type cytochrome *c* oxidase
CFU	Colony forming unit
$cfu.ml^{-1}$	CFU per millilitre
CHAPS	3-[(3-cholamidopropyl)dimethylammonio]-1-propanesulfonate
CID	Collision induced dissociation
CIO	Cyanide insensitive oxygen reductases
CPZ	Chlorpromazine
CTP	Cytidine triphosphate
Cys	Cysteine
DDM	*n*-dodecyl-β-D-maltopyranoside
DEPC	Diethylpyrocarbonate
dH_2O	Distilled water
DHAP	Dihydroxyacetone phosphate
DMPK	Drug metabolism and pharmacokinetics
DMSO	Dimethyl sulfoxide
DNA	Deoxyribonucleic acid
DOTS	Directly observed treatment, short-course
dQH_2	Decylubiquinol
DTT	Dithiothreitol
E	Enzyme

EDTA	Ethylenediaminetetraacetic acid
EI	Enzyme-Inhibitor complex
EMB	Ethambutol
ES	Enzyme-Substrate complex
ESI	Electrospray ionization
ETC	Electron transport chain
F	Fluorine
FAD	Flavin adenine dinucleotide
$FADH_2$	reduced flavin adenine dinucleotide
FAS-I	type I fatty acid synthases
FAS-II	type II fatty acid synthases
FRD	Fumarate reductase
G-3-P	Glycerol-3-phosphate
G3PDH	Glycerol-3-phosphate dehydrogenase
GABA	γ-Aminobutyric acid
GC-MS	Gas chromatography-mass spectrometry
Gln	Glutamine
Glu	Glutamic acid
Gly	Glycine
GS	Gramicidin S
GSH	Glutathione
GSSG	Glutathione disulfide
GTP	Guanosine triphosphate
H_2O	Water
H_2O_2	Hydrogen peroxide
HDQ	1-hydroxy-2-dodecyl-4(1H) quinolone
HEPES	4-(2-hydroxyethyl)-1-piperazineethanesulfonic acid
HILIC	Hydrophilic interaction liquid chromatography
His	Histidine
HIV	Human immunodeficiency virus
HTS	High-throughput screening
I	Inhibitor
IC_{50}	Half-maximal inhibitory concentration
IC_{90}	90% inhibitory concentration
ICLs	Isocitrate lyases
Ile	Isoleucine
INH	Isoniazid
IPTG	Isopropyl-β-D-thiogalactoside
K_2HPi	dipotassium hydrogen phosphate trihydrate
KatG	Catalase-peroxidase
KCN	Potassium cyanide
KDa	Kilodaltons
KDH	α-ketoglutarate dehydrogenase

KGD	α-ketoglutarate decarboxylase
KH_2Pi	Potassium dihydrogen orthophphosphate potassium
K_m	Michaelis constant, half-maximal velocity
KOR	α-ketoglutarate:ferredoxin oxidoreductase
LB	Luria-Bertani
LC-MS	Liquid chromatography-mass spectrometry
LC-MS/MS	Liquid chromatography-tandem mass spectrometry
LDH	L-lactate dehydrogenase
Leu	Leucine
LM	Lipomannan
LOD	Limit of detection
LTBI	Latent Tuberculosis infection
Lys	Lysine
m/z	Mass-to-charge ratio
MABA	Microplate alamar blue assay
ManLAM	Mannose capped lipoarabinomannans
MCC	Methylcitrate cycle
MCL	2-methylisocitrate lyase
MCS	Multiple cloning sites
MDH	Malate dehydrogenase
MDR-TB	Multidrug-resistant tuberculosis
MeOH	Methanol
MES	2-(*N*-morpholino)ethanesulfonic acid
Met	Methionine
$mg.ml^{-1}$	Milligram per millilitre
ML16	Untransformed AnML16 competent cells
MLS	Malate synthase
mM	Millimolar
MoA	Mode of action
MQ	Menaquinone
MQ-8	Menaquinone-8
MQ-9	Menaquinone-9
MQH_2	Menaquinol
MSI	Metabolomics standard initiative
Mtb	Mycobacterium tuberculosis
Mtb *bd*-I	*M. tuberculosis* cytochrome *bd*-I oxidase
MTZ	Metronidazole
MW	Molecular weight
NA	Not applicable
NA	Nicotinic acid
NAD	nicotinamide adenine dinucleotide
NADH	Reduced nicotinamide adenine dinucleotide
NADP	Nicotinamide adenine dinucleotide phosphate
NADPH	Reduced Nicotinamide adenine dinucleotide phosphate

ND	Not determined
NDH	NADH dehydrogenases
NDH-1	Type I NADH dehydrogenase
NDH-2	Type II NADH dehydrogenase
NDH-2A	Type IIA NADH dehydrogenase
NIAID	National Institute for Allergy and Infectious Diseases
nM	Nanomolar
nm	Nanometers
NO	Nitric oxide
NOS	Reactive nitrogen species
NRP	Non-replicating persistence
NRP-1	NRP phase 1
NRP-2	NRP phase 2
NRs	Nitrate reductases
OADC	Oleic Albumin Dextrose Catalase
OCF_3	trifluoromethoxy
OD	Optical density
PAS	p-aminosalicylic acid
PBS	Phosphate buffer saline
PCA	Principal component analysis
PCR	Polymerase chain reaction
PDH	Proline dehydrogenase
PEP	Phosphoenolpyruvate
Pfu	Pyrococcus furiosus
Phe	Phenylalanine
PIM	Phosphatidylinositol mannoside
PLS-DA	Partial least squares-discriminant analysis
PMF	Proton motive force
POA	Pyrazinoic acid
PPP	Pentose phosphate pathway
Pro	Proline
PTFE-coated	Polytetrafluoroethylene-coated
pTM3	pCR®II, TA/*cydABDC* construct
pTMA	pUC19/*cydABDC* construct
PZA	Pyrazinamide
Q_1H_2	Ubiquinol-1
Q_2H_2	Ubiquinol-2
QH_2	Quinol
QSAR models	Quantitative structure–activity relationship models
R^2	The linearity
Raz	Resazurin
RIF	Rifampicin
RNS	Reactive nitrogen species

ROS	Reactive oxygen species
Rru	Resorufin
RT	Retention time
S	Substrate
SAR	Structure-activity relationship
SDH	Succinate dehydrogenase
SDS-PAGE	Sodium dodecyl sulfate polyacrylamide gel electrophoresis
SEM	Standard error of the mean
Ser	Serine
SRM	Single reaction monitoring
SSA	Succinic semialdehyde
SSRs	Simple sequence repeats
STR	Streptomycin
TAPS	*N*-Tris(hydroxymethyl)methyl-3-aminopropanesulfonic acid
TB	Tuberculosis
TCA	Tricarboxylic acid
TDR-TB	Totally-drug-resistant tuberculosis
TEMED	N,N,N\\N'-tetramethylethylenediamine
Thr	Threonine
TMB44	Transformed cells grown in O_2-limited growth condition
TML16	Transformed AnML16 competent cells
TMPD	N,N,N′,N′-tetramethyl-p-phenylenediamine
TPZ	Trifluoperazine
Trp	Tryptophan
TRZ	Thioridazine
TST	Tuberculin skin testing
TTP	Thymidine triphosphate
Tyr	Tyrosine
UDP	Uracil diphosphate
UMP	Uridine monophosphate
UQH_2	Ubiquinol
UTP	Uridine triphosphate
v/v	Volume per volume
Val	Valine
VIP	Variable Influence on Projection
V_{max}	Maximum reaction velocity
w/v	Weight per volume
WHO	World Health Organization
X-gal	5-bromo-4-chloro-3-indolyl β-D-galactopyranoside
XDR-TB	Extensively drug-resistant TB
XXDR-TB	Very extensively-drug-resistant TB
µM	Micromolar

Abstract

Tuberculosis (TB) remains one of the most devastating diseases in humans. Nowadays, tuberculosis therapy is not sufficient to control the TB epidemic and only lasts for 6 months to cure patients and prevent relapse; therefore, the treatment of *Mycobacterium tuberculosis* (Mtb) is particularly challenging (1). New antibiotics, mainly those that are derived from new chemical classes, are more likely to be more effective against resistant strains. Moreover, expanding the knowledge of the mode of action of drugs has important implications in tackling TB. Only empirical approaches can be adopted in the journey of discovering new anti-tubercular drugs until a clear picture of latency and persister cells' physiology is achieved. Mtb has the extraordinary ability to survive under hypoxia, suggesting a high degree of metabolic plasticity. The flexibility conferred by a modular respiratory system is critical to the survival of Mtb, thereby also making it a promising area of research for new drug targets. This thesis aimed towards the characterisation of cytochrome *bd*-I quinol oxidase (*bd*-I), a respiratory component that is believed to operate during both the replicative and "dormant" Mtb phenotypes. The essential nature of Mtb *bd*-I, which has no human homologue, has been confirmed in a recent deep sequencing study of genes required for Mtb growth by Griffin *et al.* (2), further confirming its potential as a novel target. Recombinant Mtb *bd*-I was successfully expressed under the control of the pUC19 lac promoter in the *Escherichia coli* ML16 *bo*$_3$*/bd*-I and MB44 *bo*$_3$*/bd*-I*/bd*-II knockout strains, allowing "noise-free" measurement of the enzyme. Initial steady-state kinetics of the enzyme was presented using a range of quinol substrates, revealing a substrate preference for dQH_2 over Q_1H_2 and Q_2H_2. A number of *bd*-I inhibitors were identified and their pharmacodynamic profiles against Mtb H37Rv were determined. In addition, a pharmaco-metabolomics platform was initiated to explore the cellular response of Mtb to current first-line TB drugs as well as in house *bd*-I and type II NADH inhibitors. The initial findings are discussed in the context of the known mode of action of the drugs and future research needs in drug discovery of this devastating disease.

Chapter I

General introduction

1.1. Overview

Tuberculosis (TB) is an infectious disease caused by the bacillus *Mycobacterium tuberculosis* (Mtb), that most often affect the lungs. Despite the availability of highly efficacious treatment for decades, TB remains a major global health problem. TB is second only to HIV as the leading infectious killer worldwide (3).

Although active, drug-sensitive TB disease is curable and preventable, although the prolonged and demanding current TB drugs regimen leads to the emergence of drug resistant strains, which are difficult, complicated, and expensive to treat. Further, sub-populations of slow-growing and persistent Mtb are not targeted by the present TB drugs regimen. Moreover, the deadly synergy of TB and HIV diseases demands first-line treatments that can be fully harmonized as the current TB drugs regimen is not compatible with certain common antiretroviral (ARV) therapies used to treat the human immunodeficiency virus (HIV)/AIDS.

Nearly 50 years passed with no new TB drugs have been developed, despite the flaws with and growing resistance to current TB treatments. Therefore, a shorter, faster, simpler and affordable cure for TB could improve treatment compliance, stop the spread of the disease, save millions of lives and have tremendous global benefits. The new anti-TB treatments should also tackle drug-resistant strains of Mtb, including the organisms in the latent state and it should be compatible with the current drugs.

Targeting respiration and the electron transport chain of Mtb is framed in the context of exciting new developments in tuberculosis drug discovery due to its importance to the survival of Mtb. Currently, The drugs diarylquinolines and phenothiazines have in common the fact that both target oxidative phosphorylation in mycobacteria (4), and that the diarylquinoline TMC207 is involved in a clinical phase II trial and in a novel multi-drug regimen in late-stage clinical trials (1).

1.2. The global burden of tuberculosis in the world

TB is a global pandemic, killing someone approximately every 25 seconds. TB remains a major cause of morbidity and mortality worldwide. According to the WHO, an estimate 8.8 million incident cases of TB globally occurred in 2010, of which 1.1 million deaths were among HIV-negative cases of TB and an additional 0.35 million deaths among people who were HIV-positive (3).

Challenges and burden of TB are arising due to the occurrence of the twin pandemics, TB and HIV/AIDS, as well as the emergence of drug resistant strains of Mtb. Those challenges in conjunction with poor control programs are leading to the resurgence of the disease. An estimated 15% of the population infected with TB (1.4 million people) are co-infected with HIV (3). Further, there were an estimated 0.5 million cases of multidrug-resistant TB (MDR-TB) in 2008 (5), where patient with MDR-TB shows resistance to the two most effective first-line anti-TB drugs, rifampicin and isoniazid (6). Unfortunately, MDR-TB is present in almost all countries surveyed (3).

Latent TB, a state when Mtb remain dormant without developing or transmitting the disease, poses a massive challenge in controlling TB with estimates of about one-third of the world's population has latent TB, of which between 5% and 15% will develop active disease during the course of their lifetime (3). Additional factors that are related to the high TB burden include homelessness, poverty, increasing number of refugees and the lack of governmental support in prevention and treatment programs in developing countries. The lack of better preventive measures that block Mtb transmission or prevent establishment of Mtb infection contributed in increasing the burden of TB. The only available vaccine against TB is one-century-old Bacillus Calmette-Guérin (BCG) vaccine with incomplete protective efficacy against pulmonary TB in adults (3, 7). However, light of hope exists with 11 vaccine candidates (in clinical trials) that could offer an excellent protective efficacy (8).

The majority of the estimated TB cases in 2010 happened in Asia (59%) and Africa (26%) while smaller proportions of cases were found in the Eastern Mediterranean Region (7%), the European Region (5%) and the Region of the Americas (3%) (3).

The worldwide distribution of new TB cases per 100,000 individuals is depicted in the following Figure (1.1).

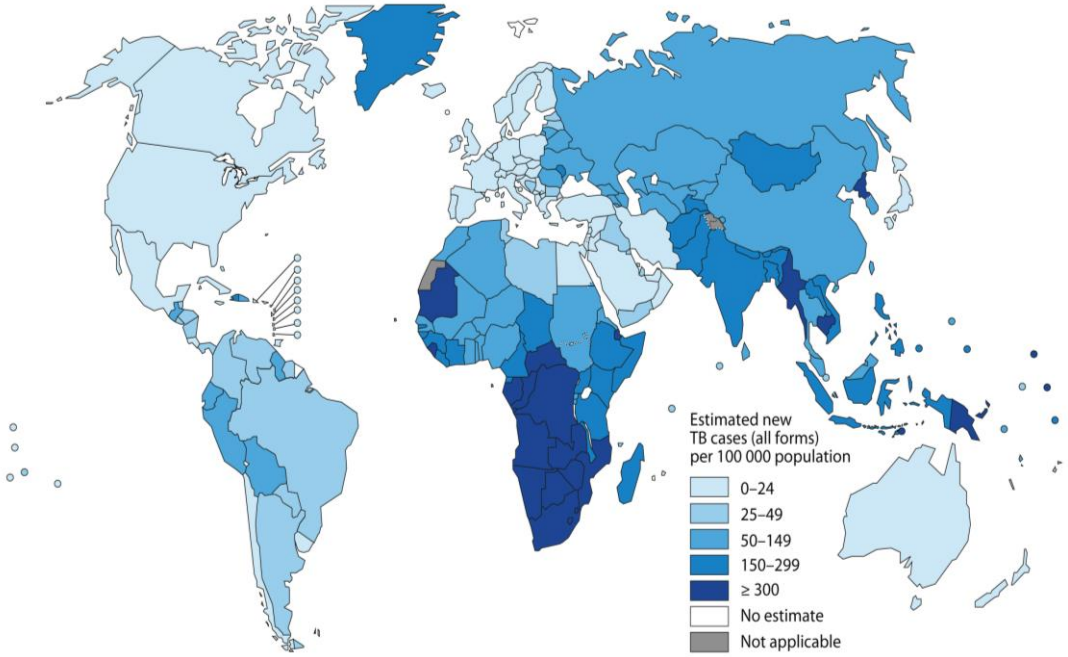

Figure 1.1: Worldwide distribution of new TB cases per 100,000 people in 2011 (3)

All this illustrates the tremendous burden that a single disease has globally. Therefore, advances in TB research are urgently needed to explore the mysteries of Mtb pathogenesis and potential drug targets that could help in eliminating the disease.

1.3. *Mycobacterium tuberculosis* (Mtb):

1.3.1. The pathogen of tuberculosis: biology and virulence factors

Tuberculosis is caused by Mtb, a slow growing aerobic-to-facultative anaerobe intracellular pathogen that parasitizes macrophages. Mtb belongs to the Mycobacterium genus, Mycobacteriaceae family, Corynebacterineae suborder, Actinomycetales order, Actinobacteria phylum in the Bacteria kingdom. Mtb are gram positive non-motile and rod-shaped bacteria. The cell wall is a major virulence factor of Mtb that relates to Mtb intrinsic drug resistance. The Mtb cell wall is built of a fascinating diversity of lipids layers, which includes a hydrophilic arabinogalactan layer linked to hydrophobic mycolic acids. This arabinogalactan/

mycolic acid layer, which lies on the top of the peptidoglycan layer, is further covered with a layer of polypeptides and mycolic acids consisting of free lipid, glycolipids, and peptidoglycolipids (Figure 1.2). The cell wall of mycobacterium is unique by the dominance of mycolic acids. Other important glycolipids including mannose capped lipoarabinomannans (ManLAM), lipomannan (LM), and phosphatidylinositol mannoside (PIM) (9). These layers constitute a barrier for both hydrophobic and hydrophilic compounds rendering the outer surface of Mtb extremely hydrophobic (10, 11).

Importantly, the capacity of Mtb to escape the host immune system and remain alive and in a dormant state is considered one of the main Mtb virulence factors. This phenomenon is called latency where Mtb remain alive in the human host, in an asymptomatic non-transmissible state and with the ability to reactivate and cause active disease, having their virulence mechanisms intact.

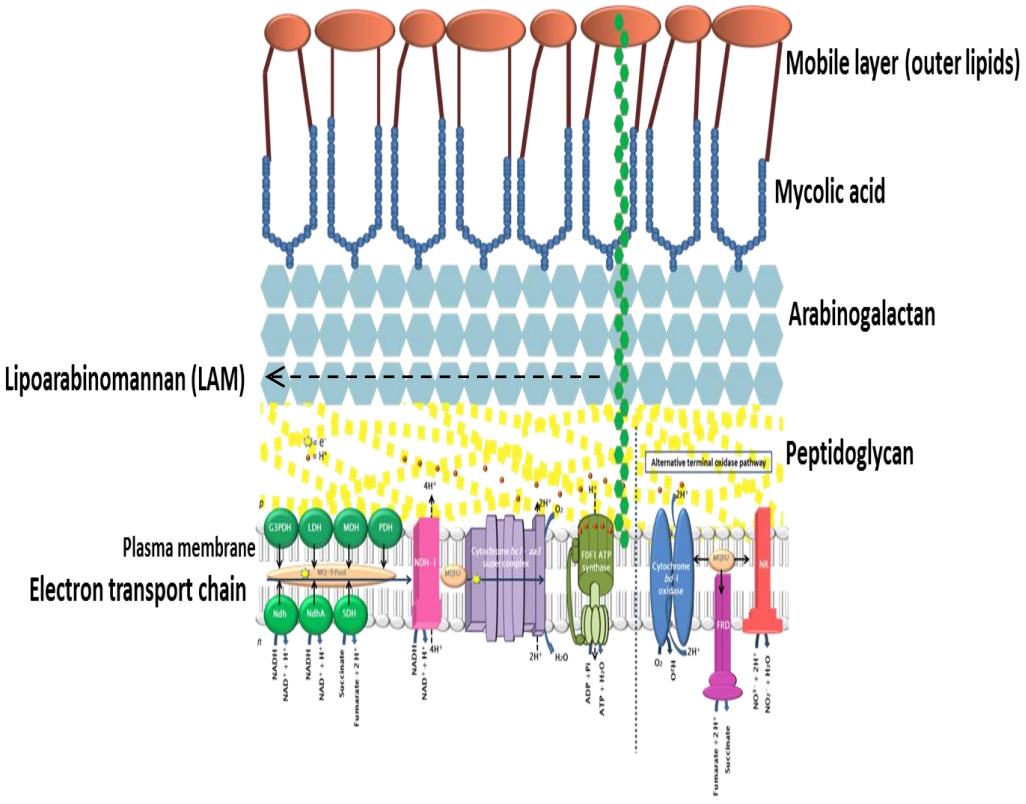

Figure 1.2: Schematic representation of the cell wall of *Mycobacterium tuberculosis*

1.3.2. Pathogenesis of tuberculosis

1.3.2.1. Life cycle of Mtb

To develop new efficient drugs, it is important to understand the disease process. The disease is spread through an aerosol route when people who are sick with active pulmonary TB expel bacteria, for instance by coughing or sneezing. Tuberculosis commonly affects the lungs (pulmonary TB) and causes symptoms that can include coughing up blood, chest pains, fever, and fatigue. However, Mtb can disseminate to other parts of the body (extrapulmonary TB) including the central nervous system, lymphatic system, bones and joints. Pulmonary TB is by far the most common form of tuberculosis, accounting for 86% of all new and relapsed cases worldwide (3).

Mtb usually enters the body by airborne droplet nuclei, which are inhaled and lodge in the alveoli in the distal airways. Mtb is then taken up by alveolar macrophages, initiating a cascade of events where either successful containment of the infection in granulomas or progression to active disease takes place. The notorious success of Mtb adaptation inside its human host refers to its ability to impair the normal maturation of the phagosome (reprogramming of macrophages after phagocytosis to prevent its own degradation). Ideally, Mtb bacteria are internalised inside macrophages in a membrane-bound organelle called the phagosome. The phagosome undergoes a maturation process along the endocytic pathway leading to fusion with late endosomes and finally lysosomes, forming the phagolysosome where some of the ingested bacilli are degraded (12). However, bacilli phagocytosed by alveolar macrophages can subsequently invade the subtending epithelial layer leading to induction of a localized inflammatory response and consequently recruitment of mononuclear cells from neighboring blood vessels. This recruitment provides fresh host cells for the bacterial population.

In immunocompetent individuals the propensity of Mtb to survive in a pathogen-friendly phagosome (granuloma) and to establish asymptomatic latent infection is a continued threat of TB infection. This is because the immune system is capable of effectively containing Mtb regardless of the fact that the infectious microorganism may not always be fully eliminated (13). The risk of active disease, disease reactivation or death exists in an immune-compromised host (e.g. HIV positive

individuals) or patients with chronic diseases such as diabetes/obesity (14). During active TB or disease reactivation, damage in lung tissue occurs and an active granuloma displays extensive pathology that eventually ruptures and releases thousands of viable, infectious bacilli into the airways. This point of the highly infectious form of the disease allows the cycle to resume. Interestingly, it is impossible to predict who will fully eradicate Mtb and who will contain latent TB infection and remain healthy due to the variance of immune system response from person to person (Figure 1.3) (15, 16).

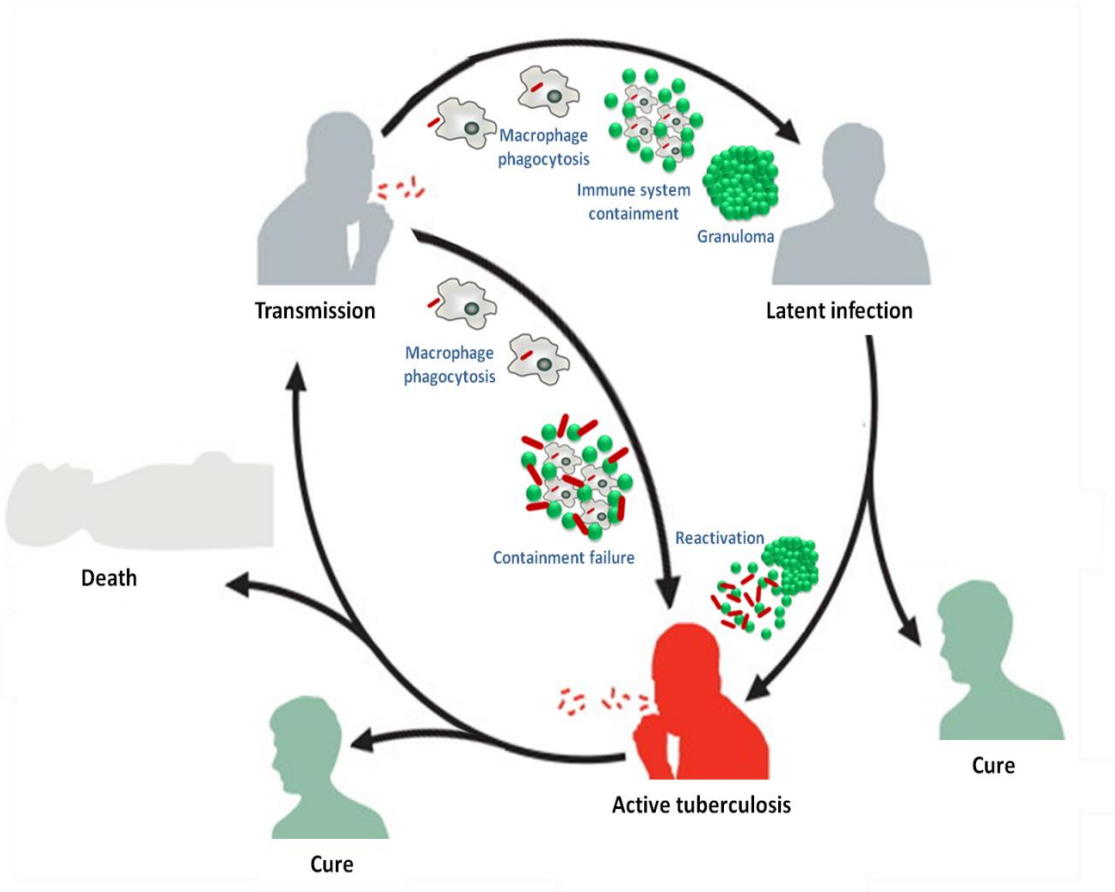

Figure 1.3: The life-cycle of *Mycobacterium tuberculosis*: from infection to host defence

Primary infection can progress toward active disease or can be contained as latent infection. Active TB can: be cured (eradication of Mtb by host's immune system); be contained as latent infection and remain healthy; or lead to death. Latent infection can: develop to active disease (reactivation); or be cured.

1.3.2.2. Granuloma

The granuloma is the characteristic feature of human latent pulmonary TB as well as an important key factor responsible for immune evasion and reactivation. Pathologists have described the lung granuloma as the hallmark of pulmonary TB. Granuloma formation is a sign of protective immunity and known to occur in the early stages of an infection episode to ensure pathogen containment. However, the features of the granuloma are still largely unknown, regardless of the efforts on *in vitro* granuloma models and on *in vivo* dissections to mimic the human granuloma environment (17, 18).

The granuloma is defined as a central core of necrotic tissue surrounded by dense layers of immune system cells, like macrophages and lymphocytes, large multinucleated cells (Langhans giant cells), dendritic cells and specialised leukocytes as well as epithelioid cells and fibroblasts. Development of the tuberculous granuloma restrains pathogen dissemination throughout the host and focuses the immune response to the site of mycobacterial persistence. This development is controlled by cytokines and chemokines produced by leukocytes and local tissue cells (17-19). Within granulomas, mycobacteria in activated macrophages adapt to a metabolic life-style that makes preferential use of fatty acids, functions under severe oxidative and nitrosative stress, increases cell-wall thickness and halts active replication (13, 20). Moreover, the highly pathogenic mycobacteria stimulate the formation of granuloma-specific foamy macrophages which have a high lipid content that constitute a nutrient-rich reservoir for long-term persistence (21).

Various animal models (e.g. guinea pigs, rabbits and nonhuman primates caseous) have been used to study granulomas using pimonidazole, an imaging agent that indicates hypoxic conditions, and metronidazole, a drug only effective against anaerobic bacteria (22). Puissegur *et al* (2004) replicated an *in vitro* model of granulomas using mononuclear cells, isolated from a BCG-vaccinated non-infected individual human blood sample and exposed to mycobacterial antigen-coated beads, or live-mycobacteria. This process lead to the production of a cellular aggregation response, similar to the granuloma (23).

1.3.2.3. Latency of Mtb

Latency, persistence, and dormancy are terms that are sometimes used interchangeably in describing Mtb and TB pathogenesis. Latency is defined as the presence of any tuberculous lesion which fails to produce symptoms of active TB. Persistence stand for actual or potential bacterial survival in the face of any stress from the host immune system (24). Dormancy has been used to describe both TB disease as well as the metabolic state of the tubercle bacillus where dormancy involves a reversible metabolic shutdown. Latent infection may be attributable to dormant bacteria as well as to bacilli with similar phenotypes as persister cells, which will be described shortly (24-26).

This dormant or latent infection presents a vast reservoir of potential reactivation and transmission of the disease, making eradication of TB a major challenge. Impairment of the immune system either by age, chronic illness or HIV/AIDS cause reactivation of these dormant bacilli that can occur at any time, even decades after the primary infection took place (27).

The existence of latent TB in an infected individual could be detected by a visible calcified granulomatous tissue under X-ray. Further, the infected individual will have a strong immune response against Mtb antigens which is detected through tuberculin skin testing (TST) (13). Unfortunately TST gives a high rate of false positives that makes it inadequate to distinguish if the immunological reaction is due to BCG vaccination or previous exposure to pathogenic Mtb. Similarly, it is difficult to distinguish if an active TB infection occurred as result of latent TB reactivation or as a new incident of infection (11, 28).

1.3.2.3.1. Replication state of dormant Mtb

The issue of defining the replication state of dormant Mtb is still controversial. However, there are two acceptable hypotheses. The first one defends a non-replication or very slow replication state, a near-static state of Mtb that permits an escape from the host immune system and a resistance against antibiotics (13). The second hypothesis proposes a dynamic state of constant replication of Mtb, enclosed by the immune system. In both states, Mtb developed an elaborate survival

mechanism in humans where the immune system in immunocompetent individuals engages a lifelong battle against latent TB infection, either eradicating the pathogenic Mtb or limiting its replication, creating a long-standing reservoir of future disease and contagion (13, 25, 28).

Yang *et al* (2011) conducted a genomics and molecular epidemiology study that support the first hypothesis, a non-replication state of Mtb during latency. However, this hypothesis is not conclusive as the study was limited by the small number of case studies and by the fact that the mutation rates of the mononucleotide simple sequence repeats (SSRs or microsatellites) in Mtb genome are unknown (29).

Other studies in the defence of the second hypothesis were that Mtb bacilli in continuous replication during latency are counted by the presence of metabolic activity within the Mtb bacilli (28, 30). Moreover, one of the strongest arguments for Mtb replication during latency comes from the fact that isoniazid, active against only replicating mycobacteria, is able to completely sterilize the host from bacteria, which suggests that at least part of the Mtb latent population is replicating (13). Gill *et al*'s (2009) study favoured the second hypothesis as well, where transformed Mtb with the unstable plasmid pBP10 were used during mice infection. This study showed loss of plasmid during chronic infection which implied a replication state of Mtb during this period (31).

1.3.2.3.2. Latency models

The acknowledegment of the consequence of the latency phenomenon in TB pathogenicity drives the research toward latency abrogation. This requires a better understanding of the physiological events that lead to latency, thus efforts to replicate this state *in vitro* were made. The Wayne model of hypoxia and the Cornell mouse model, the most utilised models, are two examples of modulating some conditions that are known to reduce Mtb metabolism and create a state that would mimic one or more features of the latency condition.

The Wayne model of hypoxia is one of the best characterized models, where the Mtb bacilli are submitted to a slow shift from aerobic to anaerobic conditions by growing

bacteria in a constantly stirred liquid medium with no disturbance on the surface of the liquid and with a defined proportion between air and liquid in sealed tubes. This specific set up leads to a gradual depletion of oxygen from the bottom to the top of the tube in a constant manner, which in turn results in a successful adaptation of the bacilli to hypoxic conditions. As the latency state is established, the Mtb bacilli enter a 2-phase state called non-replicating persistence (NRP), NRP phase 1 (NRP-1) and NRP phase 2 (NRP-2) (20, 32, 33). During NRP-1, the oxygen saturation is about 1% and the number of viable bacteria reaches stationary, although cell enlargement leads to a minute increase in the turbidity of the culture (34). Eventually, during the next phase NRP-2, the culture transfers to complete anaerobic conditions where the oxygen saturation is 0.06% and a significant reduction of metabolism with no morphological changes of bacteria take place (33, 34).

With regards to drug susceptibility, although dormant bacilli display increased tolerance, they are still susceptible to rifampicin and isoniazid once bacilli resume growth. Further, the bacilli are sensitive to metronidazole since metronidazole is only active against anaerobic or microaerophilic bacteria. This susceptibility is considered as an evidence for hypoxia in the phenomenon of latency (33, 35).

The Cornell mouse model, a drug induced model, is an alternative dormancy model where Mtb infected mice are treated with isoniazid and pyrazinamide for only 12 weeks, resulting in disappearance of active TB disease and rendering uncultivatable Mtb bacilli from mouse spleens (36). Consequently, one third of the mice show a reappearance of active and drug-sensitive Mtb. Therefore, the latent period of the disease is considered to be the 12 weeks between disappearance and then reappearance of the infection (37, 38).

A variety of other models have been established to mimic the latency state of Mtb as present in the macrophage, phagosome or granuloma environment. For example, the nutrition starvation model is based on evidence that indicated the presence of severe nutrient limitations in TB lesions (39, 40). The phosphate depletion model is another model that represents the macrophage restricted environment (41). Moreover, the prolonged stationary-phase model has been developed since similarities between persistence and the bacteria that exist in stationary phase, the non-replicating

phenomenon, has been proposed (42, 43). Recently, a novel multiple-stress model for inducing dormancy in Mtb has been suggested where the bacteria are submitted to a combination of stresses which are low oxygen, high CO_2, low nutrients and an acidic environment. The multiple-stress model can be used in high-throughput screening for drugs targeting the persistent bacteria, since it most likely resembles the latency environment in the human host (44).

1.3.2.4. Persister cells

Tubercle bacilli produce heterogeneous bacterial populations, including persisters, dormant and growing bacteria. This is due the fact that Mtb are able to reside in various microenvironmental statuses that are oxygen-rich (in cavities) or oxygen-limited (in host macrophages or in granulomatous lesions) conditions, or in other stressful conditions (e.g. nutrient starvation, oxidative stress, and acidic pH) (45). Persisters can inhabit intracellular and extracellular locations as well as different cell types, e.g. adipose tissue and sputum (24, 46, 47).

There is overlap with the bacterial dormancy (persistence) phenomenon and persisters where dormant Mtb are applicable to some but not all described persistence phenomena (26, 48). The term "persister" donates a well-defined sub-population of bacteria that survive antibiotic exposure, while "persistence" as mentioned earlier points to the bacterial survival in the face of any stress from the host immune system (24).

Although mycobacterial persisters are genetically identical to drug susceptible bacteria and have non-inheritable phenotypic resistance or tolerance to antibiotics, they are still capable of surviving the cidal action of antibiotics (24, 49). Persisters necessitate lengthy TB therapy, posing a major challenge for controlling TB. Persisters appear to be non-replicating or slowly replicating bacilli where their propagation depends on the age of the culture, the antibiotic exposure duration, and the type and concentration of antibiotics used in the culture (45, 50, 51).

The mechanisms of persister cell development are complex and may be related to those required for persistence (dormancy) in chronic infection. Single-gene mutation

studies identify several genes or pathways that might engage in Mtb persister formation or maintenance, such as energy-related pathways genes. In INH-treated mice, disruption of *cydDC* genes accelerated Mtb elimination, which entailed reduction of antibiotic resistant cells (persisters) (24, 52). *CydDC*, encoding an ABC transporter, is implicated in cytochrome *bd*-I assembly, an essential enzyme during hypoxia and for Mtb viability (2, 53).

1.3.2.5. Yin-Yang model

There is sparse information defining the subpopulations of Mtb. A yin-yang model, applicable to both patients and experimental systems, has been proposed to emphasize the heterogeneity, dynamic nature, and interconversion of the diverse Mtb subpopulations present. The hypothesis of yin-yang models is that the bacterial population consists of growing, slow-growing, and non-growing subpopulations that have different metabolic statuses which can interconvert at the level of the bacteria (24). This model also provides a possible justification of latent infection (yin) and active disease (yang) abilities to interconvert at the level of the host and behave as a continuum. Further, the rationale behind the current two-phase TB regime and the reasons of using isoniazid as chemoprophylaxis or for treatment of latent TB infection (LTBI) could be explained through the yin-yang model as well (24).

There are two yin-yang models. The first one is the yin and yang of persisters and replicating bacteria and their interconversions (Figure 1.4). This model suggests that the subpopulation of growing bacteria (yang) has a small proportion of non-growing or slowly growing persisters (yin). This proportion increases upon entry of the bacteria into the stationary phase. Furthermore, this model shows that after a 2-month intensive-phase treatment with isoniazid (INH), rifampin (RIF), pyrazinamide (PZA), and ethambutol (EMB), the remaining persister tubercle bacilli can revert to growing form that can be eliminated by INH/RIF combination in the succeeding 4-month continuance phase of treatment. This model also demonstrates the possibility of Mtb to revert from a non-growing form during LTBI to a growing form, that is INH susceptible. This in turn explains using INH as prophylactic treatment of LTBI. Moreover, this model shows the possibility of phenotypic resistance persister

tubercle bacilli to convert into genetic resistance growing bacteria and vice versa (24).

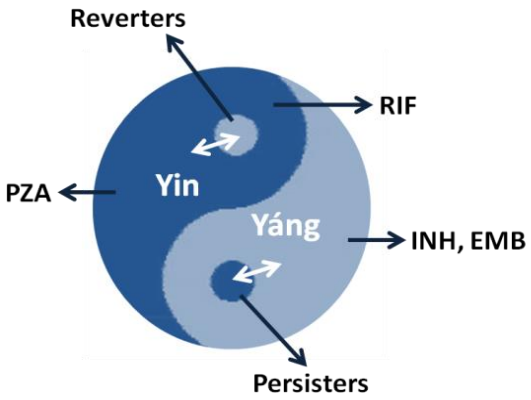

Figure 1.4: Yin and yang of persisters and replicating bacteria and their interconversions (24, 45).

The second yin-yang model is the yin and yang of latent infection and overt or active disease and their interconversions (Figure 1.5). During overt disease (yang), the growing bacterial population is the majority while non-growing bacteria or persisters are the minority and vice versa with respect to LTBI (yin). These proportions of growing and non-growing bacteria vary according to the host immune system and antibiotic treatment effectiveness (24).

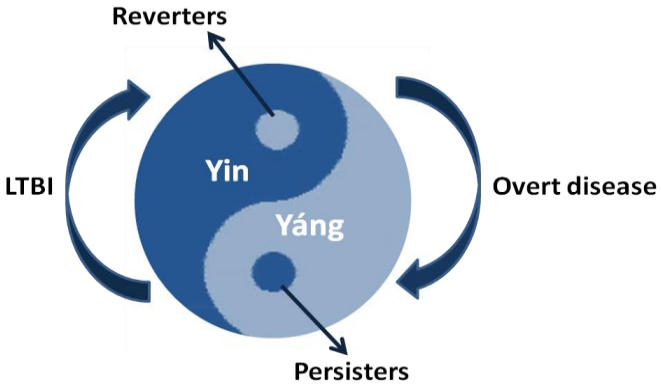

Figure 1.5: Yin and yang of latent infection and overt disease and their interconversions (24, 45).

1.4. Tuberculosis drugs:

The current TB chemotherapy evolved from numerous experimental and clinical studies where the introduction of the current front-line anti-tuberculosis drugs started in 1952 with the discovery of isoniazid (54, 55), which was then followed by pyrazinamide (1952) (56-58), ethambutol (1961) (58) and rifampicin (1967) (59-62). Recently, a variety of other second-line drugs were introduced such as kanamycin, amikacin, capreomycin, cycloserine, ethionamide and thiacetazone.

The current first-line recommended standard TB chemotherapy, called DOTS (directly observed treatment, short-course), involves a direct monitoring of the patient by trained health professionals of the patient being treated. DOTS is a six month therapy consisting of an initial two-month phase of treatment with four drugs, INH, RIF, PZA, and EMB, followed by a continuation phase of treatment with INH and RIF for another four months. The DOTS regimen is recommended by the WHO and has a cure rate of up to 85% with drug-susceptible forms of TB (63-65).

The rationale behind using the combination of drugs regimen is due to the synergistic reaction of these drugs as well as the presence of physiologically heterogeneous population of the tubercle bacilli. Moreover, this combination serves as an attempt to avoid the risk of emergence of drug-resistant strains under monotherapy and reduces anti-TB therapy from 18 months to 6 months (33, 66, 67). However, long treatment duration could be attributed to the possibility of existence of phenotypically tolerant tubercle bacilli after a 2-month intensive-phase treatment that can be killed by INH and RIF in the subsequent 4-month continuation phase of treatment (24, 68).

With regards to DOTS regimen strengths; within 2 months of treatment initiation, 99% of tubercular bacilli could be killed by the INH and RIF combination, the two most potent anti-TB drugs. Thereafter, RIF and INH are crucial for successful 6-month treatment regimens as RIF kills low or non-replicating bacilli that are not affected by any other anti-TB agents (67).

Regarding DOTS limitations, DOTS is an extremely prolonged, demanding and complex regimen results in patient non-compliance that leads to the development of deadlier heritable drug-resistant strains (69). Further, another massive challenge is to control the twin epidemics, TB and HIV/AIDS, which arises from the incompatibility of current TB therapy with certain common ARV drugs that are used to treat HIV/AIDS (70). Moreover, DOTS is ineffective in controlling MDR-TB in high MDR-TB incidence areas (71). Therefore, first-line treatments that can be fully harmonized and overcome the current TB drugs flaws are urgently needed. A detailed description of the drugs of the DOTS regimen is given below.

With respect to LTBI, the current recommended treatment of LTBI to prevent endogenous reactivation consists of 6–12 months of isoniazid. However, this regime is limited by the long duration of therapy and potential for hepatic toxicity. Therefore, shorter and more intermittent rifamycin-containing regimens have been investigated where rifampicin for 4 months is an alternative in the USA and Canada whereas in the UK, a 3-month regimen of rifampicin plus isoniazid is used with success (72-75). Remarkably, Lin *et al* (2012) showed that MTZ given for 2 months is almost as effective as using an INH/RIF combination in order to prevent reactivation of LTBI (76).

1.4.1. First-line tuberculosis drugs:

1.4.1.1. Isoniazid

Isoniazid (Figure 1.6), a pyridine derivative of nictoinamide, is the most widely prescribed first-line drug for the treatment of TB. Isoniazid (INH, isonicotinic acid hydrozide) is a highly bactericidal drug against actively growing bacilli and bacteriostatic for non-dividing Mtb. INH is a small hydrophilic compound that is thought to enter Mtb through porins in the mycobacterial cell wall (77). The accumulation of isoniazid has been also attributed to the role of an active efflux (78-80).

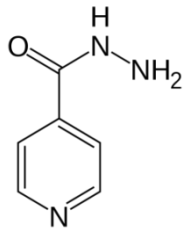

Figure 1.6: Structure of isoniazid, $C_6H_7N_3O$

INH is a pro-drug activated by the mycobacterial enzyme catalase-peroxidase (KatG), a hemoprotein possessing catalase-peroxidase, Mn^{2+}-dependent peroxidase, cytochrome P450-like oxygenase, and peroxynitritase activities (81, 82). A number of stable KatG mediated isoniazid metabolites have been identified which include isonicotinic acid, isonicotinamide and pyridine-4-carboxyaldehyde (83). However, none of these stable metabolite themselves are bactericidal and it is likely that bactericidal activity is attributed to reactive intermediate species, isonicotinic acyl radicals and anions (84).

Our knowledge of the mechanism of action of INH is limited despite numerous studies that have been done. Isoniazid is particularly effective at inhibiting the synthesis of mycolic acid needed for the Mtb cell wall (85). The synthesis of mycolic acid in Mtb is attributed to a number of proteins including an enoyl-acyl carrier protein reductase (InhA), an acyl carrier protein (AcpM) and a β-ketoacyl-ACP synthase (KasA). These proteins (InhA, AcpM and KasA) are hypothesised as targets for the isoniazid active metabolites as mutation in these proteins show a low level of INH resistance (86).

One of the proposed mechanisms by which INH is able to inhibit InhA and therefore mycolic acid synthesis is that Mtb KatG oxidizes isoniazid, a prodrug, to an isonicotinic acyl radical, which then couples to reduced nicotinamide adenine dinucleotide (NADH) (84, 87). In this theory, isonicotinic acyl radicals covalently bind to $NAD^{\bullet}$ radicals to form isonicotinic acyl NADH that is thought to be a potent inhibitor of InhA. Inhibition of InhA by the INH-NADH adduct probably results in a weakened mycobacterial cell wall and, eventually, death of the pathogen (84).

Likewise, it has been suggested that the INH activity also arises from the coupling of $INH^{\bullet}$ to reduced nicotinamide adenine dinucleotide phosphate (NADPH), forming an INH-NADPH adduct, which is an inhibitor of MabA. MabA is one of several proteins involved in the type II fatty acid synthases (FAS-II) mycolic acid synthesis pathway (88). An alternative theory on INH activity is the isonicotinic acid hypothesis (89). Here it is proposed that isoniazid is metabolised to a stable metabolite, isonicotinic acid, which remain in its ionic form at physiological pH leading to ion trapping and accumulation of isonicotinic acid in Mtb. Thereby, isonicotinic acid competes with, and displaces, nicotinic acid (NA) during the bacterial synthesis of NADH, leading to the formation of the *meta*-isomer of NADH wich inhibits InhA mediated fatty acid synthesis (90).

The origins of INH drug-resistance in Mtb can be traced to mutations in *KatG*, coding for the only identified catalase–peroxidase in Mtb (81), or to mutations in the promoter regions of InhA (91). KatG mutations are found to confer high levels of INH resistance (92). Resistance to INH in Mtb is also linked to reduced NDH-2 activity in NDH mutants, as this leads to an increase in intracellular NADH levels (93, 94). Moreover, other factors such as neutralization of isoniazid by the overproduction of arylamine N-acetyltransferase (95), limitation of NAD^{+}-binding proteins (96, 97), and the overexpression of antioxidant enzymes that compensate for the loss of function of the KatG protein (98) bestow resistance to INH.

INH has been used clinically since 1952 as a first-line antimicrobial for tuberculosis (99) and is highly regarded as an anti-TB drug, due to the fact that it is highly potent, well tolerated by the patient and relatively cheap. It is also prescribed to infants as prophylactic therapy (100, 101). Among the first-line drugs, INH is the only bactericidal agent that easily crosses the blood-brain barrier (102, 103). However, the main drawbacks of INH are INH-related severe toxicity, which is peripheral neuropathy and hepatotoxicity (104) and the fact that INH acts exclusively on actively growing bacilli.

1.4.1.2. Rifampicin

Rifampicin (RIF) (Figure 1.7) is a large lipophilic semi-synthetic derivative of the natural product rifamycin, obtained from culture filtrates of *Streptomyces mediterranei*. RIF uptake is mediated by diffusion through the cell wall, in a process that is influenced by the cell wall arabinogalactan content (77).

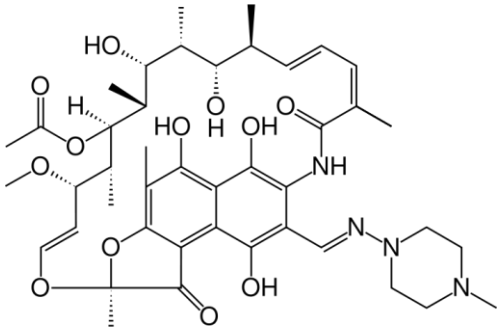

Figure 1.7: Structure of rifampicin, $C_{43}H_{58}N_4O_{12}$

RIF is a broad-spectrum antibiotic with potent bactericidal activity against both active and dormant tubercle bacilli. It inhibits RNA synthesis by binding to the central region of the β-subunit (81 bp) of RNA polymerase (encoded by the *rpoB* gene), which effectively blocks transcription (105-107). Therefore, RIF continues to exhibit some bactericidal action, even after O_2 depletion occurs (33).

Resistance to RIF is the main reason of treatment failure and fatality as it is one of the essential drugs in modern chemotherapy (108). Mutations in the 81 bp region of *rpoB* are the most common mutations associated with rifampicin resistance (approximately 96%) (105).

Importantly, simultaneous use of rifampicin and antiretroviral drugs is complicated by drug–drug interactions (DDI). This DDI is caused by the potent induction by rifampicin of a number of drug-metabolising enzymes involved in antiretroviral drugs metabolism and transport (109). Moreover, rifampicin is not highly toxic on its own, however some studies showed that the incidence of hepatotoxic effects associated with rifampicin monotherapy is around

2%, but rarely associated with fulminant hepatitis (110, 111). Otherwise, rifampicin toxicity is mostly idiosyncratic, and only a small percentage is attributable to an allergic, hypersensitivity type reaction which leads to symptoms including fever, rash, flu-like syndrome, acute renal failure, haemolytic anaemia, thrombocytopenia, and anaphylactic events (112).

1.4.1.3. Ethambutol

Ethambutol (EMB) is a bacteriostatic agent that has activity against growing bacilli but has no effect against non-replicating bacilli (Figure 1.8). EMB is a small, hydrophilic agent that is thought to cross the mycobacterial wall via the porin channels, although some evidence of active uptake exists (77).

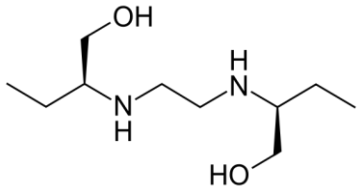

Figure 1.8: Structure of ethambutol, $C_{10}H_{24}N_2O_2$

The specific mode of action of EMB is still uncertain. EMB exerts its activity by interfering with the synthesis and assembly of arabinogalactan (113), with secondary effects upon lipoarabinogalactan (114) and mycolic acids (115), essential lipids in the Mtb cell wall. EMB is assumed to act via inhibition of three arabinosyl transferases: EmbA, EmbB, and EmbC. These arabinosyl transferases are essential in Mtb, where EmbA and EmbB are required for the synthesis of arabinogalactan, and EmbC is involved in the synthesis of LAM (116-119). EmbB has been proposed as the target of EMB in Mtb (120) although Goude *et al* (2009) found that EmbB is not the only target and that EmbC is one of the cellular targets of EMB action (119).

The genetic basis of resistance to EMB in mycobacteria has been referred to mutations in EmbCAB operon, especially EmbB. High levels of resistance were attributed to a combination of mutations in EmbB codon 306 and EmbC codon 270 (119, 121). The most frequent adverse effects associated with EMB are ocular toxicity, manifested by optic or retrobulbar neuritis, and hepatotoxicity (122, 123).

1.4.1.4. Pyrazinamide

Pyrazinamide (PZA) (Figure 1.9), a structural analogue of nicotinamide, is a paradoxical drug, showing good activity against tubercle bacilli at acid pH (124) and being more effective against old cultures than young cultures (125), and also more active at low oxygen or anaerobic conditions (126). PZA is a prodrug of active agent pyrazinoic acid (POA). PZA introduction allowed TB therapy to be shortened from 1 year to 6 months.

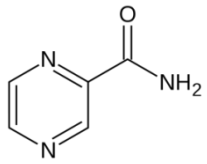

Figure 1.9: Structure of pyrazinamide, $C_5H_5N_3O$

However, it shows no activity against Mtb grown in standard culture conditions *in vitro* (127), unless acidic conditions are introduced (128) which probably facilitate the accumulation of POA inside the bacilli (129, 130). The acidic environment *in vivo* is thought to be generated by either a small decrease in phagosome pH which occurs due to binding of the early endosomes, or by early inflammation following Mtb infection (131).

Zhang and colleagues (129, 130) have reported that, PZA enters Mtb through porins and is converted to POA by the PZase/nicotinamidase enzyme. POA in turn leaves Mtb via a weak efflux pump or by passive diffusion. The presence of Mtb in acidic environment allows the POA, which is uncharged and protonated, to enter Mtb and accumulate as the rate of POA influx is greater than the efflux. Accumulation of pyrazinoic acid is thought to be vital in mediating PZA antimicrobial activity (124).

There are a number of postulated mechanisms of action of POA. The first postulated hypothesis is that the accumulation of protonated POA brings protons into the bacilli, leading to acidification of the cytosol which eventually causes disruption of the Mtb membrane energetic by collapsing the membrane potential and affecting

membrane transport. The PZA effectiveness against dormant Mtb is attributed to the reduction of its ability to maintain membrane potential (132). The second proposed hypothesis is that PZA and POA inhibit fatty acid synthesis in Mtb through type I fatty acid synthases (FAS-I) inhibition at pH 6 (acidic condition) but not at pH 6.8 (133).

The mycobacterial enzyme PZase, encoded by the *pncA* gene of Mtb, is essential for converting PZA to POA. A mutation in the gene *pncA*, which encodes PZase, is the major mechanisms of PZA resistance (134). The non-uptake of the pro-drug is an additional mechanism of resistance to the PZA that is known to exist but has not been fully investigated. It has been demonstrated that the accumulation of both PZA and nicotinamide, but not isoniazid, in mycobacteria is partially dependent on an uptake process, which could be an active transport or facilitated transport with subsequent ATP dependent metabolism (134).

In terms of tuberculosis treatment PZA is relatively non-toxic. The toxicity of PZA is dose-related (110, 135) and has the frequently described adverse events (AE) of arthralgia and hepatotoxicity (110, 136).

1.4.2. Second-line tuberculosis drugs

The emergence of strains resistant to DOTS drugs causes a major concern for TB treatment. Therefore, alternative TB drugs, known as the second-line TB drugs, are available to be used (Table 1.1). These second-line drugs include fluoroquinolones, such as ciprofloxacin, ofloxacin, levofloxacin and moxifloxacin as well as aminoglycosides, injectable agents, such as streptomycin, amikacin, kanamycin and capreomycin. Further, they include bacteriostatic second-line drugs, cycloserine, ethionamide and para-aminosalicylic acid (73). Quinolone drugs were shown to have high activity against Mtb and have been used as second-line drugs for the treatment of drug-resistant TB since the late 1980s (124).

1.4.2.1. Streptomycin

Streptomycin (STR), an aminoglycoside antibiotic, was the first effective drug against Mtb, representing the beginning of modern Mtb chemotherapy (Figure 1.10).

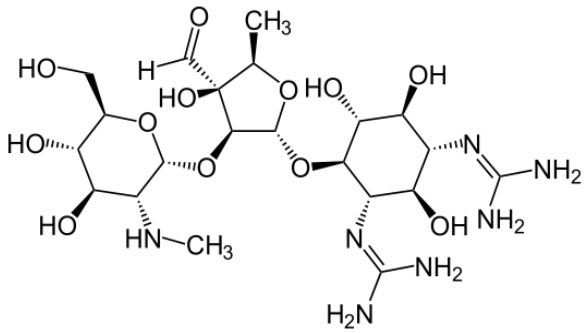

Figure 1.10: Structure of streptomycin, $C_{21}H_{39}N_7O_{12}$

Primarily, the STR mode of action is associated with interfering with protein synthesis by inhibiting initiation of mRNA translation, that in turn results in misreading of the genetic code and damaging of the cell membrane. Specifically, STR binds tightly to the conserved A site of 16S rRNA in the 30S ribosomal subunit. STR has an effect only on replicating tubercle bacilli. However, the intracellular location of the bacilli could render STR inactive (67, 123, 124).

Streptomycin remains an important drug for treating diseases caused by Mtb, but it is no longer first-line. This could be referred to number of factors, including rapid development of resistance to this drug, and since the combination of INH and STR had little overall effect and must be given by injections. STR resistance is linked to mutations in *rpsL* (S12 ribosomal protein) and *rrs* (16S rRNA) genes that encode small ribosomal subunit (67, 123, 124, 137).

1.4.3. Metronidazole, a drug against anaerobic bacteria

Metronidazole (MTZ) (Figure 1.11) is classified as a nitroimidazole and as antitubercular which kills only dormant and persister Mtb under hypoxic/anaerobic conditions. Metronidazole acts on damaging the pathogen deoxyribonucleic acid (DNA) but has poor activity against replicating tubercle bacilli. Recently, Zhang (2012) and Lin *et al* (2012) found that MTZ alone can prevent reactivation of LTBI

to active disease (35, 76). Metronidazole serves as a control in the anaerobic TB studies (138, 139). A Phase II clinical trial in South Korea sponsored by the National Institute for Allergy and Infectious Diseases (NIAID) (www.niaid.nih.gov), is currently studying the effect of adding MTZ to the treatment against MDR-TB (138).

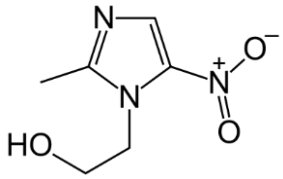

Figure 1.11: Structure of metronidazole, $C_6H_9N_3O_3$

1.4.4. Resistant tuberculosis phenotypes

The sporadic appearance of drug resistant *Mycobacterium tuberculosis* strains is an inevitable consequence of using anti-TB antibiotics. There are factors that accelerate the emergence of these resistance strains, including the aforementioned DOTS limitations, inadequate chemotherapy prescriptions, poor management of drug supplies, the use of drugs of unproved bioavailability and poor direct observation of TB patients throughout the treatment course. There are two types of resistance, TB primary resistance occurs when the person is infected with an already Mtb drug-resistant strain and TB secondary resistance (acquired resistance) occurs when TB patients who are infected with Mtb drug susceptible strains develop resistance (6, 138).

MDR-TB and extensively drug-resistant TB (XDR-TB), resistant phenotypes, are acquired by a sequence of cumulative mutations in the genes involved in individual drug resistance (140). MDR-TB is defined as TB caused by strains of *Mycobacterium tuberculosis* that are resistant to at least isoniazid and rifampicin, the backbone of any successful TB treatment programme. In the other hand, XDR-TB is a form of TB caused by bacteria that are resistant to isoniazid and rifampicin (i.e. MDR-TB) as well as to any of the second-line drugs, namely aminoglycosides, and fluoroquinolones (73). Recently, a high level of challenge in TB management has been appeared by the emergence of totally-drug-resistant tuberculosis (TDR-TB) or

very extensively-drug-resistant tuberculosis (XXDR-TB). This type of TB resistant strain, reported in Italy and Iran, is resistant to all first- and second-line drugs (141, 142).

The highest proportions of MDR-TB ever documented in a subnational area where MDR-TB has reached 0.5 million cases per year and in some countries accounts for up to 28% of new TB cases (Figure 1.12). XDR-TB was found in 5.4% of MDR-TB cases and eight countries reported XDR-TB in more than 10% of MDR-TB cases (5). A map showing the worldwide distribution of XDR-TB cases is displayed in Figure (1.13) where large parts of Africa do not have reported XDR-TB cases as result of laboratory limitations in diagnosis (WHO 2010).

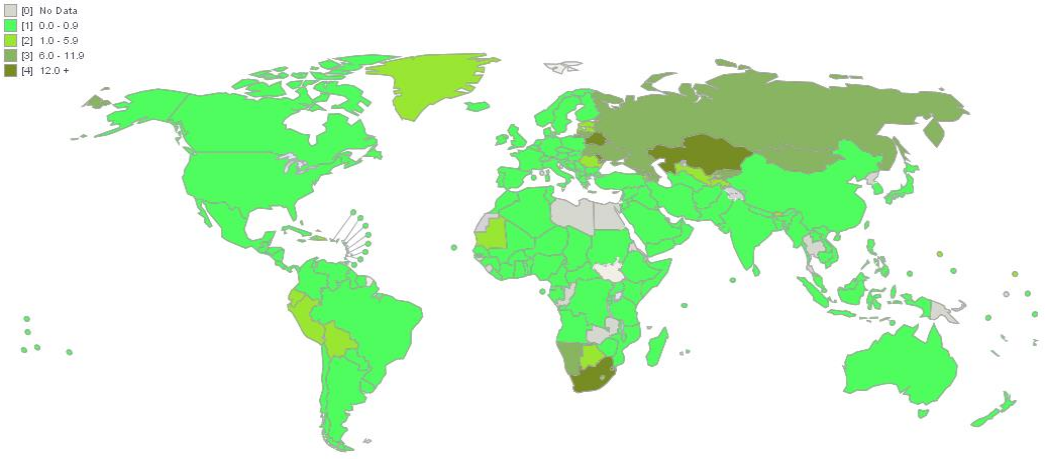

Figure 1.12: Distribution of Notified MDR-TB (population rate per 100,000) – 2010 (143)

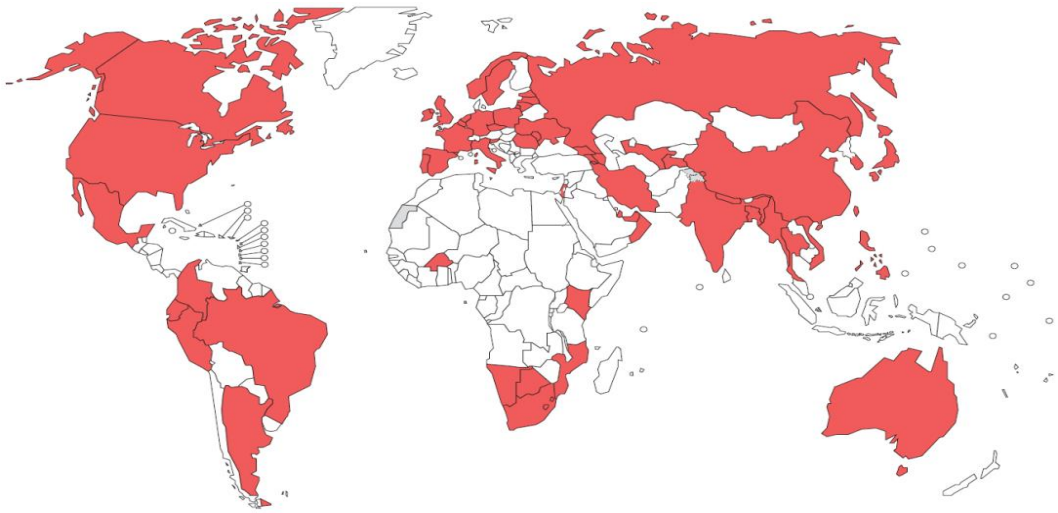

Figure 1.13: Worldwide distribution of countries reporting at least one case of XDR-TB (in red), according to WHO report, 2010 (144).

Patients with MDR TB can be cured with appropriate management based on second-line TB drugs although they are inherently more toxic and less effective than first-line drugs. Therefore, a reliable assessment of drug resistance (drug susceptibility testing, DST) is an essential prerequisite to support clinical decision making and helps to prevent the emergence of further drug resistance in patients with MDR TB. This strategy is called the DOTS-Plus strategy (145, 146) or individualized regimen. A regimen of at least four drugs should be implemented: injectable anti-tuberculosis drugs, kanamycin, amikacin or capreomycin, a fluoroquinolone, an oral bacteriostatic second-line drug and pyrazinamide. The duration of the MDR-TB treatment can last from 8 to 20 months, which could be modified according to the patient's response to therapy, with increased risks of adverse reactions after 12 months. However, this individualized regimen is difficult to apply in low income areas and thus a standardized approach has the advantages of making it easier to estimate drug needs and to train personnel in the treatment of MDR-TB patients.

The standardized approach should include at least pyrazinamide, a fluoroquinolone, a parenteral agent, ethionamide (or prothionamide), and either cycloserine or p-aminosalicylic acid (PAS) if cycloserine cannot be used. Unfortunately the current recommendations do not necessarily apply to XDR-TB patients as there is lack of evidence for the best drug regimens for treating these patients. XDR-TB patients can be cured although the probability of success with the current drugs available is much lower than in patients with ordinary TB or even MDR-TB. Effective treatment of XDR-TB depends on the speed and the accuracy of the diagnosis as well as on a good selection of the second-line drugs that are available to clinicians (147). A summary of the mechanisms of resistance involved with each of the first- and second-line drugs is displayed in Table (1.1).

Table 1.1: Summary of drugs currently used against TB and their mechanisms of resistance (67, 138, 140).

	Drug	Effect on	Mechanism of action	Target	Mutations associated with resistance
First-line Agents	**Isoniazid**	Replicating bacilli	Inhibits mycolic acid synthesis	InhA, KasA and AcpM	*katG* (Catalase-peroxidase) *inhA* (Enoyl ACP reductase)
	Rifampicin	Replicating and dormant bacilli	Inhibits RNA synthesis	RNA polymerase β-subunit	*rpoB* **(**β-subunit of RNA polymerase)
	Ethambutol	Replicating bacilli	Inhibits arabinogalactan synthesis	EmbB and EmbC	EmbB and EmbC **(**Arabinosyl transferase)
	Pyrazinamide	Dormant bacilli	Depletes membrane energy	Unknown (possibly inhibits FAS-I or alters membrane energetics)	*pncA* **(**Nicotinamidase/pyrazinamidase)
	Streptomycin	Replicating bacilli	Inhibits protein synthesis	A site of 16S rRNA in the 30S ribosomal subunit	*rpsL* (S12 ribosomal protein) *rrs* (16S rRNA)
Bacteriocidal second-line drugs	**Amikacin/Kanamycin**	Replicating bacilli	Inhibits protein synthesis	Ribosomes	*rrs* (16S rRNA)
	Capreomycin	No conclusive data	Inhibits protein synthesis	Methylated nucleotides in ribosomal subunits	*tlyA* (2'-O-methyltransferase) *rrs* (16S rRNA)
	Fluoroquinolones	No conclusive data	Inhibit DNA gyrase	DNA gyrase	*gyrA-gyrB* **(**DNA gyrase subunit A/B)
Bacteriostatic second-line drugs	**Ethionamide**	Replicating bacilli	Inhibits mycolic acid synthesis	InhA	*ethA* (Flavin monooxygenase) *inhA* (Enoyl ACP reductase)
	Para-aminosalicylic acid	No conclusive data	Inhibits folate metabolism	Possibly Dihydropteroate synthase	*inhA* (Enoyl ACP reductase) *thyA* (Thymidylate synthase)
	Cycloserine	No conclusive data	Inhibits peptidoglycan synthesis	Alanine racemase D-alanine-D-alanine ligase	*alr* (Alanine racemase) *ddl* (D-alanyl-alanine synthetase A)

1.5. *Mycobacterium tuberculosis* and a vision for the future

1.5.1. The Genomic era in the study of Mtb

The publication of the complete annotated genome of the Mtb laboratory strain H37Rv in 1998 was the beginning of the genomic era of Mtb (148). Since then, the Mtb clinical strain CDC1551 and six related mycobacteria, *M. leprae*, *M. ulcerans*, *M. avium*, *M. avium paratuberculosis*, *M. smegmatis*, and *M. bovis* have been fully sequenced (149). The annotation of Mtb genomes is an on-going process where more information is being added constantly to the annotation platform.

Sequencing the Mtb genome is considered an important milestone in modern history of TB study. Currently, the complete genome of Mtb H37Rv is available in NCBI. This culminates in a composite sequence of 4,411,532 base pairs (bp), with a G + C content of 65.6% (http://www.ncbi.nlm.nih.gov/genome/166). This G + C rich genome is a characteristic of Gram positive Actinobacteria and confers high stability of the DNA. The Mtb genome represents the second-largest bacterial genome sequence currently available after that of *Escherichia coli* (*E. coli*) (150) with 90% of a total 4047 genes identified as functional of which 3988 are protein coding genes (148, 151, 152). Another striking feature of the Mtb genome is the abundance of genes coding for enzymes involved in fatty acid metabolism (more than 250 genes) compared with only 50 genes in *E. coli* (148). Mtb also has the amazing potential to produce over 100 enzymes implicated in the β-oxidation of fatty acids and it contains both the FAS I and FAS II fatty acid synthase systems (153).

Regarding the post-genomic era, relating the annotated genome sequence to the physiological functions of a cell is considered the main goal of this era. Therefore, comparative and functional genomics has advanced since the publication of the complete genome sequence, notably through the study of the transcriptome, the proteome and the biogenesis of Mtb. The full transcriptome of Mtb has been studied using different TB experimental models, activated and naive mice macrophages (154-156). Moreover, Cappelli *et al* (2006) were the first to describe Mtb gene expression in human macrophages (157) while Rachman *et al* (2006) conducted the study on human lung tissue (surgical specimens) directly (158). Application of comparative proteomic analysis explored the critical proteins involved in Mtb

pathogenicity (159). Metabolomic-based methods offer integrated readouts of the genome and the proteome on a physiologically global scale. Specifically, metabolomics is the study of metabolite profiles, the end products of biological cell or organism processes. This approach provides the benefit of identifying and analysing metabolites in response to various physiological conditions (160, 161), for instance, studying a drug's effect upon the metabolitc level, a topic that will be discussed later (Chapter V).

Studying gene essentiality in bacteria employs familiar genome-scale methods, which are a microarray hybridization or conventional sequencing. These methods allowed mapping the sites of transposon insertions in large libraries of random mutants and identifying the regions of the genome that were unable to sustain mutation, which probably indicate the essentiality of these genes for the survival of the organism (116, 162-165). However, these methods suffer from significant drawbacks, resulting in uncertainty of an essential region location. Griffin *et al* (2011) used highly parallel Illumina sequencing to characterize transposon libraries achieving a precise identification of essential open reading frames (2). Recently, Zhang *et al* (2012) coupled high-density mutagenesis with deep sequencing and found a high level of agreement with Mtb essential genes data that were reported by Griffin *et al* (2011) (2, 166).

1.5.2. *Mycobacterium tuberculosis* metabolism

The metabolic machinery of any bacteria is made up of two tightly linked biochemical networks: the carbon metabolic pathways (carbohydrates, fatty acids and amino acids metabolism), the tricarboxylic acid (TCA) cycle and the membrane-embedded electron transport chain (ETC). The carbon metabolism provides the respiratory chain with electrons (mostly as NADH and reduced flavin adenine dinucleotide ($FADH_2$)). The ETC components allow the cell flexibility in the H^+/e^- ratio (the number of protons delivered to the periplasmic side of the membrane per electron) and rapid responsiveness in the rate of ATP synthesis in response to O_2 and carbon availability (167, 168).

Adaptation of Mtb to the host environment is a defining feature of its pathogenicity. The key of this adaptation is the metabolic reprogramming of Mtb during acute and

chronic (latent) phases of TB disease. However, biochemical knowledge of Mtb metabolic networks remains scarce.

1.5.2.1. Carbohydrate, TCA cycle

During aerobic *in vitro* growth of Mtb, various carbon sources feed into central carbon metabolic (CCM) pathways such as D-glucose (dextrose), glycerol and acetate, where each carbon source is widely catabolized into intermediates of glycolysis/gluconeogenesis, the pentose phosphate pathway (PPP) and the TCA cycle (160, 168). de Carvalho *et al* (2010) concluded that Mtb did not exhibit diauxic growth (consuming individual carbon substrates in a preferred sequence) but Mtb can catabolize multiple carbon sources simultaneously, leading to enhanced monophasic growth. For instance, while co-catabolizing glucose and glycerol, Mtb preferentially metabolized glucose into intermediates of glycolysis and PPP, and glycerol for TCA cycle intermediates. However, concurrently, Mtb also incorporated low levels of glycerol into glycolytic/gluconeogenic and pentose phosphate intermediates (160). In the absence of exogenous sugars, glycolytic intermediates are precursors for biosynthetic pathways as well which are generated by gluconeogenesis (154).

The TCA cycle is the major energy-generating pathway in aerobic organisms as it plays essential roles in cell metabolism, providing reduced equivalents for energy generation and biosynthetic reactions as well as yielding precursors for lipids, amino acids and heme synthesis. Mtb is considered an aerobic-to-facultative anaerobe bacillus and has functional genes coding for all enzymes of the standard TCA cycle regardless of its ability to survive for long periods in a hypoxic environment (33, 148). In fact, it is intriguing that the TCA cycle in Mtb is unusual in that α-ketoglutarate dehydrogenase (KDH) is replaced by α-ketoglutarate decarboxylase (KGD), which is absent in mammalian cells, and a succinic semialdehyde dehydrogenase (169, 170). In the γ-Aminobutyric acid (GABA) shunt, an alternative pathway from α-ketoglutarate to succinate via succinic semialdehyde (SSA) was proposed which replaces the succinyl-CoA in Mtb TCA cycle (169). Although this pathway supports growth on carbohydrates when the glyoxylate shunt is inoperable, Mtb still requires production of succinyl-CoA by an alternate enzyme, anaerobic-like

α-ketoglutarate:ferredoxin oxidoreductase (KOR) (171). Importantly, the presence of a functional glyoxylate shunt and KOR could bypass the requirement for KDH activity. These observations show that, unlike most organisms, Mtb employes two different pathways from α-ketoglutarate, one that functions simultaneously with β-oxidation, KOR-dependent, and one that functions in the absence of β-oxidation, KGD-dependent (171, 172).

1.5.2.2. Fatty acids metabolism, Glyoxylate shunt

During infection, Mtb switches its carbon sources of glycerol and glucose to fatty acids, where upregulation of Mtb genes involved in fatty acid catabolism has been observed *in vivo* from the lungs of mice and humans (173-175). A transcriptional profiling study of Mtb recovered from macrophages *in vitro* showed induction of genes involved in the β-oxidation of fatty acids upon converting the microbe from aerobic to anaerobic respiration (154). Mtb possesses more than 250 enzymes involved in lipid metabolism, which includes enzymes for lipid biosynthesis as well as degradation, where host cell lipids degradation is crucial for the intracellular life of the organism (148, 176).

Two pathways are required for fatty acid utilization by bacteria: the β-oxidation cycle and the glyoxylate shunt. The β-oxidation cycle is the dominant route for oxidative degradation of fatty acids in bacteria and eukaryotes, yielding acetyl-CoA and propionyl-CoA. Acetyl-CoA molecules are generated from the β-oxidation of both odd- and even-chain-length fatty acids, while propionyl-CoA comes from odd-chain-length fatty acids degradation, and can also be generated by catabolism of cholesterol, methyl-branched fatty acids and branched-chain amino acids (168, 177, 178).

The importance of the glyoxylate shunt, which has no mammalian counterpart, was demonstrated by McKinney *et al* (2000), who showed that the persistence of Mtb in macrophages and mice requires the glyoxylate shunt enzymes, isocitrate lyases (ICL 1 and 2) (172). Similarly, it has been proposed that glyoxylate cycle enzymes are activated during adaptation to the low oxygen environment of the granuloma. Upon using fatty acids as the principal carbon source, replenishment of TCA cycle

intermediates (anaplerosis) occurs via the glyoxylate cycle that converts acetyl-CoA into oxaloacetate. In the glyoxylate shunt, ICL 1 and 2 catalyse the cleavage of isocitrate into glyoxylate and succinate while malate synthase (MLS) mediates the condensation of glyoxylate and acetyl-CoA into malate (168, 175). Isocitrate lyases (ICLs) play two main roles during infection, bypassing carbon loss under limited nutrient availability by using the glyoxylate shunt and preventing accumulation of toxic propionyl-CoA (16). ICLs are jointly required for fatty acid catabolism, *in vivo* growth in the macrophage and mice, and for virulence in Mtb, as mutant bacteria lacking icl1 and icl2 cannot grow in mice and are rapidly eliminated (179). Beste *et al* (2011) demonstrated a role for ICLs and the glyoxylate shunt during slow growth rate of Mtb on glycerol suggesting that they operate under more general conditions (180).

The methylcitrate cycle in Mtb is operational with ICL 1 and 2 serving dual roles as ICLs in the glyoxylate shunt and as a 2-methylisocitrate lyase (MCL) in the methylcitrate cycle (175, 181). Propionyl-CoA is assimilated via the methylcitrate cycle which oxidizes propionyl-CoA to pyruvate (182). Mtb uses the methylmalonyl-CoA pathway to metabolize propionyl-CoA for cell wall synthesis (175). Moreover, ICLs control propionate levels when the bacterium uses specific carbon sources, such as cholesterol, fulfilling a detoxification function (177, 183). Pandey and Sassetti (2008) showed that Mtb utilizes cholesterol, a major component of host cell membranes, during Mtb persistance in the lungs of chronically infected animals as well as during the growth of Mtb within IFN-γ-activated macrophages that predominate at this stage of infection (183). During cholesterol catabolism metabolic modification is centered on propionyl-CoA and pyruvate pools that necessitate the stimulation of the propionyl-CoA-assimilating methylcitrate cycle (MCC) enzymes (184). It is becoming apparent that fatty acid metabolism is pivotal during infection and that the glyoxylate shunt could be a good target for drug development. However, the possibility of a parallel uptake of additional carbon sources such as sugars, fatty acids and amino acids from the human host during infection cannot be excluded, as been observed in cholesterol uptake mutants that grow normally in resting macrophages of infected mice (183, 184).

Although it has been suggested that mycobacteria *in vivo*-growth is lipolytic rather than lipogenic, fatty acid biosynthesis still plays an important role (148). Mycolic acids, representing essential components of the mycobacterial cell wall, are very long-chain β-hydroxy fatty acids with a long α-alkyl side chain (185). The biosynthetic pathway of mycolates involves two types of fatty acid-synthesizing systems, FAS-I and FAS-II (148). The multifunctional FAS-I polypeptide contains all the functional domains required for *de novo* fatty acid synthesis (186). Mycobacterial FAS-II elongates acyl-CoA primers generated by FAS-I to a mixture of homologous fatty acids of longer chain lengths (meromycolic acids) (187).

Redox couples in Mtb are NAD^+/NADH, $NADP^+$/NADPH and FAD/$FADH_2$, all of which are vital for both anabolic and catabolic reactions. NAD^+, an efficient electron sink, is used as a cofactor in several oxidising reactions. A constant level of NADH is maintained during various phases of growth *in vitro*, while the concentration of NAD^+, a major contributor to a change in NADH/NAD^+ ratio, is variable. A higher ratio of Mtb NADH/NAD^+ is generated during the transition from aerobic to anaerobic growth phase (188, 189). β-oxidation of fatty acids consumes NAD^+ and FADH in every cycle of fatty acid oxidation, therefore type II NADH dehydrogenase (NDH-2) induction signals the need of NAD^+ regeneration to maintain the NAD^+ pool (154). Concurrently, the β-oxidation of fatty acids yields one NADH and one $FADH_2$ molecule for every acetyl-CoA generated. Consequently, NADH and $FADH_2$ channel the electrons to the ETC, which consecutively oxidises and reduces multiple redox centres before generating ATP (188).

1.5.2.3. Amino acids metabolism

The existing knowledge about amino acid metabolism in mycobacteria is limited. Generally, L-asparagine is the preferred source of nitrogen for the growth of mycobacteria but can be replaced by L-alanine, L-glutamine or L-glutamic acid. In glycerol-enriched media, glutamate becomes the preferred source of nitrogen (190). One of the most important precursors for gluconeogenesis are free amino acids which might increase when amino acids are not utilized for protein anabolism but are oxidized by impairment of protein synthesis (191). The Mtb genome revealed a statistically significant preference for the amino acids alanine, glycine, proline,

arginine and tryptophan all of which are encoded by G + C rich codons, and a comparative reduction in the use of asparagine, isoleucine, lysine, phenylalanine and tyrosine amino acids, encoded by A + T rich codons (148).

During infection, due to the high demand for amino acids as substrates for energy production, many amino acids significantly increased in the lung, spleen, liver, and serum of Mtb-infected mice. Moreover, Shin *et al* (2011) found that intermediates of pyrimidine metabolism, uracil, uridine, and UDP-glucose, and intermediates of purine metabolism ATP, AMP, inosine, allantoin, and xanthine were high in Mtb-infected mice (191).

Central carbon metabolic pathways of Mtb are depicted in the following Figure (1.14), including the major catabolic intermediates and amino acids. Importantly, these metabolic pathways are found to be critical for the virulence of Mtb during infection.

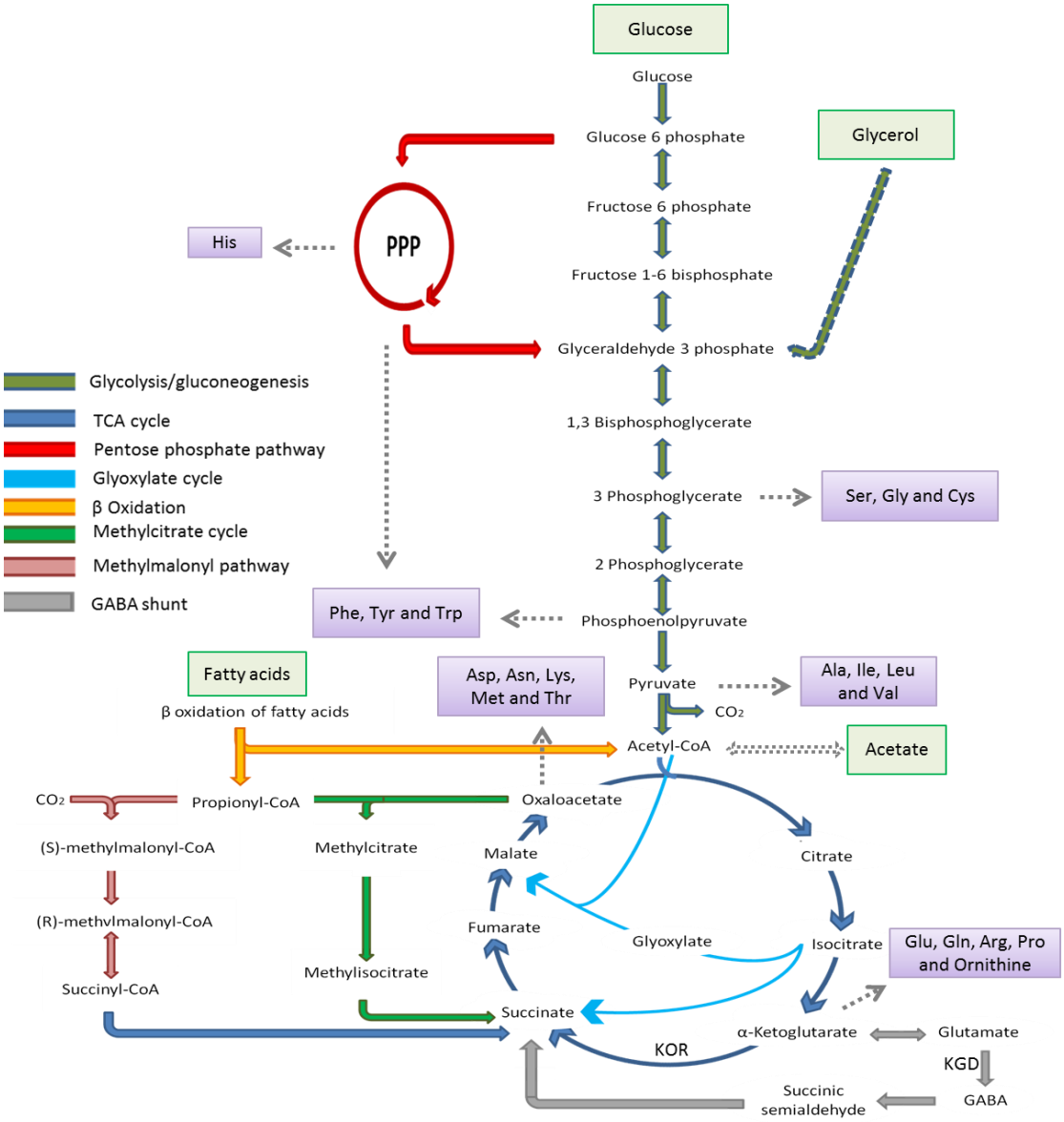

Figure 1.14: Central metabolic pathways of *Mycobacterium tuberculosis* (192-194)

Central carbon metabolic pathways depicting a bioinformatic inventory of Mtb's CCM pathways, inculding the anabolic monomers (amino acids; purple boxes) and the major catabolic intermediates from which they derive (dashed grey arrows) are shown. Major carbon substrates are shown in green boxes. The CCM pathways are colour-coded as present in the key panel. KOR, α-ketoglutarate:ferredoxin oxidoreductase and KGD, α-ketoglutarate decarboxylase. His, Histidine; Arg, Arginine; Asn, Asparagine; Asp, Aspartic acid; Ala, Alanine; Cys, Cysteine; Gln, Glutamine; Glu, Glutamic acid; Gly, Glycine; Ile, Isoleucine; Leu, Leucine; Lys, Lysine; Pro, Proline; Ser, Serine; Thr, Threonine; Trp, Tryptophan; Tyr, Tyrosine; Val, Valine; Phe, Phenaylalanine; Met, Methionine.

1.5.3. Electron transport and respiration in *Mycobacterium tuberculosis*

The importance of the flexibility, conferred by a modular respiratory system, in the survival of Mtb has led to the targeting of the ETC components in the context of developing new anti-TB drugs.

Mtb oxidizes a variety of electron donors including succinate, NADH, lactate, malate, proline and glycerol using different aerobic, microaerophilic and anaerobic respiratory systems. Consequently, the generated electrons are transported to any terminal electron acceptors that include oxygen, nitrate, nitrite and fumarate. ETC contains electron carriers in heme molecules, copper atoms or flavin prosthetic groups forms. Generally, dehydrogenases transfer electrons from cytoplasmic electron donors into the quinone pool, in the centre of the ETC, resulting in reducing menaquinone to menaquinol. Subsequently, the menaquinol is oxidized back to menaquinone by the cytochrome bc_1 complex. Successively, bc_1 complex passes electrons to a terminal oxidase, cytochrome *bd*-I oxidase. In anaerobic respiration, terminal reductases comprising nitrate reductases and fumarate reductase replace the terminal oxidase. Finally, electrons are transferred to the terminal electron acceptor. A proton motive force (PMF) forms as a result of simultaneous action between electron migration across the chain and proton passage from the cytoplasmic side into the periplasmic side of the membrane. Production of ATP is a result of gradient dissipation by movement of the protons through a membrane-associated ATP synthase back into the cytoplasm (195). The composition of the respiratory system of Mtb is shown in Figure (1.16). The biochemical properties and physiological roles of the specific respiratory system components of Mtb are described in more detail.

1.5.3.1. Electron donors

NADH:menaquinone oxidoreductases, also known as NADH dehydrogenases (NDH), are one of the main electron donors of the Mtb respiratory system. NDH play an essential role in transferring electrons from NADH to the quinone pool and in NAD^+ recycling. Mtb has three different NDH: a type I NDH (NDH-1) and two type II NDH (NDH-2 and NDH-2A). The redox activity in NDH-1 is coupled to proton translocation while in NDH-2 and NDH-2A is not. NDH-2 and NDH-2A are

single-subunit dehydrogenases that catalyse electron transferring from NAD(P)H to the quinone pool without proton translocation across the membrane (195). Studies have suggested that NDH-1 and NDH-2A are dispensable for Mtb growth *in vitro*, while NDH-2 is required for optimal Mtb growth *in vitro* (116). Further, NDH-2A was shown to have no role in the virulence of Mtb in SCID mice (2, 196). Weinstein *et al* (2005) found that the classic inhibitors of NDH-1 (rotenone, piericidin A, and pyridaben) did not inhibit overall oxidoreductase activity (197). Thus, NDH-2 is suggested to function as the main NDH of the Mtb respiratory chain (198).

Succinate dehydrogenase (SDH) is known as complex II of the ETC and catalyses the oxidation of succinate to fumarate and the reduction of the quinone. SDH is an essential part of the TCA cycle and has a role in aerobic respiration (195, 199, 200). The Mtb respiratory chain has other dehydrogenases, L-lactate (LDH), Glycerol-3-phosphate (G3PDH), malate (MDH) and proline dehydrogenase (PDH), for oxidizing the other electron donors but without identified function (195).

1.5.3.2. Quinones in *Mycobacterium tuberculosis*

Quinones are lipid-soluble molecules that have a critical role in the ETC as a reversible redox component, carrying electrons between electron donors and acceptors (201). In bacteria, quinones present in different forms, which are ubiquinone, menaquinone, and/or demethylmenaquinones, of which menaquinone is known as the sole quinone in Gram-positive bacteria (Figure 1.15). Mycobacteria have only menaquinone according to the genomic data of Mtb (148). The variant of menaquinone in Mtb contains nine isoprene units (MQ-9) (202). MQ-9 synthesized by a series of enzymes encoded by *menABCDEH* (203). Menaquinone has a lower redox potential than ubiquinone that confers less tendency to accept electrons and being reduced (195). The quinone structure consists of a hydrophobic isoprenoid unit rendering quinone soluble in the interior of the membranes (204).

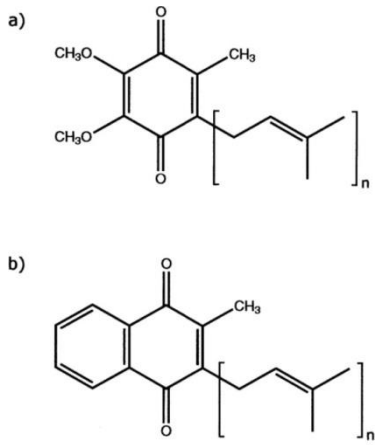

Figure 1.15: Structures of (a) Ubiquinone and (b) Menaquinone

1.5.3.3. Electron Acceptors

The cytochrome bc_1 reductase-cytochrome *c* oxidase super-complex comprises cytochrome bc_1 reductase (bc_1 complex) which catalyzes the oxidation of menaquinol (MQH_2) and the aa_3-type cytochrome *c* oxidase (CcO). Electrons from the bc_1 complex are passed through an iron-sulphur cluster and cytochrome *c* to the Cu_A atom in the CcO where the reduction of O_2 to water takes place. This catalysis is coupled with proton translocation across the membrane, resulting in greater energy conversion (195).

Cytochrome *bd*-I oxidase is a terminal oxidase that oxidizes menaquinol and reduces O_2 to water (195). Cytochrome *bd*-I oxidase has the ability to generate a PMF by trans-membrane charge separation, unlike heme-copper terminal oxidases, with a "proton pump" mechanism (205). Generation of PMF by trans-membrane charge separation is conducted by virtue of the fact that protons resulting from the oxidation of ubiquinol are released into the positive (periplasmic) side of the membrane, while the protons used to convert O_2 to H_2O are taken from the negative (cytoplasmic) side (205, 206).

Amongst the mycobacteria, Mtb is the most competent reducer of nitrate, containing two homologues of nitrate reductases (NRs) encoded by *narGHJI* and *narX*. NR catalyses the reduction of nitrate to nitrite, granting Mtb with the ability to persist

under O_2 depletion (anaerobic condition) and/or nitrate abundance conditions (195, 207).

Fumarate reductase (FRD) is more efficient at catalyzing the reduction of fumarate to succinate and the oxidation of quinol (QH_2), the reverse reaction of SDH. FRD accepts electrons from QH_2 and acts as terminal electron acceptor under anaerobic conditions. FRD is suggested to be involved in the mechanism of Mtb persistence (195, 199, 200).

In Mtb there are genes that encode a cytoplasmic NirBD nitrite reductase and sulphite/nitrite reductase, NirA. Through the action of anaerobic nitrite reductases, the nitrite resulting from degradation of reactive nitrogen intermediates or nitrate respiration can be reduced to ammonia (195).

F_0F_1 ATP synthase, encoded by the *atpBEFHAGDC* operon, is a multisubunit complex consisting of a membrane-embedded proton-pumping F_0 part and a cytoplasmic, catalytic and non-catalytic nucleotide binding domain, F_1. During aerobic respiration, the enzyme is responsible for the production of ATP by oxidative phosphorylation whereas in anaerobic respiration, it works as ATPase, pumping protons through the membrane. The F_0F_1 ATP synthase can utilize the PMF across the bacterial cytoplasmic membrane for the synthesis of ATP (195, 208).

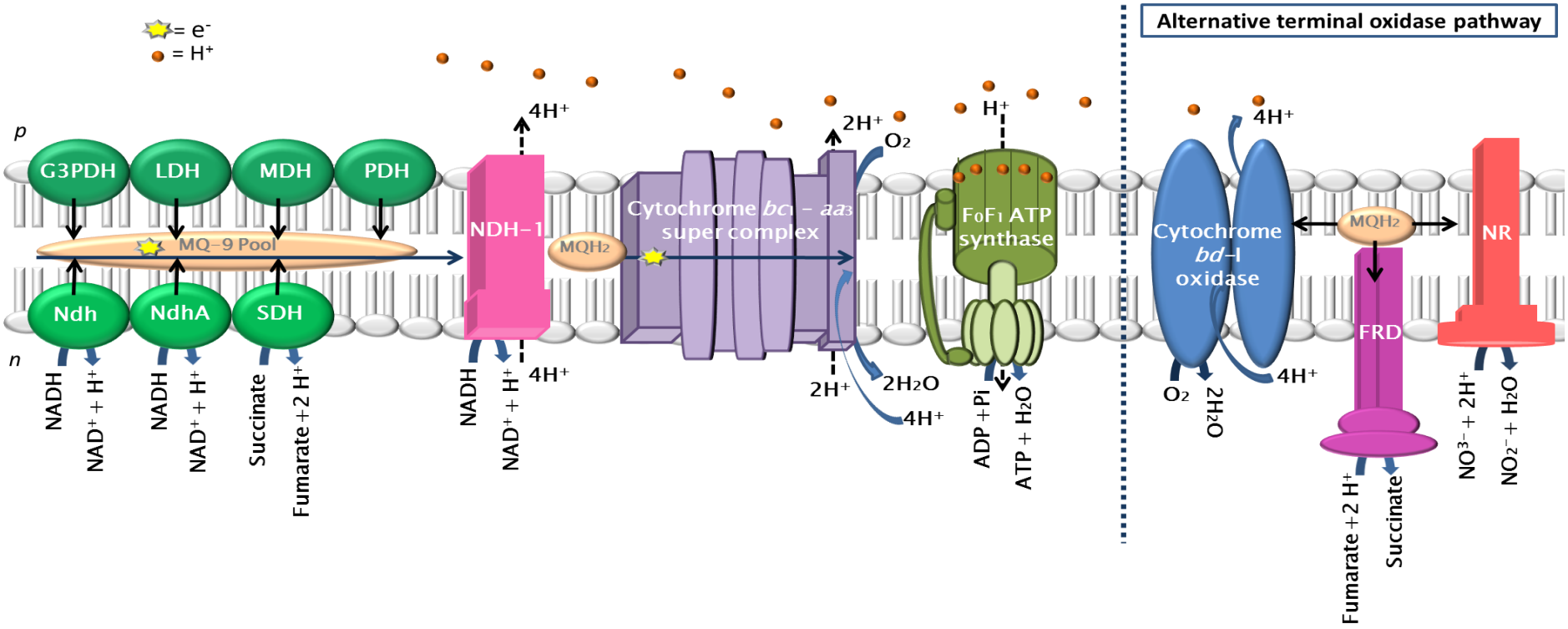

Figure 1.16: Components of the electron transport chain in *Mycobacterium tuberculosis* (209)

The chain electron donor components are Ndh/NdhA-type II NADH: (mena)quinone oxidoreductase (two isoforms), SDH-succinate dehydrogenase, G3PDH-glycerol-3-phosphate dehydrogenase, LDH-L-lactate dehydrogenase, MDH-malate dehydrogenase, PDH-proline dehydrogenase and nuo-type I NADH (complex I). Electron acceptors are cytochrome bc_1-aa_3 super complex-the cytochrome bc_1 reductase-cytochrome *c* oxidase super-complex and an alternative terminal oxidase pathway which comprises cytochrome *bd* oxidase (quinol oxidase), FRD-fumarate reductase and NR-nitrate reductase. Chain components also include F_0F_1 ATP synthase (complex V), MK-9-menaquinone-9 and MKH_2-menaquinol. *P* and *n* correspond to the positive and negative sides of the respiratory membrane with respect to proton translocation. Proton movements are indicative only and do not represent H^+/e^- ratios for the respective complexes. The orientation and topology of the subunits are indicative only.

1.5.4. Cytochrome *bd*-I oxidase

1.5.4.1. Definition

Cytochrome *bd*-I oxidase is a respiratory quinol: O_2 oxidoreductase found in many prokaryotes, including strictly anaerobic bacteria such as *Desulfovibrio vulgaris Hildenborough* (DvH) (210). Respiratory oxygen terminal oxidases are a class of enzymes at the end of the respiratory chain of organisms that couple the oxidation of a respiratory substrate, cytochrome *c* or QH_2, to the reduction of O_2 to water. This type of reaction leads to the bioenergetic function of cytochrome *bd*-I oxidase through the production of a PMF by a vectorial charge transfer of protons (211).

1.5.4.2. Subclasses

Oxygen reductases (terminal oxidases) are classified into three distinct families which are the heme-copper family, the alternative oxidase (AOX) family and the cytochrome *bd* family. The cytochrome *bd* family are quinol oxidases with no homology to any subunit of the heme-copper family or the AOX family. The cytochrome *bd* family does not have copper or non-heme iron (53, 211-214). Moreover, based on structural and spectroscopic observations, the cytochrome *bd* family is sub-classified into the A-subfamily (long Q-loop), B-subfamily (short Q-loop) and the cyanide insensitive oxygen reductases (CIO) (211). The Q-loop is a hydrophilic domain of subunit I of cytochrome *bd*-I oxidase and has been implicated as part of the quinol binding site. The long Q-loop *bd*-family members have an insert in the C-terminal portion of the Q-loop, while the short Q-loop *bd*-members do not have this insert (211, 215). At the gene sequence level, CIO has no differentiating characteristic that could distinguish CIO from other members of cytochrome *bd* family. However, CIO has been characterized by low heme *d* content and resistance to cyanide (211, 216).

Interestingly, although many aerobic prokaryotes do not contain any member of the *bd* family, some prokaryotes have more than one *bd* family member, for instance, two: *E. coli* (217, 218); three: *Vibrio cholerae* (219); and as many as six *bd*-type oxidoreductase: some *Acidithiobacillus* strains (211). In Mtb, there is only one *bd*

family member, the *cydAB*-encoded cytochrome *bd*-I oxidase (148) that serves as an alternative terminal oxidase pathway under oxygen-limited conditions (195, 209).

1.5.4.3. Physiological functions

The cellular bioenergetic function of cytochrome *bd*-I is the production of a PMF via liberation of protons upon quinol oxidation (218, 220). Cytochrome *bd*-I grants bacteria with a number of vital physiological functions. Cytochrome *bd*-I permits colonization of O_2-poor environments (221, 222), by working as an O_2 scavenger in order to prevent degradation of O_2-sensitive enzymes such as nitrogenase (223). This enzyme was found to support anaerobic photosynthetic growth as well (224). Moreover, it is of interest to note the positive correlation between the level of cytochrome *bd*-I expression and microbial pathogen virulence which was observed in tuberculosis, pneumonia, life-threatening sepsis and meningitis (211, 221, 225). Further physiological functions of cytochrome *bd*-I oxidase are in improving bacterial tolerance to nitrosative stress (211, 226, 227), contributing in detoxification of hydrogen peroxide in *E. coli* (228), suppressing extracellular superoxide production in *Enterococcus faecalis* (229), and involvement in the degradation of aromatic compounds in *Geobacter metallireducens* (230). Under conditions of nitric oxide (NO) stress, cytochrome *bd*-I was overexpressed, granting nitric oxide resistance to *E. coli* (231). It has been suggested that Mtb cytochrome *bd*-I oxidase may thus serve to maintain an energized membrane during the persistent stages of infection, NRP stage 1 and 2 (20), and forms a part of the Mtb defence system against immune-mediated oxidative damage (232). Shi *et al* (2008) wrote that cytochrome *bd*-I oxidase is a potential enzyme candidate that may defend against reactive oxygen and nitrogen species (ROS and RNS) produced by the host adaptive immunity during tuberculosis infection (233).

1.5.4.4. Cytochrome *bd* expression conditions

There are many stressful conditions that influence the expression of cytochrome *bd* family in *E. coli*. For instance, low O_2 tension (234), alkalinization of the medium (235), high temperature (236), the presence of poisons in the environment (for

example, cyanide) (237), uncouplers-protonophores (235, 238) and high hydrostatic pressure, observed in *Shewanella violacea DSS*12 (239). In Mtb, a high level of cytochrome *bd*-I expression was recorded during NRP stages 1 and 2 growth conditions, categorized by low O_2 tension and metabolic slowdown (20). In *M. smegmatis*, although the threshold pO_2 for *cyd* induction is at 1% air saturation, cyanide induces *cydAB* gene expression at 21% air saturation (Kana et al., 2001). Further, DNA microarray analyses showed an up-regulation of Mtb H37Rv *cydA* (2.7-fold) during Mg^{2+} starvation (240). *CydAB* gene expression in Mtb was up-regulated by inhibitors of CcO and during adaptation to hypoxia (241) which is probably a response to the disruption of the bc_1-aa_3 pathway (242). Similarly in *M. smegmatis*, up-regulation of cytochrome *bd*-I oxidase occurred in response to disruption of the bc_1-aa_3 respiratory pathway as well (242). However, Mtb *cydAB* gene expression showed no up-regulation during hydrogen peroxide (H_2O_2) or menadione treatment (241).

1.5.4.5. Genetics

1.5.4.5.1. Genes of *Mycobacterium tuberculosis* encoding the protein subunits and assembly factors of the cytochrome *bd*-I oxidase

The genes involved in the expression of the cytochrome *bd*-I oxidase are the *cydA* and *cydB* genes, encoding subunits I and II of the cytochrome *bd*-I oxidase, respectively. The *cydDC* genes, located immediately downstream of the *cydA* and *cydB* genes, encode an ABC-type transporter which is implicated in the assembly of functional *bd*-type oxidase (195, 232, 243-247) and in maintaining redox homeostasis in the periplasm (53, 248, 249).

1.5.4.5.2. Regulation of *cydAB* operon expression

Two global transcriptional regulators, Arc and Fnr control the expression of the *cydAB* operon (250). Arc is a two-component regulatory system, ArcA and ArcB, of which ArcA responds to the oxidation state of the quinone pool, sensed by ArcB (251). Under microaerophilic conditions (O_2 tension of 2-15% of air saturation), a

high level of phosphorylated ArcA activates the *cydAB* operon in *E. coli* (252). The Fnr regulator is active only during anaerobic growth and it serves as redox sensor. During the transition to anaerobic conditions (O_2 tension of less than 2% of air saturation), the active Fnr regulator inhibits cytochrome *bd*-I (250). However, the induction of *cyd* expression differs between organisms. For example, the threshold of O_2 tension for *cyd* induction in *M. smegmatis* (253) and Mtb (221) is suggested to be at 1% air saturation while in *E. coli* it is found to be at 10% air saturation (254).

1.5.4.6. Cofactors and substrates

The oxidation of quinols by cytochrome *bd*-I enzyme as an electron acceptor is species-specific. For example, in *E. coli* the cytochrome *bd*-I enzyme can oxidize both ubiquinol (UQH_2) and menaquinol (MQH_2) whereas in *B. stearothermophilus*, the substrate of cytochrome *bd*-I is MQH_2 and in *Azotobacter vinelandii* is UQH_2 (255, 256). MQH_2 is the substrate in Mtb as mentioned previously (195).

Cytochrome *bd*-I oxidase has a three-heme enzyme comprising two protoheme IX groups (hemes b_{558} and b_{595}) and a chlorin (heme *d*). The low-spin hexacoordinate heme b_{558} accepts electrons from a quinol (257) whereas the high-spin heme *d* is recognized as the O_2 binding site and it catalyses the reduction of O_2 to water. Construction of *cydA* and *cydB* mutants in *E. coli* located heme b_{558} on subunit I and hemes b_{595} and *d* on subunit II of cytochrome *bd* oxidase (258, 259). Using mutant strains defective in *cydB*, Green *et al* (1986) managed to express, purify and retain only heme b_{558} (*cydA*–encoded) (260). The location of heme b_{558} heme b_{595} and heme *d* is predicted to be near the periplasmic surface (215, 261). The α-band of the reduced heme *d* in the absolute absorption spectrum of *E. coli* cytochrome *bd*-I showed a peak at 628–632 nm. The α-bands of the reduced heme b_{558} and heme b_{595} at room temperature reveal maxima at 560–562 nm and at 594–595 nm respectively, in the difference absorption spectrum (262, 263).

1.5.4.7. Proposed catalytic mechanism

Cytochrome *bd*-I oxidases in *E. coli* are known to have a relatively high affinity for O_2 (K_m = 0.3 μM) and the ability to generate PMF by trans-membrane charge separation, unlike heme-copper terminal oxidases which operate with a "proton pump" mechanism (205, 213, 231). The electron transfer sequence in cytochrome *bd*-I is thought to be $QH_2 \rightarrow$ heme $b_{558} \rightarrow$ [heme $b_{595} \rightarrow$ heme d] $\rightarrow O_2$. This process will be explained in detail in Chapter (III).

1.5.4.8. Inhibitors of cytochrome *bd*-I

Quinol oxidase inhibitors are classified into two main groups: inhibitors that operate at the Q-binding site (Q-like compounds) and inhibitors that act at the O_2 binding/reducing site (heme ligands) such as cyanide, azide or nitrite. Importantly, inhibitors acting at the oxygen reduction site tend to be moderately weak (53, 211, 213). Therefore, investigations for specific inhibitors of the *bd*-I type oxygen reductases, which could be used in clinical practice, took place where aurachins C and D and their alkyl-substituted derivatives were found to be potent inhibitors against quinol oxidases (264). Gramicidin S (GS), a cationic cyclic decapeptide, was found to be a potent inhibitor against *E. coli bd*-I (IC_{50} 5.3 μM) as well. However, the membrane lipid bilayer was found to be the main target of GS rather than *bd*-I (265).

1.5.4.9. The importance of *bd*-I and latency

Tackling latent TB is a main goal in the new era of TB drug discovery, providing a promising approach for shortening the duration of current TB therapy, as seen for PZA (126), RIF (266), TMC207, a novel diarylquinoline (267) and MTZ (35). Latency is a condition that displays the ability of Mtb bacilli to adapt under any stress from the host immune system. The importance of cytochrome *bd*-I oxidase in dormant Mtb bacilli or in persister cells of Mtb during latency was proposed by different studies. Initially at the genome level, *cydAB*-encoded cytochrome *bd*-I oxidase was defined to be essential for Mtb survival (2). The critical role of the cytochrome *bd*-I oxidase was further defined in the context of Mtb bacilli adaptation to stress conditions. Transcriptional studies confirmed the significance of this

enzyme both *in vivo* and *in vitro* where the level of Mtb *bd*-I expression was higher under hypoxic conditions (20, 212, 221). Boshoff *et al* (2004) found that the *cydABDC* operon was up-regulated in response to the respiratory inhibitors such as the phenothiazines (e.g. thioridazine, TRZ), the CcO-specific inhibitors (cyanide and azide) and redox cycling agents (menadione and clofazimine). Moreover, the study found that isoniazid- and pyrazinamide-treated Mtb showed up-regulation of the *cydABDC* operon (241). Interestingly, the F_1-ATPase-defective *E. coli* and *Corynebacterium glutamicum* mutants were found to have specific up-regulation of less efficient PMF generation components, such as NDH-II and cytochrome *bd*-I, to avoid generating excess PMF (268, 269). This observation emphasises the importance of cytochrome *bd*-I during restricted conditions such as latency where ATP synthase was found to be down regulated. Importantly, single-gene mutation studies suggested that *cydDC*, encoding an ABC transporter and implicated in cytochrome *bd*-I assembly, might engage in Mtb persister formation or maintenance (24, 52).

1.5.5. Transcriptional changes in respiratory chain components of *Mycobacterium tuberculosis* among various growth models

The fact that there is a high degree of microenviromental diversity encountered by the tubercle bacillus during infection in humans originates from different extents of cavitary disease (Tuberculosis) within a single patient, and since within a lesion several immunological microenvironments exist to exert different effects on bacterial subpopulations (15, 20). As the science behind these microenvironments remains unknown, *in vitro* models have been developed to mimic the environments that are thought to be encountered by Mtb *in vivo*. Models in which the tubercle bacilli enter into a state of NRP include, but are not restricted to, carbon starvation (Loebel model) (270), O_2 depletion *in vitro* (Wayne model) (33) and the chronic stage of infection in mice (195).

Oxygen limitation is believed to be a crucial factor affecting the metabolism of Mtb during pathogenesis, since the granuloma would have such hypoxic environments (20, 25, 271). Numerous studies analysed the transcriptome of Mtb in a hypoxic model and suggested that the NRP state was associated with O_2 depletion and nitrate

reduction (221, 241, 271, 272). Bacon *et al* (2004) recorded a strong induction of the *narX* and *narK*2-encoded NR and nitrate/nitrite transporter respectively, during growing Mtb in a chemostat at 1% air saturation, signalling a shift to nitrate metabolism. In the Wayne model, a gradual O_2 depletion resulted in the initial establishment of the NRP-1 state (1% air saturation), followed by NRP-2 (0.06% air saturation), a state acknowledged by a widespread of metabolic cessation. Simultaneously, the following genes: *cydA, cydB, cydC,* and *cydD* were induced to 3.1-, 2.9-, 1.6- and 2.6-fold, respectively, while the expression level of the bc_1–aa_3 super complex remained unchanged (33, 34, 43, 221). Concomitant with these changes was the down-regulation of the intracellular ATP level of oxygen-starved bacilli (Wayne bacilli) by 5-fold compared to that of exponentially growing bacilli (273, 274).

The carbon starvation model, accompanied by O_2-limiting conditions resulted in down-regulation of 47% of aerobic respiration genes, among which were cytochrome *bd*-I oxidase, SDH and ATP synthase, and the up-regulation of genes encoding FRD and NR (195, 270). The hallmark of Mtb growth in resting bone-marrow-derived macrophages model was the reduction of aerobic respiratory components, NDH-1 and CcO, concurrently with the down-regulation of ATP synthase coding genes. These observation were indicative of low energy necessities during intracellular growth (154). Simultaneously, an induction of nitrate/nitrite transport, NR and FRD in activated macrophages were indicative of their availability as alternate electron acceptor in the intracellular environment of Mtb (275).

Regarding the transcriptional profiling of Mtb respiratory chain components using *in vivo* models, there are three distinct respiratory states defined during Mtb colonization of mouse lungs (murine model). The first respiratory state occurs during the acute phase and is characterized by a bioenergetically efficient state, as evidenced by up-regulation of genes encoding ATP synthase, NDH-1 and CcO subunits (221). The second respiratory state appears as result of NO production, a central component of the host immune response. This state is characterized by the down-regulation of bioenergetically efficient respiratory components and ATP synthase and concurrent up-regulation of microaerophilic respiration genes,

cytochrome *bd*-I oxidase and nitrate reduction and transport (221). Moreover, NO marks the appearance of the third respiratory state, characterized by the down-regulation of cytochrome *bd*-I oxidase and strong up-regulation of NRs (221). However, challenging Mtb with NO drove the organism to nitrate reduction and led to up-regulation of cytochrome *bd*-I oxidase and NDH-2 (195, 271, 276, 277).

The respiratory states of Mtb in human disease are not well characterized. Nonetheless, it is worth noting that some studies detected the expression of NR, together with FRD genes in the granulomatous region that is found in the pericavity and in the distal lung (158, 278).

1.6. Potential future anti-TB drugs

1.6.1. TB drugs global alliance

The current TB treatment regime has many challenges, which include complex dosing schedules, long treatment times, and growing rates of drug resistance. The Stop TB partnership set a goal for adequately controlling TB and to ultimately eradicate it by 2050, and for this to be a reality, new drugs, diagnostics and vaccines will be required (http://www.stoptb.org/). Generally, the Target Product Profiles of new TB drugs state that drugs need to be effective against resistant strains as well as able to treat latent infection, compatible with anti-retroviral therapy, suitable for paediatric populations and shorting and simplifing the duration of treatment (279).

1.6.2. Important drugs that target Mtb ETC

A new anti-tubercular drugs, targeting the ETC component of Mtb, is currently in clinical development and known as TMC207 (R207910, Bedaquiline). TMC207 is a novel diarylquinoline that demonstrates a potent anti-TB activity both *in vitro* and *in vivo* with the same target specificity on both replicating and dormant bacilli (280). TMC207 acts by specifically targeting the subunit *c*, encoded by the gene *atpE* of the F_1F_0-ATP synthase, causing a pronounced bactericidal effect (267). TMC207 is currently in Phase IIb clinical trials for the treatment of patients with MDR-TB (274, 281).

Phenothiazines are old drugs that re-emerged recently as potential anti-TB agents. Phenothiazines target the Mtb ETC through inhibiting type II NADH: menaquinone oxidoreductase. Warman *et al* (2012) showed that phenothiazine activity against Mtb NDH-2 is directly correlated to antitubercular activity against Mtb under both aerobic and anaerobic growth conditions. However, the potential and known toxicities of the phenothiazine class still exist. Therefore, phenothiazines could be used as potential templates on which to base future anti-TB drugs that overcome the current drawbacks (282).

1.6.3. Other future drugs candidates

Owing to the fact that each of anti-TB drugs has potential as a starting point for the discovery of a new clinical candidate, new chemical entities have progressed in clinical development based on chemical tailoring of existing drugs or drug classes. Two approved fluoroquinolones (moxifloxacin and gatifloxacin), DNA gyrase inhibitors, have shown promising results for treating resistant TB strains and shortening the duration of treatment. The parent scaffold of moxifloxacin and gatifloxacin is nalidixic acid and they are currently in phase III clinical trials where the efficacy of these drugs in replacing either INH or ethambutol in first-line therapy is being tested (138, 279, 283, 284). Furthermore, cell wall synthesis inhibitors, PA-824 and OPC-67683 (nitroimidazole family), with a remarkable antitubercular activity are in phase II clinical trials, and they are remodelling of Metronidazole. PNU-100480 is a protein synthesis inhibitor, developed from Linezolid (oxazolidinone family), and is in phase II clinical trials as well (279). Moreover, SQ109 (diamine derivative) is a new cell wall synthesis inhibitor, and targets a mycolic acid transporter (MmpL3). SQ109 is in Phase II clinical trials and shows synergistic effects with the antitubercular drugs isoniazid and rifampicin (138, 281, 285, 286).

1.7. Objectives

This thesis sets out to expand the current knowledge of the ETC of Mtb. Specifically, the thesis has focused on an important, but hitherto little studied component, the cytochrome *bd*-I quinol oxidase. A basic characterisation of this *bd*-I quinol oxidase has been undertaken as well as an initial study to determine its pharmacological potential as a drug target. As an extension to this work, an initial pharmacometabolomics study was undertaken to determine the cellular consequences of targeting this component. The specific objectives include;

- Cloning and expression of Mtb cytochrome *bd*-I oxidase (Mtb *bd*-I), using two different heterologous expression systems (ML16 (bo_3/*bd*-I) and MB44 (bo_3/*bd*-I/*bd*-II)).
- Steady state characterisation of Mtb *bd*-I in the two expression models.
- Pharmacological profiling of Mtb *bd*-I in the two expression models and chemical validation of the target.
- Set up of a pharmacometabolomics platform to assess the cellular consequence of perturbation on Mtb metabolism by known drugs and selective ETC inhibitors.

Chapter II

Generation and characterisation of a heterologous expression system for *Mycobacterium tuberculosis* cytochrome *bd*-I oxidase in an *E. coli* respiratory knockout (bo_3/*bd*-I) mutant strain.

2.1. Introduction

The aim of this study was to explore the features of the Mtb cytochrome *bd*-I oxidase (Mtb *bd*-I) through initially cloning the enzyme, followed by characterizing the expression, growth conditions and the spectroscopic signature of this enzyme.

Kana *et al* (2001) previously demonstrated the ability of recombinant Mtb cytochrome *bd*-I oxidase to restore *bd*-I activity in a *M. smegmatis* mutant strain (253). However, detailed studies of Mtb cytochrome *bd*-I in terms of functionality and inhibitor profiling have not yet been performed.

The Mtb genome encodes approximately 4,000 genes contained within 4,411,529 base pairs (148, 287, 288). The *Rv1623c*, *Rv1622c*, *Rv1621c* and *Rv1620c* genes, encoding the *cydABDC* operon (5,967 bp), are found between 1,819,963 and 1,825,887 base pairs of the Mtb genome (Figure 2.1).

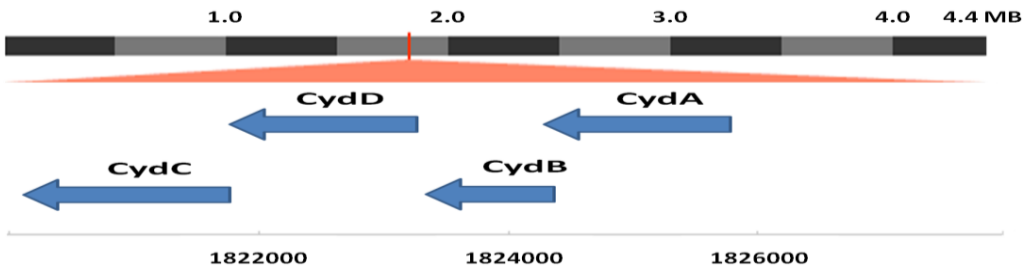

Figure 2.1: The position of the *cydAB* genes in the context of the *Mycobacterium tuberculosis* genome

The cytochrome *bd*-encoding genes (*cydA* and *cydB*) are found adjacent to genes (*cydD* and *cydC*) encoding an ABC-type transporter.

(http://genome.tbdb.org/annotation/genome/tbdb/GeneDetails).

An *Escherichia coli* bo_3/*bd*-I knockout strain was used to develop a heterologous expression system for Mtb *bd*-I. A brief description of Mtb and *E. coli* quinol terminal oxidases will be presented.

As stated previously, Mtb has two terminal oxidases, the cytochrome bc_1 reductase-cytochrome *c* oxidase super-complex and the cytochrome *bd*-I oxidase (195) (Figure 2.2, A). Cytochrome *bd*-I oxidase contains two structural subunits, subunits I and II, encoded by *cydA* and *cydB* respectively. *CydDC* of the *cydABDC* operon, encoding an ABC-type transporter, are implicated in the assembly of a functional *bd*-type oxidase and in maintaining redox homeostasis in the periplasm through exporting cysteine (53, 232, 247, 248). Cytochrome *bd*-I oxidase is an enzyme that couples the oxidation of a respiratory substrate quinol (two-electron donor) to the four-electron reduction of O_2 to water. The high-affinity cytochrome *bd*-I oxidase is able to scavenge oxygen under microaerophilic conditions. Upregulation of this enzyme *in vitro* and *in vivo* has been observed at the transition to chronic infection, providing initial evidence for the importance of cytochrome *bd*-I oxidase in the adaptation of Mtb to host immunity (221, 253, 289).

E. coli possesses three terminal quinol oxidases; cytochrome bo_3, cytochrome *bd*-I and cytochrome *bd*-II, encoded by the *cyoABCDE*, *cydAB* and *appBC* operons, respectively (218, 290) (Figure 2.2, B). Cytochrome bo_3 is from the heme-copper family of terminal oxidases while cytochrome *bd*-I and cytochrome *bd*-II are members of the cytochrome *bd*-family (211). Dassa *et al* (1991) demonstrated the homology between cytochrome *bd*-II subunits (encoded by *appC* and *appB*) and cytochrome *bd*-I subunits (encoded by cydA and cydB) with 60% and 57% homology of amino acid sequences, respectively (291). Thus, the spectral features of cytochrome *bd*-II closely resembles those of cytochrome *bd*-I, rendering them spectrophotometrically undistinguishable (217). The well-studied *E. coli* cytochrome *bd*-I oxidase has a three-heme form, which includes heme b_{558}, heme b_{595} and heme *d*, with signature peaks at 560 nm, 596 nm and 629 nm, respectively. Similarly, the difference spectrum of *E. coli* cytochrome *bd*-II showed the presence of heme *d* (626 nm), heme b_{595} (589 nm), and heme b_{558} (559 nm) (212, 217).

A)

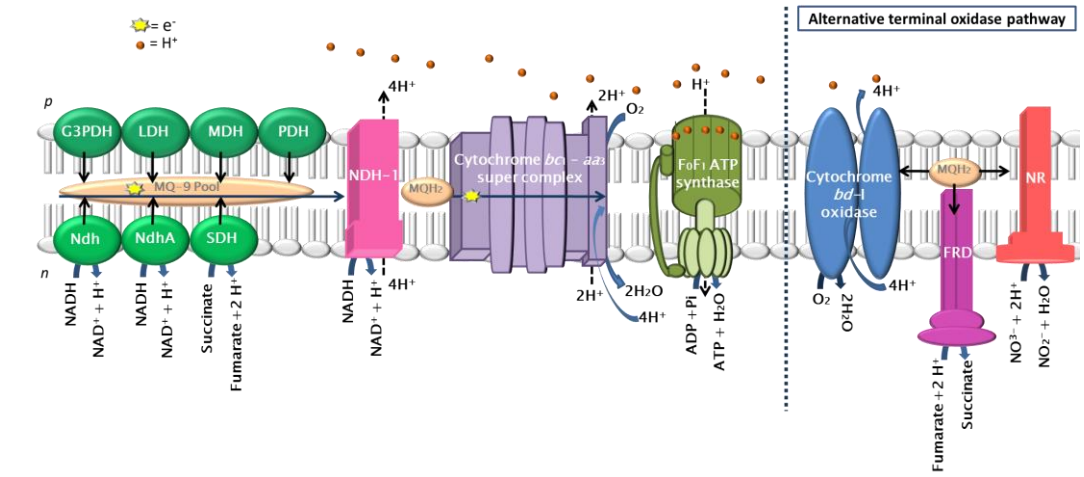

B)

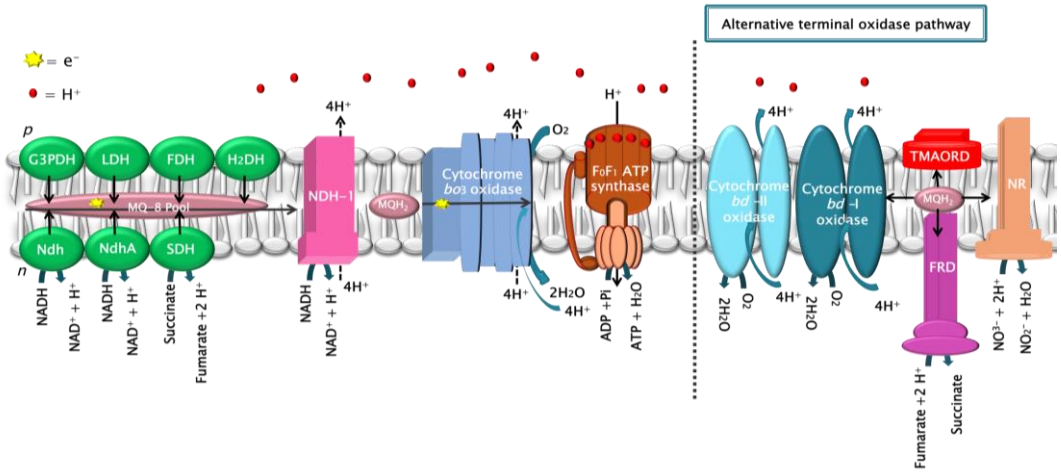

Figure 2.2: The electron transport chain of *Mycobacterium tuberculosis* and of *E. coli*

A) Components of the electron transport chain in Mtb of which cytochrome *bd*-I oxidase (quinol oxidase) is an alternative terminal oxidase. Figure adapted from Fisher *et al* (2009) (209). B) Components of the electron transport chain in *E.coli*. The chain electron donor components are Ndh/NdhA-type II NADH: (mena)quinone oxidoreductase (two isoforms), SDH-succinate dehydrogenase, G3PDH-glycerol-3-phosphate dehydrogenase, LDH-L-lactate dehydrogenase, FDH-formate dehydrogenase, H_2DH-H_2 dehydrogenase, and nuo-type I NADH (complex I). Electron acceptors are the cytochrome bo_3 oxidase and an alternative terminal oxidase pathway which is cytochrome *bd*-I oxidase, cytochrome *bd*-II oxidase, FRD-fumarate reductase, TMAORD-TMAO reductase and NR-nitrate reductase. Chain components also include the F_0F_1 ATP synthase (complex V), MQ-8-menaquinone-8 and MQH_2-menaquinol. *P* and *n* correspond to the positive (periplasmic) and negative (cytoplasmic) sides of the respiratory membrane with respect to proton translocation. Proton movements are indicative only and do not represent H^+/e^- ratios for the respective complexes. The orientation and topology of the subunits are indicative only.

Here we describe the use of the ML16, an *Escherichia coli* bo_3/*bd*-I knockout strain to express Mtb cytochrome *bd*-I terminal oxidase (Chapter II and III); the use of an *E. coli* bo_3/*bd*-I/*bd*-II triple-knockout strain for the heterologous expression of Mtb cytochrome *bd*-I is described in Chapter IV. As mentioned previously in Chapter 1.5.4.4, different cytochrome *bd* members have distinctive expression features. For example, the expression of cytochrome *bd*-I in *E. coli* and Mtb is recorded during both aerobic and microaerophilic growth conditions (20, 212), while induction of cytochrome *bd*-II in *E. coli* is associated with a shift to anaerobic growth or stationary phase, as well as with phosphate, carbon or glucose starvation (217, 218, 290, 292). Therefore, cytochrome *bd*-II in *E. coli* is likely to function under even more O_2-limiting conditions than cytochrome *bd*-I (293).

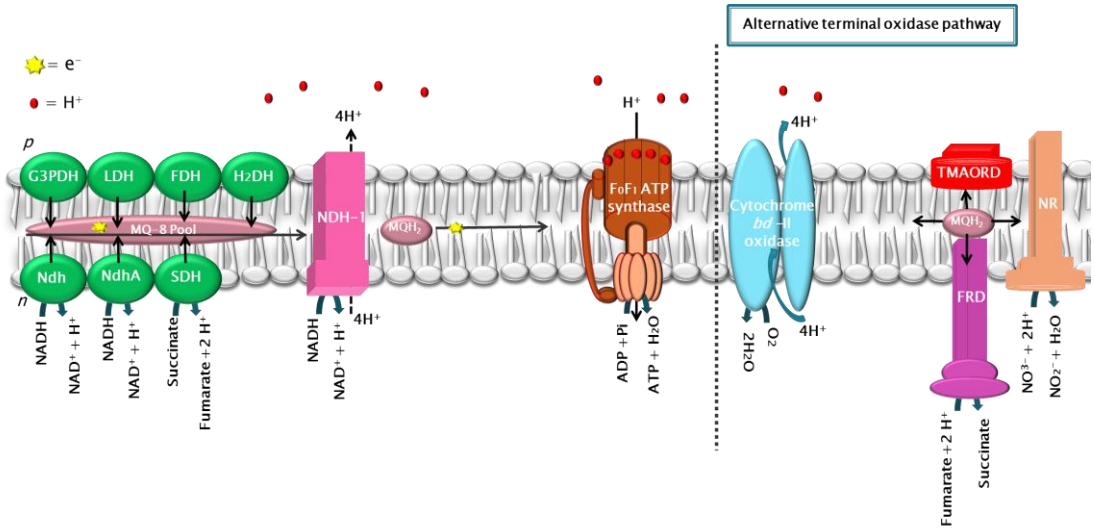

Figure 2.3: Components of the electron transport chain of ML16, an *E. coli* mutant strain

The ML16 respiratory chain has all the electron donor components of wild-type *E. coli* but only cytochrome *bd*-II oxidase, FRD-fumarate reductase, TMAORD-TMAO reductase and NR-nitrate reductase as electron acceptors. Chain components also include F_0F_1 ATP synthase (complex V) and MQH_2-menaquinol. *P* and *n* correspond to the positive (periplasmic) and negative (cytoplasmic) sides of the respiratory membrane with respect to proton translocation. Proton movements are indicative only and do not represent H^+/e^- ratios for the respective complexes. The orientation and topology of the subunits are indicative only.

Growth cycles were monitored for wild-type *E. coli*, ML16 and transformed strains with a view to studying the effect of the recombinant Mtb cytochrome *bd*-I on the transformed cells. The standard systematic growth cycle of any bacteria should include four main phases; lag phase, exponential phase, stationary phase and decline phase. Following inoculation of cells into a synthetic medium, the time which elapses before cell growth accelerates is known as the lag phase. The exponential phase is when the culture grows at a constant rate, and the growth rate is proportional to the culture density. The stationary phase refers to a culture that shows no further increase in the number of cells (i.e. non-replicating cells or the rate of death equal to the rate of growth). Entry into the stationary phase is a transition period for the cells in which cells exit from the cell cycle, maintain viability during starvation, and resume growth when starvation is relieved. During the stationary phase studies show the importance of the proteins made and the regulation of their synthesis and their essentiality for the survival of the cell, which will be discussed later (294-296). Importantly, the stationary-phase model of Mtb latency is based on studying the persistence phenomena of Mtb during this phase (42, 43). The last phase of the 'standard' bacterial life cycle is the decline phase, which is characterized by toxic waste accumulations, food depletion and bacterial death (294-296).

2.2. Material and methods

2.2.1. Amplification of *Mycobacterium tuberculosis cydABDC* operon

2.2.1.1. Primer design

Each primer described herein was designed from the published genome sequence of the *Mycobacterium tuberculosis cydABDC* operon from the TB data base (http://www.tbdb.org/). Primers were custom synthesised by Invitrogen, UK. Pairs of oligonucleotide primers (Table 2.1) for PCR reactions were designed to be complementary to the *cydABDC* operon to be replicated, with one primer designed to bind the sense strand and another for antisense strand.

Table 2.1: The oligonucleotide primers for amplifying the *cydABDC* genes from *Mycobacterium tuberculosis* H37Rv

***cydABDC* PCR primers**	**Primer sequence (5' → 3')**
Forward Primer	CCG GAG ATG ACA GAT GAA TGT CGT CG
Reverse Primer	GGC GTT ACG TGC TGA TAT CGA TGA CTC AGG

The forward and reverse primers were designed to incorporate both the initiation and termination operon.

An additional 18 internal oligonucleotide primers were designed to provide sequencing coverage of the entire 5,967 bp gene sequence. The entire operon was checked for frameshift, silent and other mutations which could affect the expression of cytochrome *bd*-I oxidase protein. The primers used for sequencing are summarised in the following table (Table 2.2).

Table 2.2: The oligonucleotide primers used for sequencing of the *cydABDC* genes

***cydABDC* sequencing primers**	**Primer sequence (5' → 3')**
Forward Primer 15	CGA TCT GCA GCA GGA ATA CC
Forward Primer 16	GGT TCG GTG TCA TCG CAG CG
Forward Primer 17	GCT CAA CGC CTA CAC CCT GC
Forward Primer 18	GGA CGT ATT GGG TTT TCC GG
Forward Primer 19	CCA TTG TGG TGA TCA CAC TGC
Forward Primer 20	CCA GTT TCA TGC CGC AGC TGA CG
Forward Primer 21	GCT GTA CTA GAC GAG TTG CCC
Forward Primer 22	CCC TTA TCT ATC ACC GGC TGG
Forward Primer 23	GCA ACG TCA TCG CCG ACT CAC AAC G
Reverse Primer 4	GGC CGG TAG TCG TTT GGT CC
Reverse Primer 5	CGC CCA TAC CGA CAT GAG CG
Reverse Primer 6	GGT TTT CAA AGC GAT GAA CAC CGC
Reverse Primer 7	GGT GGA GGT ATC CGT TCA GC
Reverse Primer 8	CCA TGA AGA TCG GTA TCA GG
Reverse Primer 9	CGG TGA GAT CAT ACG GTG CG
Reverse Primer 10	CAC GTG TTG TTC GGT GCG GG
Reverse Primer 11	GCA TGT TGG CCA GTT CGT CGA CG
Reverse Primer 12	GGC AAC AAC ATC AGG ATG GC

The primers were designed against the published *cydABDC* sequence (http://www.tbdb.org/) to bind at intervals along the inserted *cydABDC* operon.

2.2.1.2. Polymerase chain reaction of *cydABDC* operon

The *cydABDC*-encoding genes were amplified from Mtb genomic DNA prepared from a culture of Mtb H37Rv supplied by Dr. Amanda Brown (Queen Mary, University of London).

Polymerase chain reaction (PCR) reactions were carried out in a 50 µl volume, containing 2 µl (about 20 µmol) of each primer (Table 2.1), 1 µl of the DNA to be amplified (typically 10 ng), 25 µl 2x Phusion® Master Mix (New England BioLabs, UK), 1.5 µl dimethyl sulfoxide (DMSO) and 18.5 µl of sterile dH_2O. The PCR reaction for amplifing the *cydABDC* sequence was performed using a Bio-RAD PCR thermal cycler (Bio-RAD, UK). The PCR reaction involved an initial denaturation step of 98 °C for 2 min, followed by 35 cycles of (a) denaturation at 98 °C for 10 s, (b) annealing at 64 °C for 40 s and (c) polymerisation at 72 °C for 4 min, followed by a final polymerisation step of 72 °C for 7 min. PCR product was run on an ethidium bromide-containg 1% agarose gel alongside a 1 kb DNA ladder (Invitrogen, UK) to check the size of the PCR product (297). The resulting DNA bands were visualized by exposure to UV light briefly in order to avoid damaging the DNA.

It is worth mentioning that *Pyrococcus furiosus* (*Pfu*) DNA Polymerase (Fermantas, UK) and Crimson™ *Taq* DNA polymerase (New England BioLab, UK) were used at different annealing temperatures (55-65) °C with the purpose of amplifying the *cydABDC* operon, but both enzymes gave unsuccessful results. Therefore, Phusion® Master Mix (New England BioLabs, UK), a high-fidelity PCR Master Mix, was used for amplification of the *cydABDC* operon, owing to fusion of a novel Pyrococcus-like enzyme with a processivity-enhancing domain. Phusion® Master Mix is capable of amplifying long DNA templates (7.5 Kb-20 Kb) with high accuracy and fidelity (50X greater than *Taq* polymerase) (298, 299). Phusion® Master Mix has a processivity that is 10-fold greater than *Pfu* DNA polymerase and 20-fold greater than that of *Taq* DNA polymerase.

2.2.1.3. Purification of PCR products

Purification of PCR product was conducted following confirmation that the PCR product was the expected size (5,967 bp) of the *cydABDC* operon. This method is important in order to remove agarose and other contaminants away from the PCR product that may inhibit further cloning steps. The DNA fragment was purified using a QIAquick Gel Extraction Kit (Qiagen, Germany). The ~ 6000 bp *cydABDC* DNA band was excised from the agarose gel with a sterile scalpel. The gel slice was weighed before 3 volumes of buffer QG were added to 1 volume of the gel slice. The mixture was incubated at 50 °C for 10 min before being vortexed intermittently until completely dissolved gel fragments was achieved. The sample was transferred into QIAquick spin column in a 2 ml collection tube and centrifuged at high speed (13,000 *g*) for 1 min. The flowthrough was discarded and the Qiaquick column was returned to the same collection tube. In order to remove all the residual of agarose, 0.5 ml of buffer QG was added to QIAquick column and centrifuged for 1 min at 13,000 *g*. The flow through was discarded and the QIAquick column was centrifuged for a further 1 min at 13,000 *g*. For the elution step, the QIAquick column was transferred into a clean 1.5 ml microcentrifuge tube and 50 µl diethylpyrocarbonate (DEPC)-treated water (Ambion, UK) was added before centrifugation at maximum speed (13,000 *g*) for 1 min. A NanoDrop 1000 U 3.7.1 (Thermo scientific, UK) was used in order to check the purity and the concentration of the PCR product, which was then stored at -20 °C until required.

2.2.1.4. Agarose gel electrophoresis

Agarose gels were used to separate the DNA fragments in the PCR products or from the restriction enzyme digestions. In this study 1% agarose gels (Sigma Aldrich, UK) were prepared in 1 x Tris-Acetate-EDTA (TAE) consisting of 40 mM Tris, 20 mM acetic acid and 1 mM EDTA, pH 8.0 (Sigma Aldrich, UK). The mixture was heated for 2 min in a microwave oven and cooled at room temperature. Subsequently, ethidium bromide (0.25 $\mu g.ml^{-1}$) (Sigma Aldrich, UK) was added before pouring the gel solution into a gel cast on flat surface. DNA samples were mixed with 6 x loading dye (Invitrogen, UK) and loaded before being electrophoresed for 30 - 40 min at a constant current of 90 volts. Once completed, the gel was visualised by UV

illuminator (Syngene Bioimaging, UK) and analysed using Genetools analysis software (Syngene Synoptics Ltd. Cambridge, UK). The DNA fragments were compared with DNA molecular weight marker (Invitrogen, UK).

2.2.2. TA cloning

A-tailing of the PCR product was applied to add cohesive ends to the cloned DNA fragment, thus facilitating its insertion into the pCR®II, TA cloning vector (Invitrogen, UK). This reaction was achieved by incubating 7 µl (~50 ng) of the isolated fragment with 1 µl of 1 mM dATP, 1 µl of *Taq* polymerase and 1 µl x10 *Taq* polymerase buffer (New England BioLab, UK) in a total reaction volume of 10 µl at 70 °C for 20 min. The pCR®II, TA cloning vector was selected due its following advantages, eliminating any enzymatic modifications of the PCR product; allowing transcription from either direction into the insert; and not demanding PCR primers that contain restriction sites. Moreover, the pCR®II, TA cloning vector enhanced screening chances, as it possesses genes that confers ampicillin and kanamycin resistance, either one could be used for propagation. It has the *lacZ* gene as well that can be used for blue/white screening as uninterrupted *lacZ* expresses β-galactosidase, an enzyme which converts 5-bromo-4-chloro-3-indolyl β-D-galactopyranoside (X-gal) to a blue derivative in the presence of isopropyl-β-D-thiogalactoside (IPTG, which is a stable mimic of lactose and induces expression of *lacZ*). Functional β-galactosidase will not be expressed once the insertion at the multiple cloning sites (MCS) occurs, and thus no formation of coloured product occurs, resulting in white colonies, which should contain plasmid with the desired gene cloned.

Subsequently, attempts were made to ligate the A-tailed fragment into the pCR®II, TA cloning vector (Invitrogen, UK). All ligations were carried out in a 10 µl reaction volume with any shortfall of volume being made up with dH_2O. The ligation reaction contained 3 µl of A-tailed PCR product, 2 µl of pCR®II, 1 µl of each provided T4 DNA ligase and x10 buffer and 3 µl of dH_2O. The reaction was submitted for an overnight incubation at 14 °C before the ligation reactions being

transformed into TOP10 competent cells. The ligation mixture of pCR®II-TOPO and *cydABDC* operon created the pCR®II, TA/*cydABDC* construct, designated as pTM3.

2.2.3. Preparation of media:

2.2.3.1. LB Broth (Luria-Bertani medium)

All growth of cells was carried out in sterilised LB medium (Sigma Aldrich, UK). Required antibiotics were added to the LB solution when the medium had cooled below 50 °C, but prior to use.

2.2.3.2. LB agar plate media

Sterile agar plates were prepared using LB agar medium (Sigma Aldrich, UK) and required antibiotics were added to the LB solution when the medium had cooled below 50 °C, but prior to setting.

2.2.4. Transformation of One Shot® TOP10 chemically competent *E. coli*

Transformation was performed following the standard methods of Sambrook and Russell (2001) (297). The ligation mixture pTM3 was transformed into One Shot® TOP10 chemically competent *E. coli* (Invitrogen, UK) by the heat shock method. This method involved incubating a standard volume (14 µl) of Top 10 competent cells with 2 µl of recombinant plasmid DNA (pTM3) on ice for 30 min. Cells were then heat shocked at 42 °C for 1 min before being returned to ice for 2 min. About 180 µl of pre-warmed S.O.C medium (Invitrogen, UK) was added to the cells, which were then incubated at 37 °C in a shaking incubator at 200 rpm for 1 h. In order to have blue/white screen colonies for successfully ligated plasmid, 20 µl of X-Gal substrate was added to the cells. Subsequently, 150 µl of the cells were then plated to LB agar containing appropriate antibiotics (100 $\mu g.ml^{-1}$ ampicillin) and incubated overnight at 37 °C. The following day, white colonies were picked from the plates and grown in 5 ml LB medium containing 100 $\mu g.ml^{-1}$ of ampicillin at 37 °C in a shaking incubator at 200 rpm. Glycerol stocks of the plasmid-containing cells were

made from these cultures. Thereafter ampicillin was used in order to sustain plasmid transformant growth and for selectivity.

2.2.5. Glycerol Bacterial Stock

Glycerol stocks were prepared using 100 µl of 50% (v/v) sterile glycerol and 500 µl of bacterial suspension in LB medium. The bacterial suspension was kept at -80 °C for future use.

2.2.6. Mini preps

Mini preps were carried out using QiaAmp (Qiagen, UK). A white colony (plasmid-containing cell) from a fresh LB agar plate was used to inoculate 10 ml LB medium containing appropriate antibiotic (100 $\mu g.ml^{-1}$ ampicillin) and incubated overnight at 37 °C in a shaking incubator at 200 rpm. Subsequently, the culture was centrifuged for 5 min at 10,000 *g*. The supernatant was poured off and the pelleted cells were resuspended in 250 µl of cell resuspension solution (P1) before being transferred to a microcentrifuge tube. The addition of 250 µl of buffer P2 was followed by inverting the tubes 4-6 times until the cell suspension turned blue signifying lysis of the cells. The mixture was neutralized by the addition of 350 µl Buffer N3 neutralisation solution and immediately mixed thoroughly by inverting the tube before being centrifuged at 13,000 *g* for 10 min at room temperature. The cleared lysate was transferred into a QIAprep spin column and was centrifuged at 13,000 *g* for 1 min and the flowthrough was discarded. The column was washed twice, first with 500 µl of buffer PB and then with 750 µl of buffer PE solution and after each wash the column was centrifuged for 1 min at 13,000 *g* at room temperature. The flowthrough was discarded and followed by an additional 1 min centrifuge step to remove remaining wash buffer. Finally, the plasmid DNA was eluted in 50 µl of buffer EB by centrifugation at 13,000 *g* for 1 min at room temperature. The DNA concentration was measured using a NanoDrop 1000 U 3.7.1 (Thermo scientific, UK) and stored at -20 °C until required.

2.2.7. Screening of positive clones pTM3 by restriction enzyme analysis

Screening of the positives clones was conducted in order to validate successful cloning and subcloning of the inserted gene into the vectors, and successful transformation of the ligated gene into the *E. coli* host. The reaction mixture for pTM3 digestion was in a total reaction volume of 30 µl that contained 2.5 µl of pTM3, 2 µl of 10x fast digest buffer, 1 µl of *EcoR*I restriction endonuclease (Fermentas, UK) and 24.5 µl of dH_2O. The reaction was incubated at 37 °C for 15 min then inactivated at 80 °C for 5 min. Following digestion, 10 µl of digested plasmid with 2 µl of 6 x loading dye were loaded to a 1% agarose gel, containing ethidium promide (0.25 $\mu g.ml^{-1}$), run alongside 1 kb DNA ladder (Invitrogen, UK). Electrophoresis was conducted in 1 x TBE running buffer at 90 volts for 30 min and the gel was visualised under UV light.

2.2.8. Analysis by automated sequencing

pTM3 (200 ng) produced positive results by PCR and restriction enzyme analysis, and was sequenced using automated DNA sequencing (Cogenics, UK), and the 18 internal primers (Table 2.2) which were designed for the sequencing reaction.

2.2.9. Maxi prep

A maxi prep was used to obtain good yields of recombinant plasmid DNA to be used for sub-cloning of pTM3 into the pUC19 expression vector. A single colony of TOP10 competent cells containing pTM3 was inoculated into 5 ml LB broth, containing 100 $\mu g.ml^{-1}$ ampicillin before being overnight incubated at 37 °C with vigorous shaking at 200 rpm. 500 µl of this culture was added into 100 ml LB/100 $\mu g.ml^{-1}$ ampicillin broth and submitted for overnight incubation at 37 °C with vigorous shaking at 200 rpm. The culture was harvested by centrifugation at 13,000 *g* at 4 °C. The supernatant was discarded, and the bacterial pellet was resuspended completely in 1 ml of buffer P1 followed by 1 ml Buffer P2. The tube was mixed by inverting several times until the cell suspension turned blue indicating lysis of the cells. The mixture was neutralized by the addition of 1.4 ml Buffer N3 neutralisation solution and immediately mixed thoroughly by inverting the tube. The bacterial

lysate was subjected to centrifugation at 13,000 *g* for 20 min at room temperature. The cleared lysate was transferred into QIAprep spin column and centrifuged at 13,000 *g* for 1 min and then the flowthrough was discarded. The column was washed twice, firstly with 500 µl of buffer PB and then with 750 µl of buffer PE solution and following each wash the column was centrifuged for 1 min at 13,000 *g* at room temperature. The flowthrough was discarded and the column was further centrifuged for 1 min at 13,000 *g* to remove remaining wash buffer. Finally, the plasmid DNA was eluted in 50 µl of buffer EB by centrifugation at 13,000 *g* for 1 min at room temperature. The DNA concentration was measured using a NanoDrop 1000 U 3.7.1 (Thermo scientific, UK) and stored at -20 °C until required.

2.2.10. Sub-cloning of pTM3 into pUC19 expression vector

The pUC19 vector was selected for protein production as it possesses an ampicillin resistance gene that enables screening for plasmid-containing cells and helps to prevent contamination of the cell cultures. Moreover, it has a MCS in the *lacZ* gene to give flexibility in selecting the restriction enzyme or the enzymes used for cloning.

In order to express Mtb cytochrome *bd*-I oxidase protein, the cloned gene was excised from pTM3 using the restriction site *Eco*RI present in both pTM3 and pUC19 expression vectors. The digests were analysed by visualisation on a 1% agarose gel and the gene fragments gel purified (Qiagen, Germany).

The sub-cloning reactions were as follows: The first reaction was for pTM3 digestion which involved a total reaction volume of 30 µl that contained 2.5 µl plasmid DNA (pTM3), 2 µl of 10x fast digest buffer, 1 µl of *Eco*RI restriction endonuclease (Fermentas, UK) and 24.5 µl of dH_2O. The reaction was incubated at 37 °C for 15 min then inactivated at 80 °C for 5 min. Following digestion, the reaction product was run alongside 1 kb DNA ladder (Invitrogen) on a 1% Aquapor LE gel (Invitrogen, UK) containing ethidium promide (0.25 $\mu g.ml^{-1}$). The desired fragment (the operon of interest) was excised from the gel and purified using QIAquick Gel Extraction Kit (Qiagen, Germany) (Chapter 2.2.1.3) in order to

remove undesirable products that may hinder later stages of the cloning processes. The concentration of DNA yield was measured using a NanoDrop 1000 U 3.7.1 (Thermo scientific, UK).

The second reaction was for pUC19 digestion which involve a total reaction volume of 30 µl that contained 5 µl pUC19 vector, 2 µl of 10x fast digest buffer, 1 µl of *EcoR*I restriction endonuclease (Fermentas, UK) and 22 µl of dH_2O. The reaction was incubated at 37 °C for 15 min then inactivated at 80 °C for 5 min. Afterwards, dephosphorylation was carried out to prevent the re-ligation of the double-digested expression vector pUC19 which involved adding 2 µl of Antractic phosphatase buffer and 2 µl of Antractic phosphatase enzyme to the reaction. The reaction went through consequent incubation at 37 °C for 10 min and 65 °C for 10 min, respectively. Following digestion, the reaction product was run alongside 1 kb DNA ladder (Invitrogen) on a 1% Aquapor LE gel (Invitrogen, UK) containing ethidium promide (0.25 $\mu g.ml^{-1}$). The desired fragment was excised from the gel and purified using QIAquick Gel Extraction Kit (Qiagen, Germany) (Chapter 2.2.1.3) in order to remove other undesirable products that may hinder later stages of the cloning processes. The concentration of DNA yield was measured using a NanoDrop 1000 U 3.7.1 (Thermo scientific, UK).

The vector and insert were ligated in 10 µl reaction volumes, containing 1 µl of digested pUC19, 7 µl of digested pTM3, 1 µl of 10x T4 ligase buffer and 1 µl of T4 Ligase. The reaction was incubated overnight at 16 °C to create the pUC19/*cydABDC* construct (designated as pTMA).

2.2.11. Transformation of ligated expression vector into One Shot® TOP10 chemically competent *E. coli*

The ligated expression vectors (pTMA) were transformed into TOP10 *E. coli* cells following the above mentioned protocol (Chapter 2.2.4). The ligation mixture was transformed using heat-shock transformation into TOP10 chemically competent *E. coli* cells and plated on LB agar containing 100 $\mu g.ml^{-1}$ ampicillin.

2.2.12. Selection of recombinants

Viable colonies from the transformation were cultured in ampicillin-enriched LB medium and the plasmid extracted by Miniprep (Qiagen, UK) (as described in section 2.2.6). In order to confirm the success of the cloning step, restriction enzyme digests were performed and visualised on 1% agarose gels, containing ethidium promide (0.25 $\mu g.ml^{-1}$). pTMA was analyzed using *Pst*I (NEB, UK) and *EcoR*I (Fermentas, UK) restriction enzymes.

The first reaction was for digestion of pTMA in a 30 µl reaction volume, containing 3 µl of plasmid DNA (pTMA), 2 µl of 10x fast digest buffer, 1 µl of *EcoR*I restriction endonuclease (Fermantas, UK) and 24 µl of dH_2O. The reaction was incubated at 37 °C for 15 min. The second digestion reaction of pTMA was conducted using *Pst*I (NEB, UK) in a 30 µl reaction volume, containing 2 µl of plasmid DNA (pTMA), 2 µl of BSA buffer, 3 µl of buffer 3, 1 µl of *Pst*I restriction endonuclease (NEB, UK) and 22 µl of dH_2O. The reaction was incubated at 37 °C for 1 h and 50 min. Following digestion, the reactions products were run alongside 1 kb DNA ladder (Invitrogen, UK) on a 1% Aquapor LE gel (Invitrogen, UK) containing ethidium promide (0.25 $\mu g.ml^{-1}$).

2.2.13. Preparation of competent ML16 *E. coli* cells

In order to express Mtb cytochrome *bd*-I protein, specific competent cells were required to incorporate and replicate the plasmid conveying the Mtb *cydABDC* operon. Competent cells were constructed using ML16, an *E.coli* bo_3/*bd*-I knockout strain, donated by Professor Robert B. Gennis, Illinois. The ML16 (Δ*recA*, Δ*cydAB*, Δ*cyoABCDE*::Cm^r) strain lacks two types of quinol:oxygen oxidoreductase (cytochrome bo_3 and cytochrome *bd*-I terminal oxidases) but has only one type of quinol:oxygen oxidoreductase (cytochrome *bd*-II terminal oxidase). ML16 has a chloramphenicol resistance cassette as it was constructed following the protocol of Datsenko and Wanner (2000) that based on using phage-based *E. coli* homologous recombination system (300). ML16 is a derivative of *E. coli* C43 (DE3) (genotype F^- *ompT gal* $hsdS_B$ ($r_B^- m_B^-$) *dcm lon* λDE3) (301, 302).

Competent ML16 cells were produced by the magnesium chloride/calcium chloride method. This involved overnight aerobic and O_2-limited cultures. The aerobic culture condition was as follow: 200 ml LB medium (in a 500 ml flask) enriched with 2.5 $\mu g.ml^{-1}$ chloramphenicol incubated at 37 °C in a shaking incubator at 200 rpm. The O_2-limited culture involved inoculation of an overnight aerobic ML16 culture into 375 ml LB medium enriched with 2.5 $\mu g.ml^{-1}$ chloramphenicol (in a 500 ml flask), sealed with a rubber plug with a head-space ratio of 0.5 and incubated at 37 °C in a shaking incubator at 200 rpm.

Competent cells preparations were performed according to the standard protocols of Sambrook and Russell (2001) (297). 100 ml of the cultures were centrifuged (4000 *g*) for 10 min at 4 °C once an OD_{600}= 0.44 was reached. The optical density was determined using a Thermo Spectronic instrument (Genesys, UK). Then, the cells were resuspended in 30 ml ice-cold 80 mM magnesium chloride/ 20 mM calcium chloride per 100 ml of culture volume. The cells were centrifuged as before, resuspended in 4 ml of ice-cold 100 mM calcium chloride solution with the addition of 200 µl of 50% (v/v) glycerol. The cells were then aliquoted (200 µl) into cold Eppendorf tubes and stored at -80 °C until required. The competent cells were designated as AnML16 (O_2-limited grown ML16) and AML16 (aerobically grown ML16).

2.2.14. Transformation of pTMA into ML16 competent cells

A 200 µl volume of each AnML16 and AML16 competent cells were transformed with the pTMA (10 µl) by firstly co-incubating on ice for 30 min followed by heat shock at 42 °C for 90 s, before returning samples to ice for 2 min. 300 µl of pre-warmed S.O.C medium (Invitrogen, UK) was added to the cells, which were then incubated at 37 °C in a shaking incubator for 1 h at 200 rpm. 150 µl of the cells were then plated to agar plates containing appropriate antibiotic, which was a combination of both 100 $\mu g.ml^{-1}$ ampicillin and 2.5 $\mu g.ml^{-1}$ chloramphenicol to sustain plasmid transformant growth, and incubated at 37 °C aerobically and anaerobically. AnaeroGen sachet (Thermo Scientific, UK) was used to generate an anaerobic atmosphere. After 2 days of incubation, colonies were picked from the plates and grown in 5 ml LB medium containing an appropriate concentrations of antibiotic at

37 °C in a shaking incubator at 200 rpm. These cultures were then used for making glycerol stocks of the plasmid-containing cells and for larger scale cultures and plasmid preparation.

Of note, transformants of pTMA into aerobic ML16 competent cells (AML16) took 3 days to grow on agar plates and 2-3 days in 5 ml LB broth over both growth conditions (aerobic and anaerobic). In contrast, transformants of pTMA into O_2-limited ML16 competent cells (AnML16) was successful for both growth conditions (aerobic and anaerobic).

2.2.15. Large-scale culture

The successful transformant colonies were grown in selective O_2-limited conditions, 375 ml of LB (in a 500 ml flask), containing 100 µg.ml^{-1} ampicillin and 2.5 µg.ml^{-1} chloramphenicol, sealed with a rubber plug with a head-space ratio of 0.5. An negative control (untransformed AnML16 competent cells) was grown in the same selective O_2-limited condition, but without ampicillin. The inoculum size was 0.2% of 375 ml LB broth. For clarification, the two strains that were used throughout experiments were untransformed AnML16 competent cells (henceforth ML16) and transformed AnML16 competent cells (henceforth TML16).

In addition, the same successful transformant colonies were grown in aerobic conditions, 200 ml of LB (in a 500 ml flask) containing 100 µg.ml^{-1} ampicillin and 2.5 µg.ml^{-1} chloramphenicol. An negative control (untransformed AnML16 competent cells) was grown in the same aerobic conditions but without ampicillin. The inoculum size was 0.2% of 200 ml LB broth.

In similar manner, BL21(DE3) pLysS, (F $^-$*ompT hsdS*$_B$ ($r_B^- m_B^-$) *gal dcm* (DE3) pLysS (Cm^R)), was also cultured as a wild-type *E. coli* strain in both aerobic and O_2-limited growth conditions, supplemented with 34 µg.ml^{-1} chloramphenicol. BL21 (DE3) bears pLysS, a compatible chloramphenicol-resistance plasmid, that produces T7 lysozyme, a natural inhibitor of T7 RNA polymerase (303).

During both aerobic and O_2-limited growth condition, IPTG was added at the beginning of the culture (i.e. along with inocula) to 1 mM final concentration (personal communication with Dr. Ashley Warman and Dr. Nick Fisher). Cultures were incubated at 37 °C in a shaking incubator at 200 rpm for 19 h.

It is worth commenting that selecting the above mentioned growth parameters, the addition of IPTG at the beginning of the culture and incubating cells for 19 h, was reliant on ML16 growth monitoring, which showed reduction of OD_{600} after 19 h of O_2-limited incubation (described later, Figure 2.3.7.2).

2.2.16. Preparation of 50 mM KPi, 2 mM EDTA, pH 7.5 buffer

For kinetic assays 50 mM KPi, 2 mM EDTA, pH 7.5 buffer was used throughout experiments, unless otherwise stated. This buffer was prepared as follow: a 50 mM K_2HPi (dipotassium hydrogen phosphate trihydrate) + 2 mM EDTA (ethylenediaminetetraacetic acid), pH 10 solution and a 50 mM KH_2Pi (potassium dihydrogen orthophphosphate) + 2 mM EDTA, pH 5.8 solution were prepared. Subsequently, these two solutions were mixed to produce a 50 mM KPi + 2 mM EDTA buffer at pH 7.5.

2.2.17. Membrane preparations

Membrane preparations were carried out following the protocol of Fisher *et al* (2009) (209). TML16, ML16 and BL21(DE3) pLysS from both aerobic and O_2-limited large-scale cultures (grown in defined conditions as described above (section 2.2.15) were harvested by centrifugation at 4000 *g* for 10 min using a Beckman centrifuge (Beckman Coulter, UK). Following supernatant removal, the cell pellets were resuspended in buffer (50 mM KPi, 2 mM EDTA, pH 7.5) and incubated on ice with hen egg lysozyme to a final concentration 200 $\mu g.ml^{-1}$ for 10 min. The cells were broken by two passes through a standard laboratory cell disruptor (Constant Systems, UK) operating at 20,000 psi and then the debris pelleted by centrifugation at 12,000 *g* at 4 °C for 20 min. The supernatant was collected and centrifuged by ultracentrifuge at 100,000 *g* at 4 °C for 1 h, depositing the membranes as a highly

viscous pellet. This was collected and resuspended with the aid of a Potter homogenizer (Sigma Aldrich, UK) in 2 ml of 50 mM KPi, 2 mM EDTA buffer (pH 7.5) per litre of original culture volume. Glycerol was added to a final concentration of 10% (v/v) and the membrane suspension stored in 50 µl aliquots at -80 °C until required. The total protein concentration of the membrane suspension was measured by Bradford assay (Chapter 2.2.18). To maintain enzyme activity, aliquots were not repeatedly freeze-thawed, and were stable for at least 6 months when stored at -80 °C.

2.2.18. Determination of protein concentration

The Bradford assay (304) was carried out in order to determine the protein concentration used for spectral analysis and to quantify the specific enzyme activity from membrane preparations. The Bio-Rad Reagent (Bio-Rad, UK) was diluted with distilled water in 1:4 ratio. A known concentration of bovine serum albumin (BSA) (2 $mg.ml^{-1}$) was used in order to obtain a standard curve. A standard curve was generated using BSA (Sigma Aldrich, UK) at concentrations ranging from 0.2-0.9 $mg.ml^{-1}$. The protein samples were prepared in a serial dilution ranging from 1 in 2.5 to 1 in 35. Subsequently, 2 µl of each samples was plated in triplicate into a 96 well plate. The automated dispenser Varioskan (Varioskan™, Thermal Corporation) was used to dispense 200 µl of Bradford Reagent into each well. The plate was incubated in the dark for 5 min at room temperature before determining the protein concentration using Skant® Software (Varioscan™ , Thermo Corporation) reading the absorbance at 595 nm.

2.2.19. Initial spectroscopic study of Mtb cytochrome *bd*-I oxidase

Initial UV-visible spectroscopic analysis of freshly prepared membranes was carried out on a Cary 300 Bio UV/visible spectrophotometer (Varian, UK). Assays of total volume 700 µl were performed with 200 µl of the crude recombinant membrane suspended in 500 µl of (50 mM KPi, 2 mM EDTA, pH 7.5) buffer. Spectra over a wavelength range of 500 – 700 nm were recorded for the oxidised membrane alone in the presence of potassium hexacyanoferrate (III), as well as in the presence of

reductants sodium dithionite. A difference spectrum was generated by subtracting the oxidised spectrum from the reduced spectrum.

2.2.20. Growth curves

Growth was monitored by measuring the optical density (OD) at 600 nm using a Thermo Spectronic instrument (Genesys, UK) over a time course (hours) and under the same aerobic and O_2-limited growth conditions (section 2.2.15). A redox indicator (resazurin), a rapid qualitative test, was used in order to monitor the respiratory state of the cells during growth. Resazurin was added to the media to final concentration of 0.0002% (w/v) according to the protocol of Karakashev *et al* (2003) (305). Aerobic cultures exceeded the 19 h of incubation to monitor the stationary phase of the cells. Pictures were taken to record the colour change of resazurin in the medium.

2.2.21. SDS-PAGE

Sodium dodecyl sulfate polyacrylamide gel electrophoresis (SDS-PAGE) was used to separate protein samples according to their molecular weight. The percentage of resolving gel used was 10%. The monomer solution of the resolving gel consisted of acrylamide/bis-acrylamide solution, (30% w/v) (Bio-RAD, UK) distilled H_2O, 1.5 M Tris-HCl (pH 8.8) (Sigma Aldrich, UK), 10% (w/v) SDS (Sigma Aldrich, UK), 20% ammonium persulphate (APS) (Sigma Aldrich, UK) and 10 µl N,N,N\N'-tetramethylethylenediamine (TEMED) (Fluka, UK) per 10 ml gel mix. The monomer solution was mixed gently and poured into glass plates assembled by instructions from the Mini-Protean III Electrophoresis Manual (Bio-RAD, UK). The gel was covered with water-saturated ethanol to ensure an even surface and to reduce polymerisation. After the gel had polymerised, the ethanol was removed by capillary action using a paper towel. The stacking gel, a 4% monomer solution, was prepared using the following materials: 530 µl 30% (w/v) arylamide/bis (Bio-Rad, UK), 2.39 ml H_2O, 1 ml 0.5 M Tris-HCl (pH 6.8), 40 µl 10% (w/v) SDS, 40 µl of 20% APS and 6 µl TEMED. This mixture was poured over the resolving gel with the comb fitted and allowed to polymerise for 30 min at room temperature.

2.2.22. Sample Preparation for SDS-PAGE

Different protein sample dilutions (1:10, 1:25 and 1:50) were prepared using assay buffer (50 mM KPi, 2 mM EDTA, pH. 7.5). For each sample, 10 µl of the protein sample was mixed with an equal volume of DTT (dithiothreitol). Prior to gel loading, samples were boiled for 5 min at 90 °C. The proteins were separated on SDS-PAGE using 1 X SDS-running buffer (0.196 M glycine, 48 mM Tris-base, 0.04% (w/v) SDS, pH 8.3) at a constant current of 60 milliamps for 60 min. Afterwards, the gel was stained with Expedion instant blue (a Comassie Blue based staining solution) (Expedion, UK). Staining was carried out for 30 min with slow agitation before being destained in distilled water. The prestained, broad range protein marker SpectraTM Multicolor Broad Range Protein Ladder (Fermentas, UK) was used to estimate the resulting protein band sizes.

2.3. Results

2.3.1. Amplification of the *Mycobacterium tuberculosis* H37Rv *cydABDC* operon

Using specific primers (Chapter 2.2.1.1), genomic DNA of Mtb strain H37Rv was subjected to amplification by PCR. The primers (Table 2.1) were designed to facilitate amplification of the whole *cydABDC* operon, yielding a single amplicon of 5,967 bp (Figure 2.4). This figure indicates that the PCR conditions have been optimised and primers are specific for the targeted gene. This amplicon is predicted to encode proteins of 1934 amino acids using the TB data base (http://www.tbdb.org/).

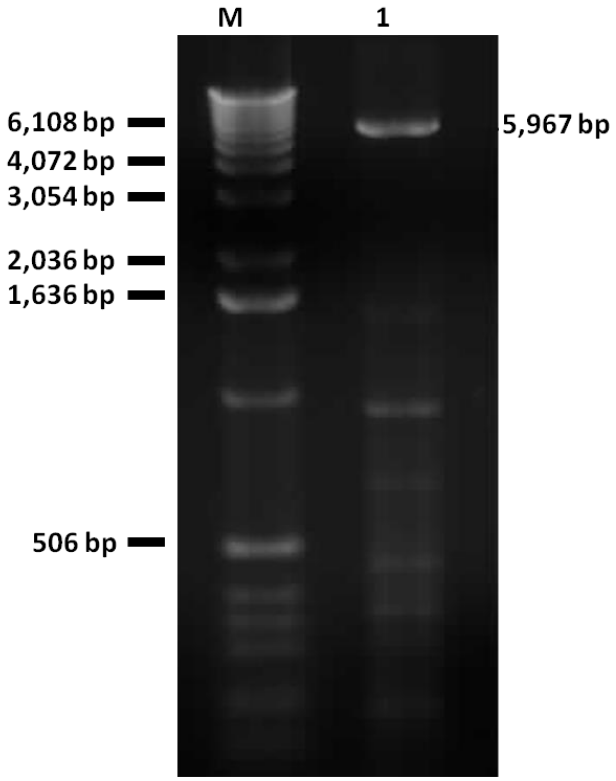

Figure 2.4: Amplification of *Mycobacterium tuberculosis* H37Rv *cydABDC* operon

The *cydABDC* operon predicted to be 5,967 bp was amplified from Mtb H37Rv genomic DNA. Lane M contains 1 kb DNA Ladder (Invitrogen), lane 1 shows the PCR products of the *cydABDC* operon that shows a single band of size ~ 6 kb. The PCR products were visualised on a 1% agarose gel containing 0.25 µg.ml^{-1} ethidium bromide (Sigma Aldrich, UK).

2.3.2. Screening of positive clones of pTM3 in TOP 10 *E. coli* host

The amplicons of the *cydABDC* operon were initially cloned to the pCR®II-TOPO® vector using the TOPO-TA cloning kit (Invitrogen, UK). TOPO-TA cloning provides fast and efficient cloning strategies for direct cloning of the PCR products into a high copy number plasmid vector. The cloning of PCR products into the TOPO vector created the 9,578 bp pCR®II-TOPO®/*cydABDC* construct (pTM3).

The success of the pTM3 cloning was validated using restriction enzyme analysis (described in Chapter 2.2.7). White colonies from each transformation were picked and cultured overnight in LB medium containing 100 $\mu g.ml^{-1}$ ampicillin. The following day, plasmid DNA was isolated using a Qiagen Miniprep kit before being subjected to restriction digest analysis**.** Figure 2.5 shows the results from digesting plasmid isolate with *EcoR*I. The positive clone produced two bands corresponding to the predicted digest fragments (3,599 and 5,979 bp). The recombinant plasmids were designated as pTM3 (Figure 2.6). In order to check pTM3 for errors, the plasmid was submitted for automated sequencing by Cogenics (UK) using 18 internal primers (Table 2.2) designed against the published *cydABDC* sequence (http://genome.tbdb.org). These oligonucleotides were designed to provide sequencing coverage of the entire 5,967 bp operon. The automated DNA sequencing, using the BLAST programme (http://blast.ncbi.nlm.nih.gov), revealed that the pTM3 is 100% identical with the published sequence and is free from errors, and that the gene could now be transferred to plasmids suited for the expression of the encoded proteins.

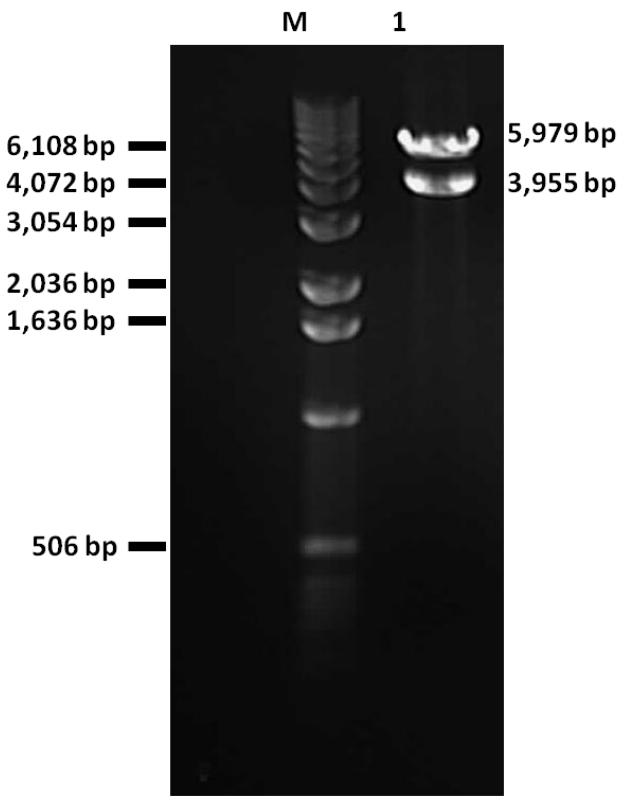

Figure 2.5: Restriction enzyme digestion analysis of a transformed colony of the pTM3 construct

The *EcoR*I restriction digest of the pTM3 plasmid was run alongside 1 Kb DNA ladder (lane M) (Invitrogen), resulting in two expected bands of 5,979 bp and 3,955 bp (lane 1) confirming that the pTM3 construct has been correctly created. Digestion was visualised by exposure to UV light following electrophoresis on 1% agarose gels containing 0.25 $\mu g.ml^{-1}$ ethidium bromide.

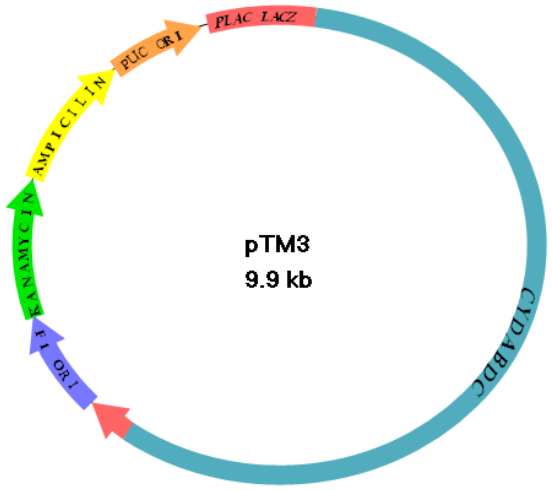

Figure 2.6: Plasmid map of pCR®II-TOPO® bearing the *Mycobacterium tuberculosis cydABDC* operon

pCR®II-TOPO® (Invitrogen, UK) was used to construct the recombinant *cydABDC* directly from a PCR reaction. The pCR®II-TOPO® Invitrogen vector is a 4.0 kb linearised vector. The pCR®II-TOPO® vector contains a *lac* promoter to allow the expression of the *lacZ* gene which encodes the first 146 amino acid of β-galactosidase. Interruption of *lacZ* by the insertion of PCR product may give rise to white colonies. The presence of both the kanamycin and ampicillin resistance genes in the vector allows for selection and maintenance in *E. coli*. The vector contains a pUC origin which allows replication, maintenance and high copy number in *E. coli*. The vector has f1 origin which allows rescue of the sense strand for mutagenesis and single-strand sequenancing. The plasmid map was generated using BVTech Plasmid (BVTech Plasmid.5.1 software).

2.3.3. Sub-cloning of pTM3 into the pUC19 expression vector

The plasmid pTM3 was sub-cloned into the pUC19 expression vector. This was carried out by digestion of the plasmid to excise the *cydABDC* insert from the TOPO vector and subsequent ligation to the pUC19 vector. pTM3 and the pUC19 vector were first digested using *EcoR*I and the appropriate fragments subsequently ligated as described in (section 2.2.10) before being transformed to TOP10 *E. coli* cells (section 2.2.11). Colonies were picked, and subjected to overnight liquid culture followed by miniprep DNA isolation. An *EcoR*I digest (Figure 2.7, A), cutting the plasmid twice in the insert region to give 5,981 bp and 2,686 bp fragments, verified the clone as correct. These data were backed up using a *Pst*I digest (Figure 2.7, B), cutting twice in the insert region to give 5,047 bp and 3,620 bp fragments. The digests confirmed the successful production of the positive recombinant plasmid,

designated as pTMA construct (pUC19/*cydABDC* construct) (Figure 2.8), which was then used in attempts to express the Mtb cytochrome *bd*-I oxidase protein.

A)

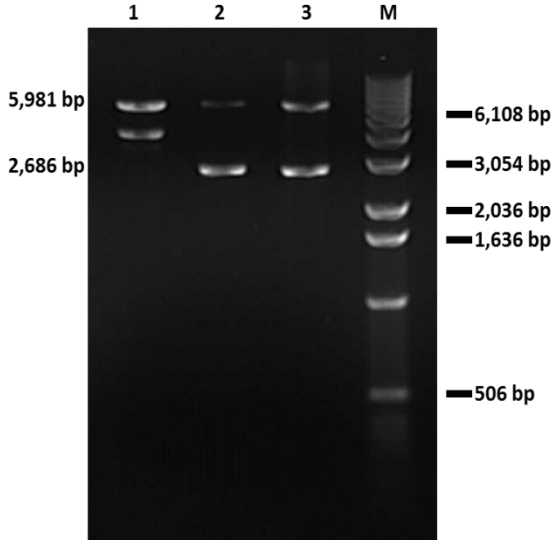

B)

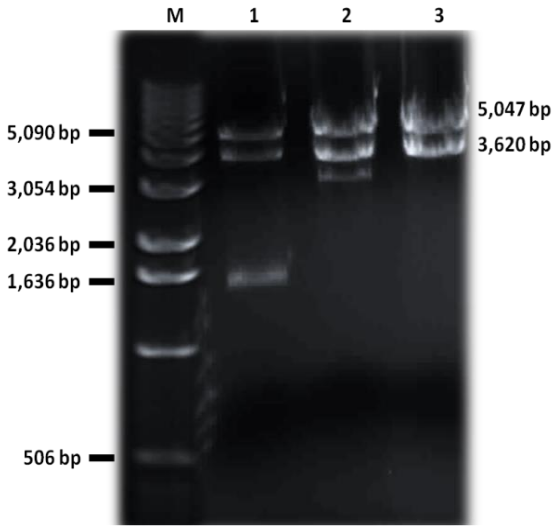

Figure 2.7: Restriction enzyme digestion analysis of transformed colonies of pTMA constructs

A) *EcoR*I restriction digests (Fermentas, UK) of three potential clones of the pTMA plasmid run alongside 1Kb DNA ladder (lane M) (Invitrogen). Two bands of 5,981 bp and 2,686 bp for the clones in lanes 2 and 3 identify the correctly cloned construct. The plasmid in lane 1 was not correctly digested by *EcoR*I digest, again confirming unsuccessful creation of the pUC19-*cydABDC* construct. B) The *Pst*I restriction digests (NEB, UK) of three potential clones of pTMA run alongside 1Kb DNA ladder (lane M) (Invitrogen, UK). Two expected bands of 5,047 bp and 3,620 bp for the clones in lanes 2 and 3 identify the correct construct. The plasmid in lane 1 was not correctly digested by *Pst*I, indicating it is not a successful pUC19- *cydABDC* clone. All digests were visualised by exposure to UV light following electrophoresis on 1% agarose gels containing 0.25 µg.ml^{-1} ethidium bromide.

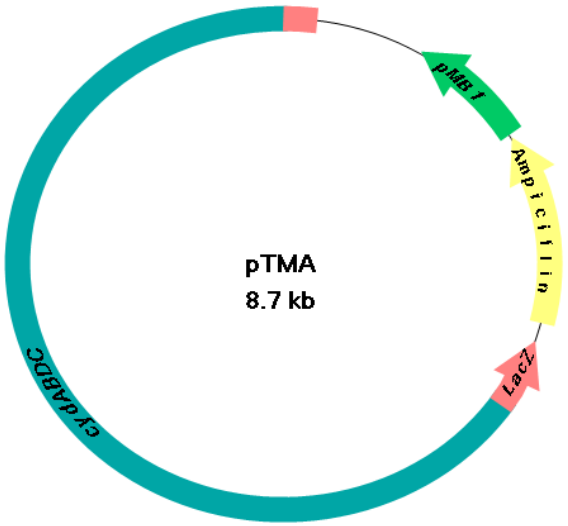

Figure 2.8: Plasmid map of the pUC19 expression vector bearing the *Mycobacterium tuberculosis cydABDC* operon

The pUC19 plasmid contains a *lacZ* gene which has similar features to pCR®II-TOPO® vector. The presence of the *lacZ* gene allows recombinants to be selected by blue/white screening. pUC19 also possesses the ampicillin resistance gene that enables selection. The plasmid construction was carried out by excising the *cydABDC* from pCR®II-TOPO® vector and ligating into the pUC19 multiple cloning sites (between *EcoR*I restriction sites). The plasmid map was generated using BVTech Plasmid (BVTech Plasmid.5.1 software).

2.3.4. The effect of recombinant *Mycobacterium tuberculosis* cytochrome *bd*-I on cell pigmentation

The colour of harvested cells during membrane preparation process was assessed with a view to examining the effect of recombinant Mtb cytochrome *bd*-I oxidase (Mtb *bd*-I) on cell pigmentation. The transformed double-knockout cells (TML16) showed a colour change to a red/brown pigmentation following harvesting both aerobic and O_2-limited cultures. In contrast, the untransformed double-knockout cells (ML16) had a light yellow pigmentation following harvesting aerobic and O_2-limited cultures (Figure 2.9).

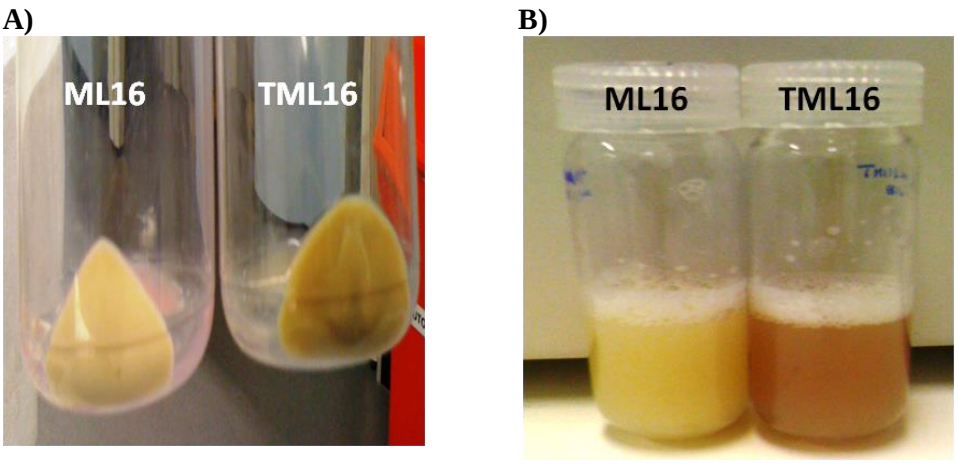

Figure 2.9: Effect of Mtb *bd*-I on cell pigmentation

A) Harvested ML16 and TML16 cells. B) The cell pellets of ML16 and TML16 were resuspended in buffer (50 mM KPi, 2 mM EDTA, pH. 7.5). ML16 had a light yellow pigmentation whereas TML16 (bearing Mtb *bd*-I) was accompanied by a change in the colour of the cells to a red/brown pigmentation.

2.3.5. Expression studies of *cydABDC* operon in the ML16 host

Successfully transformed cells (TML16) and untransformed cells (ML16) were subjected to 1 mM IPTG induction at 37 ^{o}C to express the predicted Mtb *bd*-I protein using the previously mentioned culture conditions (Chapter 2.2.15). Membranes of the induced culture were prepared (Chapter 2.2.17) and subjected to SDS-PAGE analysis (sections 2.2.21 and 2.2.22). Figure 2.10 shows the expressed proteins. There were a group of 4 bands expressed around 180 kDa in TML16, all of which might indicate the expression of *cydABDC* genes. There were also two distinct bands above and below 52 kDa which might indicate the overexpression of *cydA* and *cydB*, which will be confirmed later. However, due to the fact that the molecular weights of all *cydABDC* genes are relatively close to each other, makes it difficult to be certain to which genes these two bands relate.

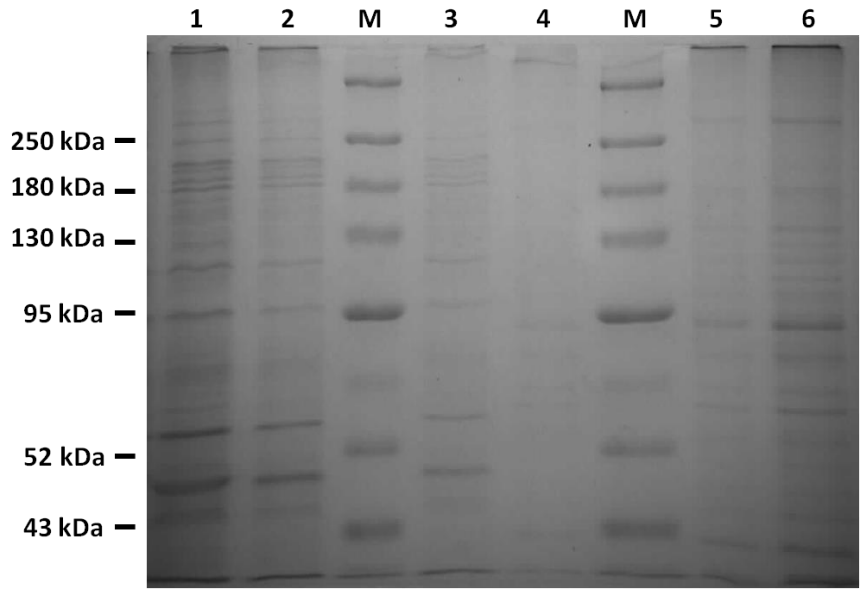

Figure 2.10: SDS-PAGE analysis of the recombinant Mtb cytochrome *bd*-I oxidase

M, marker of standard proteins whose molecular weights are indicated on the left. Lanes 1, 2 and 3 correspond to TML16 samples with different dilutions 1:10, 1:25 and 1:50 respectively, while lanes 4, 5 and 6 correspond to ML16 samples with dilutions 1:50, 1:25 and 1:10 respectively. The molecular weights of *cydA*, *cydB*, *cydD* and *cydC* genes according to the ProtParam tool (hosted by ExPASy http://web.expasy.org/protparam/) are 53 kDa, 38 kDa, 55 kDa and 59 kDa respectively. There are a group of 4 bands at around 180 kDa in TML16 samples (lane 1, 2 and 3). There are also two distinct bands above and below 52 kDa. The stock concentration of TML16 and ML16 were approximately 8 $mg.ml^{-1}$ and 4.3 $mg.ml^{-1}$, respectively.

2.3.6. Initial spectroscopic study of the *Mycobacterium tuberculosis* cytochrome *bd*-I

The difference spectra (reduced minus oxidized) of wild-type *E. coli* BL21 (DE3) LysS strain, ML16 and TML16 cells, which were grown during both aerobic and O_2-limited conditions, were recorded at room temperature using sodium dithionite as reductant and potassium hexacyanoferrate (III) as oxidant (Figures, 2.11-2.13). The significant difference between TML16 and ML16 spectra was the presence of a distinctive peak at 631 nm corresponding to that of the heterologous Mtb cytochrome *bd*-I in TML16.

2.3.6.1. Wild–type *E. coli* (BL21(DE3)pLysS) strain

A)

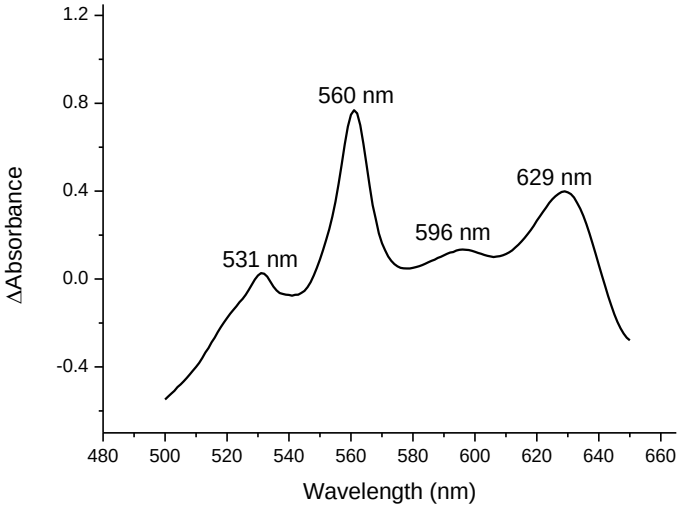

B)

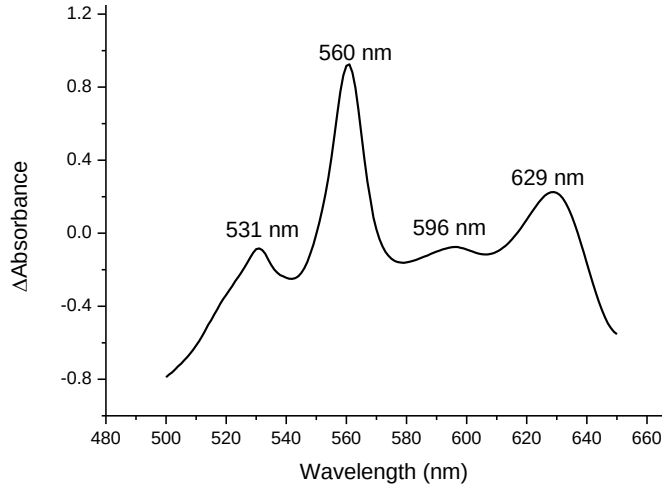

Figure 2.11: Reduced minus oxidized spectra of wild-type *E. coli* BL21 (DE3) LysS strain

The difference spectra (reduced minus oxidized) of wild-type *E. coli* BL21 (DE3) LysS strain were recorded at room temperature using sodium dithionite as reductant and potassium hexacyanoferrate (III) as oxidant. There are three distinct features spectra recorded in A) O_2-limited and B) Aerobic *E. coli* cultures, which are cytochrome *b* at 560 nm, cytochrome a_1 at 596 nm and cytochrome *d* at 629 nm. The cells were grown in O_2-limited condition using closed shaken flasks with a head-space ratio of 0.5 and induced at time = 0 h with 1 mM IPTG. The ratios of heme *d* (629 nm) with respect to heme b_{560} as a reference peak are 0.51 in O_2-limited condition and 0.3 in aerobic condition. These peaks have been normalized according to the following equation (Value-min/max-min). The final protein concentration of O_2-limited membranes was approximately 5.7 $mg.ml^{-1}$ and for aerobic membranes was approximately 4 $mg.ml^{-1}$

2.3.6.2. Double-knockout *E. coli* (ML16) strain

A)

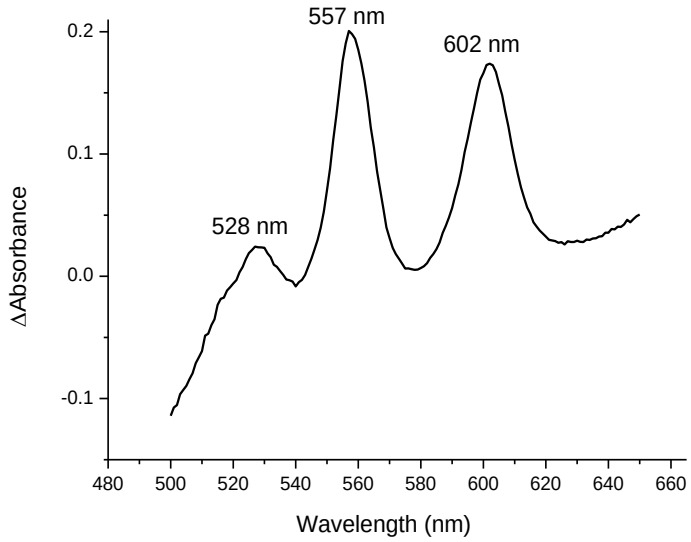

B)

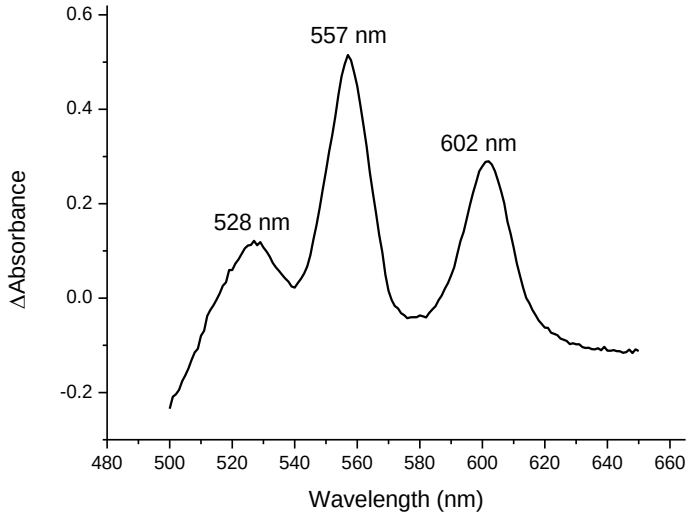

Figure 2.12: Reduced minus oxidized spectra of ML16

The difference spectra (reduced minus oxidized) of ML16 were recorded at room temperature using sodium dithionite as reductant and potassium hexacyanoferrate (III) as oxidant. There is a distinct feature in the spectra recorded in both A) O_2-limited and B) Aerobic ML16 cultures, showing peak at 602 nm. The cells were grown in O_2-limited condition using closed shaken flasks with a head-space ratio of 0.5 and induced at time = 0 h with 1 mM IPTG. The ratios of heme (602 nm) with respect to heme b_{557} as a reference peak are 0.85 in O_2-limited conditions and 0.44 in aerobic conditions. These peaks have been normalized according to the following equation (Value-min/max-min). The final protein concentration of O_2-limited membranes was approximately 1.2 mg.ml^{-1} and for aerobic membranes was approximately 2.2 mg.ml^{-1}

2.3.6.3. Transformed double-knockout *E. coli* (TML16) strain

A)

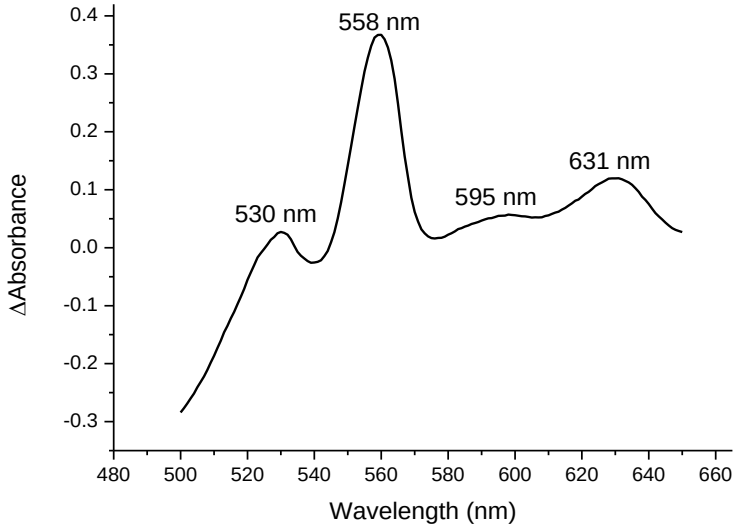

B)

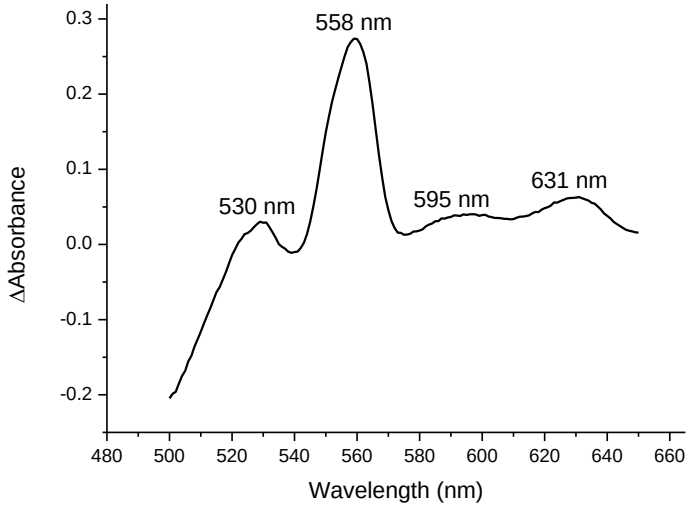

Figure 2.13: Reduced minus oxidized spectra of TML16

The difference spectra (reduced minus oxidized) of TML16 were recorded at room temperature using sodium dithionite as reductant and potassium hexacyanoferrate (III) as oxidant. Cytochrome *d* at 631 nm is a distinct feature of recombinant Mtb cytochrome *bd*-I in both A) O_2-limited and B) aerobic TML16-10 cultures. The cells were grown in O_2-limited conditions using closed shaken flasks with a head-space ratio of 0.5 and induced at time = 0 h with 1 mM IPTG. The ratios of heme *d* (631nm) with respect to heme b_{558} as a reference peak are 0.3 in O_2-limited conditions and 0.13 in aerobic conditions. These peaks have been normalized according to the following equation (Value-min/max-min). The final protein concentration of O_2-limited membranes was approximately 2.8 mg.ml^{-1} and for aerobic membranes was approximately 4.3 mg.ml^{-1}.

2.3.7. Assessment of growth phenotypes

To qualitatively evaluate the contribution of cytochrome *bd*-I to respiration, monitoring the growth of *E. coli* BL21 (DE3) LysS strain, AnML16 and TML16 cells was conducted to identify the differences between wild-type, mutant and transformed cells respectively. Resazurin (Raz), a redox indicator, shows a qualitative result for the bacterial respiratory state. In appropriate reducing conditions, Raz (blue in colour) irreversibly loses an oxygen ion to become resorufin (Rru) (Figure 2.14). Rru (orange/pink in colour) can undergo a further reduction to colourless dihydroresorufin, which is a reversible reaction by atmospheric oxygen and is mainly favoured upon total consumption of Raz (306). Raz is able to differentiate strict anaerobes (blue in colour) from microaerophiles (orange/pink in colour) and other strict aerobes (colourless) (305). Owing to the fact that Raz has a dark blue colour which is the starting colour of any culture medium, the dark blue colour in this study, therefore, did not represent a strict anaerobic bacteria respiratory state, but represents no metabolic activity or O_2 consumption.

Figure 2.14: Structures of resazurin in various oxidation states

2.3.7.1. Wild–type *E. coli* BL21(DE3) pLysS strain

The growth of BL21(DE3) pLysS (wild-type *E. coli*) was monitored through both aerobic and O_2-limited growth conditions (Figure 2.15). During the O_2-limited growth, after 6 h incubation, the colour of Raz was reduced to dark orange/pink (Rru) during the exponential phase at OD_{600} ~ 0.38. Cells achieved highest density after 12 h of incubation (OD_{600} ~ 0.44) and maintained a stationary plateau for about 10 h. Similarly, during aerobic growth, the colour of Raz after 6 h of incubation was reduced to dark orange/pink but with a slow growth rate at the beginning of exponential phase. Wild-type *E. coli* attained maximal density (OD_{600} ~ 1.5) after 42 h of aerobic incubation and maintained a stationary plateau for about 15 h before starting to decline.

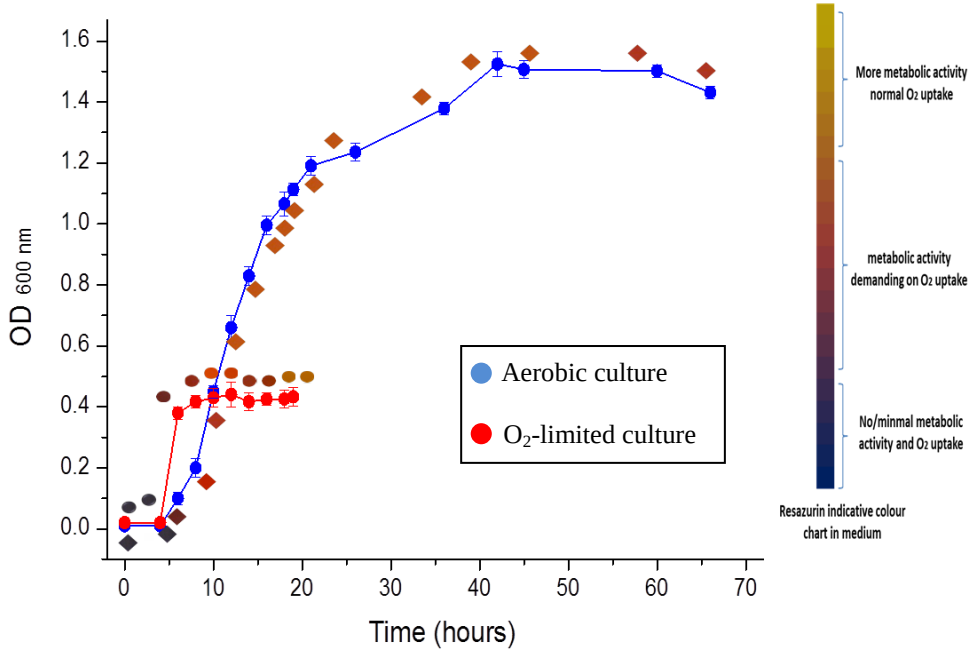

Figure 2.15: Growth of BL21 (DE3) pLysS (wild-type *E. coli*) supplemented with a redox indicator (resazurin)

Growth was monitored by recording optical density (OD_{600}) values of aerobic, shaken cultures (blue) and O_2-limited, closed, shaken flasks with a head-space ratio of 0.5 (red). The colours of the medium during the growth curve correspond to the colour of the resazurin in the medium (resazurin indicative colour chart). Wild-type *E. coli* began reducing resazurin after 6 h of aerobic incubation and achieved maximal density (OD_{600} ~ 1.5) after 42 h of aerobic incubation. During O_2-limited growth, wild-type *E. coli* also began reducing resazurin after 6 h of incubation but reached highest density (OD_{600} ~ 0.44) after 12 h of incubation. Error bars represent ± SEM of each point.

2.3.7.2. Double-knockout *E. coli* (ML16) strain

The growth of ML16 was monitored during both aerobic and O_2-limited conditions (Figure 2.16). During the O_2-limited growth and after 12 h of incubation, ML16 reached the highest density with OD_{600} ~ 0.4 following reduction of Raz after 8 h of incubation. During aerobic growth, after 8 h of incubation, the colour of the Raz was reduced to dark orange/pink (Rru) and cells recorded the highest density (OD_{600} ~1.7) after 45 h of incubation. Notably, the ML16 growth rate appeared parallel to the wild-type *E. coli* as it also reached OD_{600} ~ 1.5 after 42 h of aerobic incubation. During both aerobic and O_2-limited growth, ML16 seemed unable to maintain a stationary plateau.

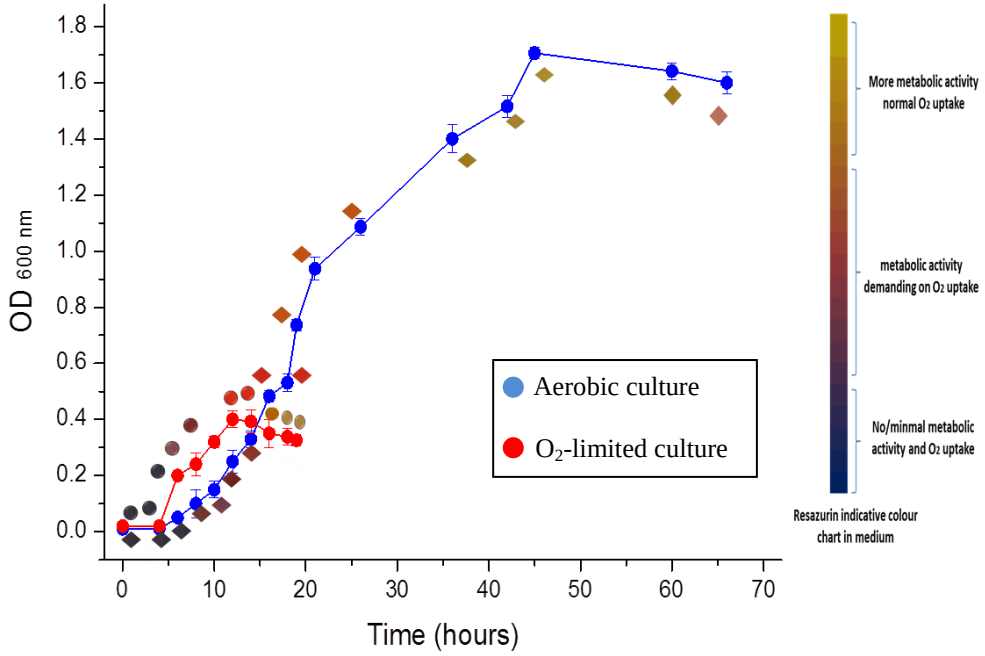

Figure 2.16: Growth of ML16 supplemented with a redox indicator (resazurin)

Growth was monitored by recording optical density (OD_{600}) values of aerobic shaken cultures (blue) and O_2-limited, closed, shaken flasks with a head-space ratio of 0.5 (red). The colours of the medium during the growth curve correspond to the colour of the resazurin in the medium (resazurin indicative colour chart). During aerobic growth, ML16 began reducing resazurin after 8 h of incubation and attained highest density (OD_{600} ~ 1.7) after 45 h of growth. The O_2-limited growth of ML16 also began reducing resazurin after 8 h of incubation and reached maximal density (OD_{600} ~ 0.4) after 12 h of incubation. Error bars represent ± SEM of each point.

2.3.7.3. Transformed double-knockout *E. coli* (TML16) strain

The growth of TML16 was monitored throughout aerobic and O_2-limited growth conditions (Figure 2.17). During O_2-limited growth, after 12 h of incubation, the colour of Raz was reduced to dark orange/pink (Rru) and TML16 attained the highest density after 16 h of incubation (OD_{600} ~ 0.22). TML16 was able to maintain a stationary plateau. During aerobic growth, reduction of Raz was observed after 12 h of incubation. TML16 achieved its highest density (OD_{600} ~ 1.2) after 45 h of aerobic incubation and maintained a stationary plateau for about 15 h before starting to decline.

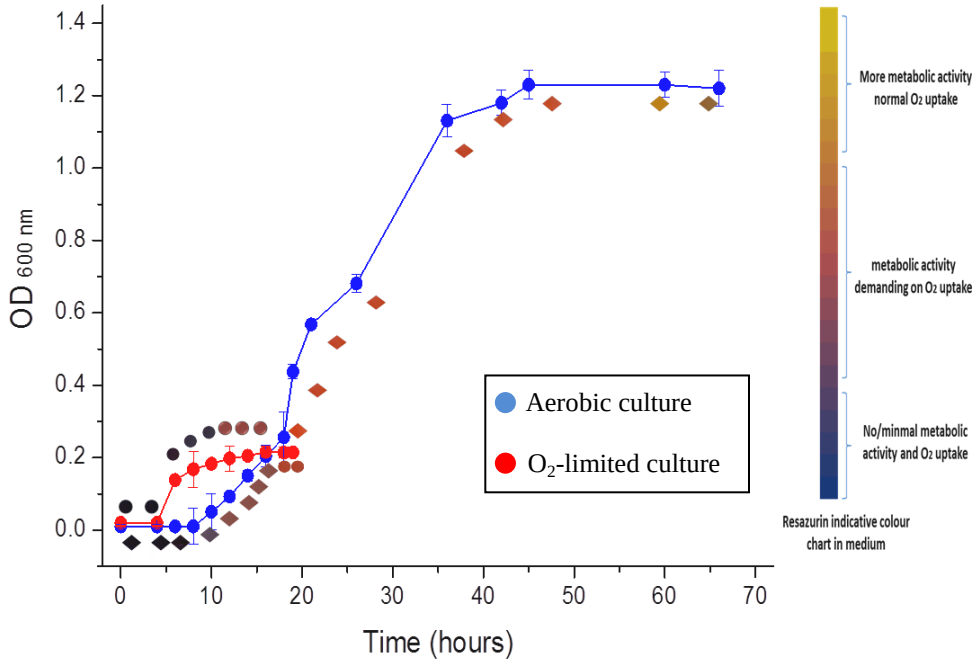

Figure 2.17: Growth of TML16 supplemented with a redox indicator (resazurin)

Growth was monitored by recording optical density (OD_{600}) values of aerobic, shaken cultures (blue) and O_2-limited, closed, shaken flasks with a head-space ratio of 0.5 (red). The colours of the medium during the growth curve correspond to the colour of the resazurin in the medium (resazurin indicative colour chart). During both aerobic and O_2-limited growth of TML16, resazurin reduction began after 12 h of incubation. TML16 attained maximal density (OD_{600} ~ 1.2) after 45 h of aerobic incubation but reached highest density (OD_{600} ~ 0.22) after 16 h of O_2-limited incubation. Error bars represent ± SEM of each point.

2.4. Discussion

The genes involved in the expression of the cytochrome *bd*-I oxidase are *cydA* and *cydB*, encoding subunits I and II of cytochrome *bd*-I oxidase. Nevertheless, cloning the whole operon *cydABDC* was a necessity due to the fact that the *cydDC* genes, located immediately downstream of *cydAB* genes, are implicated in the assembly of a functional *bd*-type oxidase (195, 243-247). This suggested a functional association between cytochrome *bd*-I oxidase and the ABC transporter owing to the adjacent location of Mtb *cydAB* and *cydDC* genes (221). The *cydABDC* organization in Mtb (148) is parallel to that observed in *M. smegmatis* (253) and *Bacillus subtilis* (215, 307). However, Kana *et al* (2001) wrote that the *cydDC* genes in *M. smegmatis* may be expressed independently from *cydAB* owing to the intergenic space between *cydAB* and *cydDC* (253). Moreover, Green *et al* (1984) was able to express cytochrome *bd*-I oxidase in *E. coli* through cloning merely *cydAB* genes (308). In *Geobacillus thermodenitrificans*, a low GC Gram-positive bacterium, coexistance of the cytochrome *bd*-I and ABC transporter genes in the same plasmid was also not necessary (309). On the contrary, an aspect regarding the necessity of *cydDC* genes has been further emphasised recently in a study of *Corynebacterium glutamicum*, a high GC Gram-positive bacterium, that showed the importance of involving *cydDC* genes in the expression plasmid for *cydAB* overexpression (310).

Essentially, using highly parallel Illumina sequencing, Griffin *et al* (2011) precisely identified essential genes (151 genes) for Mtb viability. This study showed that all *cyd*-operon genes, *cydABDC*, are essential for Mtb viability (2). This contradicted a previous study which deemed only 81 genes to be essential through the use of microarrays, and which suggested that only *cydB* is essential for Mtb (116). Remarkably, Zhang *et al* (2012) who coupled high-density insertion libraries with deep sequencing showed a 97.1% level of agreement with the data of Griffin *et al* (2011) regarding essential Mtb genes (2, 166).

With regards to the expression conditions, appropriate signalling of the regulatory components may lead to levels of cytochrome *bd*-I or *bd*-II, under specific growth conditions, that are significant to the cells. As previousely mentioned, in *E. coli* cytochrome *bd*-I has different expression conditions to that of cytochrome *bd*-II. The

expression of cytochrome *bd*-I both in *E. coli* and Mtb was recorded during both aerobic and microaerophilic growth conditions (20, 212) whereas cytochrome *bd*-II was expressed under anaerobic or starvation conditions (217, 218, 290, 292). Herein, expression studies of the recombinant Mtb cytochrome *bd*-I oxidase (Mtb *bd*-I) in an *E. coli* mutant used the low O_2 tension as a stressful condition. The spectra data showed that Mtb *bd*-I was expressed moderately in aerobic conditions and excessively under oxygen-limiting conditions. The ratio of cytochrome *d* peak to the reference peak in TML16 was higher in O_2-limited (0.3) condition than in aerobic conditions (0.13). These findings are in accordance with previous observations of cytochrome *bd*-I expression conditions in *E. coli* (234, 311), in *M. smegmatis* (253) and in this study of the wild-type *E. coli* strain.

The induction of cytochrome *bd*-I oxidase was suggested to be at 1% air saturation in *M. smegmatis* (253), at 7% air saturation in *E. coli* (246) and during transition to anaerobiosis state in *B. subtilis* (312). However, the present data suggest that the induction of Mtb *bd*-I is observed during both oxygen-rich and oxygen-limited conditions (i.e. aerobic and O_2-limited). These results further contradict the suggestion of Shi *et al* (2005) that Mtb cytochrome *bd*-I is only induced at 1% air saturation (221).

SDS-PAGE analysis of Mtb *bd*-I showed expression of two bands, which have protein mass of around 52 kDa. However, these bands were indistinguishable in terms of gene identity on SDS-PAGE since the molecular weights of all *cydABDC* genes are relatively close to each other. The protein masses of Mtb *cydA*, *cydB*, *cydD* and *cydC* subunits are 53.83 kDa, 37.63 kDa, 54.8 kDa and 59.5 kDa, respectively. Cytochrome *bd*-I in *E. coli*, a transmembrane heterodimer protein, has one copy of each subunit with molecular weight of 58 kDa for subunit I and 43 kDa for subunit II (212). Therefore, according to the spectral analysis data that confirmed the expression of Mtb *bd*-I, we can suggest that the two expressed bands could represent Mtb *bd*-I subunits I and II. According to the transformed double-knockout (TML16) protein concentration, the proteins seemed to be overexpressed as even in a highly diluted sample, the proteins bands were clearly visible. This in turn confirmed the

aforementioned Kabashima *et al* (2009) finding that *cydDC* was necessary for *cydAB* over expression (310).

Spectral properties showed different heme peaks and ratios according to growth conditions or strain differences. Reduced minus oxidized difference spectra recorded at room temperature were used to analyze the cytochrome content of wild-type *E. coli* BL21(DE3) pLysS. During both aerobic and O_2-limited growth conditions, major absorbance peaks that were observed at 560, 596, and 629 nm were characteristic of *b*-, a_1-, and *d*-type cytochromes, respectively that represent a 'normal' *E. coli* spectrum (313, 314).

Importantly, the spectra of ML16 mutant strain lacked the heme-*d* features but showed absorbance peaks at 528, 557, and a discrete peak at 602 nm, a finding consistent with specific disruption of cytochrome *bd*-I. The discrete peak at 602 nm was reported as cytochrome aa_3 in other bacteria such as the *Thiobacillus novellus* (315), *Rhizobium leguminosarum* (316) and *Bradyrhizobium japonicum* (317). However, cytochrome aa_3 in *B. subtilis* (318) and in *M. smegmatis* (253) has a peak at 600 nm rather than 602 nm. Essentially, wild-type *E. coli* BL21(DE3) did not possess the genes that code for cytochrome aa_3 oxidase, *qoxABCD*. Siegel *et al* (1973) recorded similar peak at 602 nm during a study of NADPH-sulfite reductase of *E. coli*. However, it had not been designated to a specific cytochrome component (319). Accordingly, given that macromolecular reorganization of prosthetic groups and terminal oxidase subunits could give rise to alternate oxidases, terminal components of the respiratory chain cannot be inferred only from the genome sequence (253). Likewise, the *bb'*-type terminal oxidase in *B. subtilis*, which appeared to be *bd*-type (encoded by the *cydAB* genes), had the heme-*d* substituted by high spin heme-*b* (320). This might be the case for the present ML16 spectrum as despite the presence of endogenous cytochrome *bd*-II genes, the heme-*d* absorbance peak that was expected to be present at about 628 nm - 632 nm was not recorded (217, 218, 290, 292).

The ML16 strain was transformed with a plasmid carrying the entire Mtb *cydABDC* genes that led to restoration of heme-d_{631} absorbance peak, confirming that the Mtb *cydABDC* operon was able to functionally complement the cytochrome *bd*-I defect in the *E. coli* mutant (ML16) strain. Interestingly, Kana *et al* (2001) confirmed that the presence of a plasmid carrying Mtb *cydABDC* operon restored heme-d_{631} in a cytochrome *bd*-I defective *M. smegmatis* mutant strain (253). The heme-*d* absorbance peak (about 628 nm - 632 nm) is a characteristic of the cytochrome *bd*-I oxidase in *E. coli* (263) and *B. subtilis* (Winstedt et al., 1998). The signals at 558 nm and at 595 nm were presumably due to the low-spin heme b_{558} and the high-spin cytochrome b_{595} component of the cytochrome *bd*-type oxidase complex, as were reported in the well-studied *E. coli* (313) and *A. vinelandii* (321) oxidases.

A novel, but unexplained, observation is the red/brown pigmentation observed in TML16 cultures (aerobic and O_2-limited). This could be explained by the overexpression of heme-containing cytochromes and porphyrins, which was supported by the expression studies of TML16 showing an over expression of functional recombinant Mtb cytochrome *bd*-I oxidase. Ratledge (1999) suggested that the presence of porphyrins was the main reason behind the red colour in mycobacteria (322). Significantly, a hypoxic culture of *M. smegmatis*, with 0.6% oxygen saturation, was accompanied by a change in the coloration of the cells from a light yellow pigmentation to a red pigmentation. In turn, this infers the induction of the cytochrome *bd*-I oxidase and the machinery needed for its assembly and synthesis (i.e. porphyrin/heme and cysteine biosynthesis) (289).

Regarding the growth rate of the cells, during aerobic conditions, ML16 showed a higher growth rate, reaching its highest density (OD_{600} ~ 1.7) after 45 h compared to the BL21 (DE3) pLysS (reference strain) (OD_{600} ~ 1.5) after 42 h of incubation, and to the transformed strain TML16 that which hardly exceeded OD_{600} ~ 1.2 after 45 h of incubation. Nevertheless, the ML16 growth rate seemed more similar to the reference strain as it also reached OD_{600} ~1.5 after 42 h of incubation. Kana *et al* (2001) wrote that inactivation of *M. smegmatis cydA* and/or *cydB* genes had no discernible effect on the growth rate during exponential phase, when bacteria were grown aerobically at 21 or 5% air saturation. However, Kana *et al* (2001) observed a

significantly lower growth rate of *M. smegmatis cydA* mutant than that of wild-type, when bacteria were grown at 0.5 and 1% air saturation (253). Moreover, Cohen (2011) suggested that the reduction in the growth rate could be attributed to exposing the cells to oxygen limiting conditions (294). In contrast, data showed that during O_2-limited conditions, Ml16 demonstrated a similar growth rate to the reference strain reaching an OD_{600} of ~ 0.4 after 12 h of incubation. Therefore, results suggested that the air saturation inside the flasks during O_2-limited condition could be more than 1%. In turn, TML16 cells under oxygen-limiting condition exhibited a low growth rate in comparison with both mutant and reference strains, as it reached the highest density (OD_{600} ~ 0.22) after 16 h of incubation. The slow growth rate of TML16 during both oxygen-rich and oxygen-limited conditions might be due to the adaptation of the cells to synthesize a functional recombinant Mtb cytochrome *bd*-I oxidase alongside growing under oxygen limited condition.

To qualitatively evaluate the contribution of cytochrome *bd*-I to respiration in aerobic and O_2-limited conditions, resazurin was used as a visual indicator of the oxygen depletion in cultures (305) and as an indicator of the respiratory function. Raz reacts in the presence of oxygen, acids and functional dehydrogenases and oxidoreductases of viable organisms. Raz could be reduced by strict aerobes, facultative anaerobes such as *E. coli*, aerotolerant and microaerophile organisms, but not by strict anaerobes (305, 323, 324).

ML16 and the wild-type strain cultures were shown to reduce resazurin earlier than TML16. During both aerobic and O_2-limited growth conditions, the reduction of Raz was detected respectively after 8 h and 6 h post-inoculation for ML16 and the reference strain. TML16 cell cultures were observed to reduce Raz slower, taking 12 h of incubation to reduce during both O_2-limited and aerobic growth conditions. The oxygen depletion in TML16 culture was delayed due to the fact that the host cells needed longer time to express functional cytochrome *bd*-I. Geckil *et al* (2001) noted that oxygen uptake might be particularly strict when recombinant cells are involved. This is due to the fact that the presence of the plasmid is considered a burden because of the cellular resources required for maintaining and expressing plasmid genes. In addition, the plasmid may cause perturbations in cellular metabolism (325).

However, the presence of a plasmid (pLysS) in the reference strain did not hold it back from reducing Raz during earlier time of growth rate. This could be attributed to the fact that pLysS has no noticeable effect on growth rate (303). Expectedly, ML16 reduced Raz later than the wild-type due to the lack of cytochromes *bo*$_3$ and *bd*-I in ML16 cells. Notably, although ML16 did not show a heme-*d* absorbance peak of cytochrome *bd*-II, it demonstrated normal oxygen utilization with a colourless Raz in the medium observed, which might indicate aerobic respiration.

Significantly, the demand for oxygen uptake was sustained in TML16, resembling that of the reference strain. However, ML16 showed a short period of oxygen uptake demand before it reached the regular oxygen uptake phase. The ability of the Mtb *bd*-I to restore the reference strain phenotype (oxygen consumption) is attributed to its high affinity for oxygen. Bekker *et al* (2009) showed that cytochrome *bd*-I has a 10- and 20-fold-higher affinity for oxygen than cytochrome *bd*-II and cytochrome *bo*$_3$, respectively (290). Moreover, the high demand for O_2 by both TML16 and the reference strain could also be attributed to a potential factor related to its harbouring a plasmid construct (325). In accordance with the present data, Khosravi *et al* (1990) wrote that recombinant cells require more oxygen than plasmid-free cells (326). There are other factors that could affect the oxygen depletion in cultures, and in turn the resazurin status. For instance, the mode and vigour of agitation (33) were found to have an effect on the Raz status as well as the intense light (i.e. bright sunlight), which could lead to rapid photochemical decay of resazurin (327). However, these factors could be ruled out as they were fixed throughout this study experiments and intense light exposure was avoided.

Regarding the stationary phase (non-replicating phase) viability, unlike the reference strain, both aerobically and O_2-limited grown ML16 seemed to exhibit a stationary-phase viability defect as observed in *cyd* mutant strains of *E. coli* (295) and of *A. vinelandi* (328). Remarkably, TML16 cells did display a restoration of the loss of stationary phase viability, emphasising the significance of cytochrome *bd*-I during stationary phase. The ability of Mtb *bd*-I to restore cells viability during stationary phase was further confirmed in different heterologous expression system, the TMB44 system (Chapter IV). In addition, the mycobacterial *bd*-I oxidase was

required specifically for growth under extreme microaerophilia (253). Interestingly, this observation might indicate the involvement of Mtb *bd*-I in persister cell viability. Persister cells are non-replicating subpopulation of microbes that exist during the stationary phase and have the ability to survive exposure to bactericidal antibiotics (4). Nevertheless, significant expression of Mtb *bd*-I during aerobic conditions could indicate the ability of this enzyme to compensate the loss of other terminal oxidases.

In summary, the spectroscopic evidence provided herein confirms the presence of Mtb heme-*d*-containing cytochrome in the *E. coli* mutant strain, ML16. In this and other respects, the high affinity *cydAB*-encoded cytochrome *bd*-I oxidase of Mtb displayed spectral features analogous to the well-characterized *E. coli* cytochrome *bd*-I (213). In addition, cytochrome *bd*-I oxidase demonstrated its role as an essential oxygen scavenger and as an important respiratory component of Mtb with respect to maintaining cell viability during stationary phase. Stationary phase could include slowly-replicating, non-replicating and/or persister cells. This is in agreement with the Griffin *et al* (2011) sequencing study that confirmed Mtb cytochrome *bd*-I oxidase essentiality (2) for Mtb viability, and with Dhar and McKinney (2010) who identified *cydDC* essentiality for persister cells (24, 52).

Regarding limitation and recommendations of this chapter, monitoring oxygen consumption in the cultures was limited to visual qualitative assessment using Raz. Ideally, measuring the O_2 saturation of the cultures using an O_2 electrode sensor or rotometer would be recommended. Moreover, growing cells in a chemostat could act as an alternative way of culturing TML16 whereby all the parameters in the system could be monitored, including the dissolved O_2 tension (253). Initial characterizations of the recombinant Mtb cytochrome *bd*-I oxidase including steady state kinetic and drug susceptibility studies are described in the following chapter.

Chapter III

Biochemical and pharmacological characterization of *Mycobacterium tuberculosis* cytochrome *bd*-I oxidase

3.1. Introduction

The purpose of this study was to explore the kinetic properties of recombinant *Mycobacterium tuberculosis* cytochrome *bd*-I oxidase (Mtb *bd*-I) and to highlight the potential of this enzyme as a novel drug target, thus, optimistically, fuelling the drug discovery pipeline.

The respiratory chain of Mtb can function with a variety of different membrane-bound NADH dehydrogenases, including NDH-1, NDH-2, NDH-2A, and SDH as well as LDH, G3PDH, MDH and PDH dehydrogenases, on the electron input side. In contrast, the electron accepting components of the respiratory chain include two terminal oxidases (cytochrome bc_1-aa_3 super complex and cytochrome *bd*-I oxidase) as well as reductases (NRs and FRD). The link between the electron donating and the electron accepting enzymes are the membrane mobile quinones. Donor:quinone oxidoreductases (i.e. NADH:quinone oxidoreductase) and quinol:acceptor oxidoreductase, such as quinol:oxygen oxidoreductase for *bd*, are coupled together to generate simple electron transport chains, producing a PMF. Quinones are small membrane-entrapped lipophilic molecules that are freely diffusible, which can carry two electrons and two protons in the fully reduced state (quinol) (329). Decylubiquinol (dQH_2), ubiquinol-1 (Q_1H_2) and ubiquinol-2 (Q_2H_2) are examples of synthetic quinols that are frequently utilised in enzymological studies (Figure 3.1).

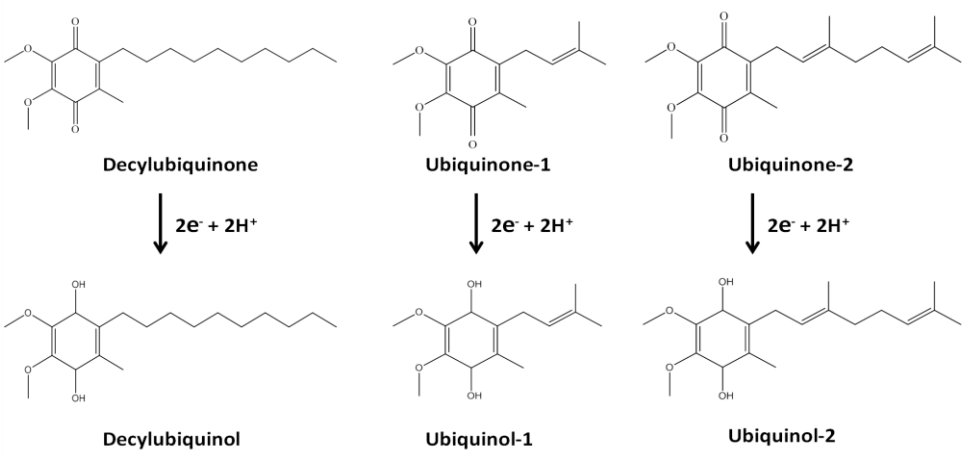

Figure 3.1: Structures of decylubiquinone, ubiquinone-1 and ubiquinone-2 and their reduced quinol counterparts

It is well known that utilization of quinol as an electron donor by cytochrome *bd*-I oxidase (*bd*-I) is species-specific. For example, *bd*-I can only oxidize menaquinol (MQH_2) in *B. stearothermophilus* and ubiquinol (UQH_2) in *A. vinelandii*. In contrast, *E. coli bd*-I can oxidize both UQH_2 and MQH_2 (255, 256), as upon changes from aerobic to anaerobic growth conditions, *bd*-I replaces UQH_2 by MQH_2 (330). Menaquinone (MQ) is the substrate in Mtb, consisting of nine isoprene units (MQ-9) while in *E. coli* it contains 8 units (MQ-8) (195, 202, 331). *In vitro*, beside the physiological substrates, short chain ubiquinols such as dQH_2, Q_1H_2 and Q_2H_2 as well as artificial electron donors, N,N,N′,N′-tetramethyl-p-phenylenediamine (TMPD) can be oxidized by *bd*-I (53, 212, 213).

Viewing the reaction pathway or catalytic cycle of an enzyme helps in understanding the enzyme catalysis and thus in planning the best inhibition mechanism of the enzyme. Cytochrome *bd*-I oxidase is an integral membrane protein with exposed surfaces to cytoplasmic and periplasmic compartments. Cytochrome *bd*-I oxidase is a terminal oxidase that oxidizes quinol/menaquinol and reduces O_2 to water. Three hemes (heme b_{558}, heme b_{595} and heme *d*) form the enzyme. Heme b_{558} is associated with subunit I of *bd*-I and is involved in QH_2 oxidation. Heme *d* is the site for capturing and, subsequently, reducing O_2 to H_2O and is predicted to be located in the second subunit (subunit II) of *bd*-I, near the periplasmic surface (195, 257, 332). Both heme b_{595} and heme *d* are located close to each other forming a di-heme active site and potentially can bind ligands; heme *d* has a higher affinity for ligands than heme b_{595}, resulting in binding of ligands to heme *d* (211, 333). The chemistry catalyzed by the enzyme is simple:

$$4e^{-1} + 4H^{+}_{IN} + O_2 \longrightarrow 2H_2O + 4H^{+}_{out}$$

The electron transfer sequence in cytochrome *bd*-I is thought to be $QH_2 \rightarrow$ heme b_{558} $\rightarrow$ [heme b_{595} $\rightarrow$ heme *d*] $\rightarrow$ O_2. Four protons per O_2 are taken up from the cytoplasmic side and four are released to the periplasmic side, thus the H^+/e^- ratio is 1. Simultaneously, reduction of O_2 to water and oxidation of quinol to quinone, performed along with the transfer of four electrons through heme b_{558} and b_{595} to the O_2 reducing site, result in the generation of a PMF by trans-membrane charge separation, which subsequently may drive ATP synthesis by the ATP synthetase (332). Generation of a PMF by trans-membrane charge separation is a consequence

of releasing protons, generated from the quinol oxidation, into the positive (periplasmic) side of the membrane, and taking protons, used to convert O_2 to H_2O, from the negative (cytoplasmic) side (205, 206). The proposed model of cytochrome *bd*-I oxidase catalytic mechanism is depicted in the following figure (Figure 3.2).

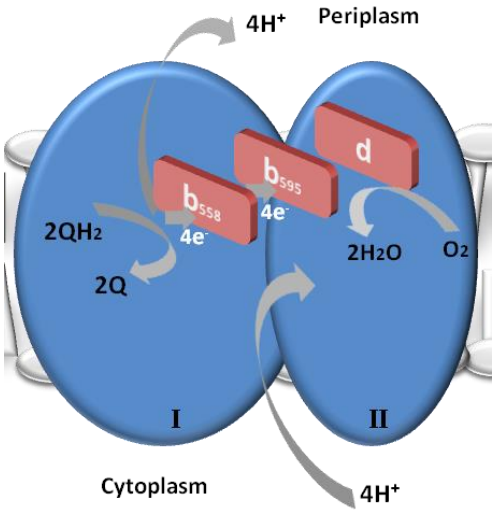

Figure 3.2: Proposed cytochrome *bd*-I model adapted from (211)

Enzyme reactions can be studied under steady state conditions. Steady state kinetics refers to a balance situation between the rate of Enzyme-Substrate (*ES*) formation and the rate of *ES* complex disappearance. During the initial phase of an enzyme reaction, the initial velocity, a slope of the product (or substrate) concentration versus time plot, typically lasts until about 10 to 15% of the initial substrate concentration has been converted into product; afterwards the velocity slows down. Enzymes can catalyse monosubstrate, bisubstrate and multiple substrate reactions. Monosubstrate reaction, the most simple enzyme reaction, involves converting a single substrate to a single product. A bisubstrate reaction involves two substrates, utilized to form one or more products. A multiple substrate reaction includes more than two substrates combining to form products (334, 335).

Under physiological conditions cytochrome *bd*-I activity varies; the detergent nature in which the purified enzyme is solubilised has an influence on its activity. For instance, solubilising *E. coli bd*-I in octylglucoside detergent rendered the enzyme inactive. However, *E. coli bd*-I shows high activity in Tween-20 (211, 336).

Concerning the importance of the pH profile, pH is known to affect the charges on the amino acids residues within the active site, resulting in structural changes of the catalytic side. Subsequently, the substrate may no longer fit into enzyme active site. Moreover, changes in pH could break the ionic bonds that stabilize the functional structure of the enzyme (194, 335). The conserved amino acids residues in the *bd*-family are His19, His186 and Met393, Arg448, and Glu99, Glu107, Ser140, Lys252 and Glu257, of which the latter two residues are involved in QH_2 binding (211, 337). The conserved amino acids residues in the *bd*-family could participate in critical proton transfer reactions and in stabilizing charges during the transition state (334).

Inhibiting the electron transport chain components of Mtb is an attractive chemotherapeutic goal as demonstrated by the diarylquinoline: TMC207 drug, targeting the mycobacterial ATP synthase complex (4, 274, 338, 339). The fact that Mtb *bd*-I, has no counterparts in mammalian mitochondria, and that it is essential for Mtb viability renders this component attractive as a drug target (Chapter 2.4) (2, 211).

Different classes of inhibitors were found to be potent against quinol oxidases, such as the natural antibiotic gramicidin S and the quinolone-type inhibitors, aurachins C and D (Figure 3.3). Derivatives of aurachin compounds showed that the critical core of the compounds is the ring structure. The compounds' effectiveness is maintained upon replacing the natural polyisoprenyl side chain with a simpler saturated aliphatic side chain; as the chain length of the R group increased, little systematic variations of inhibitor potency were observed (264, 265). A relatively similar scenario was adopted in a drug discovery programme with the objective of identifying hit compounds against *Plasmodium falciparum* NADH:ubiquinone oxidoreductase (PfNDH2) (340, 341). Based on structure-activity relationship (SAR) development, this program succeeded in identifying a novel quinolone-type inhibitor against PfNDH2. A further programme (MtbNDH2 programme) ensued with the objective of identifying selective inhibitors against NDH-2: NADH dehydrogenase, a novel enzyme target within the Mtb bacilli, adopting the same strategy as the PfNDH2 programme.

A) B)

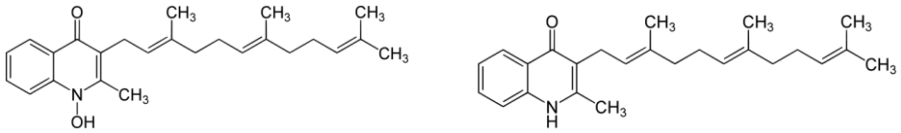

Figure 3. 3: A) aurachin C structure. B) aurachin D structure

1-hydroxy-2-dodecyl-4(1H) quinolone (HDQ) is a known inhibitor of PfNDH2 and was the core for initiating the chemoinformatics approach with the purpose of selecting compounds for high-throughput screening (HTS) (342). Therefore, quinolone-type compounds (from in house libraries) were examined against Mtb *bd*-I and Mtb H37Rv. The quinolone core (Figure 3.4) of these compounds has been the key target for SAR development investigating, the relationship between the chemical structure of a compound and its biological or pharmacological activity. SAR can be considered by viewing a series of molecules, each with a slightly different structure, and then observing the biological activity with each structural variation.

A) B)

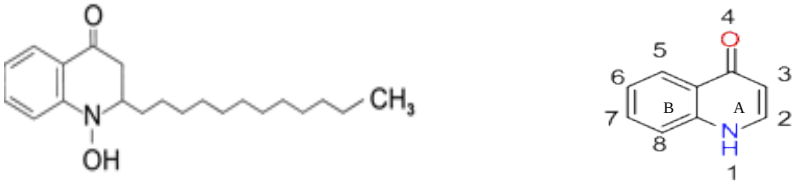

Figure 3.4: A) HDQ structure. B) The quinolone core

Eliminating the pathogenic organism is the ultimate clinical outcome of any drug designed for this purpose. Therefore, studying the pharmacokinetic and the pharmacodynamics of inhibitors as well as the kinetics of inhibitor interaction with the enzyme provides a meaningful prediction of drug efficacy *in vivo*. In this work, basic kinetic parameters of the Mtb cytochrome *bd*-I catalytic reaction were measured and compared to cytochrome *bd*-I from previously studied bacteria. Moreover, the IC_{50s} of quinolone-type inhibitors against Mtb *bd*-I and the inhibitor-enzyme interaction were studied.

3.2. Material and methods

3.2.1. Membrane preparations

Following the protocol of Fisher *et al* (2009), membrane preparations were carried out as detailed in Chapter (2.2.17) (209). It is worth mentioning that all assays were carried out using the membranes of the TML16 strain, grown under O_2-limited conditions, as it has the highest catalytic activity. The Mtb *bd*-I of the TML16 strain, grown under aerobic condition, was also examined for steady-state kinetics with dQH_2 to evaluate Mtb *bd*-I under both growth conditions (Figure 3.6, B).

3.2.2. Preparation of 50 mM KPi, 2 mM EDTA, pH 7.5 buffer

For kinetic assays 50 mM KPi, 2 mM EDTA, pH 7.5 buffer was used throughout experiments, unless otherwise stated. This buffer was prepared following the previously described protocol (section 2.2.16).

3.2.3. Preparation of decylubiquinol (dQH_2) and ubiquinol-2 (Q_2H_2)

Preparation of both dQH_2 and Q_2H_2 were performed according to the protocol of Fisher *et al* (2004) (343). Briefly, 10 mg of 2,3-dimethoxy-5-methyl-n-decyl-1,4-benzoquinone (decylubiquinone) or 10 mg of 2,3-dimethoxy-5-methyl-6-geranyl-1,4-benzoquinone (ubiquinone-2) (Sigma Aldrich, UK), were dissolved in 400 µl of nitrogen-saturated hexane. An equal volume of aqueous 1.15 M sodium dithionite was added, and the mixture shaken vigorously until colourless. The upper, organic phase was collected, the dQH_2 or Q_2H_2 were extracted off hexane and the solvent was evaporated under N_2. Subsequently, dQH_2 or Q_2H_2 were dissolved in 100 µl of 96% ethanol (acidified with 10 mM HCl). Concentrations of dQH_2 or Q_2H_2 were determined spectrophotometrically on a Cary 300 Bio UV/visible spectrophotometer (Varian, UK) from absolute spectra, using $\varepsilon_{288-320}$ = 4.14 $mM^{-1}.cm^{-1}$. Both dQH_2 and Q_2H_2 were stored at -80 ^{o}C and used within two weeks.

3.2.4. Preparation of ubiquinol-1 (Q_1H_2)

Preparation of Q_1H_2 was based on the protocol of Kihira *et al* (2012) (344) with modification where 1 ml of 40 mM ubiquinone-1 (Sigma Aldrich, UK) solubilised in DMSO was diluted 3-fold with 100 mM potassium phosphate buffer (KPi, pH 7.5). Sodium dithionite powder was added to this solution to reduce ubiquinone-1 until the yellow colour disappeared. The Q_1H_2 formed was extracted with hexane and the solvent was evaporated under N_2. Q_1H_2 was dissolved in 100 µl of 96% ethanol (acidified with 10 mM HCl). The concentration of Q_1H_2 was calculated spectrophotometrically on a Cary 300 Bio UV/visible spectrophotometer (Varian, UK) from absolute spectra, using $\varepsilon_{288-320}$ = 4.14 $mM^{-1}.cm^{-1}$. Q_1H_2 was stored at -80 ^oC and used within two weeks.

3.2.5. Steady state kinetic assays

Oxidation of quinols (dQH_2, Q_1H_2 and Q_2H_2) by Mtb *bd*-I was measured spectrophotometrically at 283 nm on a Cary 300 Bio UV/visible spectrophotometer (Varian, UK). Total reaction volume in a 1 cm pathlength quartz cuvette was 700 µl, containing 698 µl of (50 mM KPi, 2 mM EDTA, pH 7.5) buffer and 2 µl of the crude recombinant membrane to a final concentration of 3 $\mu g.ml^{-1}$. Following thorough agitation of the cuvette contents and recording the absorption spectrum, quinol was added (to a final concentration of 5 - 98 µM) and kinetic data collected for 4 min. Initial rates (computer-fitted as zero-order kinetics) were measured as a function of quinone concentration, using ε_{283} = 8.1 $mM^{-1}cm^{-1}$. Plots of initial velocity as a function of substrate concentration were fitted using the Michaelis-Menten equation (dQH_2 and Q_1H_2):

$$v = \frac{V_{\max}[S]}{K_m + [S]}$$

However, for Q_2H_2 oxidation, a modified *ping-pong bi-bi* mechanism was used for Mtb *bd*-I as per Matsumoto *et al* (2006) (345). The formula was established by Dr. Nick Fisher.

$$v = \frac{V_{\max}([S])2}{K_m 2 + K_m[S] + \left(1 + \left(\frac{[S]}{K_i}\right)n\right)[S]2}$$

Data were analysed using a Michaelis-Menten hyperbola and a modified *ping-pong bi-bi* mechanism equation in order to determine K_m and V_{max} values using Origin 8.5 (OriginLab Corp., USA). The mathematical term V_{max} refers to the maximal velocity obtained at infinite substrate concentration whereas K_m (commonly stated to as the Michaelis constant) refers to the substrate concentration that leads to half saturation of the enzyme active sites under steady state conditions (334, 335).

3.2.6. pH assay

To investigate the role of acid base catalysis in Mtb *bd*-I oxidase-catalyzed reactions, the pH dependence of kinetic parameters was determined by measurement of dQH_2 oxidation rates across the pH range of 5.5 - 8.5, employing a mixed buffer system containing 2-(*N*-morpholino)ethanesulfonic acid (MES), 4-(2-hydroxyethyl)-1-piperazineethanesulfonic acid (HEPES), and *N*-Tris(hydroxymethyl)methyl-3-aminopropanesulfonic acid (TAPS). UV-visible spectroscopic analysis of freshly prepared membranes was carried out on a Cary 300 Bio UV/visible spectrophotometer (Varian, UK). Total reaction volume in a 1 cm pathlength quartz cuvette was 700 µl, which contained 2 µl of membrane (final concentration 3 $\mu g.ml^{-1}$) suspended in 698 µl of different pH (40mM HEPES/MES/TAPS) buffer. Following thorough agitation of the cuvette contents, a UV-visible absorption spectrum was recorded at 283 nm, to which a fixed concentration of 50 µM dQH_2 was added to initiate the reaction. Specific catalytic activity ($\mu mol.min^{-1}.mg^{-1}$) was calculated using $\varepsilon_{283} = 8.1\ mM^{-1}.cm^{-1}$.

3.2.7. Detergent assays

The effect of detergents on Mtb *bd*-I oxidation rates of dQH_2 were measured spectrophotometrically using a Cary 300 Bio UV/visible spectrophotometer (Varian, UK) and a quartz cuvette of pathlength 1 cm. Assays of total reaction volume 700 µl containing 698 µl of (50 mM KPi, 2 mM EDTA, pH 7.5) buffer, 2 µl of the membranes (final protein concentration of 11.3 $\mu g.ml^{-1}$) and 0.01% (v/v) of 3-[(3-cholamidopropyl)dimethylammonio]-1-propanesulfonate (CHAPS), *n*-dodecyl-β-D-maltopyranoside (DDM), cholate, deoxycholate, Triton X-100 or Tween-80 detergents. Following thorough agitation of the cuvette contents and recording of a UV-visible absorption spectrum at 283 nm, 2.3 µl of 15 mM dQH_2 (final

concentration of 50 μM dQH_2) was added to the cuvette to initiate the reaction. Specific catalytic activity (μmol.min^{-1}.mg^{-1}) was calculated using ε_{283} = 8.1 mM^{-1}.cm^{-1}.

3.2.8. Chemoinformatics compound selection

The best 18 compounds against PfNDH2 of the mitochondrial ETC of *Plasmodium falciparum* (340) were tested against Mtb *bd*-I and Mtb H37Rv. Subsequently, 5 more compounds were chosen arbitrarily from a program established to identify hits against NDH2 complex of *Mycobacterium tuberculosis*, which were RKA-259, SCR-8-12, RKA-307, RKA-310 and MTD-403.

3.2.8.1. Preparation of inhibitor stock solutions

10 mM inhibitor stocks were prepared according to their solvent solubility (Table 3.1). Inhibitor stocks were prepared and kept at -20 ^{o}C for no longer than 1 month. Final dilutions were made with culture medium (7H9 MiddleBrook) or with DMSO and freshly prepared prior to studies being carried out. Final concentration of DMSO was maintained below 1% throughout experiments unless otherwise stated.

Table 3.1: List of the inhibitors used in inhibition studies for phenotypic profiling of H37Rv strain of Mtb

Compound	Molecular weight ($g.mol^{-1}$)	Solvent	Source
Isoniazid	137.14	DMSO	Sigma Aldrich, UK
Rifampicin	822.94	DMSO	Sigma Aldrich, UK
Ethambutol	277.23	DMSO	Sigma Aldrich, UK
Streptomycin	728.69	H_2O	Sigma Aldrich, UK
Metronidazole	171.15	DMSO	Sigma Aldrich, UK
CK-2-63	411.37	DMSO	In house synthesis in collaboration with Prof Paul O'Neill, Department of Chemistry, Uni. of Liverpool)
CK-3-22	412.36	DMSO	In house synthesis
CK-2-88	325.40	DMSO	In house synthesis
CK-3-23	339.43	DMSO	In house synthesis
CK-3-14	346.35	DMSO	In house synthesis
RKA-307	318.41	DMSO	In house synthesis
RKA-310	348.44	DMSO	In house synthesis
RKA-259	442.39	DMSO	In house synthesis
RKA-41	602.72	DMSO	In house synthesis
RKA-70	395.37	DMSO	In house synthesis
RKA-73	411.37	DMSO	In house synthesis
SCR-8-12	361.32	DMSO	In house synthesis
LT-9	343.39	DMSO	In house synthesis
SL-2-25	396.36	DMSO	In house synthesis
WDH-1U-10	403.86	DMSO	In house synthesis
WDH-1W-5	385.34	DMSO	In house synthesis
WDH-2A-9	399.37	DMSO	In house synthesis
GN-171	467.44	DMSO	In house synthesis
OB-231	428.41	DMSO	In house synthesis
OB-258	444.41	DMSO	In house synthesis
PG-128	381.35	DMSO	In house synthesis
PG-203	411.37	DMSO	In house synthesis
1-hydroxy-2-dodecyl-4(1H) quinolone	329.48	Methanol	In house synthesis
Potassium cyanide	65.12	Methanol	Sigma Aldrich, UK

3.2.8.2. Enzyme inhibition assays

Determination of IC_{50s} values for the inhibitors against Mtb *bd*-I were performed using a Cary 300 Bio UV/visible spectrophotometer (Varian, UK), and a quartz cuvette of pathlength 1 cm. Assays, of total volume 700 µl, were carried out at room temperature containing assay buffer (50 mM KPi, 2 mM EDTA, pH 7.5) and fixed concentration of membranes (3 $\mu g.ml^{-1}$) and inhibitors, which were added prior to reaction initiation with 50 µM dQH_2. IC_{50} values were calculated from plots of log dose *vs* oxidation rate using a four parameter logistic function (y = m1+(m2-m1)/(1+(m0/m3)^m4); m1=0.1; m2=150; m3=1; m4=1), using Origin 8.5 software (OriginLab Corp., USA) and initial rates were measured as a function of quinone concentration, using ε_{283} = 8.1 $mM^{-1}cm^{-1}$.

3.2.8.3. Competition assays, Lineweaver-Burk and Eadie-Hofstee Plots

Determination of K_m and V_{max} values of Mtb *bd*-I in the presence of two different inhibitor concentrations were performed using the aforementioned steady-state kinetic assays (section 3.2.5) with and without the addition of fixed concentration of inhibitors prior to reaction initiation. In order to examine the type of some inhibitors, i.e. whether they were competitive, non-competitive or uncompetitive inhibitors, Lineweaver-Burk and Eadie-Hofstee plots were generated. The Lineweaver-Burk plot is generated by plotting the reciprocal velocity (1/v) against the reciprocal substrate concentration (1/S) at two or more values of inhibitor concentrations. In contrast, the Eadie-Hofstee plot is generated by plotting the initial velocity (v) against the value of initial velocity over substrate concentration (v/[S]) at two or more values of inhibitor concentrations. Both Lineweaver-Burk and Eadie-Hofstee plots linearize the Michaelis–Menten equation and are considered useful means to present data graphically and thus identify the type of inhibition. However, the Eadie-Hofstee plot, unlike the Lineweaver-Burk plot, distributes points evenly by giving equal weight to data points in any range of substrate concentration or reaction velocity (194, 335).

3.2.9. Culture of *Mycobacterium tuberculosis*

3.2.9.1. Preparation of media:

3.2.9.1.1. Middlebrook 7H9 broth

Middlebrook 7H9 Broth (BD Diagnostic, UK) was enriched with 0.2% (v/v) glycerol, 0.05% (v/v) Tween® 80 and 10% (v/v) ADC (Albumin Dextrose Catalase) before being filtered through a sterile bottle top filter unit with a 0.22 µm membrane (Fisher Scientific, UK). ADC is an enrichment supplement composed of albumin, dextrose and catalase, constituents essential for mycobacterial growth.

3.2.9.1.2. Middlebrook 7H11 agar plate medium

Middlebrook 7H11 Agar (BD Diagnostic, UK) plates were supplemented with 0.2% (v/v) glycerol. 10% (v/v) OADC (Oleic Albumin Dextrose Catalase) was added when the medium had cooled below 50 °C, but prior to setting. OADC is an enrichment supplement composed of oleic acid, albumin, dextrose and catalase, constituents essential for mycobacterial growth.

3.2.9.2. General considerations regarding Mtb culturing

The Advisory Committee on Dangerous Pathogens (ACDP) has categorized *Mycobacterium tuberculosis* as hazard group 3. Within a containment Level 3 laboratory, a Nuaire Labguard Class II biological safety cabinet (Nuaire, USA) was for all work involving viable Mtb.

Mtb cultures were safely contained inside a Bio Transport™ Carrier box (Nalgene®, USA) inside the incubator and during moving the cultures from the incubator to the safety cabinet and vice versa. All waste generated was immersed in a solution of 5% (v/v) of Surfanios before being autoclaved. Surfanios (Anios lab, France) was used as disinfectant due to its superior ability to sterilise mycobacteria.

3.2.9.2.1. Mtb strain and growth media

Mtb strain H37Rv (ATCC#25618) was maintained in Middlebrook 7H9 Broth or Löwenstein-Jensen slopes (BD Diagnostic, UK) at 37 °C in a 5% CO_2 HERACell 150 CO_2 incubator (Thermo Scientific, UK). The continuous sub-culture of Mtb in solid or liquid medium was avoided as *in vitro* culture mutations might occur frequently due to prolonged incubation (346).

3.2.9.2.2. Culturing Mtb from frozen stocks

Mtb was retrieved from -20 °C and allowed to defrost at room temperature. 50 µl of Mtb stock was inoculated directly into 10 ml of Middlebrook 7H9 broth. Simultaneously, a pre-warmed Löwenstein-Jensen slope was inoculated using a 10 µl disposable loop (NUNC, UK) as a cell reservoir and to eliminate the presence of any contamination. Mtb cultures were incubated at 37 °C in a 5% CO_2 HERACell 150 CO_2 incubator (Thermo Scientific, UK). Following 2-3 weeks growth, an isolated Mtb colony was transferred from the slope into a 50 ml Falcon tube containing 10 ml of Middlebrook 7H9 both. The culture was vortexed and subsequently incubated for a minimum of 2 weeks before being used. The remaining Mtb in the defrosted vial were discarded in 5% (v/v) Surfanios.

3.2.9.2.3. Mtb aerobic cultures

Mtb inoculum (100 µl) was transferred to a 50 ml Falcon tube containing 10 ml of Middlebrook 7H9 broth. The culture was vortexed and incubated for a minimum of 2 weeks at 37 °C in a 5% CO_2 incubator before being used. The aerobic culture was discarded after 8 weeks of incubation.

3.2.9.2.4. Hypoxia model of growth: cultures grown in limited oxygen condition

The Wayne model of growth was adapted for Mtb growth in oxygen limited conditions (347). The creation of a microaerophilic environment (limited aeration) was attained through reducing the head-space ratio to 0.5, and 375 µl of the log-exponential phase Mtb were cultured in 50 ml Falcon tubes containing 37.5 ml of

Middlebrook 7H9 Broth. Each tube contained an autoclaved Polytetrafluoroethylene-coated (PTFE-coated) magnetic stirring bar (VWR International) with 8 × 5 mm dimensions. Subsequently, tube was closed tightly and sealed with Parafilm® (Pechiney Plastic Packaging Company, USA). Cultures were incubated in a 5% CO_2 incubator at 37 °C, stirring at 120 rpm on a Biostir 4 magnetic stirrer (Wheaton Industries Inc, USA) (282).

3.2.9.2.5. Mtb growth curves

In order to plot growth curves for aerobic Mtb cultures (Chapter 3.2.9.2.3), the culture turbidity was monitored twice a week at 600 nm using a WPA CO 8000 Biowave cell density meter (Biochrom, UK). The generation time, defined as the time for Mtb cells to double in number, was assessed by plotting a curve of time versus the OD_{600} values of the culture.

With the purpose of monitoring the growth of Mtb hypoxic cultures, a set of 19 cultures were made following the aforementioned method (section 3.2.9.2.4) and used to monitor the growth of the hypoxic culture. At selected times, one tube was opened and an aliquot of culture was collected before checking the turbidity at OD_{600} using the portable WPA CO 8000 Biowave cell density meter (Biochrom, UK). Once the culture was opened and used, it was discarded.

Assuring the same provenance of bacteria, a 2 week culture of Mtb at OD_{600} ~ 0.9 was selected and used throughout all experiments. The generated growth curves (Appendix I, Figures A - D) were used as additional information about the growth rate of aerobic and hypoxic Mtb cultures that were used in this thesis.

3.2.10. *Mycobacterium tuberculosis* drug sensitivity assays

Mtb drug sensitivities were determined using Mtb drug sensitivity assay, microplate alamar blue assay (MABA assay) as per Hartkoorn *et al* (2007) and Warman *et al* (2012) (282, 348) with modification. All compounds were initially prepared in 400 µM in DMSO. Serial dilutions of each compound were made in DMSO, of which 2.5 µl were plated in triplicate to wells of a 96-well microplate (NUNC, UK) containing

47.5 µl growth medium. Compounds were plated alongside drug-free controls containing growth medium with 2.5% DMSO and positive controls containing supra-IC_{90} concentrations of isoniazid. Outer wells of assay plates contained sterile H_2O with the purpose of reducing the evaporation over the course of the experiment.

Subsequently, Mtb culture (aerobic or hypoxic) was diluted to the turbidity of a McFarland Standard number 1 (Pro-Lab Diagnostics, UK) (OD_{600} = 0.3), corresponding to a bacterial concentration of 3×10^8 colony forming units per ml ($cfu.ml^{-1}$), which was further diluted to obtain a final concentration of 1×10^7 $cfu.ml^{-1}$. All dilutions were made using Middlebrook 7H9 Broth. Mid-log phase Mtb diluted to $1x10^7$ $cfu.ml^{-1}$ (50 µl) were plated in all wells, except the wells that contained sterile H_2O. Plates were incubated for 7 days at 37 °C in a CO_2 incubator.

Afterwards, 20 µl 2:1 alamarBlue®:Tween 80 was added to the plates and further incubated for 24 hours. AlamarBlue® solution (ABD Serotec, USA) was used as indicator of Mtb growth as growth can be observed as a change in the colouration of the alamarBlue® solution. Afterwards, 10% paraformaldehyde (Sigma Aldrich, UK) was freshly prepared and filtered through a 0.22 µm pore filter before being added to each well of sterilise plates. It is important to filter 10% paraformaldehyde solution in order to eliminate particles that could affect the photometric reading of the plate. Following two hours of plate incubation with 10% paraformaldehyde, plates were wiped thoroughly with 5% (v/v) Surfanios and assay results were determined by measurement of well absorbance at 570 nm and 600 nm using an Opsys MR™ Microplate Reader (Dynex Technologies, USA). Using these data and drug-free wells data, the half-maximal inhibitory concentration (IC_{50}) for each compound was calculated. The IC_{50} represents the concentration of a drug which causes 50% of growth inhibition. The IC_{90} (90% inhibitory concentration) refers to the concentration of drug which causes 90% of growth inhibition. IC_{50} values were calculated from plots of log dose *vs.* percentage of growth fitted with a four parameter logistic function (Origin 8.5 software).

For anaerobic cultures, plates were prepared as described for aerobically grown Mtb and subsequently were sealed within GasPak EZ pouches (BD, UK) containing an indicator to confirm the maintaining of anaerobic conditions over the course of the

experiment. Afterwards, plates were incubated anaerobically at 37 °C in a CO_2 incubator for 7 days and subsequently were moved to an aerobic environment and incubated for a further 7 days. Plates were assayed (addition of alamarBlue® and 10% paraformaldehyde) as previously described for aerobic cultures. In addition to isoniazid controls, metronidazole controls were included to confirm anaerobic conditions had been achieved (139). IC_{50} values of anaerobic cultures were calculated in the same manner as for aerobic cultures.

3.2.11. Time-kill studies

Time-kill studies were carried out using the method of Warman *et al* (2012) (282). A mid-log phase aerobic Mtb H37Rv culture (Chapter 3.2.9.2.3) was diluted to approx. $1x10^7$ cfu.ml^{-1} and subsequently added to equal volumes of drug-containing growth medium in the wells of a 24-well plate. Drugs were present at a final concentration of 5x IC_{90} (90% inhibitory concentration), as determined from modified MABA assays (Tables 3.3 and 3.5). A drug-free control was included in order to monitor normal culture growth. After 1, 2, 4, and 7 days, aliquots of the cultures were withdrawn and centrifuged at 10,000 *g* for 10 min. Pelleted materials were resuspended in drug free Middlebrook 7H9 media (lacking Tween-80 and ADC). Subsequently, serial dilution (1:10 - 1:10^6) were made before plating to solid growth medium (Middlebrook 7H11 agar plates) (Becton Dickinson UK Ltd, Cowley, Oxford, UK) supplemented with 10% OADC, 0.2% (v/v) glycerol, and 0.05% (v/v) Tween-80). An aliquot of day 0 drug-free inoculum was similarly processed to determine the initial bacterial load of all wells. After 14 days of incubation at 37 °C in a CO_2 incubator, cfu.ml^{-1} values were determined by colony counting.

3.2.12. Statistical analysis

To study the significance of the presence of different detergents on Mtb *bd*-I activity, Mann-Whitney U test was applied whereas spearman's correlation function was applied to study the association between aerobically cultured Mtb H37Rv and enzyme IC_{50} data using GraphPad 5 Software (USA).

3.3. Results

3.3.1. Detergent assay

The activity of Mtb *bd*-I was examined in the presence of different detergent types. There was an increase in Mtb *bd*-I activity in the presence of 0.01% of cholate, deoxycholate, CHAPS and DDM whilst the presence of Triton X-100 and Tween-80 led to noticeable decreases in activity (Figure 3.5). The effects of these detergents were assessed for the double-knockout *E. coli* strain (ML16) as well and showed that detergents did not have any effect on dQH_2 oxidation activity, confirming the expression of Mtb *bd*-I in the transformed double-knockout *E. coli* strain (TML16).

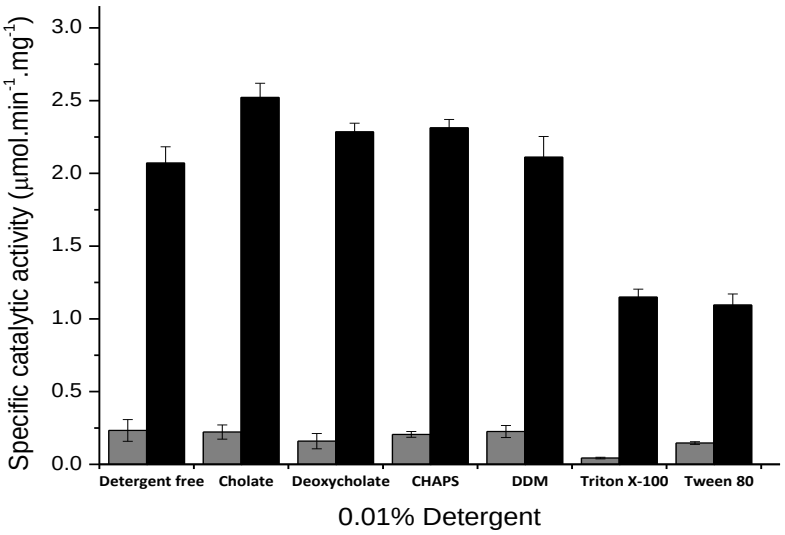

Figure 3.5: The effect of detergents on Mtb *bd*-I activity in 50 mM KPi, 2 mM EDTA, pH 7.5 buffer

The transformed double-knockout *E. coli* strain, TML16 (dark grey bars), showed increases of Mtb *bd*-I activity in the presence of 0.01% cholate, deoxycholate, CHAPS or DDM but a notable decrease in the presence of Triton X-100 and Tween-80. The effect of detergents was also examined on the double-knockout *E. coli* strain, ML16 (light grey bars). The values are the average of experimental triplicates ± SEM. The data showed no significant effect between the presence and the absence of detergent ($P > 0.05$) (GraphPad 5 Software, USA).

3.3.2. pH assay

To determine the most favourable conditions for kinetic studies of Mtb *bd*-I, the optimum pH was examined (Figure 3.6). The pH dependence of the dQH_2 Mtb *bd*-I oxidase activity showed a bell-shaped curve from which the greatest Mtb *bd*-I activity was at pH 7.5, but low activity values were recorded at more acidic and alkaline pH values.

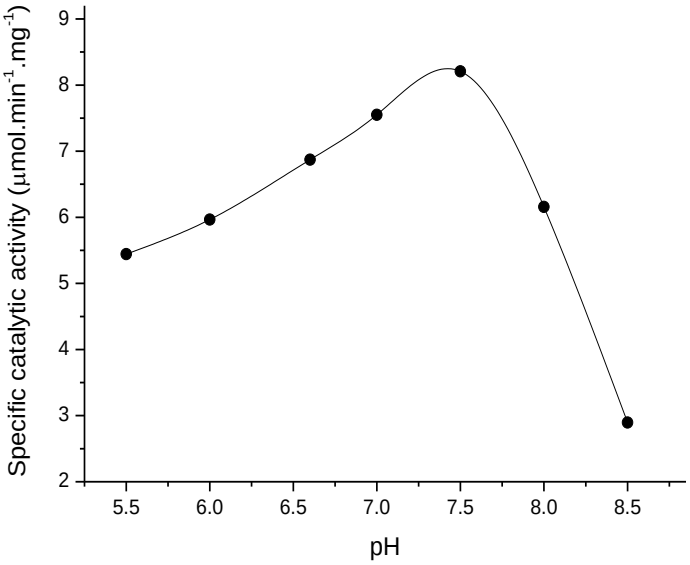

Figure 3.6: pH dependence of Mtb *bd*-I activity.

The rate of dQH_2 oxidation by Mtb *bd*-I was determined in a mixed buffer system containing 40 mM HEPES/MES/TAPS. The optimal activity of Mtb *bd*-I was observed at pH 7.5 but it decreased at more acidic and alkaline pH. The values were obtained by calculating an average of two independent replicate experiments ± SEM (Origin 8.5 software).

3.3.3. Kinetic characterization of Mtb *bd*-I

Initial kinetic characterisation of crude Mtb *bd*-I membranes revealed a typical biphasic activity with a fast linear phase followed by a second slower phase in presence of dQH_2 and Q_1H_2 substrates (Figures 3.7, A and 3.8 respectively). In contrast, Mtb cytochrome *bd*-I showed sigmoidal behaviour with low concentrations of Q_2H_2 (Figure 3.9), in agreement with previous studies (345, 349).

Mtb *bd*-I demonstrated a preference for dQH_2. Apparent K_m data for substrate analogues were determined spectrophotometrically (Figures 3.7 – 3.9) identifying a rank order preference for $dQH_2 > Q_1H_2 > Q_2H_2$ with K_m values of 19.25 ± 1.3, 51.55 ± 8.9, and 65.21 ± 15.31 µM respectively. Examining Mtb *bd*-I membranes of TML16 strain, grown in aerobic conditions revealed similar K_m data (21.52 ± 3.57 µM) to that from O_2-limited condition (19.25 ± 1.3 µM). The specific catalytic activity values of Mtb *bd*-I during O_2-limited condition was 9.01 ± 0.23 µmol.min^{-1}.mg^{-1} and during aerobic condition was 5.1 ± 0.29 µmol.min^{-1}.mg^{-1} (Table 3.2).

Given the fact that the assay was performed in an oxygen-rich environment, for 'air-oxidized' cytochrome *bd*-I (i.e. the oxygen reduction rate almost constant) the oxidation rate of quinols was not affected. Therefore, the data gave a monophasic shape although *bd*-I was expected to exhibit a bisubstrate catalytic reaction. The Michaelis-Menten equation for dQH_2 and Q_1H_2 oxidation was applied. However, under oxygen-limiting growth conditions, enzyme kinetics may be affected as the oxidation of quinols would be tightly coupled to dioxygen reduction rate (345).

Table 3.2: Kinetic parameters of Mtb *bd*-I activity

	K_m ± SEM (µM)	**specific catalytic activity ± SEM (µmol.min^{-1}.mg^{-1})**
dQH_2 (O_2-limited)	19.25 ± 1.3	9.01 ± 0.23
dQH_2 (aerobic)	21.52 ± 3.57	5.1 ± 0.29
Q_1H_2	51.55 ± 8.9	5.26 ± 0.52
Q_2H_2	65.21 ± 15.31	8.65 ± 2.5

3.3.3.1. Decylubiquinol (dQH_2)

A)

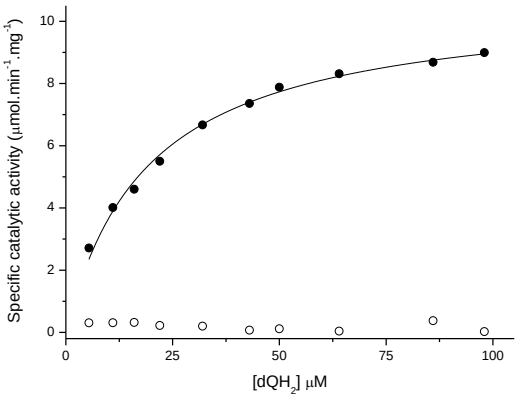

B)

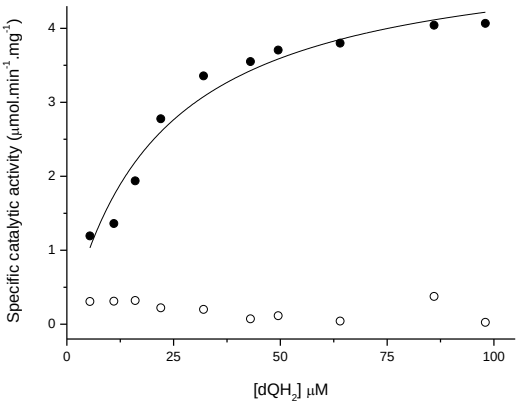

Figure 3.7: Steady-state decylubiquinol:Mtb *bd*-I activity

Steady-state kinetics of Mtb *bd*-I were measured spectrophotometrically at 283 nm. The oxidation of decylubiquinol (dQH_2) by the Mtb *bd*-I (closed circles) was analysed using the Michaelis-Menten equation. The apparent K_m (µM) and specific catalytic activity (µmol.min^{-1}.mg^{-1}) values were calculated to be respectively A) 19.25 ± 1.3 and 9.01 ± 0.23, during O_2-limited growth condition and B) 21.52 ± 3.57 and 5.1 ± 0.29 during aerobic growth condition. ML16 (open circles) was tested as a negative background. The reactions were initiated by the addition of dQH_2 (5 - 98 µM). The points are the mean initial rates of experimental duplicate obtained at each dQH_2 concentration indicated. Data were fitted using the Michaelis-Menten function using rectangular hyperbola (Origin 8.5 software).

3.3.3.2. Ubiquinol-1 (Q_1H_2)

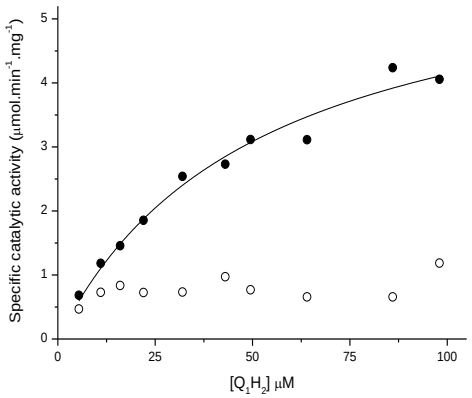

Figure 3.8: Steady-state ubiquinol-1:Mtb *bd*-I activity

Steady-state kinetics of Mtb *bd*-I were measured spectrophotometrically at 283 nm. The oxidation of ubiquinol-1 (Q_1H_2) by the Mtb *bd*-I (closed circles) was analysed using the Michaelis-Menten equation. The apparent K_m (µM) and specific catalytic activity (µmol.min^{-1}.mg^{-1}) values were calculated to be 51.55 ± 8.9 and 5.26 ± 0.52 respectively. ML16 (open circles) was tested as a negative background. The reactions were initiated by the addition of Q_1H_2 (5 - 98 µM). The points are the mean initial rates of experimental duplicates obtained at each Q_1H_2 concentration indicated. Data were fitted using the Michaelis-Menten function (Origin 8.5 software).

3.3.3.3. Ubiquinol-2 (Q_2H_2)

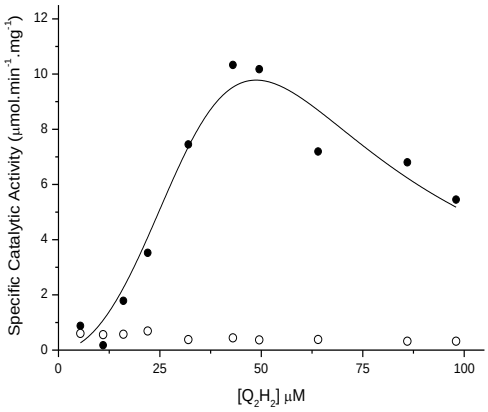

Figure 3.9: Steady-state ubiquinol-2: Mtb *bd*-I activity

Steady-state kinetics of Mtb *bd*-I were measured spectrophotometrically at 283 nm. The oxidation of ubiquinol-2 (Q_2H_2) by Mtb *bd*-I (closed circles) was analysed using the modified *ping-pong bi-bi* mechanism for cytochrome *bd*-I. The apparent K_m (µM) and specific catalytic activity (µmol.min^{-1}.mg^{-1}) values were calculated to be 65.21 ± 15.31 and 8.65 ± 2.5 respectively. ML16 (open circles) was tested as a negative background. The reactions were initiated by the addition of Q_2H_2 (5 - 98 µM). The points are the mean initial rates of experimental duplicates obtained at each Q_1H_2 concentration indicated. Data were fitted using a modified *ping-pong bi-bi* function (Origin 8.5 software).

3.3.4. Drug sensitivity assays

3.3.4.1. Growth inhibition studies

Growth inhibition assays were performed to confirm the phenotypic profiles of the current DOTS therapeutic drugs against Mtb H37Rv strain (Table 3.3). Owing to lab to lab data variations, this experiment provides personal data for time to kill and metabolic experiments. Literature data of DOTS drugs indices were reported in number of studies (348, 350, 351). In this experiment, first line anti-TB agents were all effective against Mtb strain H37Rv, (Figure 3.10) as an example. The metronidazole data served as validation of the adaptation of the Wayne model and the achievement of hypoxic conditions. Metronidazole does not have a significant inhibitory effect against aerobic Mtb but has a bactericidal effect against Mtb grown under severe hypoxia (139). Pyrazinamide was not included as it is completely inactive at a neutral pH (i.e. the pH of standard drug sensitivity assays) and is known to be effective only in acidic pH (130).

Table 3.3: Bactericidal IC_{50s} and IC_{90s} values of inhibitor compounds tested against *Mycobacterium tuberculosis*

Compound	Mtb H37Rv (aerobic)		Mtb H37Rv (Wayne model)
	IC_{50} ± SEM (µM)	**IC_{90} (µM)**	**IC_{50} ± SEM (µM)**
Rifampicin	$1\times10^{-3} \pm 0.004\times10^{-3}$	2.21×10^{-3}	$3\times10^{-3} \pm 0.003\times10^{-3}$
Ethambutol	2.15 ± 0.24	4.61	2.14 ± 0.07
Isoniazid	1.66 ± 0.21	2.38	1.67 ± 0.40
Streptomycin	0.14 ± 0.01	0.23	$80\times10^{-2} \pm 0.08\times10^{-2}$
Metronidazole	ND	-	80 ± 10.70

The IC_{50s} values were established using the modified MABA assay**.** The values are mean **±** SEM of two independent replicate experiments. IC_{50s} values were calculated using a four parameter logistic function (Origin 8.5 software). IC_{90} values were calculated along with IC_{50} determinations.

ND-not determined.

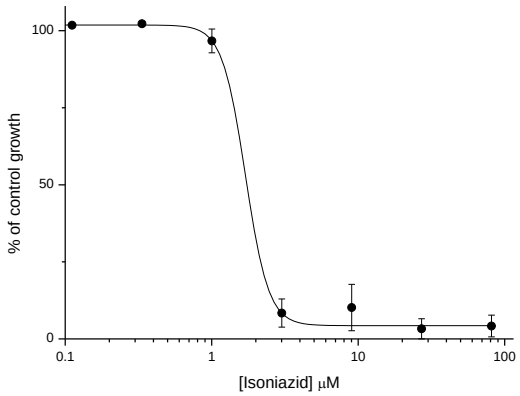

Figure 3.10: IC_{50} determination of isoniazid concentrations against Mtb aerobic growth

The percentages of growth were calculated, utilizing control wells to represent 100 % growth. The IC_{50} for isoniazid was calculated as 1.66 ± 0.21 μM using a four parameter logistic function (Origin 8.5 software). The values are mean ± SEM of two independent replicate experiments.

3.3.4.2. Enzyme and growth inhibition studies, quinolone-type compounds

As a step towards identifying and validating a novel Mtb *bd*-I inhibitor, a collection of quinolone-type inhibitors (in house compounds) were tested against Mtb *bd*-I. The flow of Mtb *bd*-I and Mtb H37Rv inhibition studies is depicted in Figure 3.11 that shows the rank order of compound potency against Mtb *bd*-I and Mtb H37Rv, ranging from the least potent to the most potent. Inhibition studies with these inhibitors showed significant attenuations of quinol oxidation activity in a concentration-dependent manner (as an example see Figure 3.12). The IC_{50s} values were determined for 23 compounds with each compound screened at 8 concentrations (with 3-fold dilution steps between points), all of which were replicated. Generally, IC_{50} values ranged between approximately 3 x 10^{-3} and 70 μM (Table 3.4). In order to examine SAR of these compounds, the inhibitors were classified into groups according to their structures. Hundreds of compounds were screened through a single point inhibition screening assay. In this screening, all compounds were examined at final concentration of 5 μM and processed normally using the MABA assay (Mtb) in aerobic condition. Consequently, those compounds that showed 50% or more inhibition processed to a full IC_{50} modified MABA assay (Mtb). The in house labratory data of single point screening assay at 5 μM concentration of quinolone-type compounds using the modified MABA assay (Mtb) is shown in Table (3.4). ClogP values of all quinolone-type inhibitors were

calculated; ClogP is a well-established measure of the compound's hydrophilicity from which high ClogP value indicates low hydrophilicity and thus poor absorption or penetration (Table 3.4).

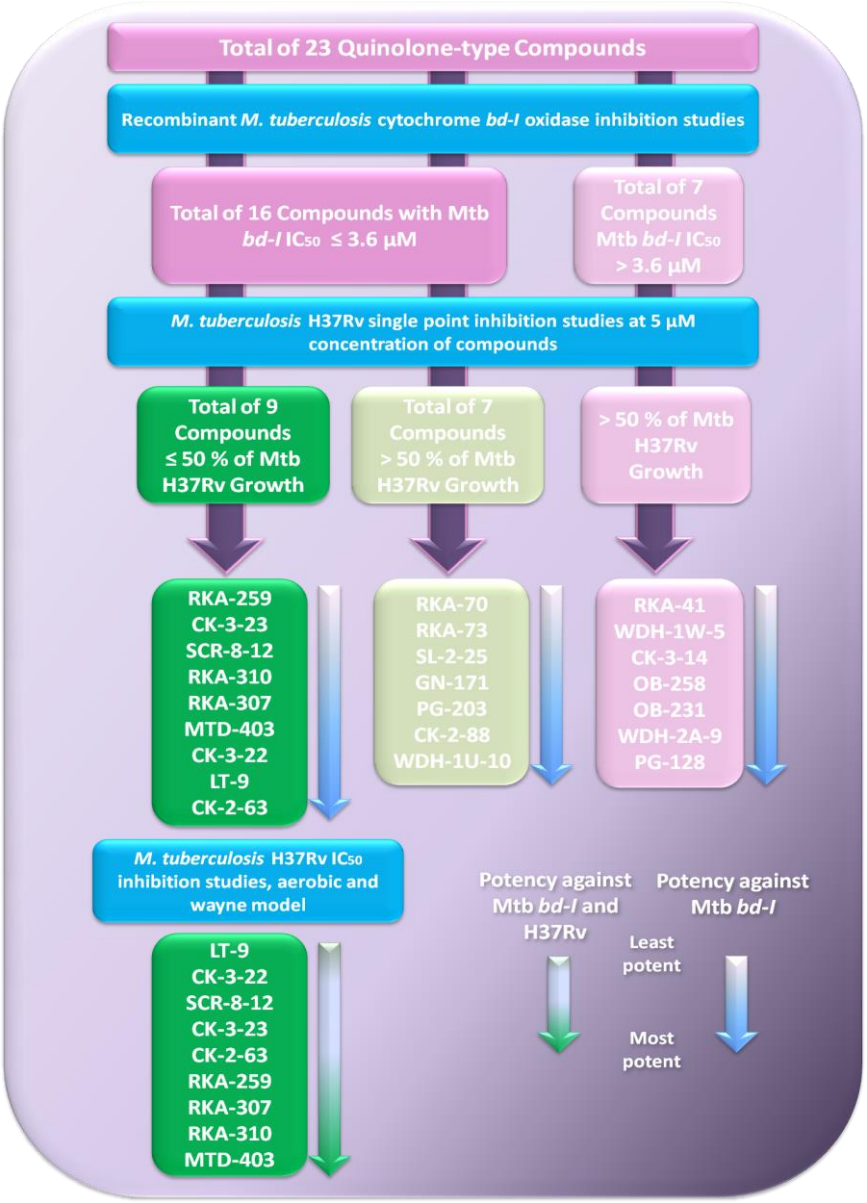

Figure 3.11: The quinolone-type compounds flow chart of potency against Mtb *bd*-I and *Mycobacterium tuberculosis* H37R

Table 3.4: The physical characteristics of the quinolone-type compounds used in this study

Compound	Structure	ClogP	*bd*-I, IC_{50} ± SEM (µM)	Growth of Mtb H37Rv (aerobic) at 5 µM of [compounds] (%)*
CK-3-22	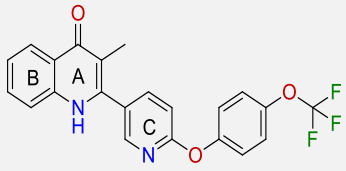	5.49	0.14 ± 0.02	19.52
CK-3-14	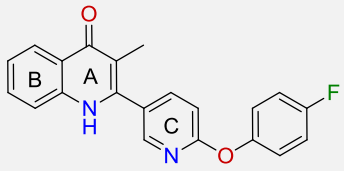	4.12	10.6 ± 6.58	100
RKA-259	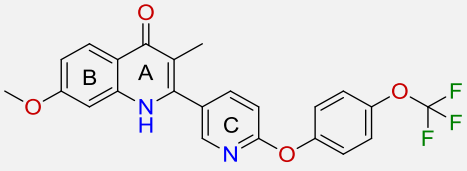	5.36	3.6 ± 1.67	12.61
RKA-307	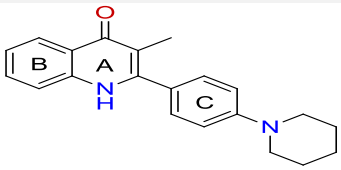	4.06	0.44 ± 0.08	1.83
RKA-310	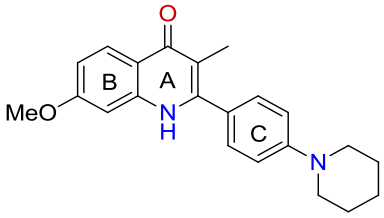	3.96	1.4 ± 0.17	No growth
MTD-403	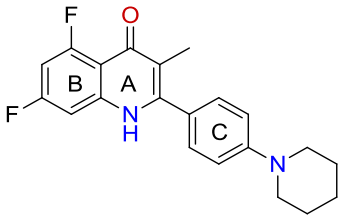	4.38	0.27 ± 0.06	No growth
SCR-8-12	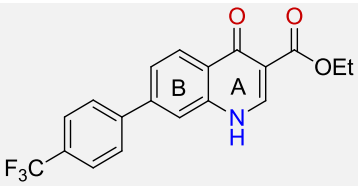	3.62	3.55 ± 1.1	No growth

Table 3.4: (*continued*)

CK-2-88	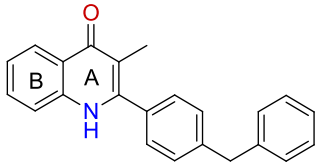	5.14	0.02 ± 0.01	90.51
CK-3-23	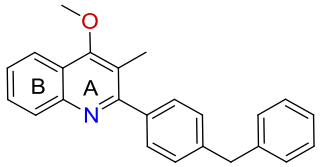	6.67	3.6 ± 0.57	6.62
CK-2-63	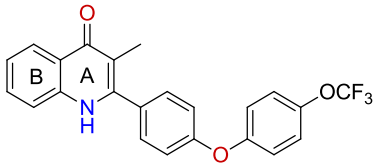	6.11	$3 \times 10^{-3} \pm 1 \times 10^{-4}$	37.81
PG-203	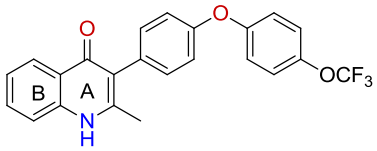	5.23	0.07 ± 0.02	100
RKA-70	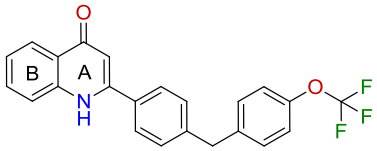	6.32	0.75 ± 0.36	100
RKA-73	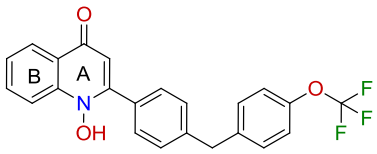	6.18	0.31 ± 0.06	100
LT-9	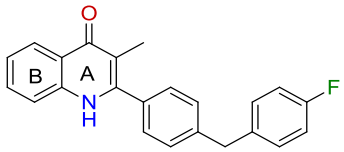	5.30	0.1 ± 0.02	34.74
RKA-41	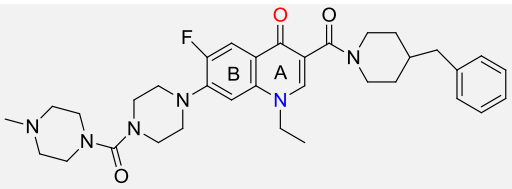	3.68	70.3 ± 29.98	ND
SL-2-25	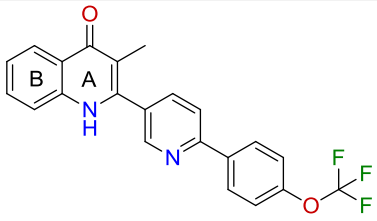	5.33	0.29 ± 0.07	88.91

Table 3.4: (*continued*)

WDH-1U-10	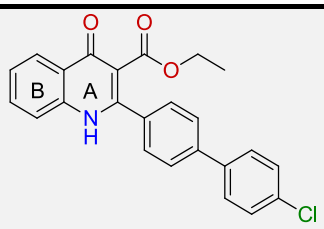	4.95	0.012 ± 1 x 10^{-3}	82.22
WDH-1W-5	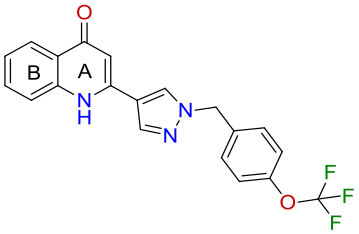	4.29	15.8 ± 1.23	61.31
WDH-2A-9	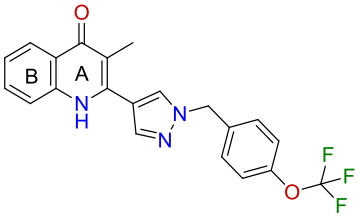	4.64	6.5 ± 2.26	97.42
GN-171	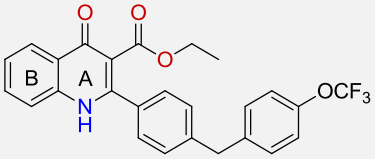	6.34	0.25 ± 0.09	100
OB-231	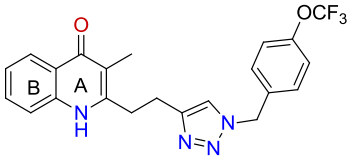	4.55	7.8 ± 1.64	93.42
OB-258	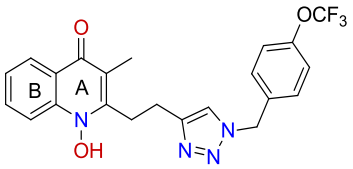	4.42	8.8 ± 2.87	94.81
PG-128	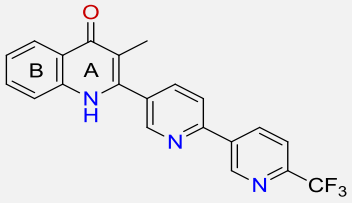	3.82	4.47 ± 0.86	95.63

The quinolone-type compounds were grouped according to their chemical structures along with their code, ClogP values and the mean of IC_{50s} values against Mtb *bd*-I ± SEM of experimental duplicates. Values were determined spectrophotometrically (Mtb *bd*-I). IC_{50s} values were calculated using a four parameter logistic function (Origin 8.5 software). * In house laboratory data of a single point screening assay at 5 µM concentration of quinolone-type compounds using the modified MABA assay (Mtb H37Rv).

The in house laboratory data of the quinolone-type inhibitors were used in this study to show the full phenotypic profiles of these compounds. Growth inhibition assays were determined against Mtb H37Rv, using the modified MABA assay, under aerobic and anaerobic growth conditions for the quinolone-type inhibitors. Out of 23 compounds tested against Mtb *bd*-I and screened through single point screening assay, 9 compounds showed ≤ 50% of growth at 5 μM concentration, all of which were examined through a full IC_{50} modified MABA assay (Mtb) (Table 3.5).

Table 3.5: IC_{50s} values from growth inhibitory assays of quinolone-type compounds

Compound	Mtb *bd*-I	Mtb H37Rv (aerobic)		Mtb H37Rv (Wayne model)
	IC_{50} ± SEM (μM)	IC_{50} ± SEM (μM)*	IC_{90} (μM)	IC_{50} (μM)*
LT-9	0.1 ± 0.02	>10	ND	NA
CK-3-22	0.14 ± 0.02	1.97 ± 0.05	4.95	>10
SCR-8-12	3.55 ± 1.12	3.45 ± 0.15	4.55	6.41
CK-3-23	3.6 ± 0.57	2.89 ± 0.11	6.53	1.63
CK-2-63	$3 \times 10^{-3} \pm 0.1 \times 10^{-3}$	3.7 ± 0.19	6.73	1.61
RKA-259	3.6 ± 1.67	1.03 ± 0.03	2.08	1.42
RKA-307	0.44 ± 0.08	1.57 ± 0.03	3.11	3.92
RKA-310	1.4 ± 0.17	0.81 ± 0.04	1.96	0.61
MTD403	0.27 ± 0.06	0.27 ± 0.01	0.85	0.41

Values were calculated spectrophotometrically (Mtb *bd*-I) or using the modified MABA assay (Mtb). The values are the mean of at least two replicates. IC_{50s} values were calculated using a four parameter logistic function (Origin 8.5 software).

* In house laboratory data**.** ND-not determined. NA-not applicable as aerobic IC_{50} was > 10 μM.

The following graphs (Figure 3.12) show examples of the inhibitory effects of two quinolone-type compounds tested against Mtb *bd*-I.

A)

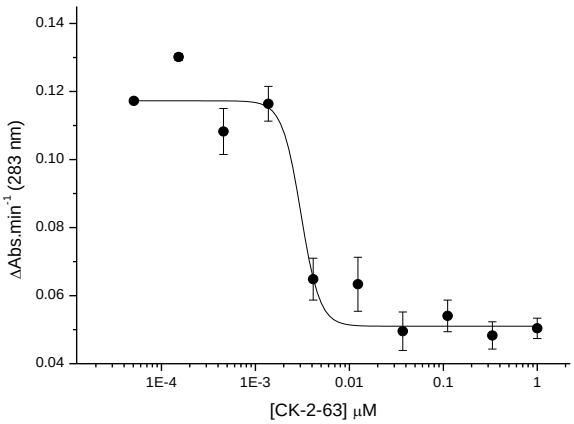

B)

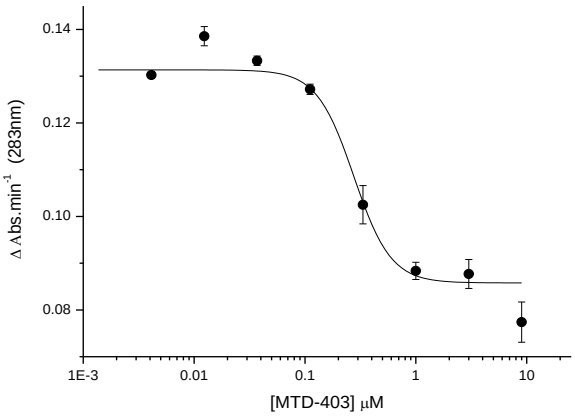

Figure 3.12: Determination of the IC_{50s} for CK-2-63 and MTD-403 against Mtb *bd*-I activity

The IC_{50s} values for A) CK-2-63 and B) MTD-403 in the decylubiquinol:Mtb *bd*-I assay were determined spectrophotometrically at 283 nm. The IC_{50s} values are $3 \times 10^{-3} \pm 0.1 \times 10^{-3}$ μM and 0.27 ± 0.06 μM for CK-2-63 and MTD-403, respectively. The values are the average of experimental duplicates ± SEM at each point. The data were fitted using a four parameter logistic function (Origin 8.5 software).

The following Table (3.6) shows other compounds used for characterization of Mtb *bd*-I. Heme ligands (e.g., cyanide, azide or nitric oxide) are known to act at the O_2 binding/reducing site of the cytochrome *bd*-I oxidase (211). Thus, the IC_{50} of potassium cyanide (KCN) was calculated to be 429.11 ± 126.85 μM against Mtb *bd*-I. In addition, the IC_{50} of HDQ, a quinolone-like inhibitor that has high affinity for alternative NADH dehydrogenases, was calculated to be 231.93 ± 116.4 μM.

Table 3.6: The IC_{50s} determination of KCN and HDQ against Mtb *bd*-I activity

Compound	Structure	ClogP	Mtb *bd*-I, IC_{50} ± SEM (μM)
KCN		ND	429.11 ± 126.85
HDQ	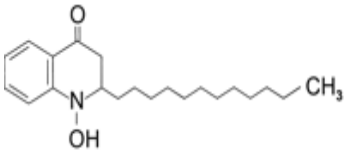	6.52	231.93 ± 116.43

The IC_{50s} values for KCN and HDQ in the decylubiquinol:Mtb *bd*-I assay were determined spectrophotometrically at 283 nm. IC_{50s} values are the mean ± SEM of experimental duplicates. IC_{50s} values were calculated using a four parameter logistic function (Origin 8.5 software).

3.3.5. Correlation Study

Scatter trends in activity for the compounds were observed with regards to aerobically cultured Mtb H37Rv and enzyme IC_{50} data. This is most clearly demonstrated by a plot of Mtb *bd*-I IC_{50} against aerobically cultured Mtb H37Rv IC_{50} (Figure 3.13) in which no significant correlation was apparent (Table 3.5). However, excluding LT-9, CK-3-22, CK-2-63 and RKA-259 resulted in a two star (**) significant correlation (*P* value < 0.01).

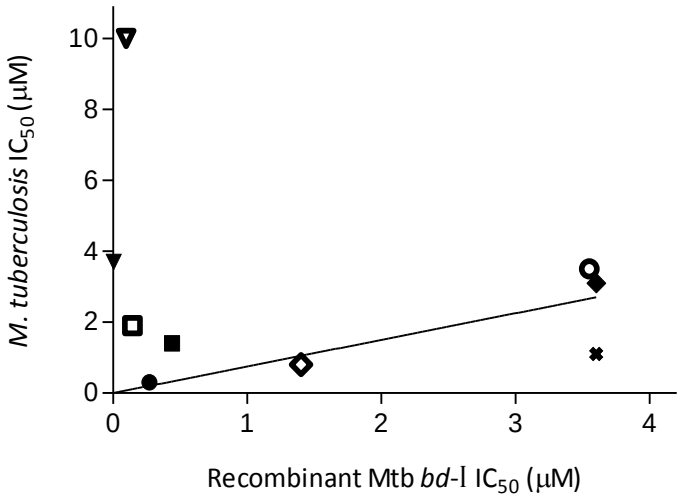

Figure 3.13: Scatter plot of the IC_{50s} of quinolone-type compounds against Mtb *bd*-I and aerobically cultured *Mycobacterium tuberculosis* H37Rv

The IC_{50s} of MTD-403 (closed circle), RKA-307 (closed square), CK-3-22 (open square), RKA-310 (open diamond), CK-3-23 (closed diamond), SCR-8-12 (open circle), CK-2-63 (closed inverted triangle), LT-9 (open inverted triangle), and RKA-259 (cross) compounds against Mtb *bd*-I and aerobically cultured Mtb H37Rv were plotted using a correlation function in GraphPad Prism (GraphPad 5 Software, USA). The data showed no significant correlation between enzyme inhibition and *in vitro* antitubercular activity (*P* > 0.05). The values are the IC_{50s} of the compounds are detailed in Table 3.5.

3.3.6. Time-kill studies

According to the *in vitro* definition, bacteriostatic agents inhibit bacterial growth whereas bactericidal agents kill bacteria. The bactericidal/static nature of 8 quinolone-type inhibitors was determined by time-dependent kill kinetic studies (Figure 3.14, compounds were presented at 5 x IC_{90}). Whilst untreated Mtb showed significant growth over 7 days, all quinolone-type compounds showed bacteriostatic

activities with the exception of SCR-8-12, CK-3-22 and CK-3-23. SCR-8-12 revealed a significant reduction in viable counts (cfu.ml^{-1}) of Mtb within the first 4 days and by day 7 no viable organisms remained. SCR-8-12 activity is similar to the bactericidal activity of streptomycin (STR). In particular, CK-3-22 and CK-3-23 did not exhibit any significant reduction in viable counts over 7 days while RKA-310 displayed lower viable counts than control over 7 days but without any significant decline. LT-9, RKA-307 and MTD-403 demonstrated nearly the same bacteriostatic nature where viable counts of bacteria started to decline by day 7. This phenomenon is more obvious in CK-2-63 activity, which showed reduction of Mtb viable count by day 7. Ethambutol (EMB) reduced the viable counts significantly over 7 days but it failed to completely attenuate growth. The bactericidal/static nature of RKA-259 was not determined due to time limitation.

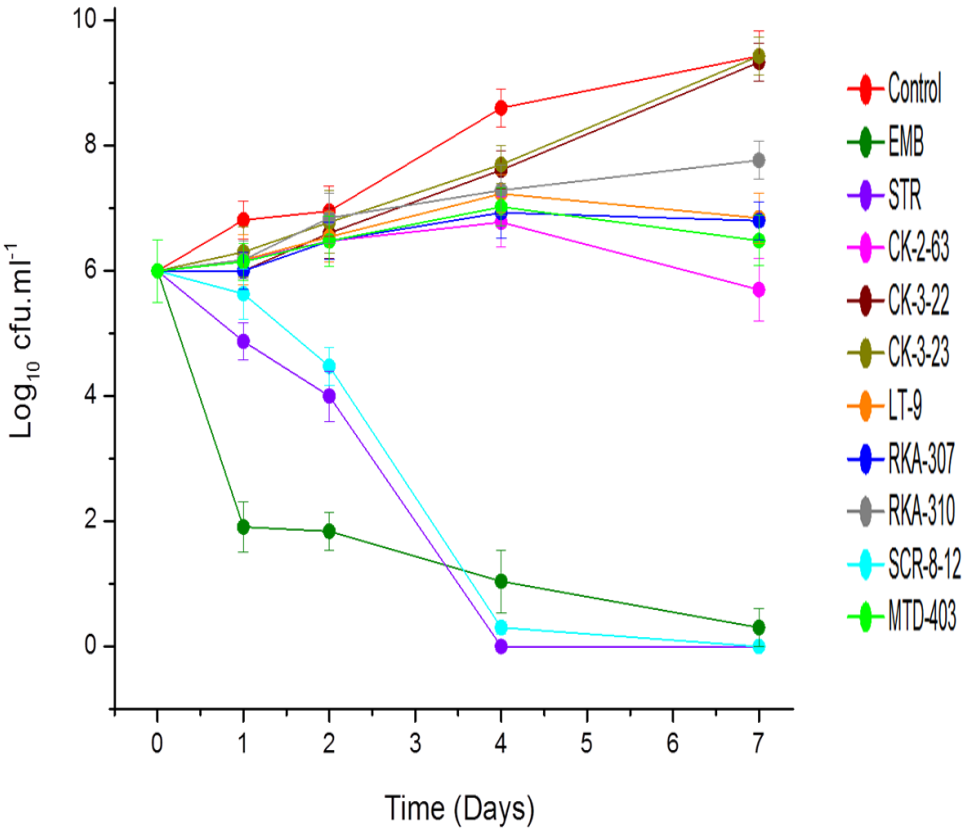

Figure 3.14: Time-kill curves for untreated and drug-treated Mtb H37Rv

Time-kill curves for untreated cells, ethambutol, streptomycin, CK-2-63, CK-3-22, CK-3-23, LT-9, MTD-403, SCR-8-12, RKA-310, and RKA-307. Compounds were present at 5 x IC_{90} (established from MABA assays) and cfu.ml^{-1} were determined at the appropriate time points. Points are the mean of experimental duplicates. Error bars represent ± SEM of each point.

3.3.7. The mechanism of inhibition of Mtb *bd*-I activity by quinolone-type inhibitors

To study the mechanism of inhibition and to distinguish the interaction between Mtb *bd*-I and the substrate, dQH_2 and quinolone-type inhibitors, the steady state kinetics of Mtb *bd*-I were studied with respect to the substrate and inhibitors. The main division of inhibitors are irreversible and reversible inhibitors. The enzyme catalytic activity is completely destroyed by irreversible inhibitors but completely restored following reversible inhibitors removal. Most drugs bind to their enzyme target through reversible interactions. The enzymatic reaction begins with the reversible binding of substrate (*S*) to the free enzyme (*E*) to form the enzyme-substrate (*ES*) complex. Inhibitors (*I*) can bind directly to the free form of the enzyme, to an *ES* complex, or to both. To describe *S* binding to the enzyme-inhibitor (*EI*) complex, a constant α must be used. The constant α defines the degree to which inhibitor binding affects the affinity of the *E* for *S*. According to the inhibitors influence on enzyme kinetic behaviour and parameters, inhibitors were divided into three types, competitive, non-competitive and uncompetitive inhibitors (335, 352). Matsumoto *et al* (2006) described that competitive inhibition is characterised by no alteration of the maximum velocity (V_{max}) while non- and un-competitive inhibition cause attenuation of V_{max} (345). Reversible modes of inhibitor interactions with enzymes and their effect on the *S* binding affinity and consequently on kinetic parameters are depicted in Table 3.7.

Table 3.7: Diagnostic signatures and binding features of reversible inhibition modalities (335, 345, 352, 353)

Inhibition modality	Diagnostic signature in Lineweaver-Burk plot	Diagnostic signature in Eadie-Hofstee plot	Enzyme-Inhibitor binding	Affinity of *EI* complex to *S*	Effect on parameters	
					K_m	V_{max}
Competitive, α = ∞	Intersecting lines that converge at the y-axis	lines intersecting the y-axis at V_{max}	Inhibitor binds exclusively to the free enzyme	*EI* complex excludes further *S* binding	Increase	No effect
Non-competitive, α > 1	Intersecting lines that converge to the left of the y-axis and above *x*-axis	Parallel lines	Inhibitor binds to the free enzyme	*EI* complex decreases affinity of *S* binding	Increase	Decrease
Non-competitive, α = 1	Intersecting lines that converge to the left of the y-axis and on the *x*-axis		Inhibitor binds to the free enzyme and *ES* complex equally	*EI* complex has no change in affinity of *S* binding	No effect	Decrease
Non-competitive, α < 1	Intersecting lines that converge to the left of the y-axis and below the *x*-axis		Inhibitor binds with greater affinity to the *ES* complex	*EI* complex augments affinity of *S* binding	Decrease	Decrease
Uncompetitive, α	Parallel lines	lines intersecting the x-axis at $V_{max/}\ K_m$	Inhibitor binds exclusively to the *ES* complex	Inhibitor requires the prior formation of the *ES* complex for binding and inhibition	Decrease	Decrease

In order to uncover the mechanism of inhibition of Mtb *bd*-I by CK-2-63, SL-2-25, MTD-403, PG-203 and SCR-8-12, the data were first fitted using the Michaelis-Menten function to calculate K_m and V_{max} (converted to specific catalytic activity) parameters. Then data were transformed to Lineweaver-Burk plot and Eadie-Hofstee plots with view to examine the properties as depicted in Table 3.7. The mode of quinolone-type compound inhibition is summarized in the following Table 3.8 and the data for each inhibitor are depicted in Figures 3.15 - 3.19. The 5 quinolone-type compounds were selected arbitrarily.

Table 3.8: Mechanism of inhibition of Mtb *bd*-I by quinolone-type inhibitors in presence of varying concentrations of dQH_2 substrate

Inhibitor		K_m ± SEM (µM)	Specific catalytic activity ± SEM (µmol.min^{-1}.mg^{-1})	Mechanism of inhibition
CK-2-63	**4 nM**	25.8 ± 3.5	6.95 ± 0.42	Non-competitive, α > 1
	12 nM	28.3 ± 5.2	5.93 ± 0.55	Or mixed-type of inhibition
SCR-8-12	**3 µM**	12.3 ± 1.1	8.85 ± 0.23	Competitive
	9 µM	10.2 ± 1.3	8.62 ± 0.27	
MTD-403	**110 nM**	8.5 ± 0.9	8.45 ± 0.22	Competitive
	330 nM	7.9 ± 0.7	8.5 ± 0.18	
SL-2-25	**110 nM**	7.4 ± 3.4	6.0 ± 0.46	Uncompetitive
	330 nM	7.7 ± 0.7	4.45 ± 0.91	
PG-203	**110 nM**	7.7 ± 1.5	4.1 ± 0.17	Uncompetitive
	330 nM	8.7 ± 1.6	2.88 ± 0.13	

Steady-state kinetics of treated Mtb *bd*-I were measured spectrophotometrically at 283 nm. The oxidation of dQH_2 by Mtb *bd*-I in the presence of inhibitors was analysed using the Michaelis-Menten equation. The apparent K_m (µM) and specific catalytic activity (µmol.min^{-1}.mg^{-1}) values were calculated. The reactions were initiated by the addition of gradient concentration of dQH_2 (5 - 98 µM). The values are the mean initial velocity of experimental duplicates obtained at each point. The data were fitted using the Michaelis-Menten function (Origin 8.5 software). The K_m and specific catalytic activity parameters were compared to untreated Mtb *bd*-I parameters of dQH_2 substrate oxidation (K_m = 19.25 ± 1.3 µM, specific catalytic activity = 9.01 ± 0.23 µmol.min^{-1}.mg^{-1}).

3.3.7.1. Inhibition mechanism of Mtb *bd*-I by CK-2-63

A)

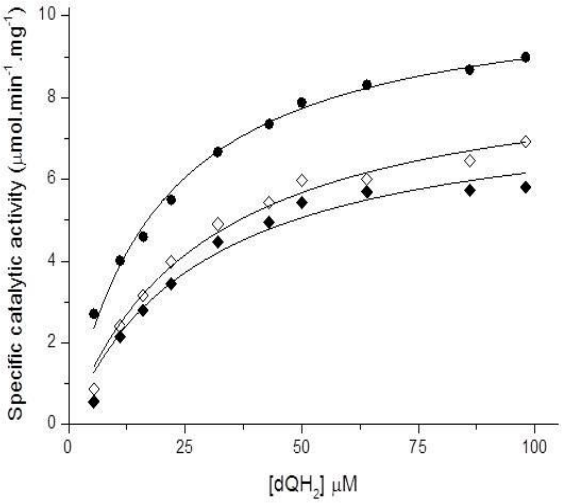

B) **C)**

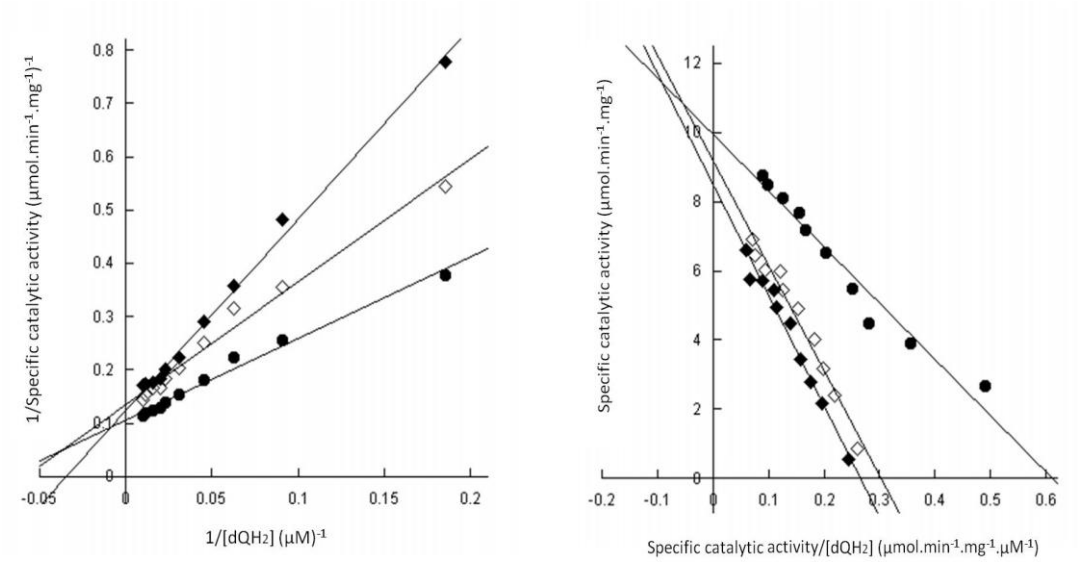

Figure 3.15: Substrate titration of steady state velocity for Mtb *bd*-I in the presence of the CK-2-63 inhibitor

A) Steady-state kinetics of Mtb *bd*-I at varying dQH_2 (5-98 µM) concentration with no inhibitor (closed circle), with 4 nM CK-2-63 (open diamond) and with 12 nM CK-2-63 (closed diamond) were fitted using the Michaelis-Menten function (Origin 8.5 software). B) Data as in (A) were fitted using the double reciprocal Lineweaver Burk plot. CK-2-63 shows a non-competitive ($\alpha > 1$) mode of inhibition with intersecting lines that converge to the left of the y-axis and above *x*-axis. C) Data as in (A) were fitted using the Michaelis-Menten function Eadie-Hofstee plot. CK-2-63 shows a mixed mode of inhibition; the lines are not parallel neither intersecting at V_{max} values. The points are the mean initial velocity of experimental duplicates obtained at each dQH_2 concentration indicated. The data were fitted using Kalidagraph (Synergy software).

3.3.7.2. Inhibition mechanism of Mtb *bd*-I by SCR-8-12

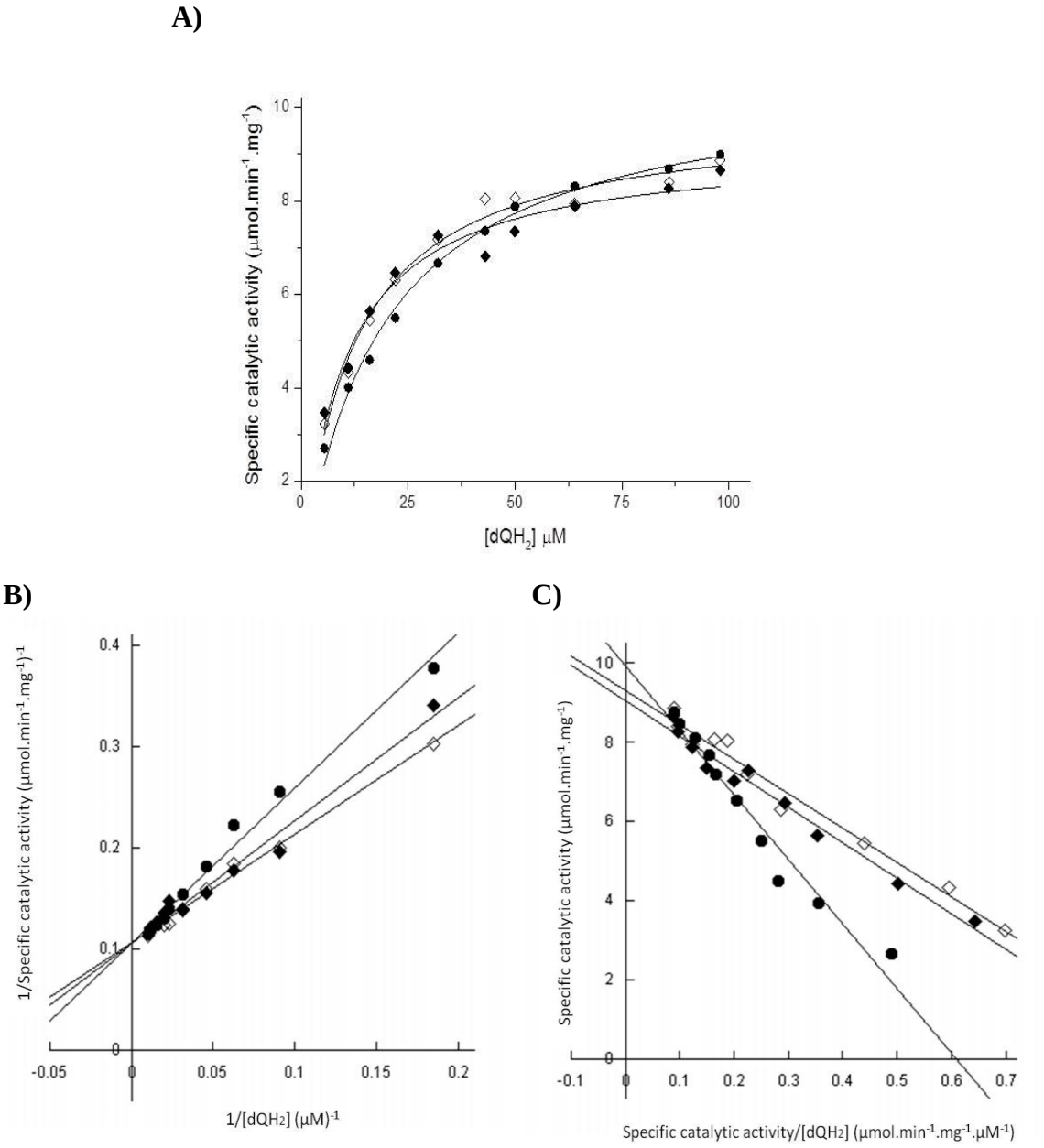

Figure 3.16: Substrate titration of steady state velocity for Mtb *bd*-I in the presence of the SCR-8-12 inhibitor

A) Steady-state kinetics of Mtb *bd*-I at varying dQH_2 (5-98 µM) concentration with no inhibitor (closed circle), with 9 µM SCR-8-12 (closed diamond) and with 3 µM SCR-8-12 (open diamond) were were fitted using the Michaelis-Menten function (Origin 8.5 software). B) Data as in (A) were fitted using the double reciprocal Lineweaver Burk plot. SCR-8-12 shows a competitive mode of inhibition with intersecting lines that converge at the y-axis. C) Data as in (A) were fitted using the Eadie-Hofstee plot. SCR-8-12 shows a competitive mode of inhibition with intersecting lines at V_{max} values. The points are the mean initial velocity of experimental duplicates obtained at each dQH_2 concentration indicated. The data were fitted using Kalidagraph (Synergy software).

3.3.7.3. Inhibition mechanism of Mtb *bd*-I by MTD-403

A)

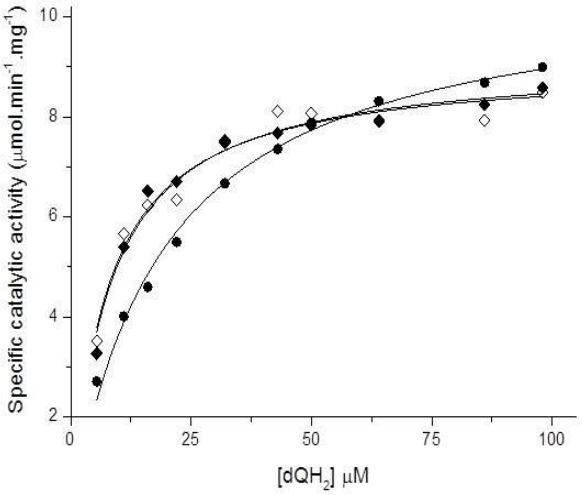

B) **C)**

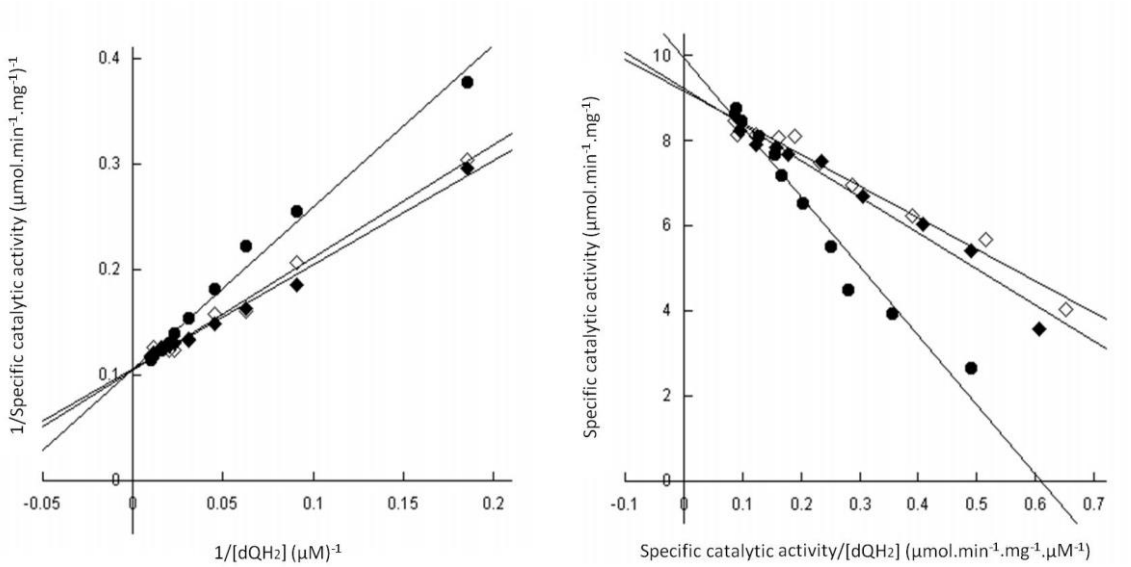

Figure 3.17: Substrate titration of steady state velocity for Mtb *bd*-I in the presence of the MTD-403 inhibitor

A) Steady-state kinetics of Mtb *bd*-I at varying dQH_2 (5-98 µM) concentration with no inhibitor (closed circle), with 330 nM MTD-403 (closed diamond) and with 110 nM MTD-403 (open diamond) were were fitted using the Michaelis-Menten function (Origin 8.5 software). B) Data as in (A) were fitted using the double reciprocal Lineweaver Burk plot. MTD-403 shows a competitive mode of inhibition with intersecting lines that converge at the y-axis. C) Data as in (A) were fitted using the Eadie-Hofstee plot. MTD-403 shows a competitive mode of inhibition with intersecting lines at V_{max} values. The points are the mean initial velocity of experimental duplicates obtained at each dQH_2 concentration indicated. The data were fitted using Kalidagraph (Synergy software).

3.3.7.4. Inhibition mechanism of Mtb *bd*-I by SL-2-25

A)

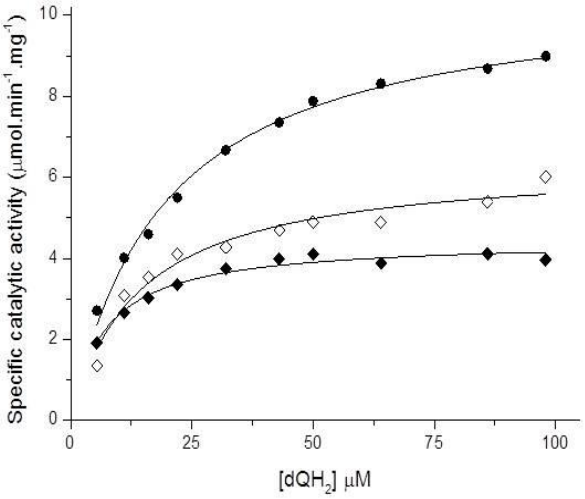

B) **C)**

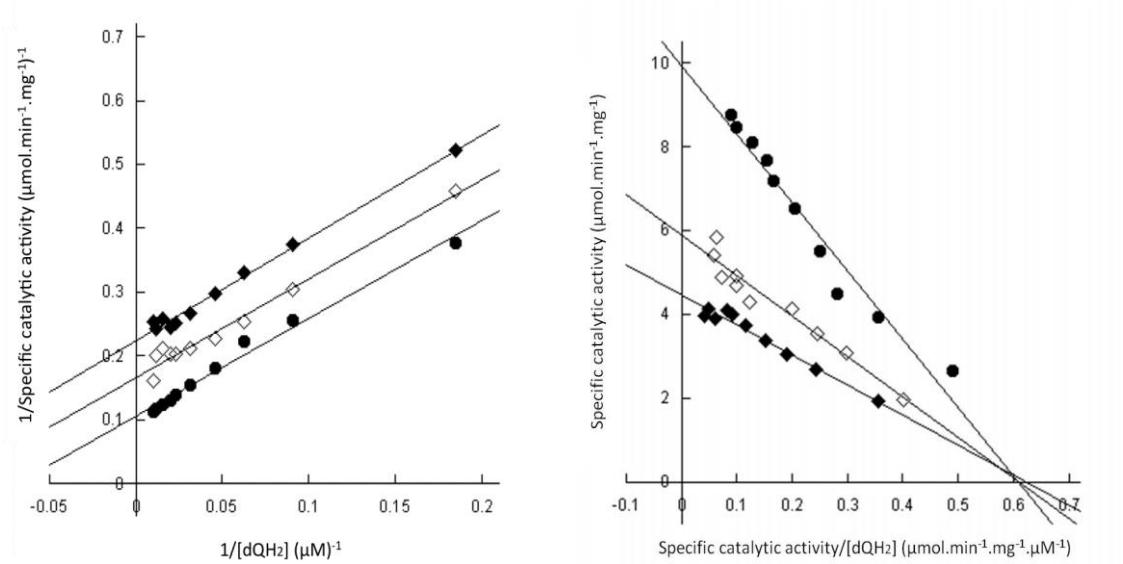

Figure 3.18: Substrate titration of steady state velocity for Mtb *bd*-I in the presence of the SL-2-25 inhibitor

A) Steady-state kinetics of Mtb *bd*-I at varying dQH_2 (5-98 µM) concentration with no inhibitor (closed circle), with 330 nM SL-2-25 (closed diamond) and with 110 nM SL-2-25 (open diamond) were fitted using the Michaelis-Menten function (Origin 8.5 software). B) Data as in (A) were fitted using the double reciprocal Lineweaver Burk plots. SL-2-5 shows an uncompetitive mode of inhibition with parallel lines. C) Data as in (A) were fitted using the Eadie-Hofstee plot. SL-2-5 shows an uncompetitive mode of inhibition with intersecting lines at V_{max}/K_m values. The points are the mean initial velocity of experimental duplicates obtained at each dQH_2 concentration indicated. The data were fitted using Kalidagraph (Synergy software).

3.3.7.5. Inhibition mechanism of Mtb *bd*-I by PG-203

A)

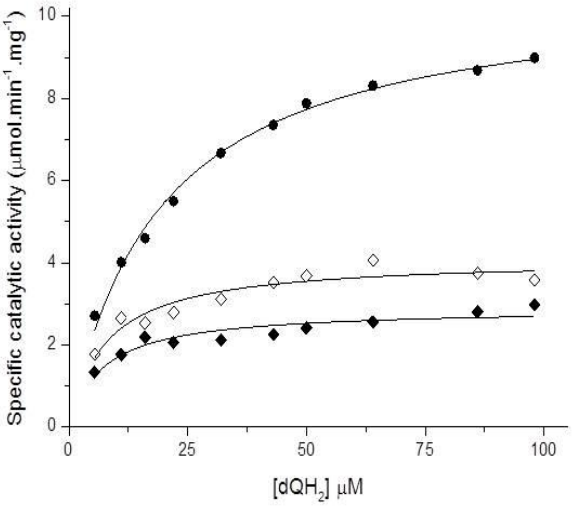

B) **C)**

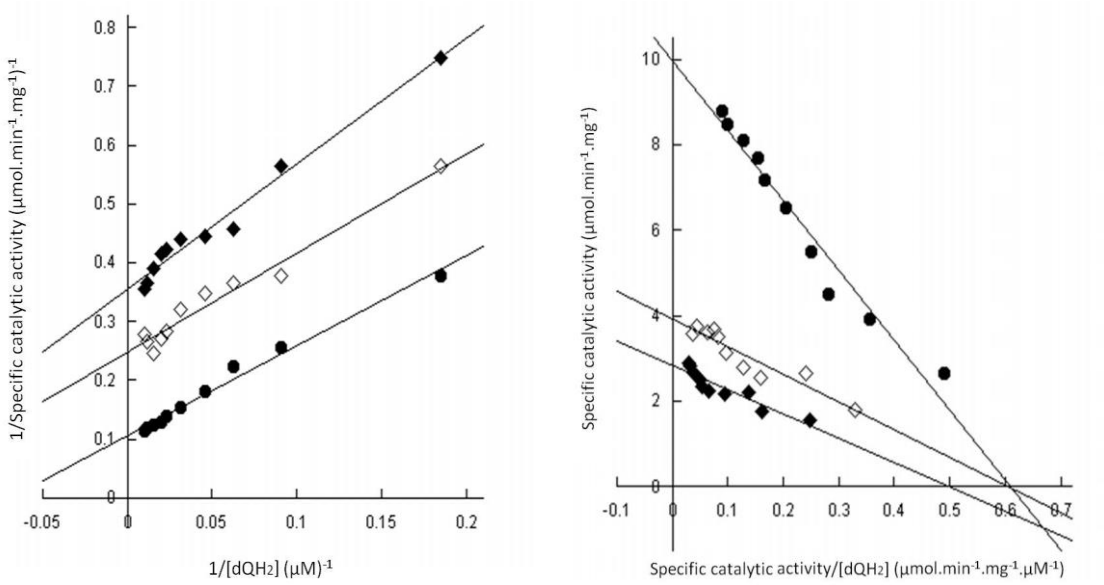

Figure 3.19: Substrate titration of steady state velocity for Mtb *bd*-I in the presence of the PG-203 inhibitor

A) Steady-state kinetics of Mtb *bd*-I at varying dQH_2 (5-98 µM) concentration with no inhibitor (closed circle), with 330 nM PG-203 (closed diamond) and with 110 nM PG-203 (open diamond) were fitted using the Michaelis-Menten function (Origin 8.5 software). B) Data as in (A) were fitted using the double reciprocal Lineweaver Burk plot. PG-203 shows an uncompetitive mode of inhibition with parrallel lines. C) Data as in (A) were fitted using the Eadie-Hofstee plot. PG-203 shows an uncompetitive mode of inhibition with intersecting lines at V_{max} /K_m values. The points are the mean initial velocity of experimental duplicates obtained at each dQH_2 concentration indicated. The data were fitted using Kalidagraph (Synergy software).

3.4. Discussion

A detailed understanding of the drug target and the mechanism of drug-target binding helps immensely in developing a lead. An initial characterization of recombinant Mtb cytochrome *bd*-I oxidase (Mtb *bd*-I) will be discussed in this chapter. There are several aspects of enzymes characterizations that merit consideration, some of which will be discussed here. The pH and detergent influences on Mtb *bd*-I activity were considered. In addition, substrate preference, catalytic behaviour and potential of Mtb *bd*-I as a drug target were studied.

A heterologous expression system (TML16) for Mtb *bd*-I characterization was developed using an *Escherichia coli bo*$_3$*/bd*-I knockout strain (ML16; *recA*, *cydAB*, *cyoABCDE*::Cm^r). Steady-state kinetics of Mtb *bd*-I for dQH_2 oxidation were performed using crude recombinant membrane of TML16 strain that was grown aerobically and under O_2-limited condition. The apparent K_m (μM) and specific catalytic activity (μmol. min^{-1}.mg^{-1}) values were calculated to be respectively 19.25 ± 1.3 and 9.01 ± 0.23, during O_2-limited growth condition and 21.52 ± 3.57 and 5.1 ± 0.29 during aerobic growth condition. The K_m values of Mtb *bd*-I from both growth conditions were similar, but not the specific catalytic activity values. This was justified through the fact that K_m is a characteristic of an enzyme for its substrate and is independent of the enzyme concentration used in the experiment. However, catalytic activity value varies with the amount of enzyme used and hence it has no absolute value (335). Therefore, all the experimental assays in this chapter were performed using crude recombinant membranes from O_2-limited grown TML16 as it had the highest catalytic activity.

Steady-state kinetics of Mtb *bd*-I oxidase revealed a substrate preference for dQH_2 over Q_1H_2 and Q_2H_2 (K_m = 19.25 μM, 51.5 μM and 65.2 μM). The reported K_m value of dQH_2 oxidation in *E. coli* (85 μM) (290) is much higher than that of Mtb *bd*-I, indicating the high affinity of dQH_2 for Mtb *bd*-I. Q_1H_2 is the preferred substrate for studying cytochrome *bd*-I in various organisms, recording a broad range of K_m values. The apparent K_m values estimated for cytochrome *bd*-I Q_1H_2 oxidation by *E. coli*, *Azotobacter vinelandii*, *Klebsiella pneumonia*, *Cyanobacterium synechocystis* and *Photobacterium phosphoreum* range from 40 μM to 280 μM. The initial steady-state kinetics of Mtb *bd*-I were consistent with previous studies whereby Mtb *bd*-I

conclusively catalyses the conversion of quinol to quinone with concomitant O_2 reduction. Importantly, the catalytic behaviours of Mtb *bd*-I in oxidation of dQH_2 and Q_1H_2 were similiar to its counterparts in other bacteria, following a monosubstrate reaction (described by the Michaelis-Menten equation) (212, 213, 321, 336, 345, 349, 354-357).

Regarding the enzyme kinetics of Q_2H_2 oxidation, different K_m values were reported for the *E. coli* cytochrome *bd*-I, 50 µM (356), 60 µM (358) and 42 µM (345). *Cyanobacterium synechocystis* cytochrome *bd*-I had a K_m value of 8 µM for Q_2H_2 oxidation (349). Although Mtb *bd*-I showed comparable kinetic to *E. coli bd*-I, it seemed to have the lowest affinity for the Q_2H_2 substrate. Notably, kinetic analysis with a wide range of substrate concentrations revealed that the oxidase activity of Mtb cytochrome *bd*-I showed sigmoidal concentration dependence at low concentrations of Q_2H_2, and marked substrate inhibition at high concentrations of Q_2H_2. In a structure-function study on the ubiquinol-2 analogs, the substrate inhibition of *E. coli bd*-I oxidase was related to the 6-diprenyl group and to the 3-methoxy group on the quinone ring (345). The peculiar kinetics were considered as a unique feature of *bd*-type quinol oxidase since in a similar Q_2H_2 concentration range, the alternative *E. coli* terminal oxidase, the cytochrome bo_3 heme-copper quinol oxidase, never exhibits such sigmoidality or substrate inhibition (358, 359). Vladimir (2003) noted that the substrate inhibition is often observed in the nonphysiological reaction and at high substrate concentrations where the substrates usually act as uncompetitive inhibitors and forming a dead-end complex (335, 352). In agreement with the Matsumoto *et al* (2006) study, the kinetic mechanism of Q_2H_2 oxidation by Mtb *bd*-I can be explained by a modified *Ping-Pong bi-bi* mechanism (following a bisubstrate reaction) (345).

The reaction of 'air-oxidized' Mtb *bd*-I with dQH_2 and Q_1H_2 substrates generated a monophasic kinetic plot, whereas with Q_2H_2 a biphasic kinetic plot was observed. Mtb cytochrome *bd*-I oxidase kinetic beheviour is in agreement with previously recorded kinetic behaviour in *E. coli* (211, 290, 345). However, there is discord between the orders of substrate preference ($dQH_2 > Q_1H_2 > Q_2H_2$, this study, and $Q_2H_2 > Q_1H_2 > dQH_2$, (345)). Importantly, the discrepancies in the kinetic parameter values and the substrate preference are referred to species-specificity and to the type

of protein used (recombinant or purified protein). Morover, further differences according to the degrees of the protein purification were recorded as well (345, 358). Steady-state kinitics of Mtb *bd*-I signified the uniqueness of cytochrome *bd*-I mechanism for the substrate oxidation and dioxygen reduction in accordance with previous studies.

Studying optimum conditions for enzyme activity and determination of those in which Mtb cytochrome *bd*-I oxidase was highly active was essential for future biophysical characterization. Regarding the pH significance, Wilson (2010) wrote that the enzyme activity is pH dependent. Therefore, the pH dependence of Mtb *bd*-I dQH_2 oxidase activity was studied, showing the highest activity of the enzyme (optimum pH of Mtb *bd*-I) at pH 7.5, with lower activity was observed at more acidic and alkaline pH values. Similarly, Lorence *et al* (1984) found that ubiquinol-1 oxidase activity of *E. coli* cytochrome *bd*-I oxidase had a broad optimum pH at and above pH 7.5 but low enzyme activity at acidic pH 6.5 - 5.5 (336). These effects of pH could be results of a combination of factors, the ionization state of amino acids residues of the catalytic side, the binding of substrate to enzyme, the ionization of substrate and the alteration of protein structure (particularly at extremes of pH) (194, 335).

Furthermore, the specific activity of Mtb *bd*-I was affected differently by detergents. High ubiquinol oxidase activity was observed in the presence of cholate, or deoxycholate, CHAPS, or DDM. However, in the presence of Triton X-100 or Tween-80, the decylubiquinol oxidase activity was notably reduced. In contrast, there was high ubiquinol-1 oxidase activity of *E. coli* cytochrome *bd*-I oxidase in the presence of γ-palmitoyl-L-α-alysophosphatidylcholine, or Tween-20, but it was totally inactive in presence of octylglucoside, cholate, or high concentrations of Triton X-100 (336). It is noteworthy that CHAPS, cholate and deoxycholate are ionic detergents while Tween-80, Triton X-100 and DDM are non-ionic detergents. Importantly, substrate binding, product formation and release can be critically affected by the ionization of different groups on the enzyme (334).

The cytochrome *bd*-family, as mentioned before (section 1.5.4.2), is subdivided into the A-subfamily with a long Q-loop, such as *E. coli bd*-I, and the B-subfamily with a

short Q-loop, such as *Bacillus stearothermophilus* and Mtb (215, 360). However, the functional role of different sizes of the Q-loop is not clear yet (211). Importantly, some of the short Q-loop cytochrome *bd*-I oxidase are cyanide insensitive oxygen reductases (CIO) such as *Pseudomonas aeruginosa bd*-I, which is distinguished by low heme *d* content (216). Herein, recombinant Mtb cytochrome *bd*-I was found to be a cyanide sensitive oxidase with an IC_{50} of 429.11 μM. These data are in comparable with the short Q-loop *B. stearothermophilus* enzyme that showed a similar IC_{50} value (~500 μM) against the duroquinol oxidase activity of the purified cytochrome *bd*-I (360). The long Q-loop purified *E. coli bd*-I was shown to be cyanide sensitive with an IC_{50} of 2 mM (213).

It worth mentioning that cyanide is a known bacterial cytochrome *bd*-I inhibitor, likely to act at the site of oxygen reduction. However, it does not have a potent inhibition activity (211, 213). Therefore, identifying a novel inhibitor that acts on the quinol oxidation site was the main focus of the current research.

HDQ, the core of quinolone-type inhibitors, is a known cytochrome *bd*-I inhibitor as seen in *Desulfovibrio vulgaris Hildenborough* (DvH) (210). Correspondingly, the HDQ data showed an inhibition effect of Mtb *bd*-I activity with an IC_{50} of 231 μM. Therefore, a total of 23 quinolone-type inhibitors were examined against both Mtb *bd*-I and the Mtb H37Rv strain (single-point screening at 5 μM of inhibitor concentration), from which the potency screen produced 9 compounds with an IC_{50} < 4 μM against Mtb *bd*-I.

Medicinal chemistry manipulation of the core template was the basis of inhibitor development with a view to maximize solubility and activity. The best 18 hits in the PfNDH2 programme were tested against Mtb *bd*-I, in addition to 5 more compounds, which were chosen arbitrarily from the MtbNDH2 programme. Some of these compounds are structurally related. The first structurally related group is the CK-3-22 (the primary template), RKA-259 and CK-3-14 group. CK-3-22 (ClogP = 5.49) has a nitrogen in ring C to improve solubility, which showed an IC_{50} of 140 nM against Mtb *bd*-I and good inhibition of Mtb H37Rv growth at 5 μM single-point screening. Furthermore, CK-3-22 has the trifluoromethoxy (OCF_3) group, acknowledged to improve the stability and lipophilicity of biologically active

molecules and hence improve *in vivo* uptake and transport (361, 362). Regarding RKA-259, although adding 7-methoxy into the CK-3-22 template enhanced inhibitor potency against Mtb H37Rv, it reduced RKA-259 effectiveness against Mtb *bd*-I with IC_{50} of 3.6 μM. In CK-3-14, replacing the OCF_3 group with fluorine (F) decreased the ClogP value (4.12). Fluorine is probably the next most favourite hetero-atom after nitrogen for incorporation into small molecules. However, inhibitor potency against both Mtb *bd*-I (IC_{50} = 10.6 μM) and Mtb H37Rv was reduced. In contrast, in the RKA-307, MTD-403 and RKA-310 group, adding 5,7-difluoro into RKA-307 (the primary template, ClogP = 4.06), which had a good activity against both Mtb *bd*-I (440 nM) and Mtb H37Rv, led to increased inhibitor potency in the MTD-403 compound without marked changes in the ClogP value. MTD-403 had a potent activity against both Mtb *bd*-I (IC_{50} = 270 nM) and Mtb H37Rv. This highlights the fact that fluorine as a substituent in active ingredients plays a significant role (361). Notably, although adding 7-methoxy into the RKA-307 template enhanced RKA-310 potency against Mtb H37Rv, it decreased RKA-310 activity against Mtb *bd*-I with an IC_{50} of 1.4 μM.

CK-2-88 is a primary template for 6 other compounds, which are CK-2-63, CK-3-23, RKA-70, RKA-73, PG-203 and LT-9. Although CK-2-88 (ClogP = 5.14) exhibited a potent activity against Mtb *bd*-I (IC_{50} of 20 nM), a weak inhibition effect against Mtb H37Rv was observed. Addition of OCF_3 into CK-2-88, as seen in previous compounds, conferred a potent CK-2-63 compound with IC_{50} of 3 nM against Mtb *bd*-I and a good inhibition profile against Mtb H37Rv. However, the solubility of CK-2-63 was decreased slightly as demonstrated in its ClogP value (ClogP = 6.11). On the other hand, swapping the substitution pattern in CK-2-63 at the 2 and 3 positions resulted in a more soluble PG-203 compound (ClogP = 5.23) with less potency against Mtb *bd*-I (IC_{50} of 70 nM) and with no inhibition activity against Mtb H37Rv. CK-3-23 (ClogP = 6.67) is CK-2-88 with the addition of 4-methoxy group, the compound was active but less potent and less soluble than CK-2-63. To improve the activity of CK-2-63, the replacement of O with CH_2 and H at the 3-position with CH_3 gave RKA-70 (ClogP = 6.32) with low effectiveness against both Mtb *bd*-I and H37Rv. Moreover, addition of *N*-hydroxy into the RKA-70 template to give RKA-73 did not show any significant improvement. LT-9 is CK-2-88 with F in the side chain

that showed better activity against Mtb H37Rv. However, this addition did not result in any significant improvement against Mtb *bd*-I from that of CK-2-88.

SCR-8-12 was developed as a bc_1 inhibitor against malaria and it showed good inhibition activity against both Mtb *bd*-I and H37Rv. Fluoroquinolone type compounds are used for the treatment of TB and currently constitute the second line of anti-TB therapy as they play a key part in the treatment of MDR-TB (147). However, RKA-41, a fluoroquinolone type compound, did not reveal good inhibitory activities against Mtb *bd*-I. SL-2-25 has an OCF_3 group and nitrogen as well to improve solubility. It showed a good activity against Mtb *bd*-I with an IC_{50} of 290 nM but was not active against Mtb H37Rv. WDH-1W-5 has a pyrazole in the side chain and gave poor activity against both Mtb *bd*-I and H37Rv. WDH-2A-9 is WDH-1W-5 with an addition of methyl at the 3-position to improve solubility. This addition improved WDH-2A-9 activity against Mtb *bd*-I with an IC_{50} of 6.5 μM, but retained poor inhibition activity against Mtb H37Rv. WDH-1U-10 has an ester group at the 3-position and Cl in the side chain, which confered potent activity against Mtb *bd*-I with an IC_{50} of 12 nM, but poor activity against Mtb H37Rv. GN-171 has an OCF_3 group instead of a Cl, this showed good activity with an IC_{50} of 250 nM against Mtb *bd*-I, but poor activity against Mtb H37Rv. Although PG-128 has an extra nitrogen in its side chain to improve solubility, it did not exhibit good activity against H37Rv and had an IC_{50} of 4.47 μM against Mtb *bd*-I. OB-231 has an extended side chain and its analogue OB-258 has a *N*-hydroxy group to look at its effect on activity. Both compounds showed poor activity against Mtb *bd*-I and H37Rv with IC_{50} values of 7.8 μM and 8.8 μM respectively, against Mtb *bd*-I.

From the quinolone-type inhibitors, a total of 9 inhibitors discussed above showed generally an acceptable inhibition profile with $IC_{50} < 4$ μM against Mtb *bd*-I and with 50% or more inhibition against Mtb H37Rv (single-point screening at 5 μM inhibitor concentration). These inhibitors were submitted for full IC_{50} evaluation during both aerobic (replicating Mtb H37Rv) and anaerobic, Wayne model, (non-replicating Mtb H37Rv) conditions. Some of these compounds showed a poor activity against replicating Mtb H37Rv, such as LT-9 although it had good activity against Mtb *bd*-I. Further, CK-3-22 showed good activity against both Mtb *bd*-I and replicating Mtb H37Rv, but not against non-replicating Mtb H37Rv. SCR-8-12 showed a similar IC_{50} (~ 3.5 μM) against both Mtb *bd*-I and replicating Mtb H37Rv,

but it was less potent against non-replicating Mtb H37Rv. Although CK-2-63 was more potent than CK-3-23 against Mtb *bd*-I, both inhibitors exhibited largely similar inhibition profiles with regard to replicating/non-replicating Mtb H37Rv. The similarity of growth inhibition assays might be due to the fact that both CK-2-63 and CK-3-23 were developed from the same template (CK-2-88). The potency of RKA-259 against replicating/non-replicating Mtb H37Rv was significantly better than that of RKA-307, although the latter was more potent than RKA-259 against Mtb *bd*-I. The phenotypic profile of RKA-310 against replicating/non-replicating Mtb H37Rv was even better than the previous compounds. RKA-310, following chemistry refinement, was replaced by an optimised version of the quinolone-type inhibitor, MTD-403. MTD-403 showed a potent inhibition profile against both Mtb *bd*-I and Mtb H37Rv. It should be noted that there was no significant correlation between Mtb *bd*-I and Mtb H37Rv growth inhibition assays. This might be due to the fact that the solubility and permeability characteristics of these inhibitors against bacteria would have an impact on how inhibitors behave (341); in addition to the possibility that these compounds may have multiple targets which would also confound a direct correlation with Mtb kill.

Interestingly, although there was no significant correlation between Mtb *bd*-I and Mtb H37Rv growth inhibition assays, excluding LT-9, CK-3-22, CK-2-63 and RKA-259 resulted in a highly significant correlation (P value < 0.01) with the remaining compounds. The significant correlation might suggest that Mtb *bd*-I (an ETC component) is a potential target for the tested quinolone-type inhibitors. This suggestion is further enforced by HepG2 data for mitochondrial toxicity assessment where CK-3-22, CK-3-23, CK-2-63, RKA-259, RKA-307, RKA-310 and MTD-403 showed much lower IC_{50s} in HepG2 cells cultured in galactose-containing media than that cultured in glucose-containing media (personal communication with Dr. Gemma Nixon). Therefore, HepG2 assays proved that inhibitors targeting the ETC. Briefly, IC_{50s} values of quinolone-type inhibitors were determined using HepG2 cells that were cultured in the presence of glucose or galactose. If the inhibitors target a mitochondrial component, HepG2 cultured in glucose-containing media will continue growing as they adapt to produce ATP through glycolysis while cells growing in the presence of galactose will be attenuated as ATP production will be through oxidative phosphorylation (363). Interestingly, SCR-8-12 did not show any

difference of IC_{50} values during both assays (with glucose or galactose), suggesting that SCR-8-12 had a different mode of action than other inhibitors, as also demonstrated by the time-kill data.

Bactericidal inhibitors are superior to bacteriostatic ones in reducing resistance development and in shortening the treatment period. However, the clinical importance of *in vitro* bactericidal inhibitors is rarely observed (364). The bactericidal/static nature of inhibitors on extra-cellular Mtb (Mtb grown in liquid culture) could be affected by various factors such as time scale of incubation, the metabolic state of Mtb (replicating or non-replicating Mtb), and the physiological conditions of the experiment (364-366). Evaluating the bactericidal/static nature of the quinolone-type inhibitors showed no bactericidal activity over 7 days with the exception of SCR-8-12. CK-3-22 and CK-3-23 treated Mtb exhibited almost identical behaviour to untreated Mtb over 7 days. In contrast, RKA-310 treated Mtb showed a low number of viable bacteria compared to that of untreated Mtb but without significant decline of viable count over 7 days of incubation. The bacteriostatic activities of LT-9, RKA-307, CK-2-63 and MTD-403 showed reduction of viable counts by day 7. These quinolone-type inhibitors, in addition to RKA-310, might display similar bactericidal/bacteriostatic activities, as demonstrated by the diarylquinoline TMC207, a selective inhibitor of mycobacterial ATP synthase. It is worth mentioning that the bactericidal nature of the TMC207 is characterized by a bacteriostatic phase in the first 7 days followed by a dose-related bactericidal phase (365). Therefore, the bactericidal/static nature of CK-3-22 and CK-3-23 might be apparent if the time scale of drug incubation exceeded 14 days. Significantly, SCR-8-12 showed a bactericidal activity that is similar to the standard drugs, streptomycin and isoniazid (366-369). SCR-8-12 seemed to operate by a different mode of action than other quinolone-type inhibitors, as supported by the aforementioned HepG2 data. Noticeably, de Steenwinkel *et al* (2010) found that isoniazid displayed a concentration-dependent killing manner while rifampicin was revealed to be a strongly time-dependent killing agent (366). Dhillon *et al* (2010) wrote that the bactericidal activity of TMC207 on extra-cellular Mtb was time but not dose-dependent for at least the first 12 days of drug incubation. Moreover, TMC207 killing was observed to be faster in tuberculous lesions than in aerobic culture, and it increased as treatment continued (365).

Examining the classification and mechanism of enzyme inhibition is of importance in terms of studying the mechanism by which an enzyme promotes its catalytic activity and revising how the inhibitor structures might be modified to increase their potency (335). The double reciprocal Lineweaver Burk data revealed that CK-2-63 is a non-competitive inhibitor implying that CK-2-63 might bind to the free enzyme that consequently might result in reducing substrate affinity binding. However, the Eadie-Hofstee plot of CK-2-63 was not conclusive, suggesting that CK-2-63 may exhibit a mixed-type of inhibition. SCR-8-12 and MTD-403 appeared to be competitive inhibitors. Competitive inhibitors are known to bind exclusively to the free enzyme, which subsequently leads to exclusion of any further substrate binding. Competitive inhibition is usually reflected by affecting the apparent value of K_m but not the value of V_{max} (353). However, SCR-8-12 and MTD-403 showed a decrease in the K_m value rather than an increase which means that the affinity of Mtb *bd*-I for the substrate increased; hence inhibitors seemed not to be binding to the quinol oxidation site. Copeland (2005) wrote that inhibitors that displayed the kinetic signatures of competitive inhibitors are not necessarily bound to the enzyme active site (353). SL-2-25 and PG-203 (CK-2-63 substitute) are reported to be uncompetitive inhibitors. This, in turn, suggests that as uncompetitive inhibitor they may exclusively bind to the enzyme substrate complex (353).

Identifying and developing potential Mtb *bd*-I and Mtb H37Rv quinolone-type inhibitors as novel therapeutic agents is conceivable. To this end, MTD-403 has been found to be the optimum compound. MTD-403 displayed an excellent therapeutic index (no toxicity) and permeability (well absorbed in gut). However, it was found to be metabolized very quickly. Hence, further optimisation work to improve the drug metabolism and pharmacokinetics (DMPK) properties of the template is ongoing (personal communication with Dr. Gemma Nixon). Moreover, further medicinal chemistry quantitative structure–activity relationship models (QSAR models) are needed to improve MTD-403.

Studying the enzyme active site in terms of the binding of a substrate(s) to the enzyme catalytic site and the subsequent conversion of the substrate(s) to product(s) is critical to gain a complete understanding of the way enzymes work. To gain such understanding, a wide range of strategies could be adopted in future, such as X-ray

crystallographic studies, irreversible inhibitor with radioisotope studies and kinetic studies. In addition to the kinetics studies of Mtb *bd*-I that were carried out in this study, measuring the oxygen affinity of Mtb *bd*-I is considered one of the basic kinetic characterizations of this enzyme. Unfortunately, lack of laboratory facilities hindered this investigation (231, 370-372).

Regarding the limitations of this study, although time-kill data were informative, increasing the time scale from 7 days to at least 14 days is recommended. Moreover, as carried out by Dhillon *et al* (2010) using various concentration of inhibitors is advised to examine the dose effect on eliminating Mtb (365).

Chapter IV

Generation and characterisation of a heterologous expression system for *Mycobacterium tuberculosis* cytochrome *bd*-I oxidase in an *E. coli* respiratory knockout (bo_3/*bd*-I/*bd*-II) mutant strain

4.1. Introduction

The aim of this chapter was to construct an additional expression system for *Mycobacterium tuberculosis* cytochrome *bd*-I terminal oxidase (Mtb *bd*-I) characterization. This system was used as a validation tool for the main Mtb *bd*-I biochemical features, obtained through using the ML16 strain.

Mtb *bd*-I characterization was accomplished using ML16, an *E. coli* bo_3/*bd*-I knockout (Chapter II and III). Owing to the challenges of expressing Mtb *bd*-I, an *E. coli* bo_3/*bd*-I/*bd*-II knockout strain (MB44) was used in order to have an additional possibility of successful expression of Mtb *bd*-I (Figure 4.1). However, although successful expression of Mtb *bd*-I using the MB44 strain was achieved, characterization studies of Mtb *bd*-I were carried out using the ML16 strain since the MB44 strain was too weak and difficult to grow to form the foundation of robust Mtb *bd*-I characterization studies.

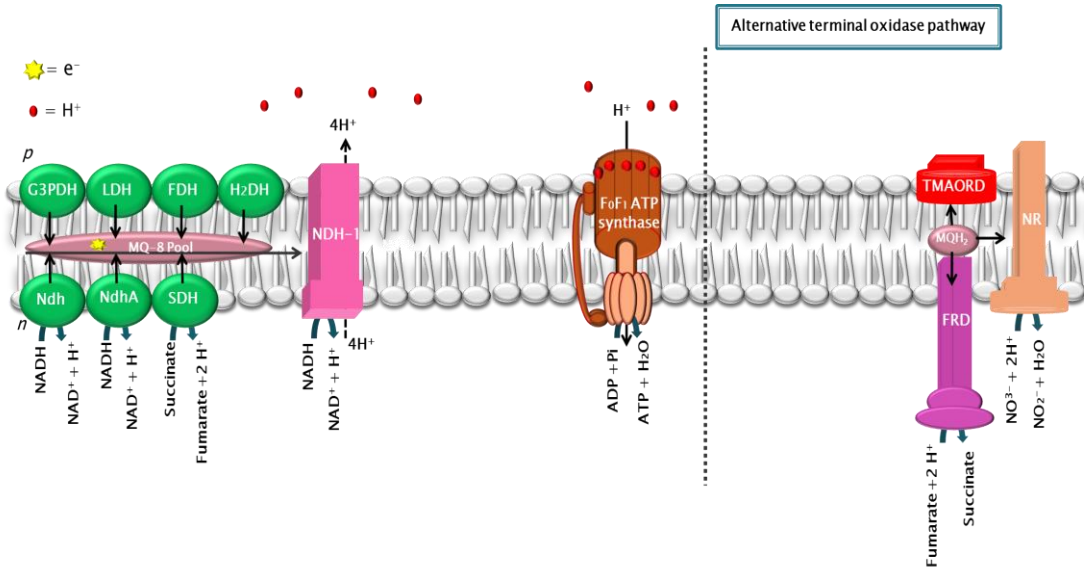

Figure 4.1: Components of the electron transport chain of MB44, an *E. coli* mutant strain

The chain has the entire electron donors found in wild type *E. coli* and only FRD-fumarate reductase, TMAORD-TMAO reductase and NR-nitrate reductase as electron acceptors. Chain components also include the F_0F_1 ATP synthase (complex V), MQ-8-menaquinone-8 and MQH_2-menaquinol. *P* and *n* correspond to the positive (periplasmic) and negative (cytoplasmic) sides of the respiratory membrane with respect to proton translocation. Proton movements are indicative only and do not represent H^+/e^- ratios for the respective complexes. The orientation and topology of the subunits are indicative only.

MB44 is a mutant *E. coli* BW25113 strain (Δ*cydB*::*Kan*^{r} Δ*cyoB* Δ*appB* Δ*nuoB*) lacking all three *E. coli* terminal quinol oxidases, cytochrome bo_3, cytochrome *bd*-I and cytochrome *bd*-II, encoded by the *cyoABCDE*, *cydAB* and *appBC* operons, respectively. Cytochrome *bd*-I and cytochrome *bd*-II are under the cytochrome *bd*-family in *E. coli* and have similar spectral signatures. However, as discussed earlier (Chapter 2.4), they have different expression conditions. Moreover, Bekker *et al* (2009) recorded different K_m values of quinol oxidation by cytochrome *bd*-I and cytochrome *bd*-II, which were 85 μM and 250 μM respectively (211, 290).

Bekker *et al* (2009) constructed MB44 with a kanamycin marker for selectivity. MB44 has phenotypic characteristics which require growth in LB medium enriched with 50 mM glucose and 50 $\mu g.ml^{-1}$ kanamycin. Moreover, MB44 has no significant respiratory activity; but in aerobic conditions, it catabolises glucose as an energy source by full homolactic fermentation into lactate. In contrast, it exhibits mixed acid fermentation in oxygen-limited conditions, producing lactate, acetate and succinate (194, 290).

4.2. Materials and methods

4.2.1. Preparation of competent cells

Competent cells were constructed using MB44, an *E. coli* bo_3/*bd*-I/*bd*-II knockout strain, donated by Dr. Martijn Bekker, University of Amsterdam, Nieuwe. The MB44 strain lacked all forms of quinol:oxygen oxidoreductase (i.e. cytochrome bo_3, cytchrome *bd*-I and cytchrome *bd*-II terminal oxidases). Following the protocol of Datsenko and Wanner (2000), MB44 was constructed to contain a kanamycin resistance cassette (300). Dr. Martijn Bekker informed me that MB44, a derivative of *E. coli* K-12 strain MG1655, grew in the presence of 50 $\mu g.ml^{-1}$ kanamycin and 50 mM glucose (290).

Competent MB44 cells were produced by the magnesium chloride/calcium chloride method. The aerobic culture condition was as follows: inoculation of overnight MB44 culture into 200 ml LB medium (in a 500 ml flask) enriched with 50 mM glucose and 50 $\mu g.ml^{-1}$ kanamycin, and incubated at 37 °C in a shaking incubator at 200 rpm. Generation of the O_2-limited culture involved inoculation of an overnight MB44 culture into 375 ml LB medium enriched with 50 mM glucose and 50 $\mu g.ml^{-1}$ kanamycin (in a 500 ml flask), sealed with a rubber plug with a head-space ratio of 0.5 and incubated at 37 °C in a shaking incubator at 200 rpm.

Competent cell preparations were performed according to the standard protocols of Sambrook and Russell (297). 100 ml of the cultures were centrifuged at 4000 *g* for 10 min at 4 °C once cell density reached OD_{600} ~ 0.25. Subsequently, cells were processed as described earlier in section 2.2.13. The competent cells were designated as AnMB44 (Anaerobic growth MB44) and AMB44 (Aerobic growth MB44).

4.2.2. Transformation of pTMA into MB44 competent cells

A volume of 200 µl of AnMB44 and AMB44 competent cells were transformed with the pTMA (10 µl) and processed as described previously (Chapter 2.2.14), with the exception of plating the cells to LB agar plates enriched with 50 mM glucose, 100 $\mu g.ml^{-1}$ ampicilin and 50 $\mu g.ml^{-1}$ kanamycin. Antibiotics were added to sustain plasmid transformant growth. Plates were incubated overnight at 37 °C aerobically

and anaerobically. After 3 days of incubation, colonies were picked from the plates and grown in 5 ml LB medium containing an appropriate concentration of antibiotic at 37 °C in a shaking incubator at 200 rpm. These cultures were then used for making glycerol stocks of the plasmid-containing cells and for larger scale cultures and plasmid preparation. The positive transformed cells were designated as TMB44 (O_2-limited growth TMB44) and ATMB44 (Aerobic growth TMB44).

Importantly, as experienced earlier with ML16 transformation (2.2.14), transformation of pTMA to AMB44 gave a strain that was less effecient to continue with; it took 3-4 days to grow on agar plates and about 3 days to grow in 5 ml LB medium over both growth conditions (aerobic and anaerobic). Importantly, transformation of pTMA to AnMB44 was successful for both growth conditions (aerobic and anaerobic).

4.2.3. Optimization of Mtb *bd*-I expression conditions

The general growth conditions were as follow: aerobic growth involved 200 ml of LB (in a 500 ml flask), containing 100 µg.ml^{-1} ampicilin and 50 µg.ml^{-1} kanamycin. The selective O_2-limited condition involved 375 ml of LB (in a 500 ml flask), containing 100 µg.ml^{-1} ampicilin and 50 µg.ml^{-1} kanamycin, sealed with a rubber plug with a head-space ratio of 0.5. Cultures were incubated at 37 °C in a shaking incubator at 200 rpm.

At first, the growth condition of TML16 that led to successful expression of Mtb *bd*-I (Chapter 2.2.15) was applied to TMB44 cells with a difference in medium supplementation (i.e. addition of 50 mM glucose). This growth condition included an addition of 1 mM IPTG along with inoculum and a total incubation time of 19 h. However, these parameters did not lead to successful expression of Mtb *bd*-I. Therefore, increasing the incubation time to 48 h was applied because the MB44 growth curve showed a continuation of growth up to 48 h (Figure 4.7), which will be discussed later. Simultaneously, the time of induction using IPTG was changed (induction after 24 h of incubation) due to the length of the incubation period, as extended IPTG inductions may result in protein degradation (personal

communication with Dr. Ashley Warman). Nevertheless, no successful expression of Mtb *bd*-I was detected. Optimization of the glucose concentration was the next step. Different glucose concentrations were used; 25 mM, 10 mM, 5 mM and 1 mM. The successful expression of Mtb *bd*-I was observed at 1 mM glucose. The final growth parameters were incubating for 48 h, addition of IPTG after 24 h of incubation and supplementation of the medium with 1 mM glucose.

It worth mentioning that after optimizing the glucose concentration and having successful expression of Mtb *bd*-I, TMB44 cells were grown in 1 mM glucose for 19 h and with addition of IPTG at the beginning along with inoculum, resembling the TML16 expression condition. However, no successful expression of Mtb *bd*-I was detected.

4.2.4. Large-scale culture of TMB44, AnMB44 and BL21(DE3)pLysS strains

The successful transformation colonies (TMB44) were grown in selective O_2-limited conditions, 375 ml of LB enriched with 1 mM glucose (in a 500 ml flask), containing 100 µg.ml^{-1} ampicilin and 50 µg.ml^{-1} kanamycin, sealed with a rubber plug with a head-space ratio of 0.5. IPTG was added after 24 h of incubation to 1 mM final concentration. Cultures were incubated at 37 °C in a shaking incubator at 200 rpm for 48 h. A negative control (untransformed MB44 competent cells) was grown in the same selective O_2-limited condition but without the addition of ampicilin. The inoculum size was 0.2% of 375 ml LB broth. Hereafter, the positive transformed cells were designated as TMB44 whereas the negative untransformed cells were designated as MB44.

Also, the same successful transformation colonies were grown in aerobic conditions, using 200 ml of LB enriched with 1 mM glucose (in a 500 ml flask) containing 100 µg.ml^{-1} ampicilin and 50 µg.ml^{-1} kanamycin. IPTG was added after 24 h of incubation to 1 mM final concentration. Cultures were incubated at 37 °C in a shaking incubator at 200 rpm for 48 h. A negative control (untransformed MB44 competent cells) was grown in the same selective O_2-limited condition, but without the addition of ampicilin. The inoculum size was 0.2% of 375 ml LB broth.

BL21(DE3) pLysS was cultured as wild-type *E.coli* strain following similar aforementioned aerobic and O_2-limited growth conditions, supplemented with only 34 $\mu g.ml^{-1}$ chloramphenicol.

4.2.5. Membrane preparations

Membrane preparations were carried out following the protocol of Fisher *et al* (2009) which was described previously in detail (section 2.2.17) (209).

4.2.6. Determination of protein concentration

The Bradford assay (304) was carried out as described in detail previously (section 2.2.18).

4.2.7. Initial spectroscopic study of Mtb *cydABDC* operon

Initial UV-visible spectroscopic analysis of freshly prepared membranes was carried out on a Cary 300 Bio UV/visible spectrophotometer (Varian, UK) following a previously described methodology (Chapter 2.2.19). Reduced minus oxidized spectra of the wild-type *E. coli* BL21 (DE3) LysS strain, MB44 and TMB44 cells were recorded over only O_2-limited conditions. Difficulties with having a decent volume of crude membrane from aerobically grown MB44 and TMB44 cells hampered the process of obtaining spectra.

4.2.8. Growth curves

Growth was monitored by measuring the optical density at 600 nm using a Thermo Spectronic instrument (Genesys, UK) over a time course (hours) under the above mentioned aerobic and O_2-limited growth conditions (section 4.2.4). A redox indicator (resazurin) was used following the previously explained protocol (section 2.2.20).

4.2.9. Preparation of dQH_2, Q_1H_2 and Q_2H_2

Preparation of both dQH_2 and Q_2H_2 were performed according to the protocol of Fisher *et al* (2004) (343). Preparation of Q_1H_2 was based on the protocol of Kihira *et al* (2012) (344) with modification. Detailed methods were previously presented (section 3.2.3. and 3.2.4).

4.2.10. Steady-state kinetic assays

Quinol oxidation (dQH_2 and Q_1H_2) by Mtb *bd*-I was measured spectrophotometrically at 283 nm on a Cary 300 Bio UV/visible spectrophotometer (Varian, UK). The method was described previously (section 3.2.5).

4.2.11. Enzyme inhibition assay

Determination of an IC_{50} value for MTD-403 against Mtb *bd*-I was performed using a Cary 300 Bio UV/visible spectrophotometer (Varian, UK) following the previously described protocol (section 3.2.8.2).

4.3. Results

4.3.1. The effect of recombinant Mtb cytochrome *bd*-I on cell pigmentation

During the membrane preparation process the transformed triple-knockout cells (TMB44) showed a colour change to a red/brown pigmentation following harvesting aerobic and O_2-limited cultures. In contrast, the triple-knockout cells (MB44) had a light yellow pigmentation following isolation from both aerobic and O_2-limited cultures (Figure 4.2).

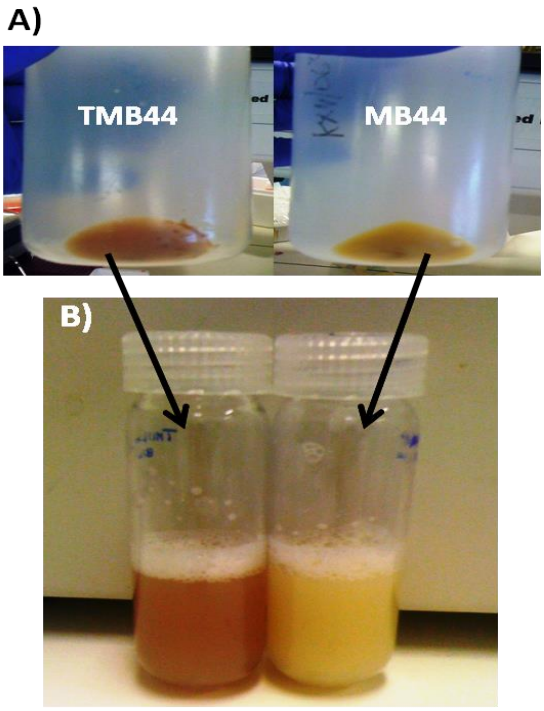

Figure 4.2: Effect of recombinant Mtb cytochrome *bd*-I expression on cell pigmentation

A) Harvested triple-knockout cells (MB44) and transformed triple-knockout cells (TMB44). B) The cell pellets of MB44 and TMB44 were resuspended in buffer (50 mM KPi, 2 mM EDTA, pH. 7.5). MB44 had a light yellow pigmentation whereas TMB44 (expressing the recombinant Mtb cytochrome *bd*-I) was accompanied by a change in the coloration of the cells to a red/brown pigmentation.

4.3.2. Initial spectroscopic study of the Mtb *cydABDC* operon

Reduced minus oxidized spectra of the wild-type *E. coli* BL21 (DE3) LysS strain, MB44 and TMB44 cells, growing at O_2-limited condition, were recorded at room temperature using sodium dithionite as reductant and potassium hexacyanoferrate (III) as oxidant (Figures 4.3 - 4.5). The presence of a distinctive peak at 631 nm was the significant difference between TMB44 and MB44 spectra which corresponded to that of the heterologous Mtb cytochrome *bd*-I in TMB44.

4.3.2.1. Wild–type *E. coli* BL21(DE3) pLysS strain

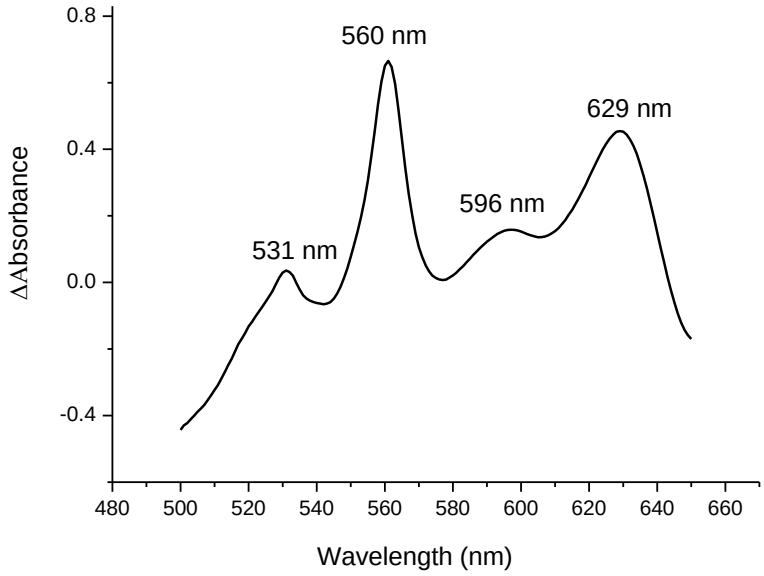

Figure 4.3: Reduced minus oxidized spectrum of wild-type *E.coli* BL21(DE3) pLysS strain

Reduced minus oxidized spectra of the wild-type *E. coli* BL21 (DE3) LysS strain was recorded at room temperature using sodium dithionite as reductant and potassium hexacyanoferrate (III) as oxidant. There are three distinct features spectra recorded in O_2-limited grown *E. coli*, which are cytochrome *b* at 561 nm, cytochrome a_1 at 596 nm and cytochrome *d* at 629 nm. The cells were grown for 48 h using closed shaken flasks with a head-space ratio of 0.5 and induced with 1 mM IPTG after 24 h of incubation. The ratio of heme *d* (629 nm) with respect to heme b_{560} as a reference peak is 0.71 in O_2-limited conditions. These peaks have been normalized according to the following equation (Value-min/max-min). The final protein concentration of the membranes was approximately 6.3 $mg.ml^{-1}$

4.3.2.2. Triple-knockout *E. coli* (MB44) strain

A)

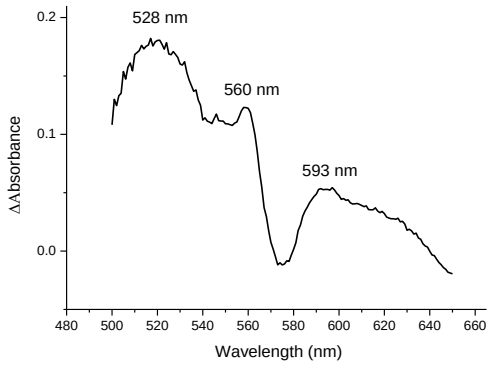

B)

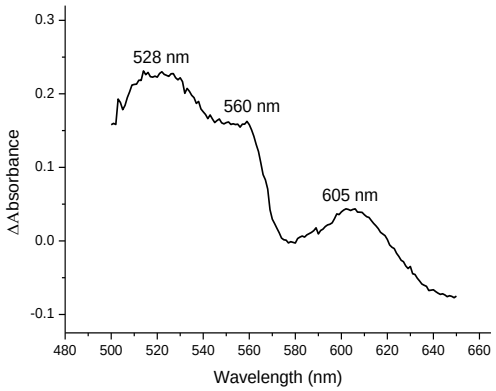

C)

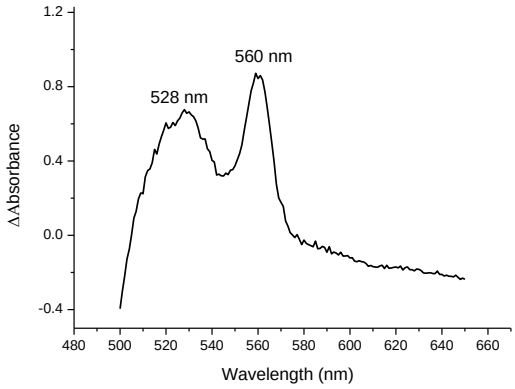

Figure 4.4: Reduced minus oxidized spectra of MB44

Reduced minus oxidized spectra of MB44 were recorded at room temperature using sodium dithionite as reductant and potassium hexacyanoferrate (III) as oxidant. The cells were grown in O_2-limited condition for 48 h using closed shaken flasks with a head-space ratio of 0.5 and induced with 1 mM IPTG after 24 h of incubation. A), B) and C) are spectra of MB44 crude membranes from different cultures batches. There are consistent peaks at ~ 528 nm and 560 nm in all membranes. A) and B) show a broad peak at ~600 nm that is not present in C) crude membranes. The final protein concentrations of A, B and C membranes were approximately 1, 1.3 and 2 $mg.ml^{-1}$

4.3.2.3. Transformed triple-knockout *E. coli* (TMB44) strain

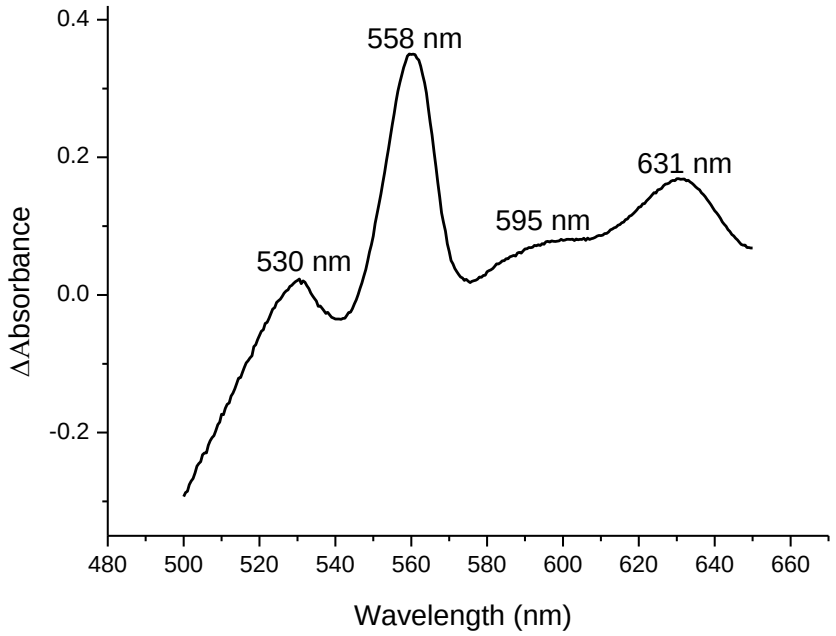

Figure 4.5: Reduced minus oxidized spectrum of TMB44

A reduced minus oxidized spectrum of TMB44 was recorded at room temperature using sodium dithionite as reductant and potassium hexacyanoferrate (III) as oxidant. Cytochrome *d* at 631 nm is recorded as distinct feature of recombinant Mtb cytochrome *bd*-I. The cells were grown in O_2-limited conditions for 48 h using closed shaken flasks with a head-space ratio of 0.5 and induced with 1 mM IPTG after 24 h of incubation. The ratio of heme *d* (631 nm) with respect to heme b_{558} as a reference peak is 0.34 in O_2-limited condition. These peaks have been normalized according to the following equation (Value-min/max-min). The final protein concentration of membrane was approximately 3 $mg.ml^{-1}$

4.3.3. Assessment of growth phenotypes

To qualitatively assess the contribution of Mtb cytochrome *bd*-I to respiration, monitoring the growth of wild-type, mutant and transformed cells was performed to identify the differences between *E. coli* BL21 (DE3) LysS, MB44 and TMB44 strains, respectively. Resazurin (Raz), a redox indicator, showed a qualitative result for the bacterial respiratory state, as discussed previously (2.3.7).

4.3.3.1. Wild–type *E. coli* BL21(DE3) pLysS strain

The growth of BL21(DE3) pLysS (wild-type *E. coli*) was monitored through both aerobic and O_2-limited growth conditions (Figure 4.6). During O_2-limited growth, the colour of the Raz was changed to dark orange/pink (Rru) after 6 h of incubation, during the exponential phase. Cells achieved highest density after 48 h incubation (OD_{600} ~ 0.5) and maintained a stationary plateau for about 12 h. Similarly, during the aerobic growth, the colour of Raz was changed to dark orange/pink after 6 h of incubation. Wild-type *E. coli* reached its highest density (OD_{600} ~1.6) after 48 h of aerobic incubation and maintained a stationary plateau for 12 h before starting to decline.

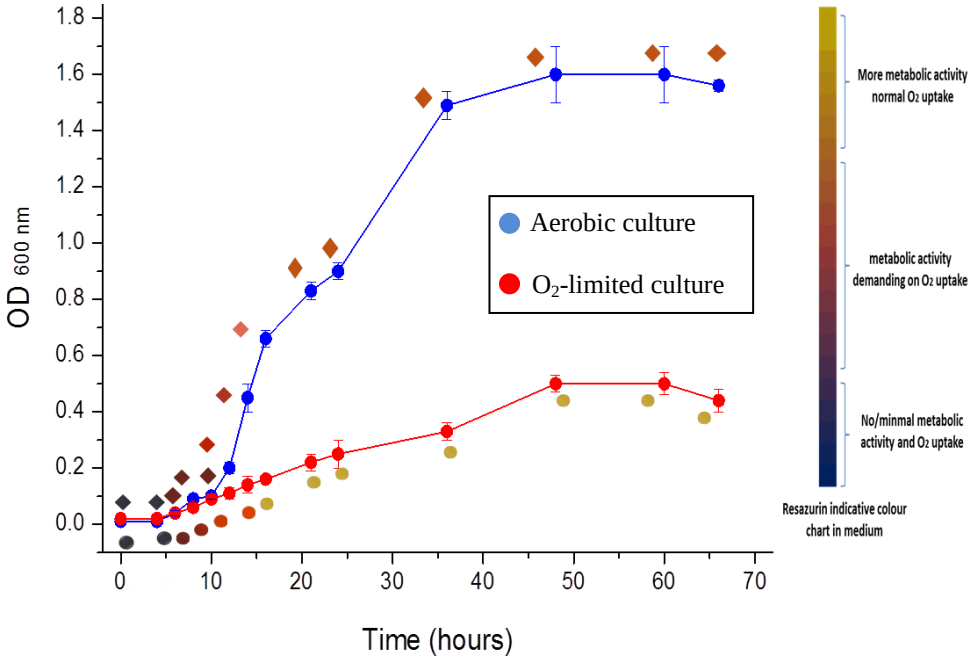

Figure 4.6: Growth of BL21(DE3) pLysS (wild-type *E. coli*) in vitro supplemented with resazurin.

Growth was monitored by recording optical density (OD_{600}) values of aerobic, shaken cultures (blue) and O_2-limited, closed, shaken cultures with a head-space ratio of 0.5 (red). The colours of the medium during the growth curve correspond to the colour of the resazurin in the medium (resazurin indicative colour chart). During both aerobic and O_2-limited growth, wild-type *E. coli* began reducing resazurin after 6 h of incubation and achieved maximal density after 48 h with OD_{600} ~ 1.6 and OD_{600} ~ 0.5 for aerobic and O_2-limited incubation, respectively.

4.3.3.2. Triple-knockout *E. coli* (MB44) strain

The growth of MB44 was assessed during aerobic and O_2-limited growth conditions (Figure 4.7). During both growth conditions, MB44 reached highest density after 48 h incubation with OD_{600} ~ 0.26 and started reducing Raz, after 10 h incubation. MB44 did not maintain a stationary plateau during both growth conditions and started to decline just after reaching its highest density.

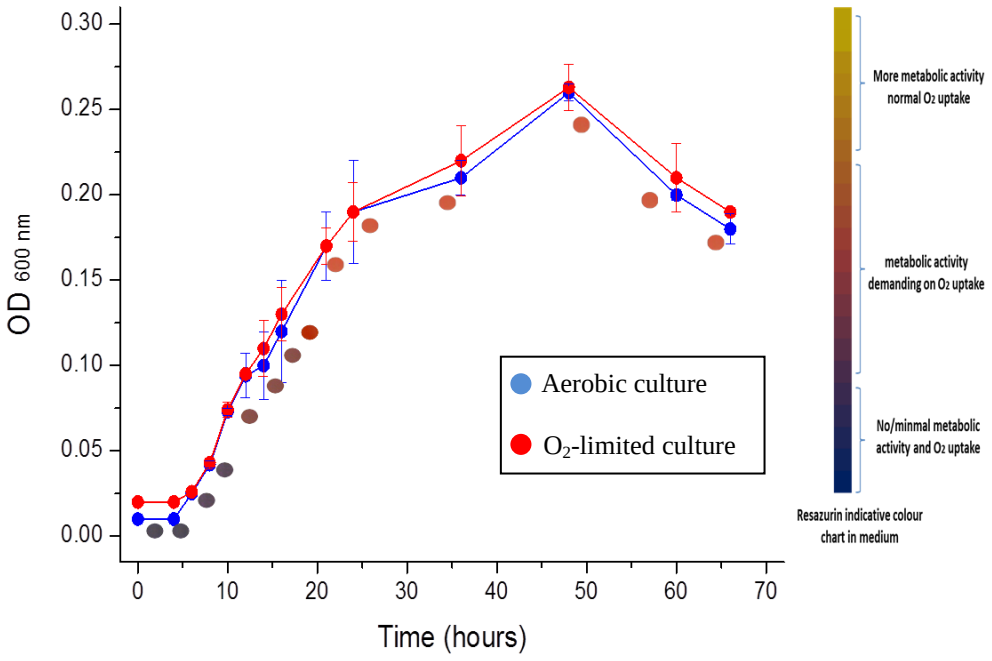

Figure 4.7: Growth of MB44 in vitro supplemented with resazurin

Growth was monitored by recording optical density (OD_{600}) values of aerobic, shaken cultures (blue) and O_2-limited, closed, shaken flasks with a head-space ratio of 0.5 (red). The colours of the medium during the growth curve correspond to the colour of the resazurin in the medium (resazurin indicative colour chart). During both aerobic and O_2-limited growth conditions, MB44 began reducing resazurin after 10 h incubation and attained highest cell density (OD_{600} ~ 0.26) after 48 h of growth.

4.3.3.3. Transformed triple-knockout *E. coli* (TMB44) strain

The growth of TMB44 was observed all through aerobic and O_2-limited growth conditions (Figure 4.8). Similar behaviours were observed during both growth conditions, the colour of the Raz was changed after 8 h incubation. TMB44 achieved highest density after 44 h incubation (OD_{600} ~ 0.53) and succeeded in maintaining a stationary plateau for about 14 h.

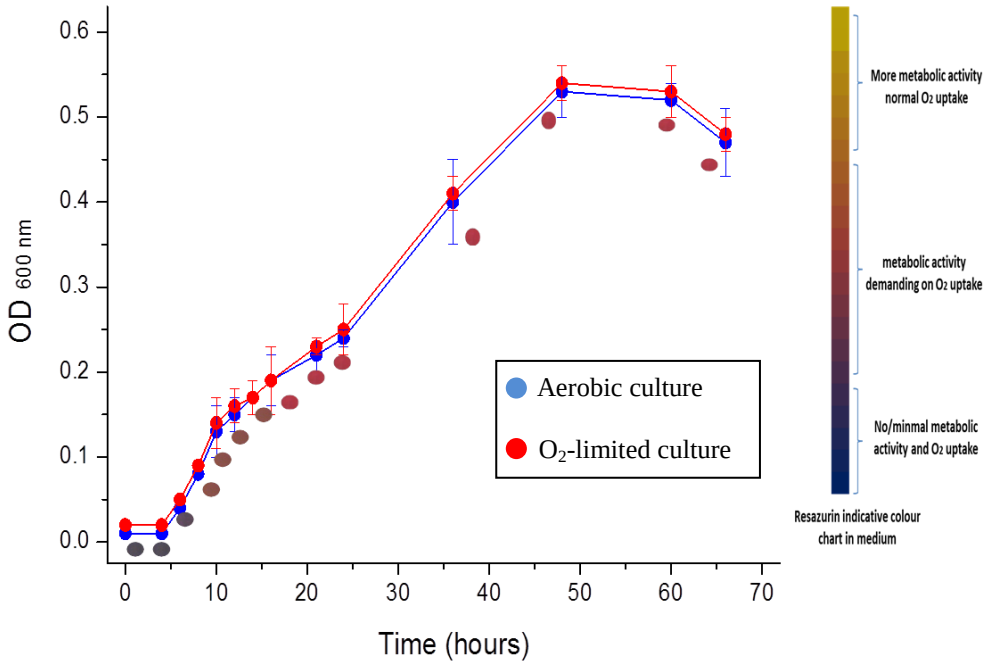

Figure 4.8: Growth of TMB44 in vitro supplemented with resazurin

Growth was monitored by recording optical density (OD_{600}) values of aerobic, shaken cultures (blue) and O_2-limited, closed, shaken flasks with a head-space ratio of 0.5 (red). The colours of the medium during the growth curve correspond to the colour of the resazurin in the medium (resazurin indicative colour chart). During both aerobic and O_2-limited growth conditions, resazurin reduction began after 8 h incubation and cells attained highest density (OD_{600} ~ 0.53) after 44 h incubation.

4.3.4. Kinetic analysis of the recombinant Mtb cytochrome *bd*-I oxidase

Initial kinetic characterisation of crude TMB44 membranes was performed as per TML16 in order to compare the Mtb *bd*-I data from two different expression systems. Examining Mtb *bd*-I in TMB44 membranes revealed similar K_m data to that of TML16 (section 3.3.3). Apparent K_m data for substrate analogues were determined spectrophotometrically (Figure 4.9) identifying a rank order preference for dQH_2 > Q_1H_2 with K_m values of 22.57 ± 2.1 µM and 51.83 ± 6.1 µM respectively. The specific catalytic activity values of Mtb *bd*-I for dQH_2 oxidation was 6.21 ± 0.51 µmol.min^{-1}.mg^{-1} and for Q_1H_2 was 1.74 ± 0.26 µmol.min^{-1}.mg^{-1} (Table 4.1). The kinetic parameters of Q_2H_2 oxidation were not determined due to limited quantities of the membrane preparations and time restrictions. However, preliminary data for Q_2H_2 showed that TMB44 demonstrated similar kinetics to TML16 (section 3.3.3.3), i.e. substrate inhibition at high Q_2H_2 concentrations. Due to limited quantities of MB44 membrane preparations and time restrictions, full kinetics studies were not performed. However, MB44 did not show any quinol oxidation activity at 50 µM dQH_2 or Q_1H_2.

Table 4.1: Kinetic parameters of Mtb *bd*-I activity

	K_m ± SEM (µM)	**Specific catalytic activity ± SEM (µmol.min^{-1}.mg^{-1})**
dQH_2 TML16	19.25 ± 1.3	9.01 ± 0.23
dQH_2 TMB44	22.57 ± 2.1	6.21 ± 0.51
Q_1H_2 TML16	51.55 ± 8.9	6.27 ± 0.53
Q_1H_2 TMB44	51.83 ± 6.1	1.74 ± 0.26

The kinetic parameters of Mtb *bd*-I in both expression systems, TML16 and TMB44, are presented.

A)

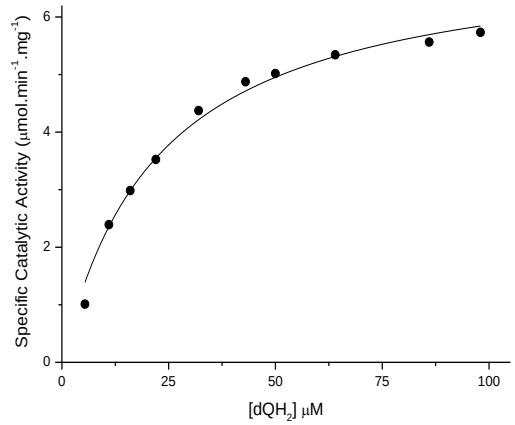

B)

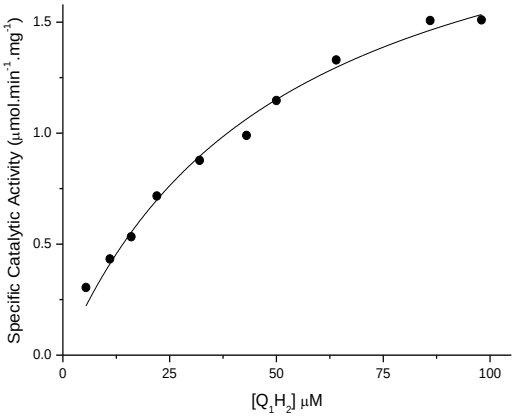

Figure 4.9: Steady-state decylubiquinol/ubiquinol-1: Mtb *bd*-I activity

Steady-state kinetics of Mtb *bd*-I were measured spectrophotometrically at 283 nm. A) The oxidation of dQH_2 was analysed and the apparent K_m (µM) and specific catalytic activity ($\mu mol.min^{-1}.mg^{-1}$) values were calculated to be 22.57 ± 2.1 and 6.21 ± 0.51 respectively. B) The oxidation of Q_1H_2 was analysed and the apparent K_m (µM) and specific catalytic activity ($\mu mol.min^{-1}.mg^{-1}$) values were calculated to be 51.83 ± 6.1 and 1.74 ± 0.26 respectively. The reactions were initiated by the addition of different concentrations of dQH_2 /Q_1H_2 (5 - 98 µM). The points are the mean initial rates of experimental duplicate obtained at each dQH_2/Q_1H_2 concentration indicated. Data were fitted using the Michaelis-Menten function using rectangular hyperbola (Origin 8.5 software).

4.3.5. Drug sensitivity assays

Inhibition studies of quinolone-type inhibitors against the recombinant Mtb cytochrome *bd*-I oxidase revealed a number of potent compounds against both Mtb *bd*-I and Mtb H37Rv. Herein, the most potent compound so far (MTD-403) was tested against Mtb *bd*-I from the TMB44 expression system (Figure 4.10). MTD-403 gave a similar IC_{50} value (330 ± 160 nM) to that obtained from the TML16 expression system (270 ± 60 nM) against Mtb *bd*-I (Chapter 3.3.4.2).

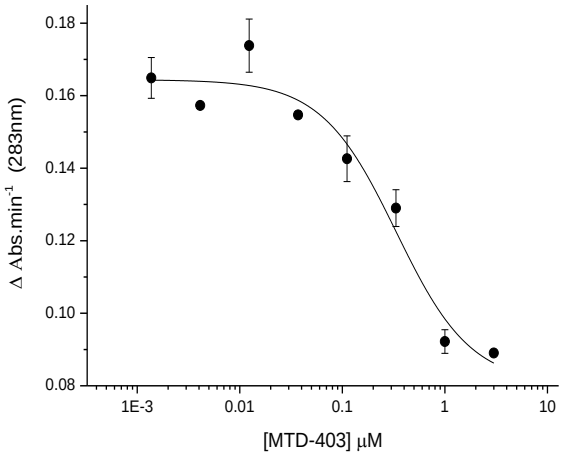

Figure 4.10: Determination of the IC_{50} for MTD-403 against Mtb *bd*-I activity

The IC_{50} value for MTD-403 in the decylubiquinol:Mtb *bd*-I assay was determined spectrophotometrically at 283 nm. The IC_{50} value is 0.33 ± 0.16 μM. The value is derived using averages of experimental duplicates ± SEM at each point. The data were fitted using a four parameter logistic function (Origin 8.5 software).

4.4. Discussion

The aforementioned phenotypic features of the MB44 strain were observed during expression studies of Mtb *bd*-I. MB44 was able to grow only in the presence of glucose and although the medium was enriched with a high concentration of glucose (50 mM), this mutant could only attain a low cell density (OD_{600} ~ 0.26) during the process of competent cells preparations. In accordance with these observations, Dassa *et al* (1991) showed that a triple *E. coli* mutant strain, SBS2019 (Δ*cyo*Δ*cyd*Δ*appB*::*TnphoA*), was not able to grow without the presence of a fermentative carbon source (glucose) and displayed drastic growth inhibition in the presence of oxygen. This growth inhibition was attributed to the accumulation of ROS in the cells. Moreover, SBS2019 was observed to form micro-colonies after prolonged incubation (291). Furthermore, it has been reported that ECOM3 (MG1655, Δ(*cydAB appBC cyoABCD*)::*FRT-kan-FRT*) is another triple *E. coli* mutant strain which was only capable of growth in the presence of glucose (373). These observations confirm that MB44 exhibited similar phenotypes to its counterparts of triple-knockout strains.

Regarding the expression conditions of Mtb *bd*-I, appropriate signalling of the regulatory components of cytochrome *bd*-I was discussed previously (section 2.4). Although appropriate expression conditions of Mtb *bd*-I were achieved in the double-knockout *E. coli* (ML16) strain, applying similar conditions to transformed MB44 (TMB44) was not successful in expressing Mtb *bd*-I. This observation was attributed to the strain phenotype differences. As mentioned above, MB44 demonstrates weak growth which leads to the extended incubation time of 48 h and induction of cells after 24 h of incubation, but these changes were not sufficient to express Mtb *bd*-I. Therefore, enlightened by the observation of Bekker *et al* (2009), enhancing the expression of cytochrome *bd*-II in *E. coli* in glucose-limited condition, limiting glucose supplementation in the medium was applied (290). Remarkably, Mtb *bd*-I was successfully expressed in MB44 cells under glucose limited conditions (1 mM glucose) and induction after 24 h of the 48 h incubation time. Since MB44 cells were slow growing cells, leaving MB44 to grow for the first 24 h without the stress of induction was the reason behind addition of IPTG after 24 h of incubation,

besides avoiding protein degradation as a result of long IPTG exposure (personal communication with Dr. Ashley Warman).

According to growth conditions or strains phenotypes, spectral analysis revealed different heme peaks. Reduced minus oxidized difference spectra recorded at room temperature were used to analyze the cytochrome content of MB44, TMB44 and wild-type *E. coli* BL21 (DE3) pLysS (reference strain). Difficulties in generating good yields of membrane severely limited the scope of further studies. Although there were differences in growth conditions, the reference strain which was induced after 24 h of incubation (reference strain-2) showed similar absorbance peaks of *b*-, a_1- and *d*-type cytochromes (at 560, 596, and 629 nm) to that studied previously, the reference strain that was induced at the beginning of incubation (reference strain-1) (section 2.4). These data were also comparable to the literature for "normal" wild-type *E. coli* BL21 spectra (313, 314).

Regarding MB44 spectra, although this mutant was harvested from relatively large cultures (27 L), the absorbance peaks were not always discernable due to poor membrane yields; a consequence of low cell density. However, there were two consistent peaks at 528 and 560 nm, which are characteristic peaks of *E. coli b*-type cytochromes (313, 314). Some of the MB44 membranes demonstrated peaks at 593 and 605 nm. MB44 does not have endogenous cytochromes (unlike ML16 which has cytochrome *bd*-II). Therefore, these unexpected peaks in MB44 could be attributed to the background noise of the spectra. Significantly, TMB44 spectra revealed similar spectral signatures to that of TML16 (Chapter 2.4), confirming the Mtb *bd*-I expression. The heme-*d* absorbance peak (approx. 628 - 632 nm) is a characteristic feature of the cytochrome *bd*-I oxidase in *M. smegmatis*, in *E. coli* and in *B. subtilis* (253, 263, 307).

TMB44 cultures displayed red/brown pigmentation as observed with TML16 cells (Chapter 2.4). This observation was attributed to the increased expression of heme-containing cytochromes; hence confirming the expression of cytochrome *bd*-I oxidase (289).

With regards to the growth rate, the reference strain-2 showed a relatively slow growth rate during O_2-limited conditions, compared to reference strain-1 (Chapter 2.4). Reference strain-2 reached its highest density (OD_{600} ~ 0.5) after 48 h incubation whereas reference strain-1 recorded the maximum at 12 h incubation with OD_{600} ~ 0.44. The growth delay in reference strain-2 induction could be attributed to a combination of factors, oxygen limitation and delayed IPTG induction. During aerobic conditions there were no significant differences between reference strain-1 and -2.

As expected, MB44 growth rate was too weak and slow during both growth conditions (aerobic and O_2-limited) in comparison with reference strain-2 and the ML16 strain (Chapter 2.4). MB44 hardly reached an OD_{600} ~ 0.26 while ML16 exceeded an OD_{600} ~ 1.7 and OD_{600} ~ 0.4 during aerobic and O_2-limited growth, respectively. MB44 data were in agreement with the findings of previous studies in which quinol oxidase mutant strains were reported to have weak and slow growth phenotypes, which in turn could be explained by the toxic effect of oxygen-derived compounds accumulating in the cells (290, 291, 373).

Significantly, TMB44 exhibited a more "healthy" growth rate than MB44 cells and restored the reference strain-2 growth rate during O_2-limited growth condition. During aerobic growth, although TMB44 showed a higher growth rate (maximal OD_{600} ~ 0.5) than MB44 (maximal OD_{600} ~ 0.26), expression of Mtb *bd*-I did not restore reference strain-2 growth rate (maximal OD_{600} ~ 1.6). This might be due to the adaption of the cells to synthesize a functional recombinant Mtb cytochrome *bd*-I oxidase, i.e. TMB44 cells under additional pressure of harnessing cellular resources to maintain and express plasmid genes. In addition, the plasmid may cause disruption in cellular metabolism which might hold back cell growth (325). Moreover, the time of IPTG induction might have an influence on cell growth.

To evaluate the contribution of cytochrome *bd*-I to respiration during growth, resazurin was used as a visual qualitative indicator of oxygen depletion in cultures and respiratory function (305). Reference strain-2 showed a similar initial resazurin reduction to the previously discussed reference strain-1 (Chapter 2.4). However, as

reference strain-2 was induced after 24 h of incubation unlike reference strain-1 (induction was at the beginning of the incubation), reference strain-2 showed a normal O_2 uptake state during O_2-limited growth conditions. The absence of IPTG pressure during the first 24 h of cell replication could be a justification for this observation. Remarkably, during aerobic and O_2-limited growth conditions, TMB44 started reducing resazurin (after 8 h of incubation) earlier than TML16 (12 h during O_2-limited and aerobic incubation). However, TMB44 showed similar resazurin colouration to that of TML16, which indicates a high demand on O_2 consumption (Chapter 2.4). During both growth conditions, the reduction of resazurin by MB44 was noticed after 10 h of incubation. The colour of resazurin during MB44 cultures was not a representation of O_2 uptake, but of the presence of acids (305, 323, 324). As mentioned earlier, MB44 during aerobic conditions operates full homolactic fermentation, producing lactate, and during oxygen-limited conditions it has a mixed acid fermentation that could explain the reduction of resazurin (218, 290).

With regards to the stationary phase (non-replicating phase) viability, the MB44 strain exhibited a stationary-phase viability defect. However, TMB44 during both aerobic and O_2-limited conditions was able to restore the loss of viability in the stationary phase similar to reference strain-2 and to the TML16 strain. The defect of MB44 in maintaining a stationary phase was in accordance with *cyd* mutant strains ML16 (this study, section 2.4) in *E. coli* (295) and an *A. vinelandi cydAB* mutant (328). These findings again confirm the importance of cytochrome *bd*-I during the non-replicating stage and the ability of Mtb *bd*-I to compensate for the loss of other terminal oxidases.

Importantly, steady-state kinetics of Mtb *bd*-I oxidase from TMB44 showed similar kinetic parameters (K_m values) for dQH_2 and Q_1H_2 and substrate preference (dQH_2 > Q_1H_2) to that of TML16 (section 2.4). These data confirm Mtb *bd*-I oxidase characteristics for dQH_2 and Q_1H_2 substrates. As discussed before, the variance in V_{max} values was due to the differences in the amount of enzyme used (335). Moreover, MTD-403, the optimum quinolone-type inhibitor against Mtb to date, was tested against Mtb *bd*-I oxidase from the TMB44 membrane preparation in order to

further confirm Mtb *bd*-I characterization. The IC_{50} of MTD-403 was similar to that obtained using the TML16 strain.

In summary, Mtb *bd*-I was successfully heterologously expressed in an *E. coli* triple-knockout system. The steady state kinetic features and inhibitory profile were consistent with those previously observed using the double-knockout system (TML16), supporting the validity of the latter. The slow growth rate and poor yields derived from the TMB44 and MB44 lines, however, make these systems unsuitable for large scale use, as is required for drug discovery or protein purification.

Chapter V

Pharmaco-metabolomics of *Mycobacterium tuberculosis*

5.1. Introduction

The objective of this chapter was to begin to study the pharmaco-metabolomics of Mtb first line and developing drugs. The broader objective is to generate a metabolomics fingerprint for drugs with validated modes of action (MoA) and to determine whether the fingerprints are consistent with proposed MoA of new drugs.

Metabolomics is a systematic study that quantitatively and/or qualitatively profiles the living system metabolome. The metabolome gives a holistic view of the living system when combined with other ‘‘omics’’ approaches, transcriptomics and proteomic (374, 375). Considering the global increasing rates of MDR-and XDR-TB (143, 144), expanding the knowledge of the drug MoA will allow more rational development of new drugs to bypass resistance to current TB therapy. Knowledge of the Mtb response at the transcriptomic, proteomic or metabolomic level to novel compounds, as well as to the clinically used drugs, usually offers a credible proof of the affected metabolome pathways and thus understanding their MoA. Moreover, important secondary effects of antimicrobial drug action would be revealed, which in turn allows for the development of co-drugs that target such secondary responses as a new direction of antimicrobial therapy (376).

Metabolic changes signal the organism response to a drug’s perturbation and the ability of the organism to adapt to the disruption. However, envisaging targets that would have a cidal effect on replicating and non-replicating Mtb is hampered by incomplete understanding of such metabolic responses to target disruption by new drugs and by the current anti-TB therapies (241). Moreover, this process is also limited by a lack of complete understanding of drugs MoA. Most of the studies on anti-TB drugs MoA have centred on the primary target and its associated mutations that count for emerging resistant strains. The MoAs of current TB drugs (DOTS) on the Mtb metabolome are not well characterized. Studying the perturbations of the Mtb metabolome by DOTS are limited to transcriptional and proteomic studies (241, 376).

In this chapter, the front line anti-TB drugs (isoniazid (INH), rifampicin (RIF), ethambutol (EMB) and streptomycin (STR) were examined along with two of the

previously tested Mtb *bd*-I in house quinolone-type inhibitors, CK-2-63 and RKA-307, and trifluoperazine (TPZ), a phenothiazine-based compound, targeting type II NADH:quinone oxidoreductase, to understand various metabolic alterations of Mtb bacilli upon exposure to these drugs. The mode of action of these inhibitors was previously described (Chapter 1.4.1) and is depicted in Figure (5.1). The central carbon metabolites were included in this study owing to their critical roles during TB infection (Chapter 1.5.2, Figure 1.14). Moreover, redox couples, bioenergetic couples and some of the amino acid metabolites were also included. As the Mtb rely on lipids *in vivo* (172-175), some key metabolites that link fatty acids metabolism with TCA cycle and glyoxylate shunt were included such as acetyl-CoA, propionyl-CoA, succinyl-CoA and methylmalonyl-CoA (16). However, other metabolites of fatty acid metabolism were not incorporated due to method limitation, which will be discussed later in this chapter.

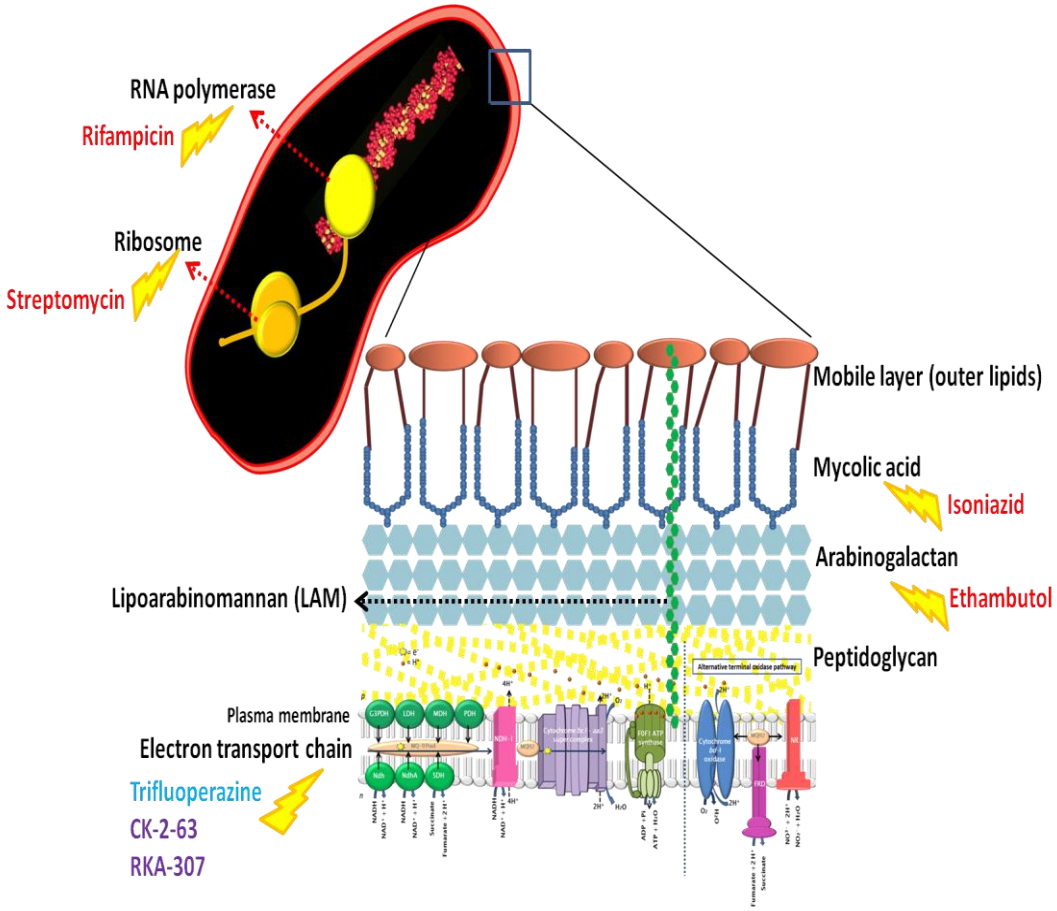

Figure 5.1: Schematic diagram of the proposed mode of action of DOTS and Mtb respiratory inhibitors

Recently, high-resolution mass spectrometers have emerged in the field of microbial metabolomics, driving the research towards obtaining profiles of a large number of low-molecular-weight compounds (metabolites) in highly complex biological samples. Metabolites, the intermediates of biochemical reactions, have a critical role in linking different operating metabolic pathways within the living cells that generate a tight controlled metabolic network. Liquid chromatography-mass spectrometry (LC-MS)-based metabolomics experiments have different approaches, targeted analysis or non-targeted profiling. Targeted analysis aims at measuring a predefined set of known metabolites whereas non-targeted profiling is based on identification and quantitation of unknown metabolites (374, 377).

The metabolome of living cells has a large variety of metabolites that differ in chemical structures and properties. The metabolome complexity is a result of wide-ranging chemical compounds that range from hydrophilic carbohydrates, volatile alcohols and ketones, amino and non-amino organic acids, hydrophobic lipids, and complex natural products to ionic inorganic species which makes identifying the complete metabolome at the same time virtually unfeasible (378).

Studying the metabolome is a multiple-step process which typically includes cell growth, metabolism quenching, metabolome extraction, and sample concentration, metabolites detection by LC-MS or another advanced method and finally data analysis (378). The quenching step is based on arrest of all metabolic activities that exist in living cells and typically accomplished through quick alteration in temperature or pH (379). There are different approaches for quenching the metabolism of cells grown in liquid culture (the common physiological condition of most microbes) that have been reviewed in details by Rabinowitz (2007), of which the quench the harvest method was applied in this study (380). Here, quenching and extraction are combined as a 40:40:20 acetonitrile:methanol:water solution results in extraction of the intracellular metabolites because of disruption of the cell wall, as well as metabolism quenching. Importantly, at the metabolome quenching step, isotopic internal standards can be added to the quenching solvents in order to obatin precise quantitaive data (377).

Regarding the extraction step, an ideal extraction aims to extract all or most of the metabolites in their original state (i.e., the extraction solvent should stop any further physical and chemical alterations of the metabolites) and in a quantitative manner. More than one solvent is usually used as one mixture during the extraction procedure in order to be compatible with all types of metabolites. For instance, polar solvents like methanol or methanol–water mixtures are used to extract polar metabolites, whereas non-polar solvents like chloroform or hexane are used for lipophilic compounds extraction (377, 381).

Prior to sample analysis, a concentration step is required to remove all the solvent(s) from the samples due to high sample dilutions that result in lower concentration of metabolites, although risking of metabolome alterations is expected. Therefore, removing solvents is needed to enhance metabolite signals at the detection phase and to avoid any interference of these solvents with the subsequent analysis. There are different methods of metabolite concentration, of which the most efficient and common one is through using a nitrogen gas stream to evaporate solvent (378).

In terms of metabolites detection and analysis, a highly sensitive and selective technique, liquid chromatography-tandem mass spectrometry (LC-MS/MS), was applied. LC-MS/MS is an analytical chemistry technique that combines physical separation, ionization and characterization of one or more compounds using tandem mass spectrometry. LC-MS includes three essential steps which are liquid chromatography separation, ionization, and separation and quantitation of the ions by mass spectrometry. This method is able to profile over a hundred cellular metabolites in a single chromatographic separation. The mass spectrometry spectrum presents masses of the ionized molecule and its fragments which are the total of the component atoms masses. Specificity arises from two orthogonal dimensions of separation: chromatographic retention time (RT) and mass-to-charge ratio (m/z), and in modern instruments the specificity is further increased by multiple rounds of MS (‘‘tandem mass spectrometry’’ or ‘‘MS/MS’’) (377, 382).

5.2. Material and methods

5.2.1. Preparation of targeted metabolomics solutions

5.2.1.1. Solvents and Chemicals

Water (H_2O; VWR International Ltd, UK), acetonitrile (CH_3CN; Fisher Scientific, UK) and methanol (CH_3OH; Fisher Scientific, UK) were all HPLC grade. Ammonium acetate ($C_2H_3O_2NH_4$) was purchased from VWR International Ltd (UK). Mass spectroscopy grade formic acid (CH_2O_2, ≥ 98%) and ammonium hydroxide (NH_4OH) were obtained from Sigma Aldrich (UK).

5.2.1.2. Quenching solution

The quenching solution consisted of 40:40:20 acetonitrile (ACN): Methanol (MeOH): water (H_2O) + 0.1 M formic acid and was spiked with 200 μM of internal standards, β-alanine and DL-arabinose for positive and negative modes, respectively. Solutions were prepared and stored at -20 °C (383).

5.2.1.3. Extraction solution

The extraction solution consisted of only 40:40:20 ACN:MeOH:H_2O and was prepared in a similar manner to the quenching solution (section 5.2.1.1).

5.2.1.4. Mobile phase solvents

The mobile phase solvent consisted of two main solvents, solvent A [20 mM ammonium acetate + 20 mM ammonium hydroxide in 95:5 water: acetonitrile (pH 9.45)] and solvent B (acetonitrile, ACN). Before use, the mobile phase was filtered through a sterile bottle top filter unit with a 0.22 μm membrane (Fisher Scientific, UK), sonicated and degassed using a sonicator (Fisher Scientific, UK) for 15 min. This mobile phase was used due to its compatibility with the luna aminopropyl column used in this study, as tested by Rabinowitz's lab (384, 385).

5.2.2. Preparation of inhibitor stock solutions

10 mM inhibitor stocks were prepared according to their solvent solubility as detailed before in section 3.2.8.1. 10 mM stock solutions were prepared and kept at -20^{o}C for no longer than 1 month. Final dilutions were made with culture medium (7H9 MiddleBrook) and freshly prepared prior to studies being carried out (Table 4.1). The effect of DOTS drugs, isoniazid, ethambutol, rifampicin and streptomycin, on Mtb H37Rv metabolites were examined along with quinolone-type inhibitors, CK-2-63 and RKA-307.

5.2.3. Culture of *Mycobacterium tuberculosis*

Cultures of *Mycobacterium tuberculosis* H37Rv were carried out as described previously (section 3.2.9). Briefly, aerobic cultures of Mtb H37Rv were grown to mid-log phase at 37 °C in 10 ml growth medium (Middlebrook 7H9 broth) supplemented with 10% (v/v) ADC, 0.2% (v/v) glycerol, and 0.05% (v/v) Tween® 80.

5.2.4. Protocol for sampling metabolites from Mtb H37Rv culture

Currently, the protocol for microbial metabolomics analysis is still in the proof-of-concept stage, thus protocols are typically developed for a specific study (379). There are several protocols used to extract metabolites from bacteria. The most common used are filter-based cell culture, batch liquid culture and chemostats. Filter-based cell culture and chemostats were excluded due to CTL3 facilities limitation. The metabolite extraction processes involve two main steps, metabolism quenching and metabolites extraction. Quenching metabolism was accomplished using a cold quenching solution, 40:40:20 ACN:MeOH:H_2O. This mixture was found to be effective in quenching metabolism and in extracting nucleotide triphosphates from *E. coli*. Metabolite extraction was attained by centrifugation (380, 382).

Following the protocol of Rabinowitz (2007), metabolite sampling from Mtb H37Rv liquid culture was applied with modification (380). The quenching solution 40:40:20

ACN:MeOH:H_2O was acidified with 0.1 M formic acid and spiked with 200 µM of internal standards, β-alanine and DL-arabinose. The addition of formic acid in the quenching solution helps protecting nucleotide triphosphates against degradation. This quenching solution was used to simultaneously quench metabolism and initiate the extraction process. Moreover, it is worth mentioning that 40:40:20 ACN:MeOH:H_2O solution was used for Mtb H37Rv metabolite extraction because it was verified to kill all viable Mtb H37Rv where it has been used in previous Mtb studies (160, 241). To further confirm this before commencing the experiment, the following ratios 1:6, 1:8 and 1:10 of Mtb H37Rv culture: 40:40:20 ACN:MeOH:H_2O solution were cultured grown on 7H11 agar plates and incubated at 37 °C in a 5% CO_2 HERACell 150 CO_2 incubator (Thermo Scientific, UK). After 5 weeks of incubation, no colony growth was recorded at all ratios. Therefore, 1:8 (Mtb H37Rv culture: quenching solution) ratio was used for quenching process in this study. Importantly, the 40:40:20 ACN:MeOH:H_2O mixture at cold temperature is considered a general efficient quenching and appropriate solvent for metabolite extraction due to its compatibility to hydrophilic interaction liquid chromatography (HILIC) compounds which cover most of the polar and some of the non-polar metabolites (241, 378, 383, 384).

5.2.4.1. Experiment set-up

Drug-containing growth medium was placed in the wells of 24-well plates. Drugs were present at a final concentration of IC_{90} (90% inhibitory concentration), as determined from modified MABA assays (section 4.3.4, Tables 4.3 and 4.5). The IC_{90} value of TPZ (36.02 µM) was obtained from the Warman *et al* (2012) study (282). With a view to capture the primary effects of the drugs/inhibitors on Mtb metabolic, IC_{90} was chosen as the final concentration rather than using IC_{50} through consulting previously published studies (241, 386). A drug-free control (vehicle control) was included in order to monitor normal culture growth. Exponentially growing Mtb H37Rv cells were harvested at an OD_{600} of ~1 by centrifugation at 0 °C, using an Eppendorf 5804R refrigerated centrifuge (Eppendorf, UK), at 5000 *g* for 10 min. Pelleted materials were resuspended in a cold drug free Middlebrook 7H9 Broth (lacking glycerol, Tween® 80 and ADC). Subsequently, the culture was

added to equal volumes of drug-containing growth medium (final concentration of culture corresponded to OD_{600} of 0.5, 1 x 10^8 cfu.ml^{-1}) in the wells of 24-well plates. The final concentration of culture was chosen following the protocol of Griffin *et al* (2012) (184). The 24-well plate was incubated at 37 °C in a 5% CO_2 HERACell 150 CO_2 incubator (Thermo Scientific, UK). ampho

5.2.4.2. Metabolites extraction

Following pre-determined incubations of 0, 1, 2, 3, 6 and 7 days, aliquots of the cultures were withdrawn and the extraction step initiated. The Mtb H37Rv culture was quenched using cold quenching solution in ratio 1:8 (culture: quenching solution). Subsequently, samples were vortexed for 30 s before centrifugation at 5000 *g* for 15 min at 0 °C using an Eppendorf 5804R refrigerated centrifuge (Eppendorf, UK). Afterward, supernatants were collected in a sterilized tube and the remaining pelleted materials were resuspended in a cold extraction solution (40:40:20 ACN:MeOH:H_2O). In similar manner, samples were vortexed, centrifuged and supernatants were pooled with the preceding supernatant. Pooled supernatant was filtered using a 0.22 μM Millex® filter unit (Millipore, UK). The samples were transferred to the LC-MS/MS lab and stored at -80 °C to be processed through LC-MS/MS no later than a week from sampling.

5.2.5. LC-MS/MS samples preparation

According to the protocol of Biagini *et al* (2012), samples were transferred to glass vials and dried under a stream of nitrogen. Mobile phase solvent A (pH 9.45) was used to resuspend the dried samples. Afterwards, samples were vortexed, filtered using a 0.22 μM filter unit (Phenomenex-RC, UK) and transferred to Chromacol LC-MS/MS glass vials (Chromacol, Thermo Fisher Scientific Inc., UK) (387).

5.2.6. Preparation of standards stock for calibration curve standards

Following the protocol of Biagini *et al* (2012) that was established by PhD student Murad Mubaraki, standards stocks were prepared according to their solvent solubility at specific concentrations for each metabolite (Sigma Aldrich, UK) (Table 5.1). Consequently, 100 µl of each metabolite was merged in one standard mixture before the preparation of 16 serial dilutions of the standard mixture, which was carried out using HPLC grade water. These 16 standard levels were processed through the extraction step and prepared for LC-MS/MS analysis in a similar manner to that described earlier (section 5.2.4.2 and 5.2.5). These standard levels were analysed through LC-MS/MS (section 5.2.7) before generating the calibration curves by plotting the area ratio of the metabolite standard (The area under the curve (AUC) of metabolite divided by AUC of internal standard) against its concentration. The linearity for each metabolite was evaluated by using linear regression.

Table 5.1: Metabolite primary stocks concentration for calibration curve standards

Metabolites	MW ($g.mol^{-1}$)	Primary Stock Concentration (mM)	Solvent
Glucose	180.16	11.10	H_2O
Fumarate	116.07	17.23	H_2O
Succinate	118.09	16.93	H_2O
Malate	134.09	14.91	H_2O
α-ketoglutarate	146.11	13.68	MeOH
(Iso)-Citrate	192.12	10.41	MeOH
PEP, Phosphoenolpyruvate	168.04	11.90	H_2O
G-3-P, Glycerol-3-phosphate	170.05	11.62	H_2O
Hypoxanthine	136.12	14.70	DMSO
Lactate	90.08	44.40	H_2O
DHAP, Dihydroxyacetone phosphate	170.06	23.52	H_2O
Oxaloacetate	132.07	151.43	H_2O
Acetyl-CoA	809.57	12.35	MeOH
Succinyl-CoA	867.60	5.76	H_2O
Propionyl-CoA	823.60	6.07	H_2O
Methylmalonyl-CoA	867.61	2.31	H_2O
Alanine	89.09	22.44	H_2O
Asparagine	132.12	15.13	H_2O
Aspartate	133.1	15.02	H_2O
Glutamine	146.14	13.68	H_2O

Table 5.1 (*Continued*)

Metabolites	MW ($g.mol^{-1}$)	Primary Stock Concentration (mM)	Solvent
Glutamate	147.13	13.59	H_2O
Arginine	174.2	11.48	MeOH
Proline	115.13	17.37	H_2O
Serine	105.09	19.03	H_2O
Valine	117.15	17.07	H_2O
Threonine	119.12	16.78	H_2O
Cysteine	121.16	33.02	H_2O
(Iso)-leucine	131.17	15.24	H_2O
Lysine	146.19	13.68	H_2O
Methionine	149.21	13.40	H_2O
Histidine	155.15	12.89	DMSO
Phenylalanine	165.19	12.10	MeOH
Tryptophan	204.23	9.79	H_2O
Tyrosine	181.19	11.03	H_2O
Ornithine	132.19	15.13	MeOH
Citrulline	175.19	11.41	H_2O
NAD	663.43	3.01	H_2O
NADH	664.43	3.00	DMSO
GSH, Glutathione	307.32	6.50	H_2O
GSSG, Glutathione disulfide	612.63	3.26	H_2O
NADP	744.41	2.69	H_2O
NADPH	745.41	2.68	DMSO
FAD, flavin adenine dinucleotide	785.55	2.54	MeOH
Carbamoyl-l-aspartate	176.12	11.35	MeOH
Orotate	156.10	12.81	DMSO
Dihydroorotate	158.11	12.64	MeOH
Carbamoyl-P	141.02	212.76	DMSO
UMP, Uridine monophosphate	324.18	6.16	H_2O
UDP, Uracil diphosphate	404.16	4.94	H_2O
UTP, Uridine triphosphate	484.14	4.13	H_2O
CTP, Cytidine triphosphate	483.15	4.13	MeOH
TTP, Thymidine triphosphate	482.16	4.14	H_2O
AMP, Adenosine monophosphate	347.22	5.76	H_2O
ADP, Adenosine diphosphate	427.20	4.68	H_2O
ATP, Adenosine triphosphate	507.18	3.94	H_2O
GTP, Guanosine triphosphate	523.18	3.82	H_2O

5.2.7. Analysis using LC-MS/MS

Following the protocol of Biagini *et al* (2012) an Accela Autosampler HPLC system (Thermo Fisher Scientific) was used with modification for the metabolites separation using an Luna aminopropyl column (250 × 2 mm with a 5-µm particle size) (Phenomenex, USA) (387). The mobile phase consisted of solvent A [20 mM ammonium acetate + 20 mM ammonium hydroxide in 95:5 water:acetonitrile (pH 9.45)], prepared as described before and solvent B (acetonitrile). The chromatographic gradients were as follows: t = 0, 15% A; t = 15 min, 100% A; t = 33 min, 100% A; t = 35 min, 15% A; t = 45 min, 15% A. Injection volume, flow rate, column temperature, and autosampler temperature were set at 20 µl, 150 µl.min^{-1}, 15 °C, and 15 °C, respectively.

For metabolite detection, a TSQ Quantum Access Triple-Stage Quadrupole mass spectrometer (Thermo Electron Corporation) was used. Electrospray ionization (ESI) was employed for the metabolite detection and analysis of metabolites. ESI spray voltage was 4000 V and 5500 V for positive and negative modes, respectively. Nitrogen was used as sheath gas at 30 psi and as the auxiliary gas at 10 psi. Argon was used as the collision gas at 1.5 mTorr. The capillary temperature was 320 °C and 270 °C for positive and negative modes, respectively. Scan time for each single reaction monitoring (SRM) event transition was 0.1 s with a scan width of 1 m/z. Xcalibar (Thermoscientific) software was applied to conduct the instrument control, data acquisition, and data analysis. LC-MS/MS parameters including retention time (RT), product and precursor mass, and collision induced dissociation (CID) are presented in Appendix II (Tables 1 and 2). The linearity (R^2), linearity range and limit of detection (LOD) are presented in Appendix II (Table 3).

5.2.8. Data treatment and analysis

Using known concentrations of standards for each of the 56 SRMs, calibration curves were generated and thus metabolite concentrations levels were quantified. AUC of the integrated peak represented the signal for each metabolite. Figure 5.2 shows an example of a LC-MS/MS chromatogram of the AMP metabolite. An example of calibration curve of AMP is shown in Figure 5.3. Calibration curves of all metabolites are presented in Appendex III (Figures 1-19). Each metabolite signal was normalized to the signal of the internal standard DL-arabinose (negative mode) or β-alanine (positive mode) in the same sample.

Principal component analysis (PCA), partial least squares-discriminant analysis (PLS-DA) and heat maps were generated through the MetaboAnalyst web server (http://www.metaboanalyst.ca/MetaboAnalyst/faces/Home.jsp) (388). Afterwards, data were plotted using GraphPad prism 5 Software Inc. for each metabolite in order to determine the important results.

A)

B)

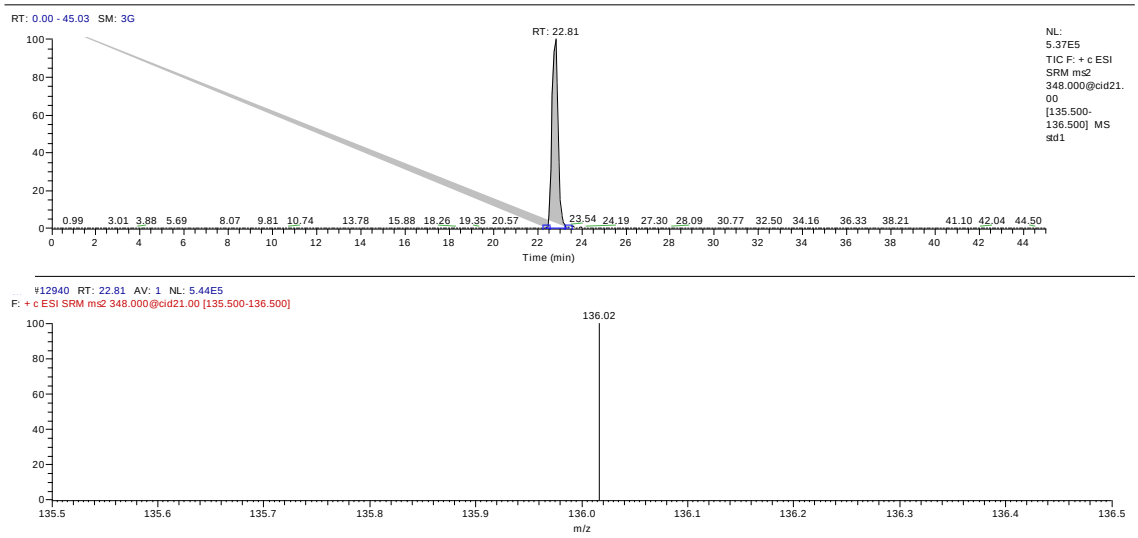

Figure 5.2: LC-MS/MS chromatogram of AMP

A) Chromatographic separation of AMP peak shows retention time (RT) at ~22.8 min. B) SRM scan of ionized AMP shows the detection of its product ion at a mass-to-charge (m/z) of 136.

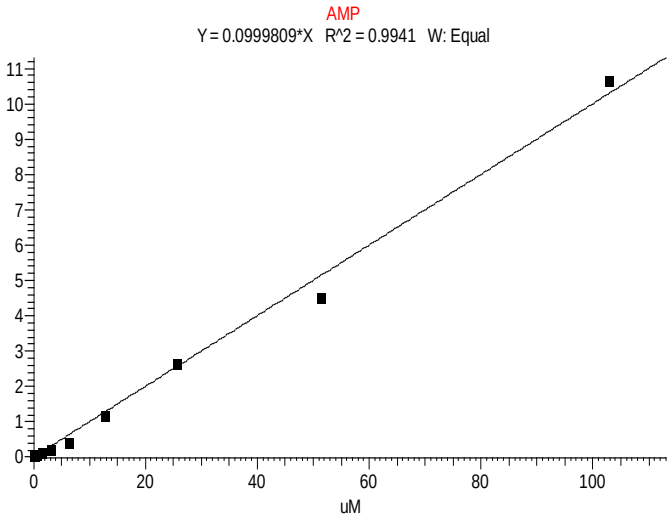

Figure 5.3: Standard calibration curve of AMP

The line of best fit for the calibration curve was generated using equal weighted linear regression as the mathematical model of best fit, showing $R^2 > 0.99$. AMP concentration in experimental samples was calculated from the resulting area ratio and the regression equation of the calibration curve.

5.3. Results

Generated data were initially processed using the MetaboAnalyst web server (388) where multivariate statistical analysis using PCA and PLS-DA was performed on the ratio of log_2 transformed datasets. All data were expressed as the normalized levels of metabolites to the number of Mtb cells in untreated and drug-treated samples. Afterwards, datasets were analyzed through hierarchical cluster analysis generating a heatmap. Finally, the importance of drug-treated metabolite *versus* untreated metabolites (vehicle control) was examined for each metabolite individually (GraphPad prism 5 Software Inc.). Out of 56 metabolites examined by LC-MS/MS, only 25 metabolites were analysed by the MetaboAnalyst web server. All redox couples, bioenergetics metabolites and some of amino acid metabolites: asparagine, arginine, serine and cysteine were not detected by LC-MS/MS as they were below LOD. Moreover, 7 CCM metabolites: PEP, DHAP, lactate, acetyl-CoA, succinyl-CoA, methylmalonyl-CoA and propionyl-CoA were not detected (below LOD, Appendix II, Table 2).

5.3.1. PCA and PLS-DA

Comparative analyses of metabolomics data are greatly facilitated by using PCA and PLS-DA. PCA converts high dimensional data into lower-dimensional plots without loss of information through developing a small number of artificial variables (principal components). PCA is a commonly used unsupervised technique, as it requires no a priori knowledge of class of the sample. PCA is usually presented in terms of component scores that account for most of the variance in the observed variables of the data. Similarly, PLS-DA uses a supervised technique to determine pattern on the original data. PLS-DA classifies the data into two blocks, one between class variation and the other within class. Thus, PLS-DA separates the more meaningful data from the less meaningful (388, 389). 2-D PCA showed that RKA-307-treated Mtb H37Rv clusters away from the untreated Mtb H37Rv and other drugs/inhibitors treated clusters (Figure 5.4, A), which is also observed with the 3-D PCA. The TPZ-treated Mtb H37Rv cluster was more defined with the 3-D PCA (Figure 5.4, B). PLS-DA was applied to further improve and refine the clustering and positioning of the variables and to assess the significance of class discrimination. 2-D PLS-DA (Figure 5.5, A) displayed discrimination of clusters for the CK-2-63-, TPZ- and RKA-307-treated Mtb H37Rv. Moreover, INH-, EMB-, RIF- and STR-treated Mtb clusters overlapped with untreated Mtb H37Rv as displayed by 2-D PLS-DA. Interestingly, 3-D PLS-DA (Figure 5.5, B) showed even better clustering of the data from which TPZ-, CK-2-63- and RKA-307-treated Mtb H37Rv were found to be in the same side but with different directions. In contrast, RIF-treated Mtb showed a defined cluster while INH- and STR-treated Mtb H37Rv demonstrated quite close distance clusters. EMB-treated Mtb H37Rv cluster was close to the untreated Mtb H37Rv cluster.

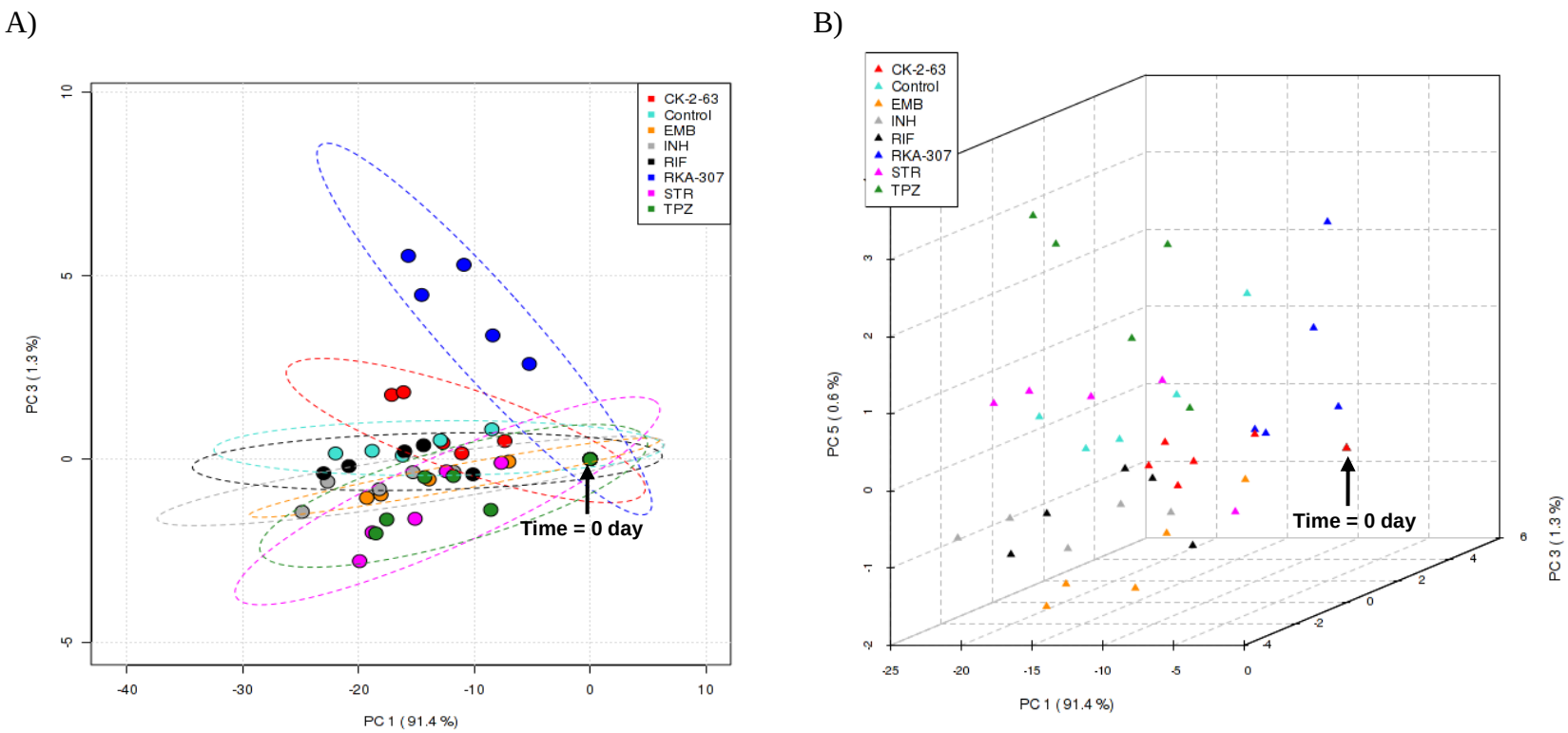

Figure 5.4: 2-D and 3-D PCA score plots for Mtb H37Rv upon exposure to different drugs and inhibitors

The samples (the time course points) on both plots are colour coded as following: untreated Mtb H37Rv samples (light blue), Mtb H37Rv samples treated with isoniazid (INH, grey), ethambutol (EMB, orange), rifampicin (RIF, black), streptomycin (STR, pink), trifluoperazine (TPZ, green), CK-2-63 (red) and RKA-307 (dark blue). A) 2-D PCA score plot shows two distinct clusters with different directions. The first cluster includes untreated Mtb H37Rv samples and drug-treated samples with INH, EMB, RIF, STR, TPZ and CK-2-63 whereas the second cluster includes only RKA-307-treated Mtb. B) 3-D PCA score plot displays no clear cluster except for that of RKA-307- and TPZ-treated Mtb. Each time-point for each metabolite represents the normalized average of two independent replicates which were divided by the corresponding average values derived from Mtb harvested at time 0 day (arrow indicted) to generate the corresponding ratios. Ratios were $\log_2$ transformed and plotted using the metaboanalyst web server (388).

A)

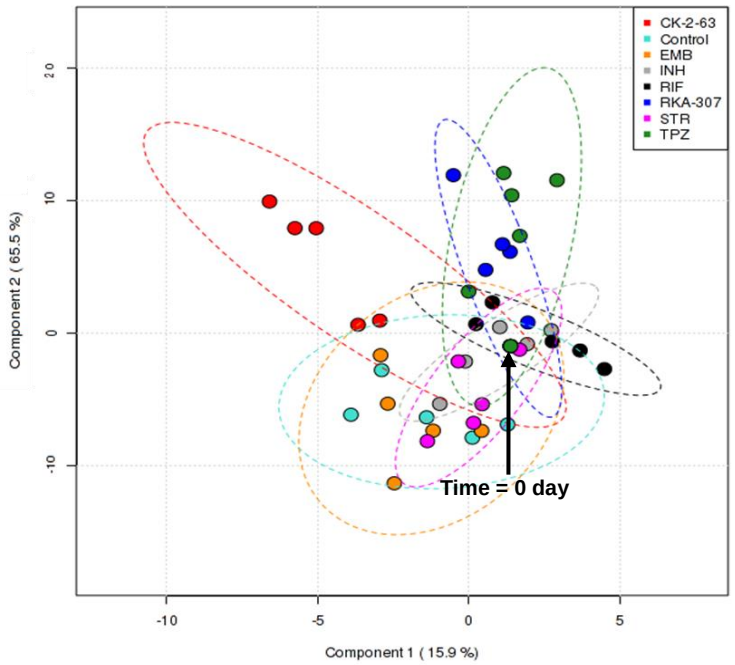

B)

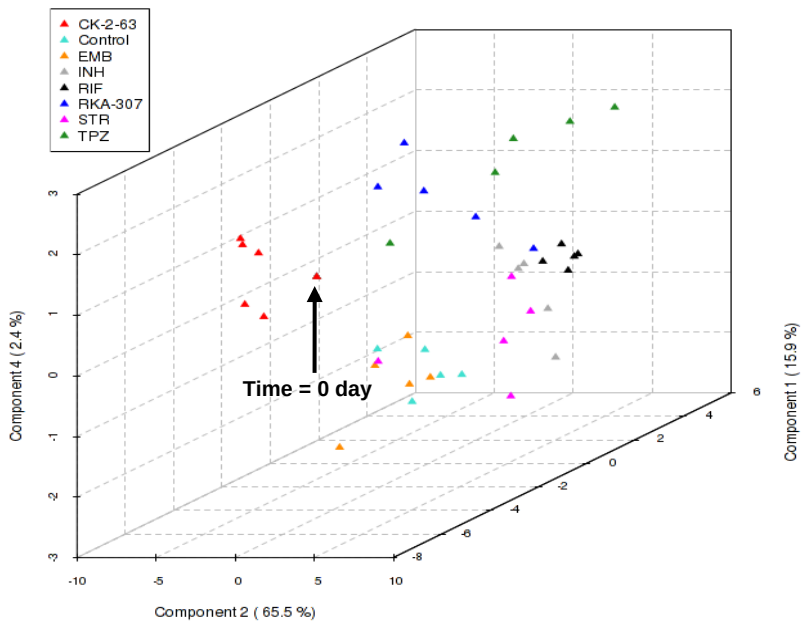

Figure 5.5: 2-D and 3-D PLS-DA scores for Mtb H37Rv upon exposure to different drugs and inhibitors.

The samples (the time course points) on both plots are colour coded as following: untreated Mtb H37Rv samples (light blue), Mtb H37Rv samples treated with isoniazid (INH, grey), ethambutol (EMB, orange), rifampicin (RIF, black), streptomycin (STR, pink), trifluoperazine (TPZ, green), CK-2-63 (red) and RKA-307 (dark blue). A) 2-D PLS-DA score plot shows four distinct clusters with different directions which are TPZ-, RKA-307-, CK-2-63- and RIF-treated Mtb whereas untreated Mtb H37Rv, INH-, EMB- and STR-treated Mtb clusters are overlapped. B) 3-D PLS-DA score plot displays TPZ-, CK-2-63- and RKA-307- treated Mtb in the same side but different directions. INH- and STR-treated Mtb display approximately close distance clusters whereas RIF-treated Mtb cluster shows a separate cluster. EMB-treated Mtb cluster is close to untreated Mtb cluster. Each time-point for each metabolite represents the normalized average of two independent replicates which were divided by the corresponding average values derived from Mtb harvested at time 0 day (arrow indicted) to generate the corresponding ratios. Ratios were $\log_2$ transformed and plotted using the metaboanalyst web server (388).

5.3.2. Heat map profile of the Mtb metabolome

The heat map is presented here as a visual aid for the similarity measures between the samples through expressing the relative difference of the dynamic changes in a scale of red and green colour (Figure 5.6). In comparison with untreated Mtb, RKA-307-treated Mtb had the most visual differences of the dynamic changes, which included most of the CCM metabolites and some of amino acid metabolites. In contrast, Mtb treated with other drugs showed less visual differences of the dynamic changes in comparison with untreated Mtb. Individual analysis of each metabolite will be presented in the following section (Chapter 5.3.4).

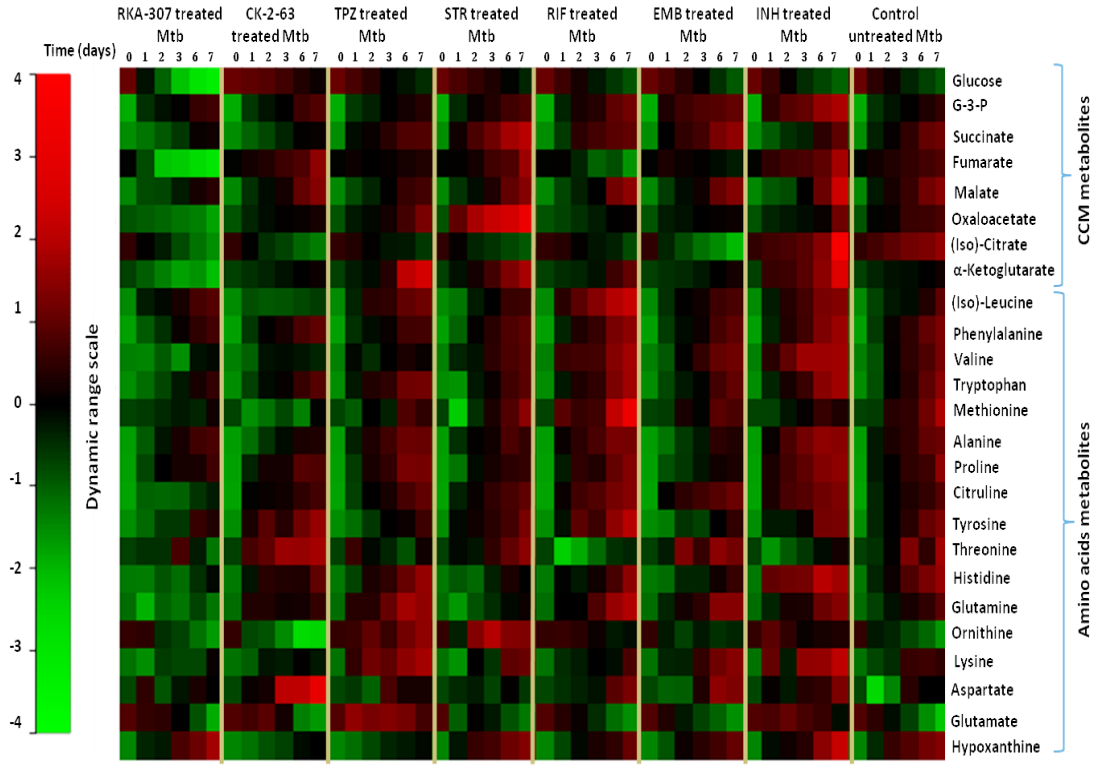

Figure 5. 6: Heat map profile of drug-treated and untreated Mtb H37Rv metabolome

The heat map shows the dynamic changes of 25 metabolites in Mtb H37Rv treated with the following drugs/inhibitors: isoniazid (INH), ethambutol (EMB), rifampicin (RIF), streptomycin (STR), trifluoperazine (TPZ), CK-2-63 and RKA-307 and in untreated Mtb H37Rv (vehicle control). Each time-point for each metabolite represents the normalized average of two independent replicates which were divided by the corresponding average values derived from Mtb harvested at time 0 day to generate the corresponding ratios. Ratios were $\log_2$ transformed and plotted on a colour dynamic range scale using the metaboanalyst web server (388). Rows correspond to metabolites measured by LC-MS/MS. Columns correspond to the time course from day 0 to day 7 for each of treated and untreated Mtb H37Rv. Green and red colours represent decreases and increases of metabolites ratio, respectively. Black colour indicates the baseline. G-3-P, glycerol-3-phosphate.

5.3.3. Biochemical time–dependent of metabolite profiles in Mtb H37Rv.

Following examination of the clusters and the dynamic change of the samples, time-dependent graphs of untreated Mtb H37Rv and Mtb H37Rv treated with the following drugs/inhibitors: INH, EMB, RIF, STR, TPZ, CK-2-63 and RKA-307 for 25 metabolites were plotted (GraphPad prism 5 Software Inc.).

INH-treated Mtb showed a notable increase in the level of glycerol-3-phosphate (G-3-P), α-ketoglutarate, valine, alanine and lysine. In addition, the levels of malate and hypoxanthine increased by day 7. Glutamate and ornithine utilization and threonine production were considerably low, compared to the drug-free control Mtb (Figures 5.7-5.9). Regarding EMB-treated Mtb (Figures 5.10-5.12), the level of fumarate production was remarkably low whereas, the level of (iso)-citrate was notably reduced, compared to the drug-free control Mtb. Moreover, the level of alanine, proline and histidine was notably decreased in EMB-treated Mtb

Compared to the untreated control Mtb, RIF-treated Mtb showed the following effects: the level of fumarate and (iso)-citrate was found to be notably decreased whereas the level of ornithine was shown to be considerably less utilized and threonine drastically less produced than that of untreated Mtb. Moreover, RIF-treated Mtb showed an important increase in (iso)-leucine and valine levels (Figures 5.13-5.15). Concerning STR-treated Mtb, succinate, oxaloacetate and ornithine level displayed substantial accumulation whereas (iso)-citrate and proline levels were notably decreased. Furthermore, the histidine level was found to be lower compared to the drug-free control Mtb (Figures 5.16-5.18).

TPZ-treated Mtb was found to have a remarkable reduction of (iso)-citrate, valine and malate levels and low production of hypoxanthine and threonine. Moreover, a considerable accumulation of ornithine and α-ketoglutarate levels and low utilization of glutamate were observed, compared to the drug-free control Mtb (Figures 5.19-5.21).

CK-2-63-treated Mtb (in comparison with untreated control Mtb) showed a notably low production level of alanine, valine, proline, (iso)-leucine, succinate and

hypoxanthine. Moreover, (iso)-citrate found to be considerably decreased while aspartate was remarkably increased in CK-2-63-treated Mtb. A complete inhibition of methionine consumption was also observed following CK-2-63-treatment (Figures 5.22-5.24).

With regards to RKA-307-treated Mtb, most of the TCA cycle metabolites (Figure 1.13, Chapter 1.6.2), which were succinate, malate and oxaloacetate were shown to have low production levels. Moreover, fumarate, (iso)-citrate and α-ketoglutarate revealed remarkable levels of reduction compared to the drug-free control Mtb. The following amino acids: citrulline, glutamine, valine, threonine, proline and histidine were found to be drastically decreased, in comparison with the untreated control Mtb (Figures 5.25-5.27).

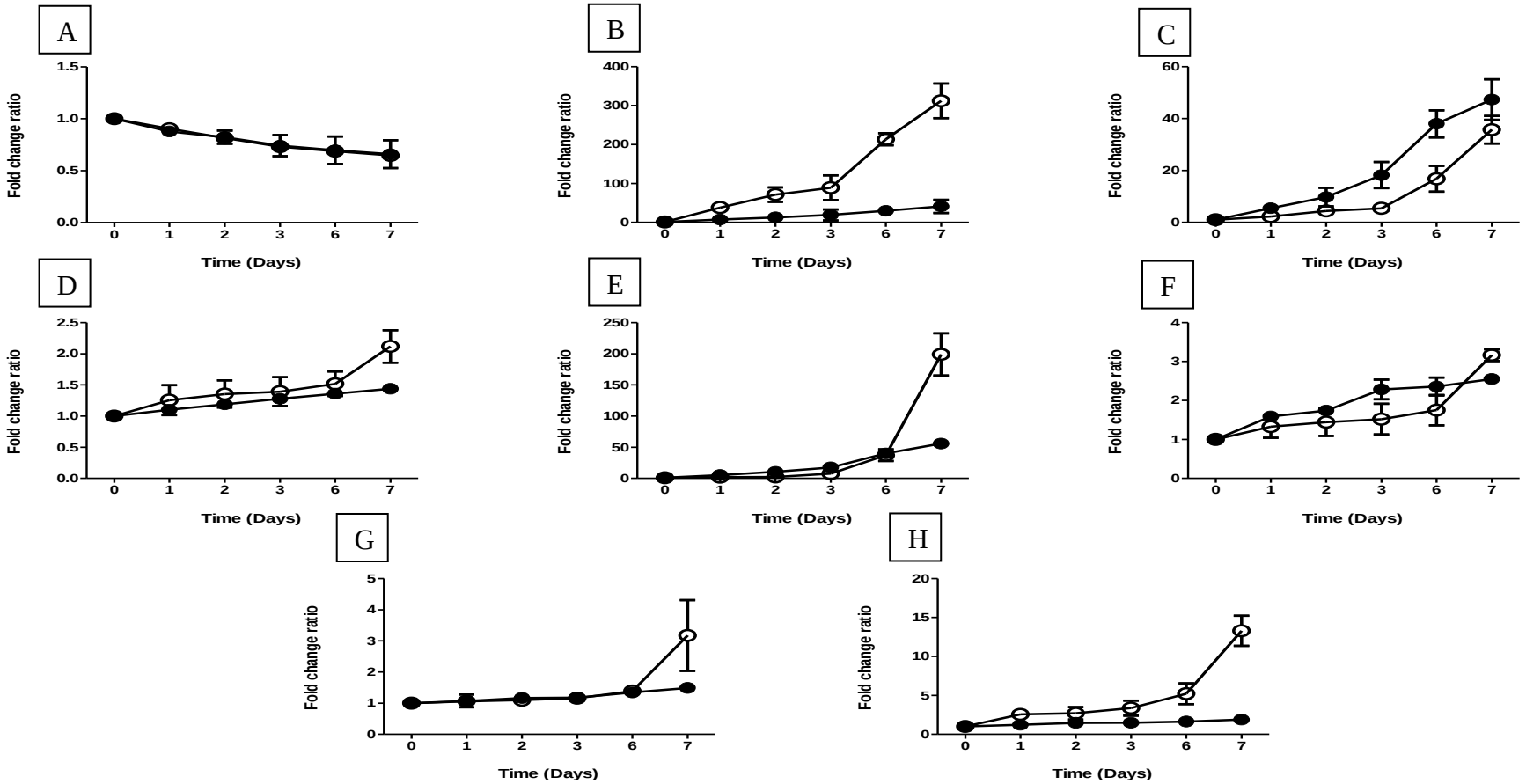

Figure 5.7: Time-dependent changes of Mtb H37Rv metabolites in INH-treated and untreated control cells

The following metabolites levels in untreated (closed circle) and INH-treated (open circle) cells were determined by LC-MS/MS, A) Glucose, B) Glycerol-3-phosphate (G-3-P), C) Succinate, D) Fumarate, E) Malate, F) Oxaloacetate, G) (iso)-citrate and H) α-Ketoglutarate. The final concentration of Isoniazid (INH) was at IC_{90} (2.38 µM). The points represent the mean ± SEM of duplicate independent experiments. In INH-treated Mtb H37Rv, G-3-P, malate and α-Ketoglutarate show a substantial increase (GraphPad prism 5 Software Inc.).

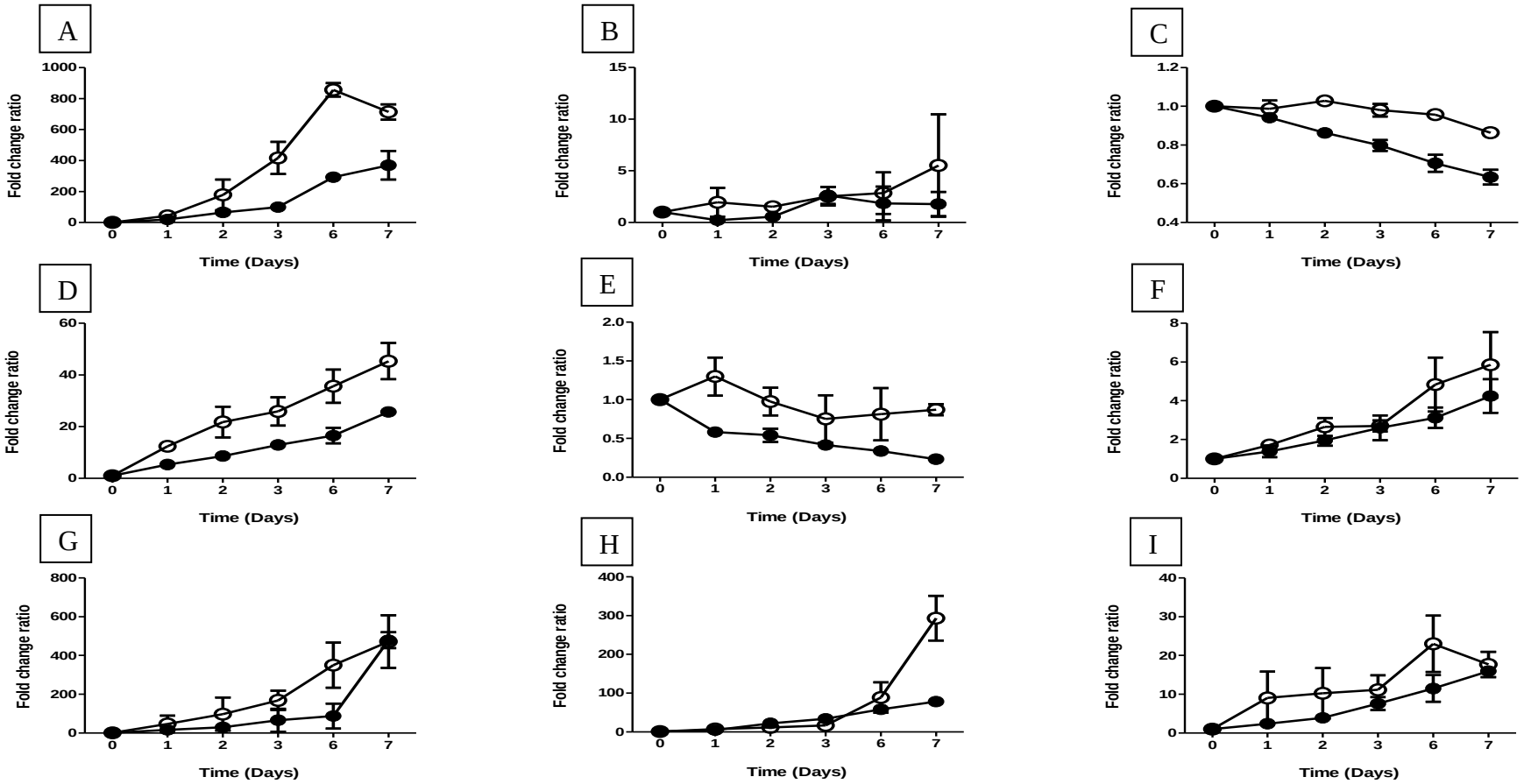

Figure 5.8: Time-dependent change of Mtb H37Rv metabolites in INH-treated and untreated control cells

The following metabolites levels in untreated (closed circle) and INH-treated (open circle) cells were determined by LC-MS/MS, A) Alanine, B) Aspartate, C) Glutamate, D) Citrulline E) Ornithine, F) Glutamine, G) Proline, H) Hypoxanthine and I) Histidine. The final concentration of Isoniazid (INH) was at IC_{90} (2.38 µM). The points represent the mean ± SEM of duplicate independent experiments. In INH-treated Mtb H37Rv, glutamate and ornithine show notably low levels whereas alanine and hypoxanthine show obvious increase (GraphPad prism 5 Software Inc.).

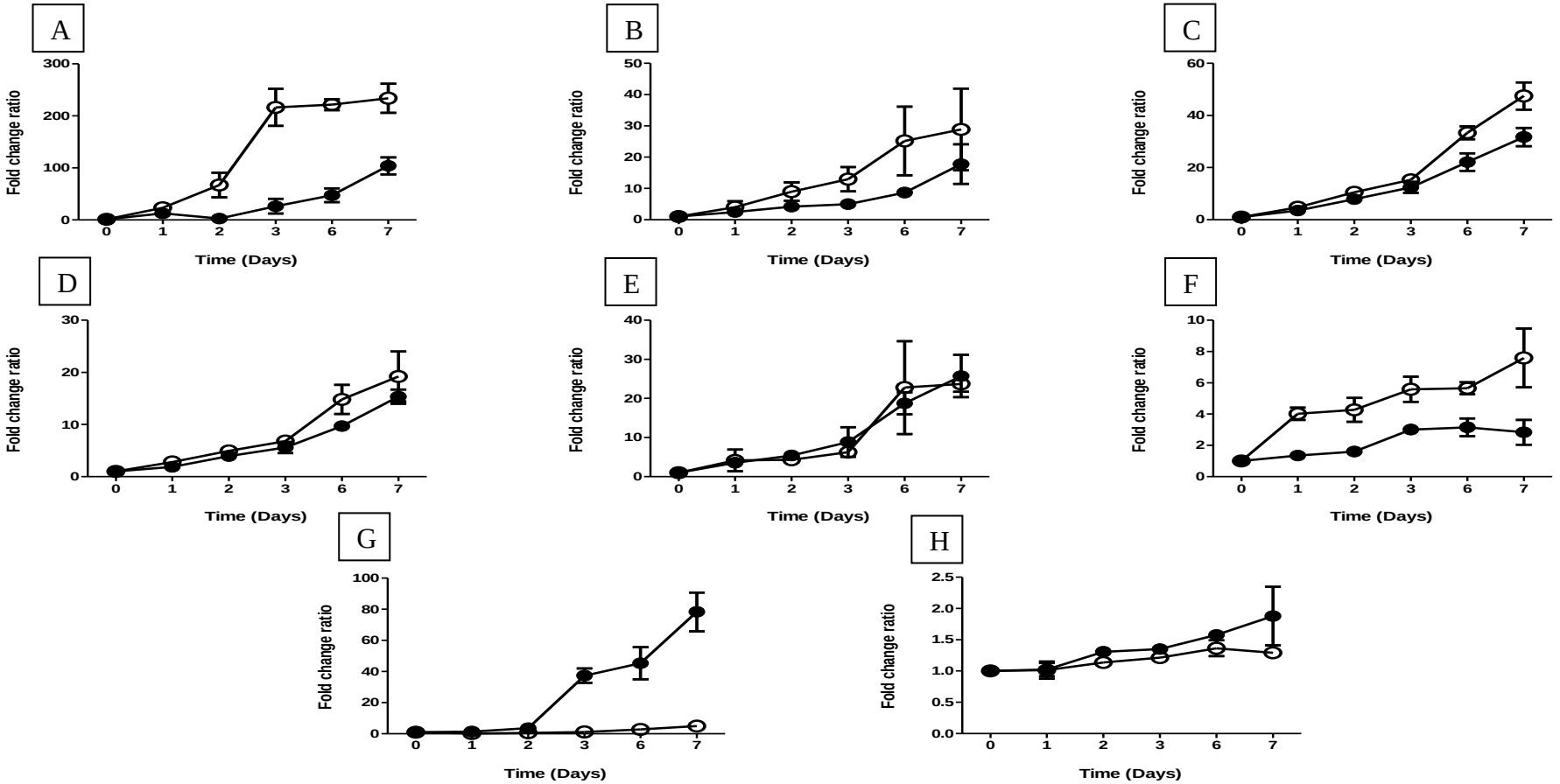

Figure 5.9: Time-dependent changes of Mtb H37Rv metabolites in INH-treated and untreated control cells

The following metabolites levels in untreated (closed circle) and INH-treated (open circle) cells were determined by LC-MS/MS, A) Valine, B) (iso)-leucine, C) Phenylalanine, D) Tryptophan E) Tyrosine, F) Lysine, G) Threonine and H) Methionine. The final concentration of Isoniazid (INH) was at IC_{90} (2.38 µM). The points represent the mean ± SEM of duplicate independent experiments. In INH-treated Mtb H37Rv, valine and lysine show notable increase; threonine shows a clearly low level (GraphPad prism 5 Software Inc.)

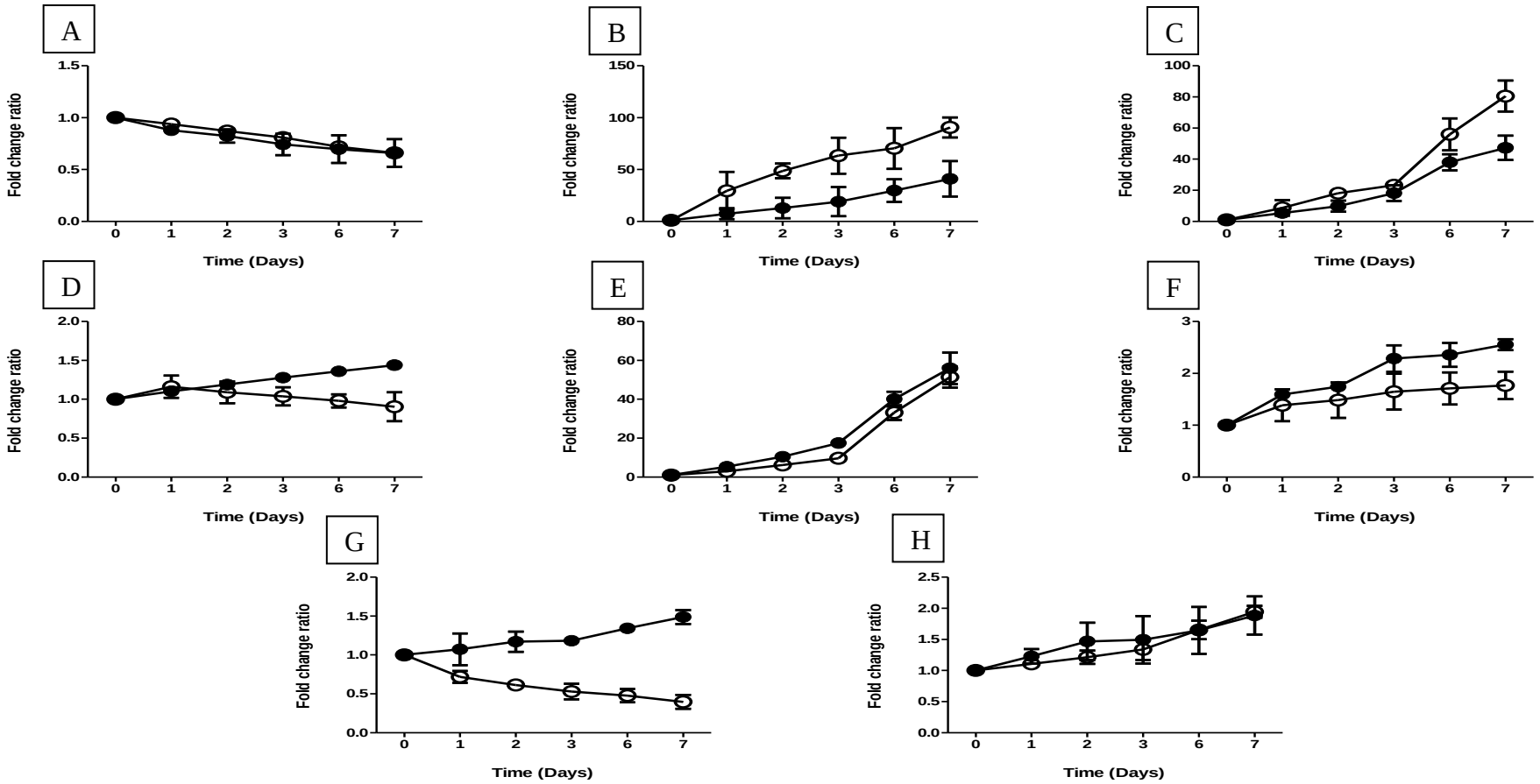

Figure 5.10: Time-dependent changes of Mtb H37Rv metabolites in EMB-treated and untreated control cells

The following metabolite levels in untreated (closed circle) and EMB-treated (open circle) cells were determined by LC-MS/MS, A) Glucose, B) Glycerol-3-phosphate (G-3-P), C) Succinate, D) Fumarate, E) Malate, F) Oxaloacetate, G) (iso)-citrate and H) α-Ketoglutarate. The final concentration of Ethambutol (EMB) was at IC_{90} (4.61 µM). The points represent the mean ± SEM of duplicate independent experiments. In EMB-treated Mtb H37Rv, fumarate and (iso)-citrate show noticeable decreases (GraphPad prism 5 Software Inc.).

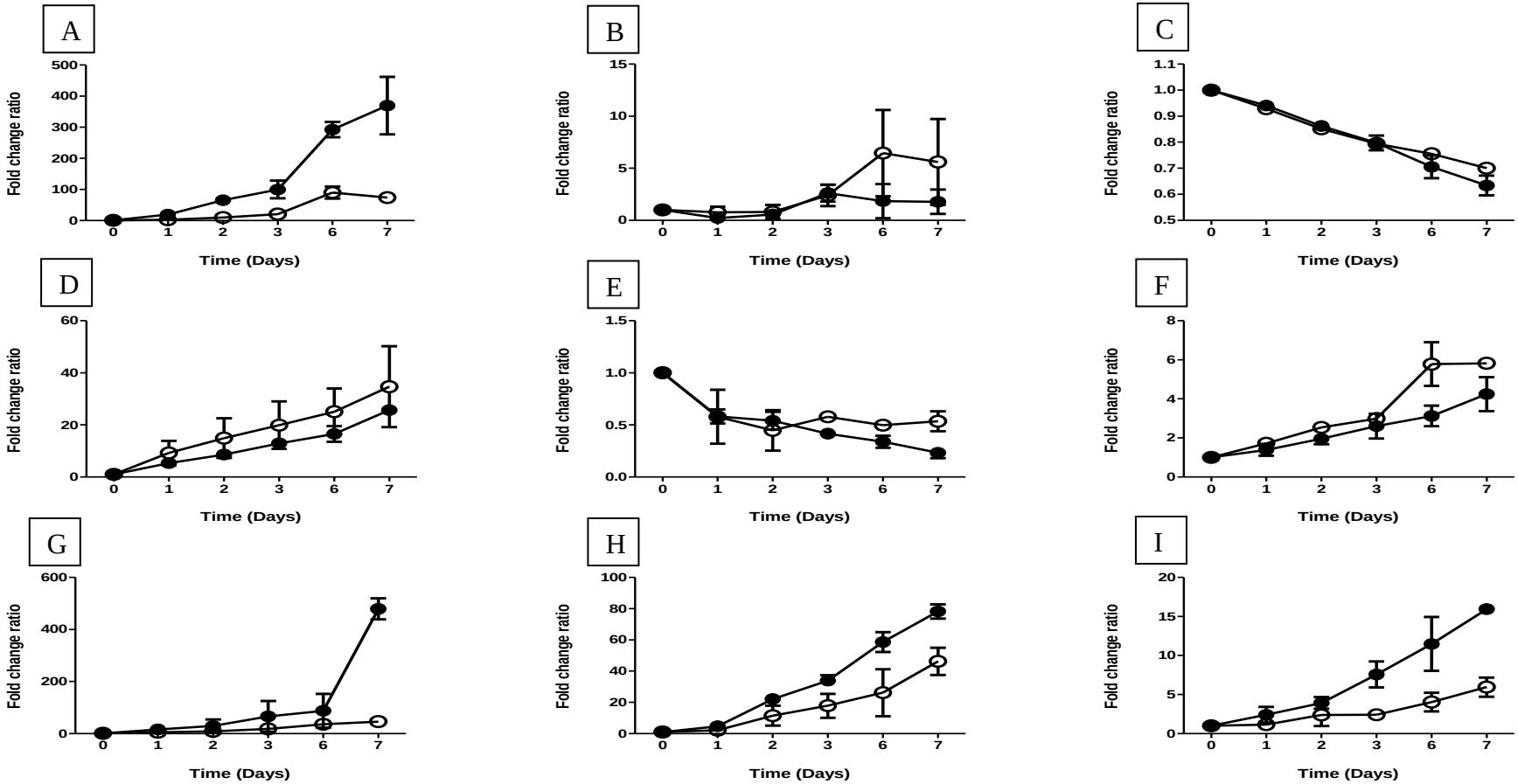

Figure 5.11: Time-dependent changes of Mtb H37Rv metabolites in EMB-treated and untreated control cells

The following metabolite levels in untreated (closed circle) and EMB-treated (open circle) cells were determined by LC-MS/MS, A) Alanine, B) Aspartate, C) Glutamate, D) Citrulline E) Ornithine, F) Glutamine, G) Proline, H) Hypoxanthine and I) Histidine. The final concentration of Ethambutol (EMB) was at IC_{90} (4.61 µM). The points represent the mean ± SEM of duplicate independent experiments. In EMB-treated Mtb H37Rv, alanine, proline and histidine show notable decrease (GraphPad prism 5 Software Inc.).

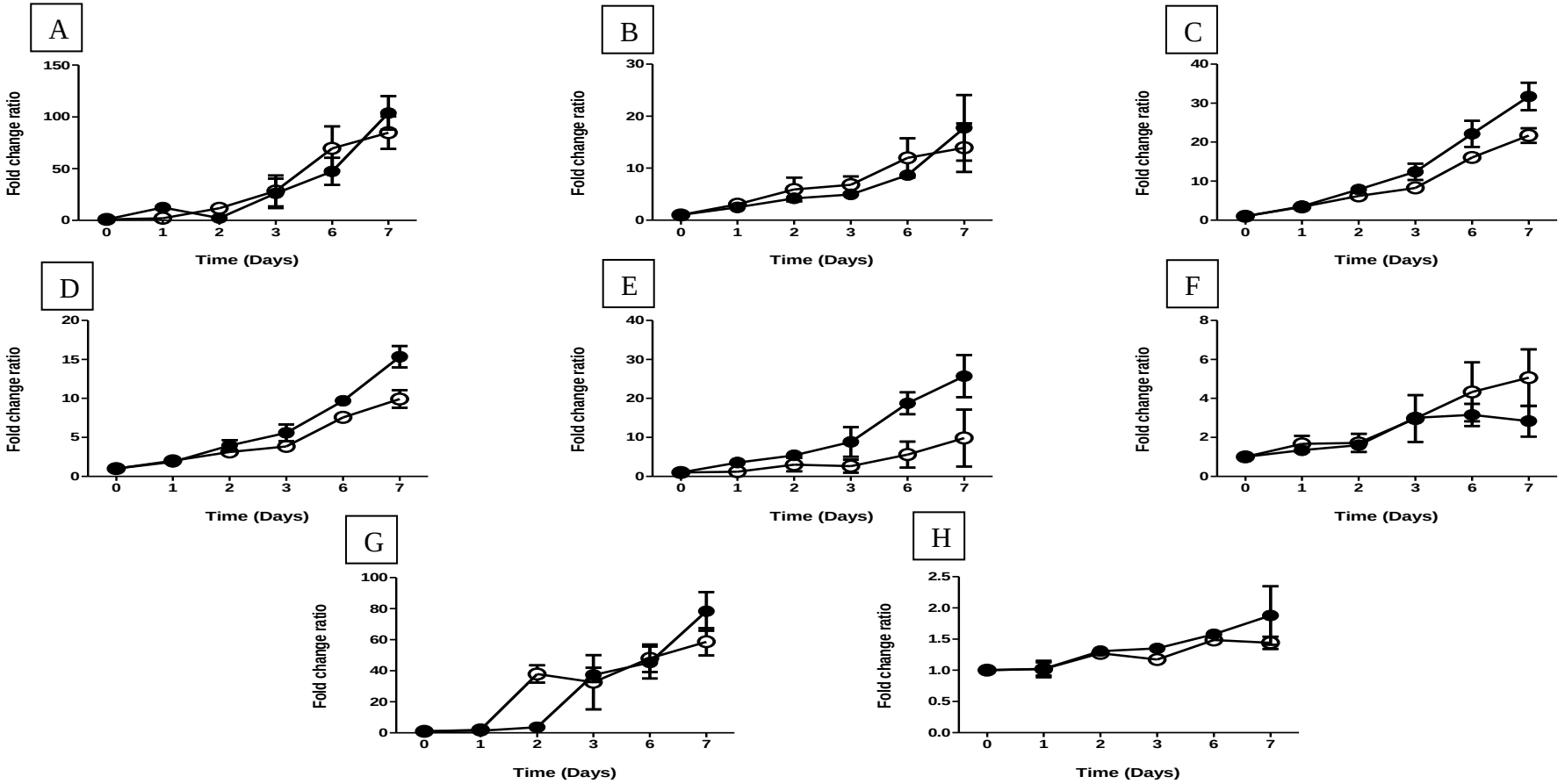

Figure 5.12: Time-dependent changes of Mtb H37Rv metabolites in EMB-treated and untreated control cells

The following metabolite levels in untreated (closed circle) and EMB-treated (open circle) cells were determined by LC-MS/MS, A) Valine, B) (iso)-leucine, C) Phenylalanine, D) Tryptophan E) Tyrosine, F) Lysine, G) Threonine and H) Methionine. The final concentration of Ethambutol (EMB) was at IC_{90} (4.61 µM). The points represent the mean ± SEM of duplicate independent experiments. There are no noticeable changes among metabolites (GraphPad prism 5 Software Inc.).

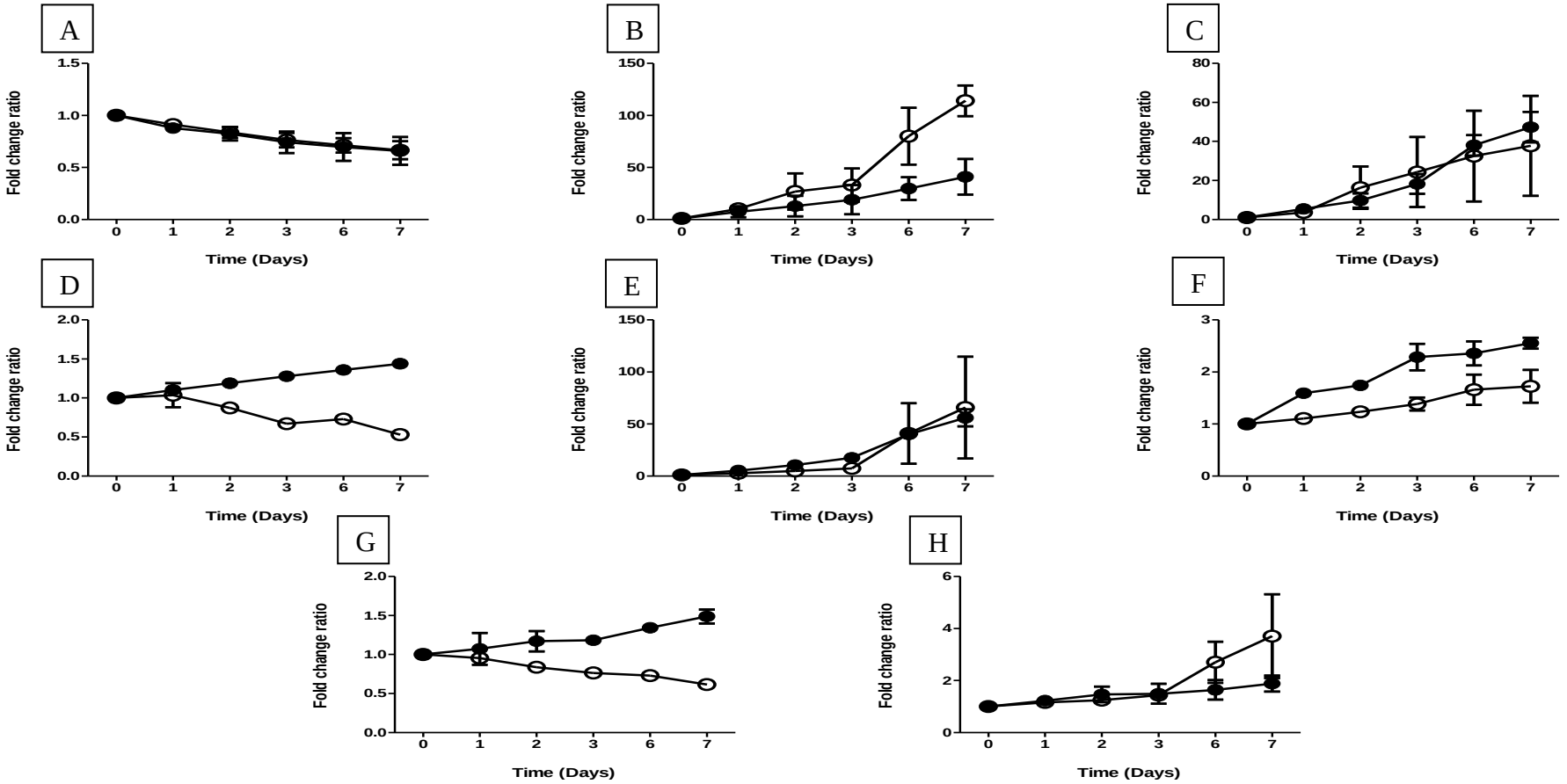

Figure 5.13: Time-dependent changes of Mtb H37Rv metabolites in RIF-treated and untreated control cells

The following metabolite levels in untreated (closed circle) and RIF-treated (open circle) cells were determined by LC-MS/MS, A) Glucose, B) Glycerol-3-phosphate (G-3-P), C) Succinate, D) Fumarate, E) Malate, F) Oxaloacetate, G) (iso)-citrate and H) α-Ketoglutarate. The final concentration of Rifampicin (RIF) was at IC_{90} ($2.21x10^{-3}$ μM). The points represent the mean ± SEM of duplicate independent experiments. In RIF-treated Mtb H37Rv, fumarate and (iso)-citrate show remarkable decreases (GraphPad prism 5 Software Inc.).

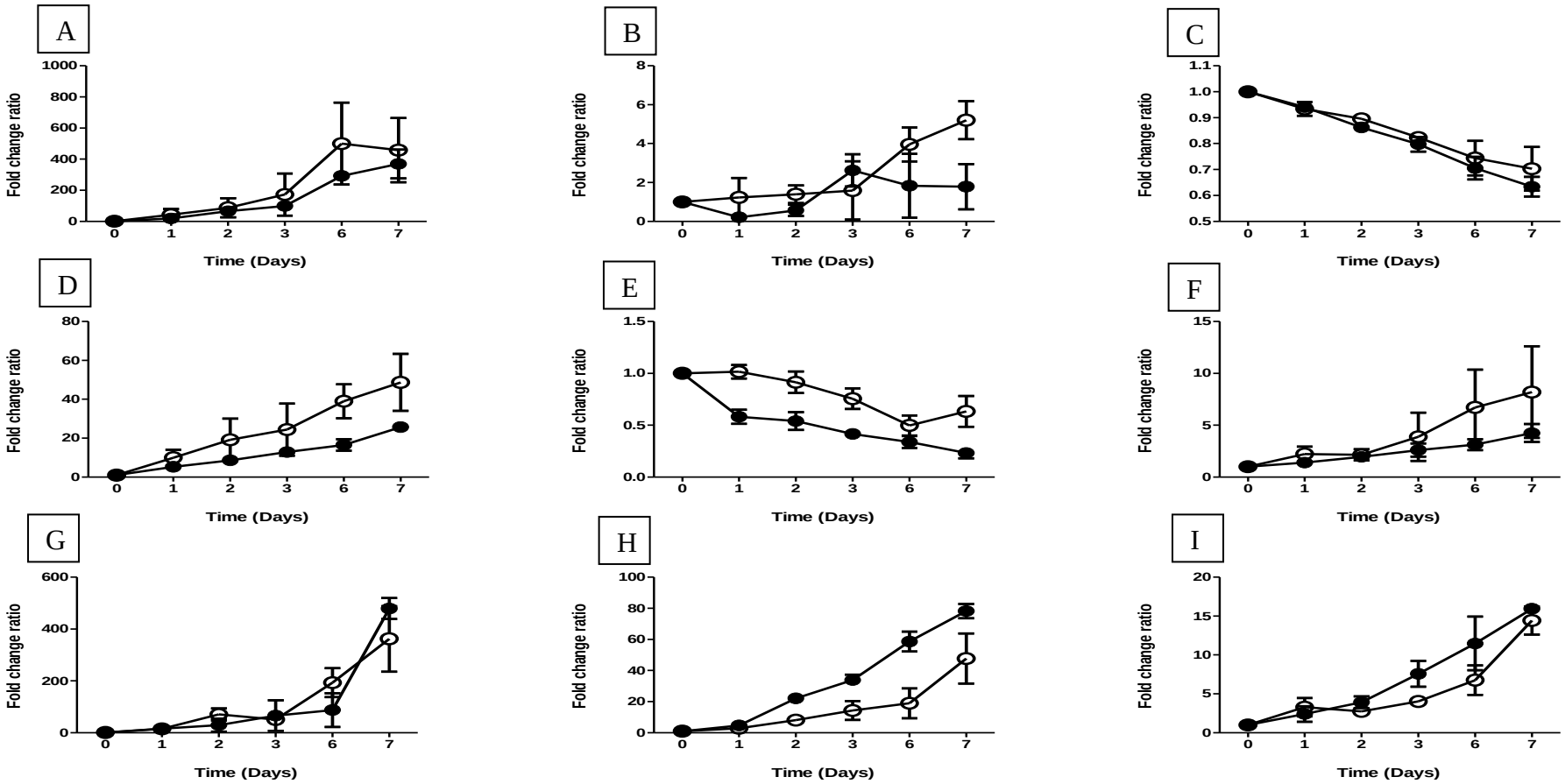

Figure 5.14: Time-dependent changes of Mtb H37Rv metabolites in RIF-treated and untreated control cells

The following metabolite levels in untreated (closed circle) and RIF-treated (open circle) cells were determined by LC-MS/MS, A) Alanine, B) Aspartate, C) Glutamate, D) Citrulline E) Ornithine, F) Glutamine, G) Proline, H) Hypoxanthine and I) Histidine. The final concentration of Rifampicin (RIF) was at IC_{90} ($2.21x10^{-3}$ µM). The points represent the mean ± SEM of duplicate independent experiments. In RIF-treated Mtb H37Rv, ornithine shows low levels (GraphPad prism 5 Software Inc.).

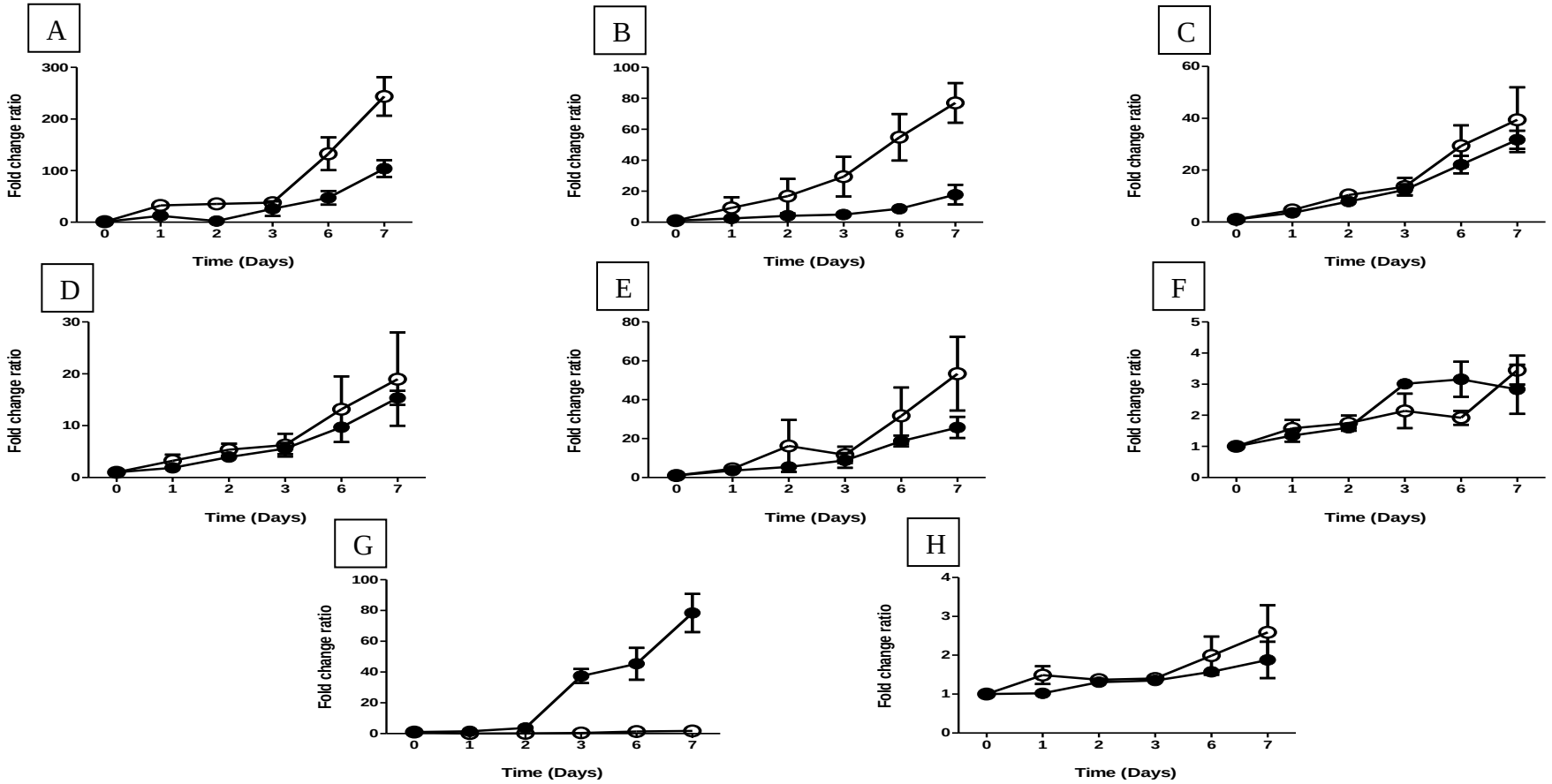

Figure 5.15: Time-dependent changes of Mtb H37Rv metabolites in RIF-treated and untreated control cells

The following metabolite levels in untreated (closed circle) and RIF-treated (open circle) cells were determined by LC-MS/MS, A) Valine, B) (iso)-leucine, C) Phenylalanine, D) Tryptophan E) Tyrosine, F) Lysine, G) Threonine and H) Methionine. The final concentration of Rifampicin (RIF) was at IC_{90} ($2.21x10^{-3}$ µM). The points represent the mean ± SEM of duplicate independent experiments. In RIF-treated Mtb H37Rv, (iso)-leucine and valine show considerable increase whereas threonine shows very low production (GraphPad prism 5 Software Inc.).

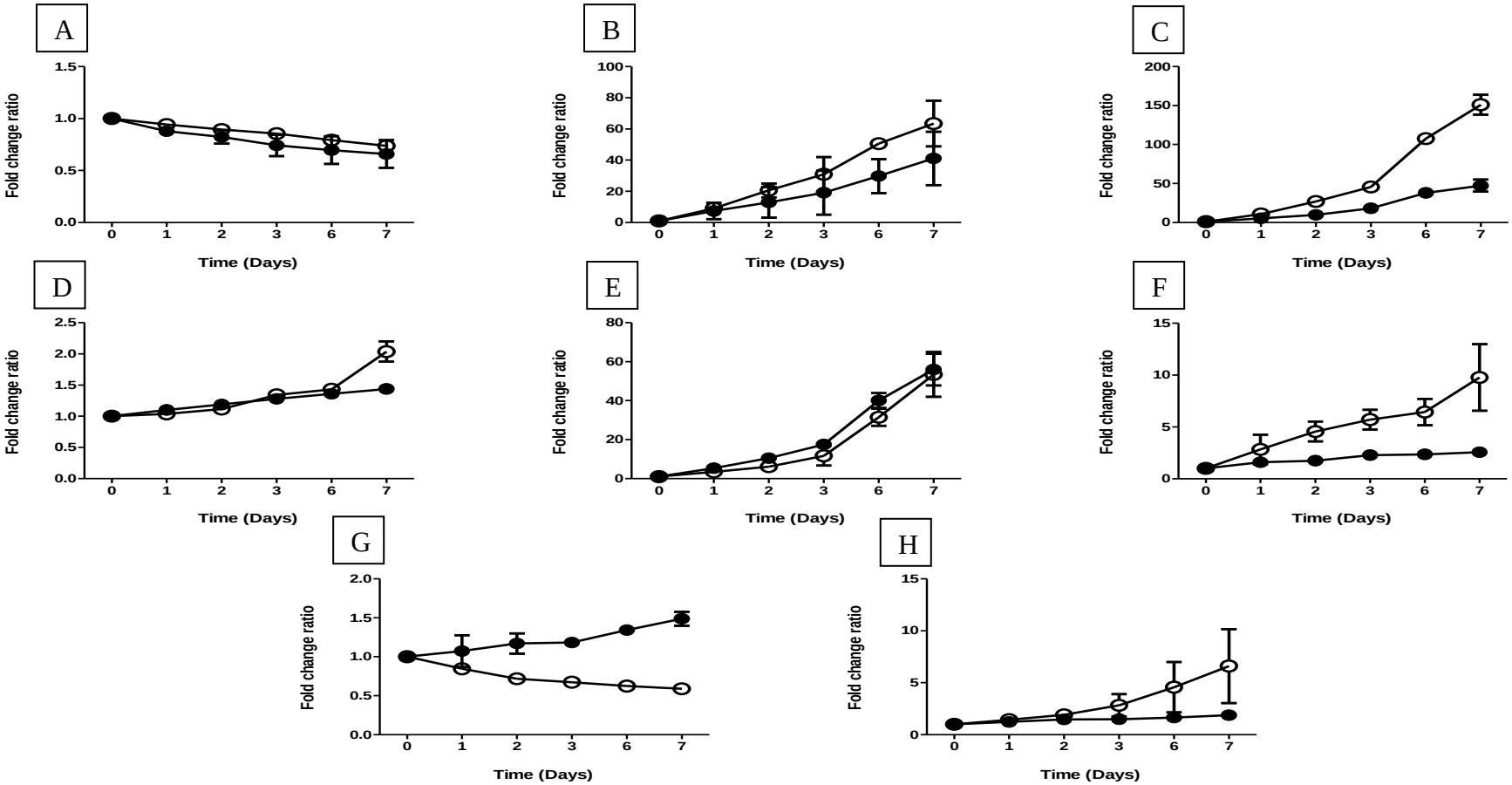

Figure 5.16: Time-dependent changes of Mtb H37Rv metabolites in STR-treated and untreated control cells

The following metabolites levels in untreated (closed circle) and STR-treated (open circle) cells were determined by LC-MS/MS, A) Glucose, B) Glycerol-3-phosphate (G-3-P), C) Succinate, D) Fumarate, E) Malate, F) Oxaloacetate, G) (iso)-citrate and H) α-Ketoglutarate. The final concentration of Streptomycin (STR) was at IC_{90} (0.23 µM). The points represent the mean ± SEM of duplicate independent experiments. In STR-treated Mtb H37Rv, succinate and oxaloacetate show a clear increase whereas (iso)-citrate shows a remarkable decrease (GraphPad prism 5 Software Inc.).

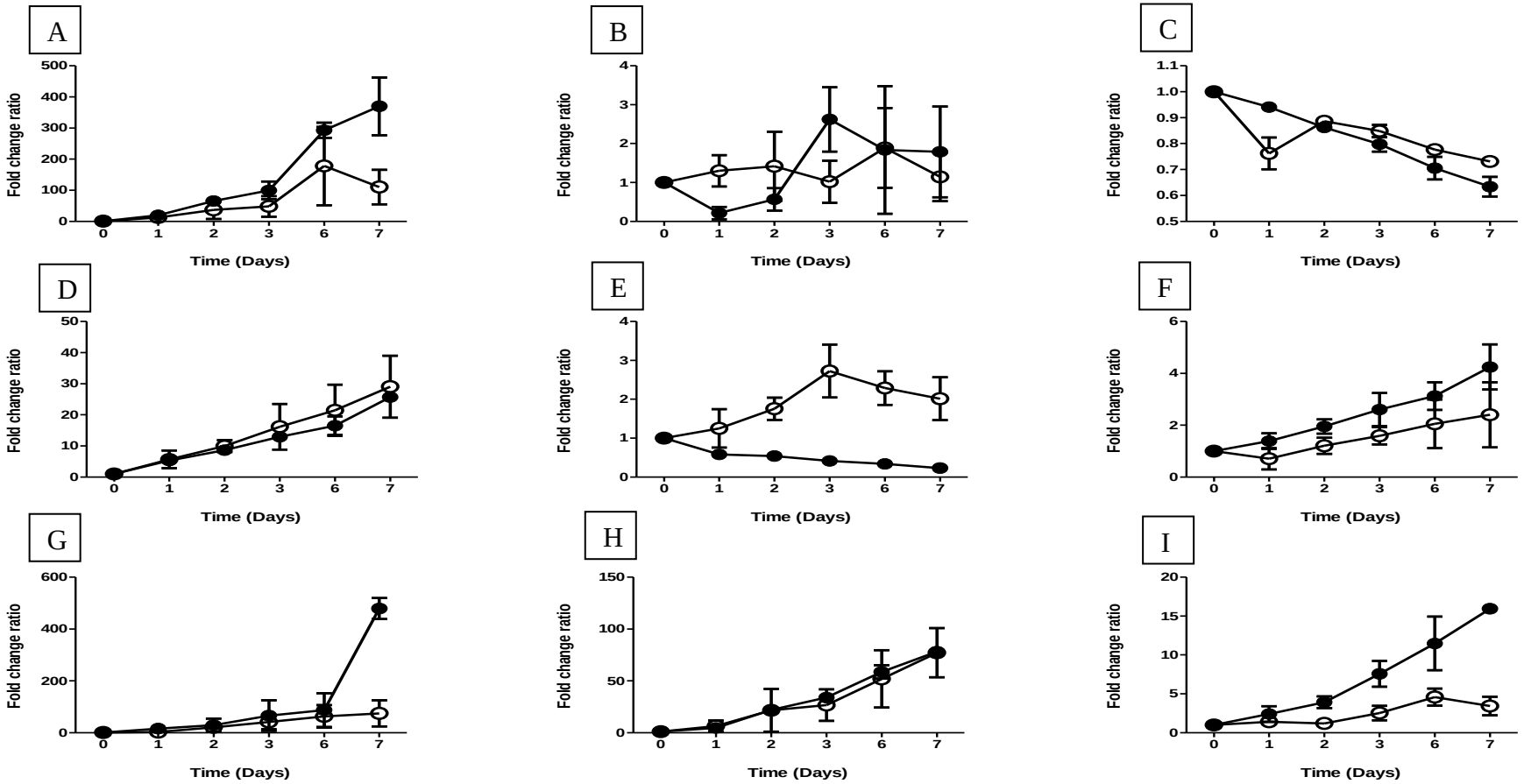

Figure 5.17: Time-dependent changes of Mtb H37Rv metabolites in STR-treated and untreated control cells

The following metabolite levels in untreated (closed circle) and STR-treated (open circle) cells were determined by LC-MS/MS, A) Alanine, B) Aspartate, C) Glutamate, D) Citrulline E) Ornithine, F) Glutamine, G) Proline, H) Hypoxanthine and I) Histidine. The final concentration of Streptomycin (STR) was at IC_{90} (0.23 µM). The points represent the mean ± SEM of duplicate independent experiments. In STR-treated Mtb H37Rv, ornithine shows considerable increase whereas histidine and proline are present at low level (GraphPad prism 5 Software Inc.).

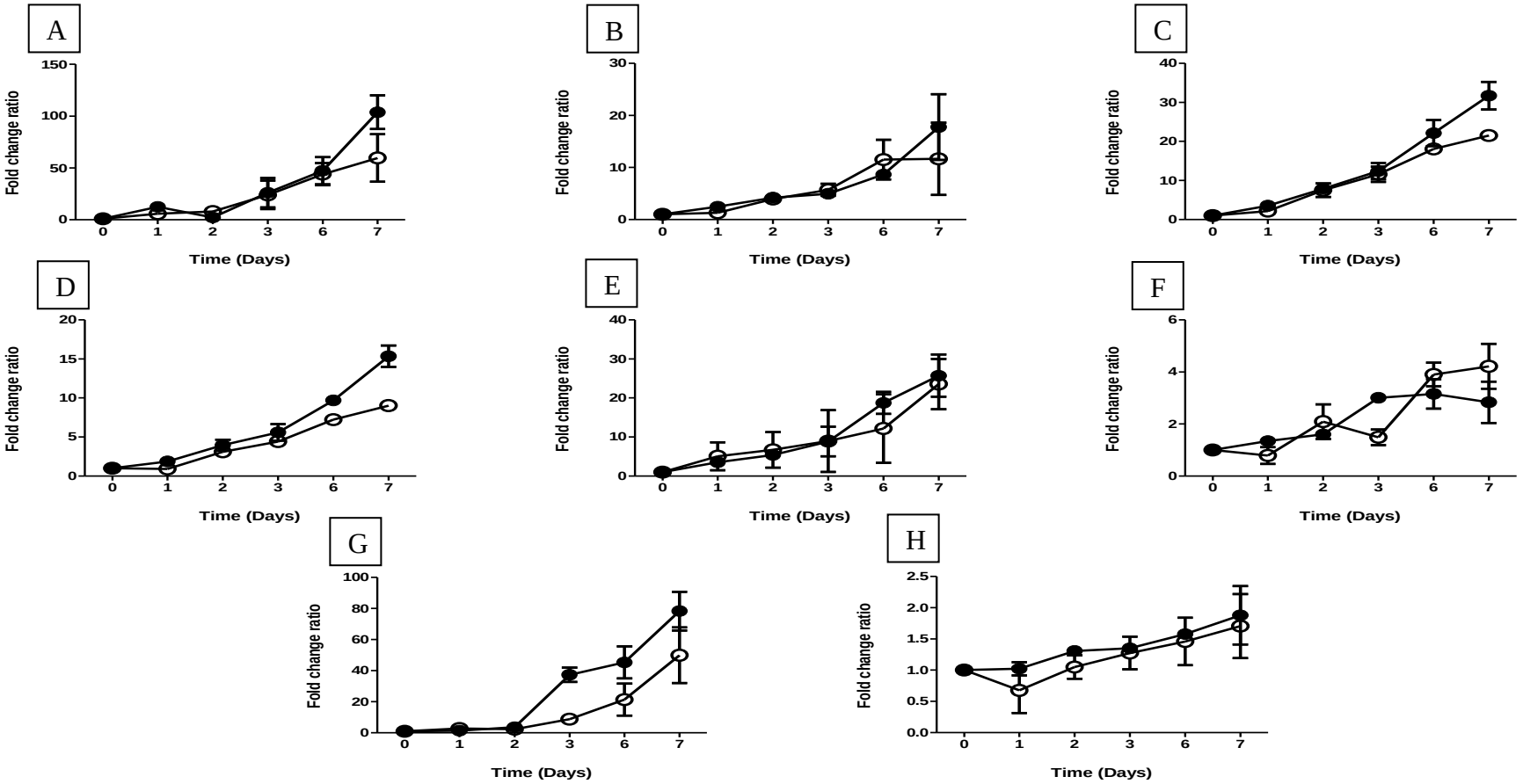

Figure 5.18: Time-dependent changes of Mtb H37Rv metabolites in STR-treated and untreated control cells

The following metabolite levels in untreated (closed circle) and STR-treated (open circle) cells were determined by LC-MS/MS, A) Valine, B) (iso)-leucine, C) Phenylalanine, D) Tryptophan E) Tyrosine, F) Lysine, G) Threonine and H) Methionine. The final concentration of Streptomycin (STR) was at IC_{90} (0.23 µM). The points represent the mean ± SEM of duplicate independent experiments. There are no noticeable changes among metabolites (GraphPad prism 5 Software Inc.).

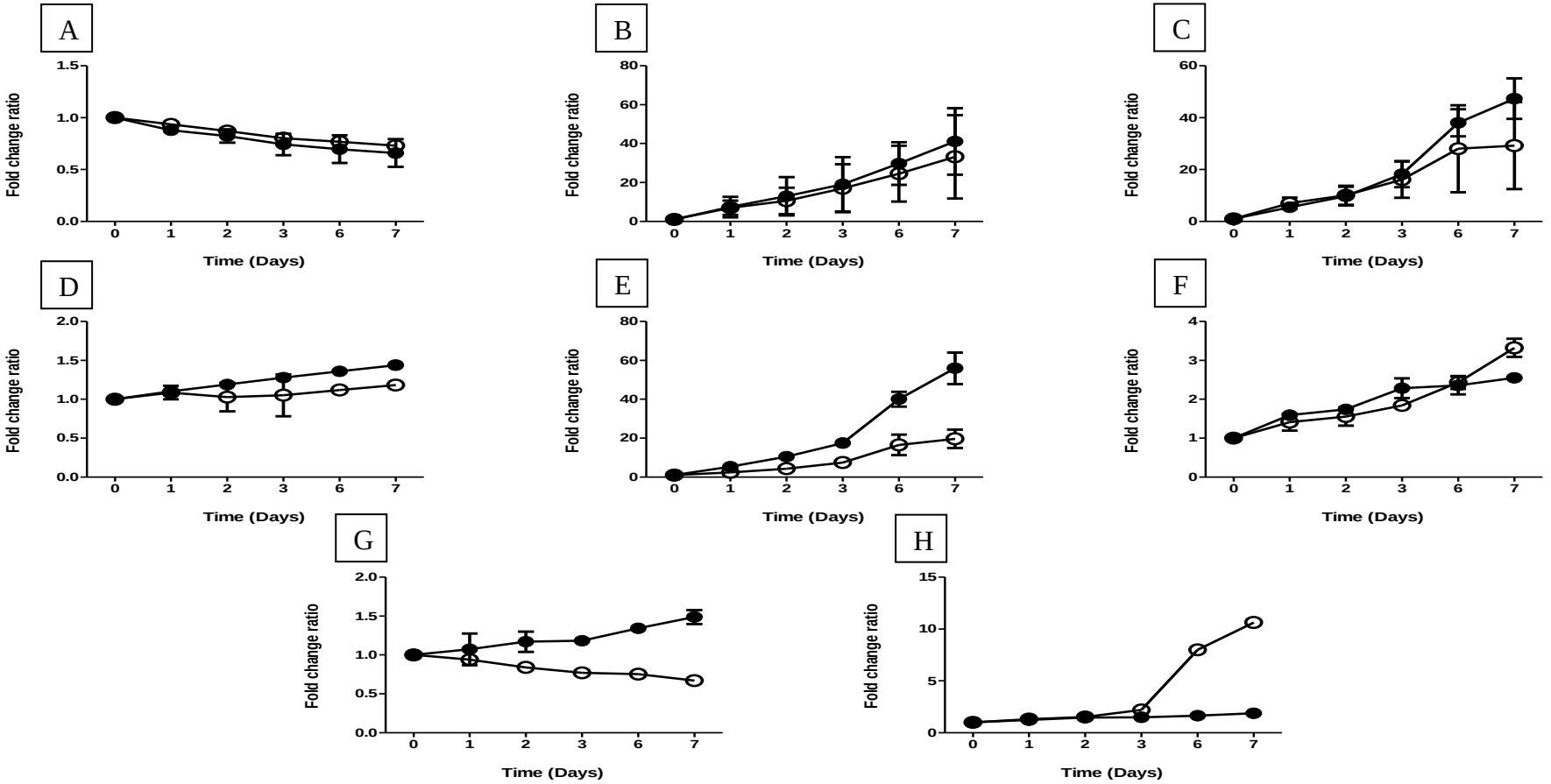

Figure 5.19: Time-dependent changes of Mtb H37Rv metabolites in TPZ-treated and untreated control cells

The following metabolite levels in untreated (closed circle) and TPZ-treated (open circle) cells were determined by LC-MS/MS, A) Glucose, B) Glycerol-3-phosphate (G-3-P), C) Succinate, D) Fumarate, E) Malate, F) Oxaloacetate, G) (iso)-citrate and H) α-Ketoglutarate. The final concentration of Trifluoperazine (TPZ) was at IC_{90} (36.02 µM). The points represent the mean ± SEM of duplicate independent experiments. In TPZ-treated Mtb H37Rv, malate and (iso)-citrate show a notable decrease while α-Ketoglutarate shows a clear increase (GraphPad prism 5 Software Inc.).

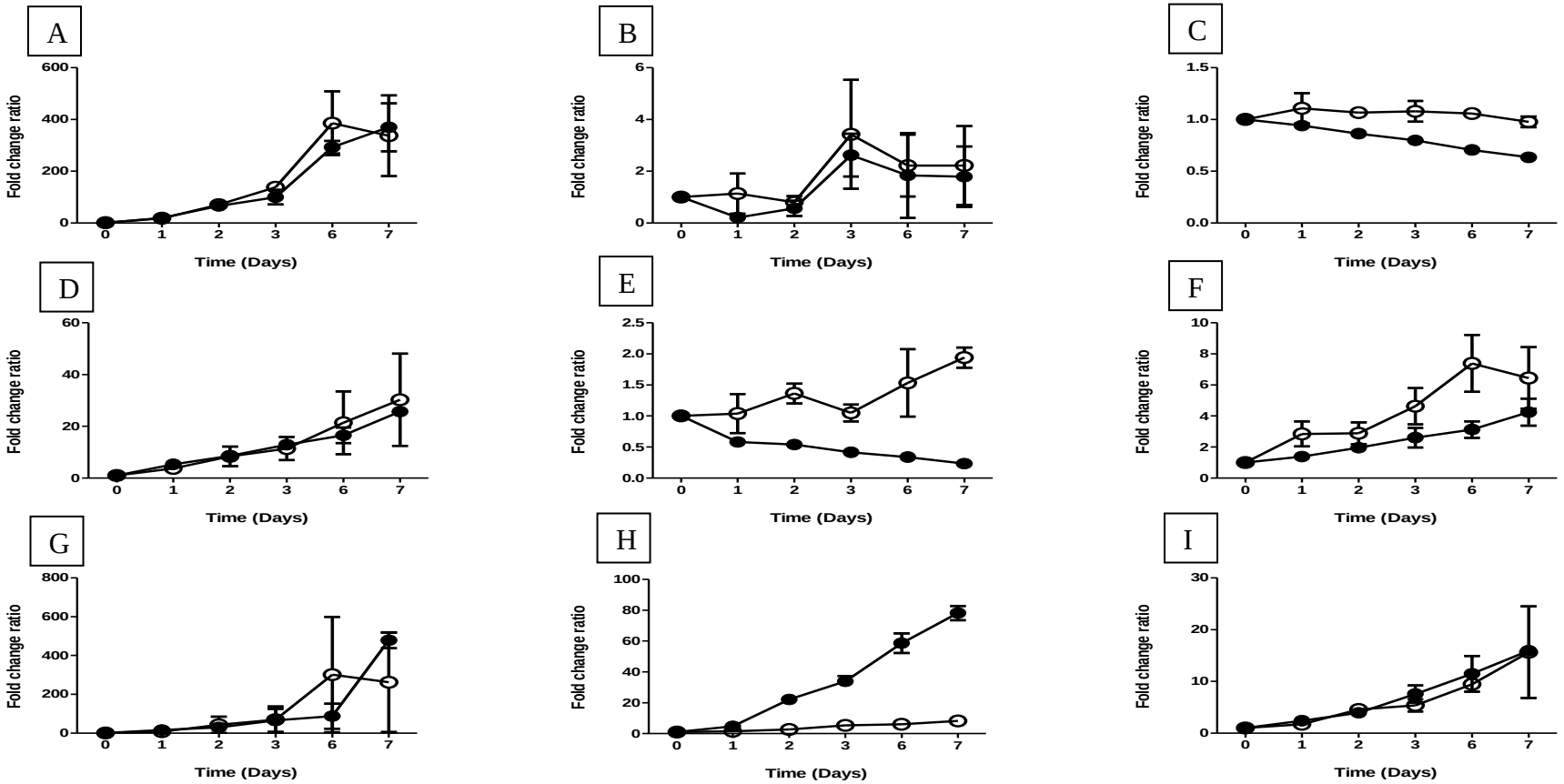

Figure 5.20: Time-dependent changes of Mtb H37Rv metabolites in TPZ-treated and untreated control cells

The following metabolite levels in untreated (closed circle) and TPZ-treated (open circle) cells were determined by LC-MS/MS, A) Alanine, B) Aspartate, C) Glutamate, D) Citrulline E) Ornithine, F) Glutamine, G) Proline, H) Hypoxanthine and I) Histidine. The final concentration of Trifluoperazine (TPZ) was at IC_{90} (36.02 µM). The points represent the mean ± SEM of duplicate independent experiments. In TPZ-treated Mtb H37Rv, glutamate shows low utilization; ornithine is notably increased and hypoxanthine is present at low levels (GraphPad prism 5 Software Inc.).

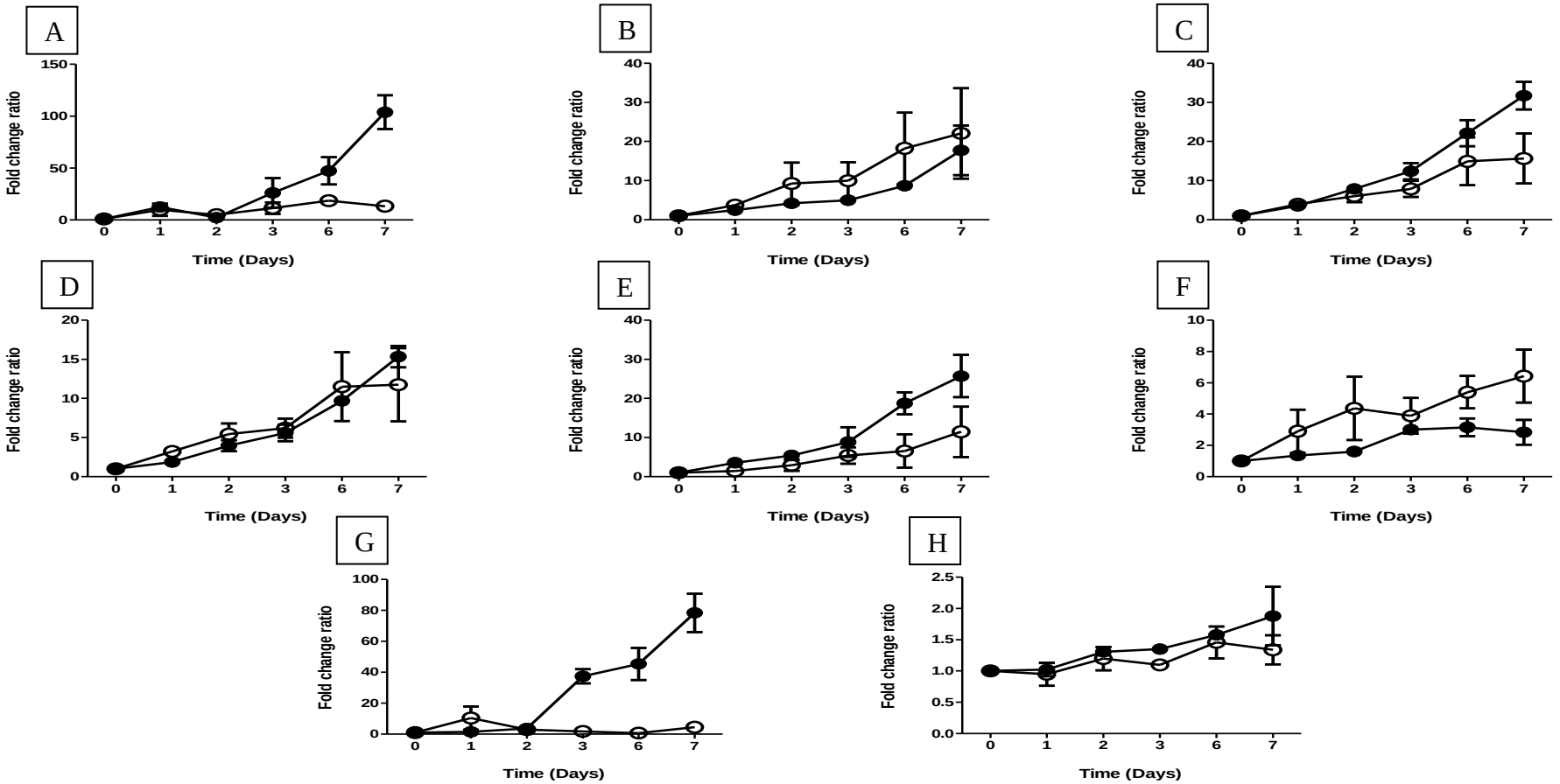

Figure 5.21: Time-dependent changes of Mtb H37Rv metabolites in TPZ-treated and untreated control cells

The following metabolite levels in untreated (closed circle) and TPZ-treated (open circle) cells were determined by LC-MS/MS, A) Valine, B) (iso)-leucine, C) Phenylalanine, D) Tryptophan E) Tyrosine, F) Lysine, G) Threonine and H) Methionine. The final concentration of Trifluoperazine (TPZ) was at IC_{90} (36.02 µM). The points represent the mean ± SEM of duplicate independent experiments. In TPZ-treated Mtb H37Rv, threonine and valine are present at very low levels (GraphPad prism 5 Software Inc.).

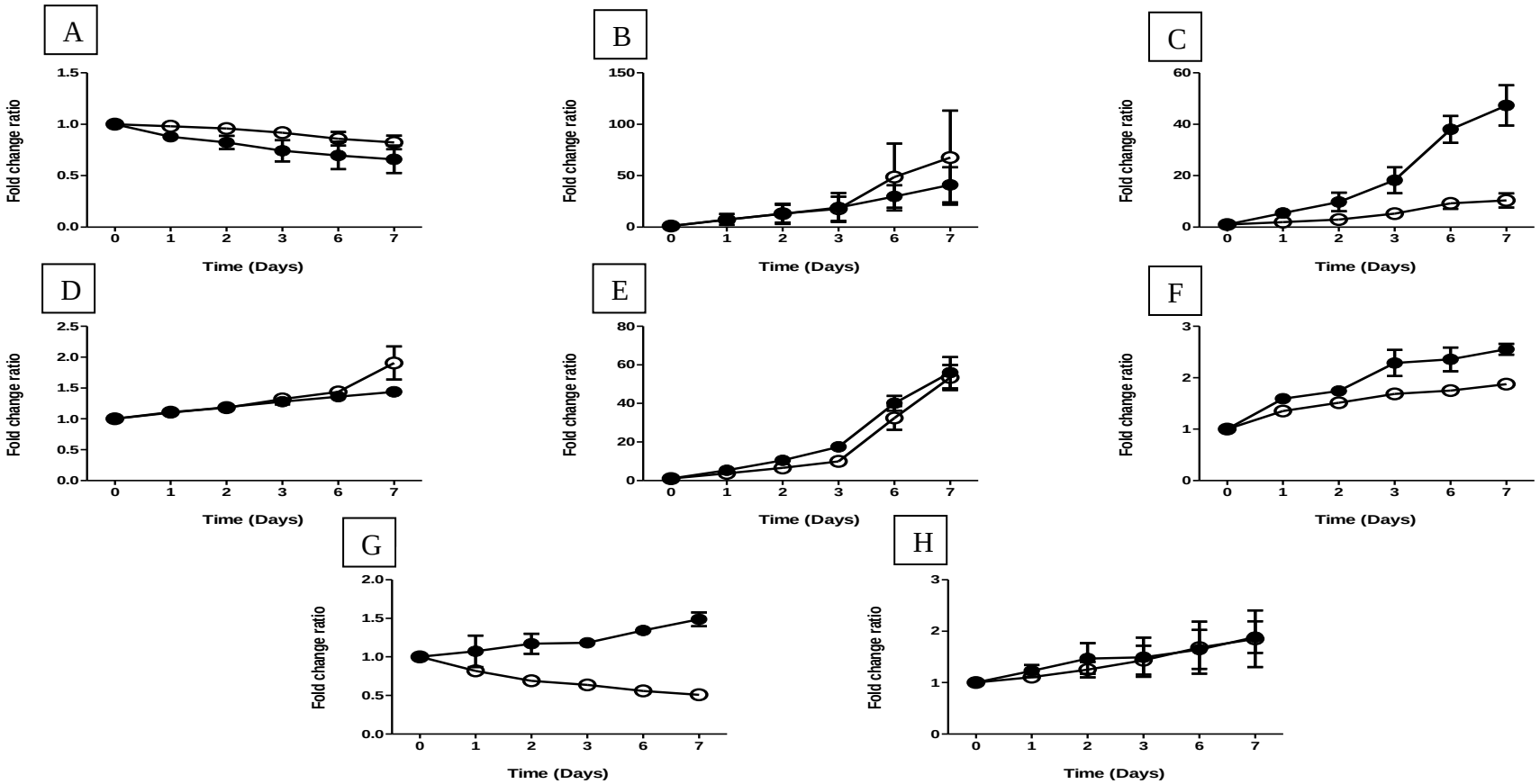

Figure 5.22: Time-dependent changes of Mtb H37Rv metabolites in CK-2-63-treated and untreated control cells

The following metabolite levels in untreated (closed circle) and CK-2-63-treated (open circle) cells were determined by LC-MS/MS, A) Glucose, B) Glycerol-3-phosphate (G-3-P), C) Succinate, D) Fumarate, E) Malate, F) Oxaloacetate, G) (iso)-citrate and H) α-Ketoglutarate. The final concentration of CK-2-63 was at IC_{90} (6.73 µM). The points represent the mean ± SEM of duplicate independent experiments. In CK-2-63-treated Mtb H37Rv, succinate is at low levels and (iso)-citrate is also considerably decreased (GraphPad prism 5 Software Inc.).

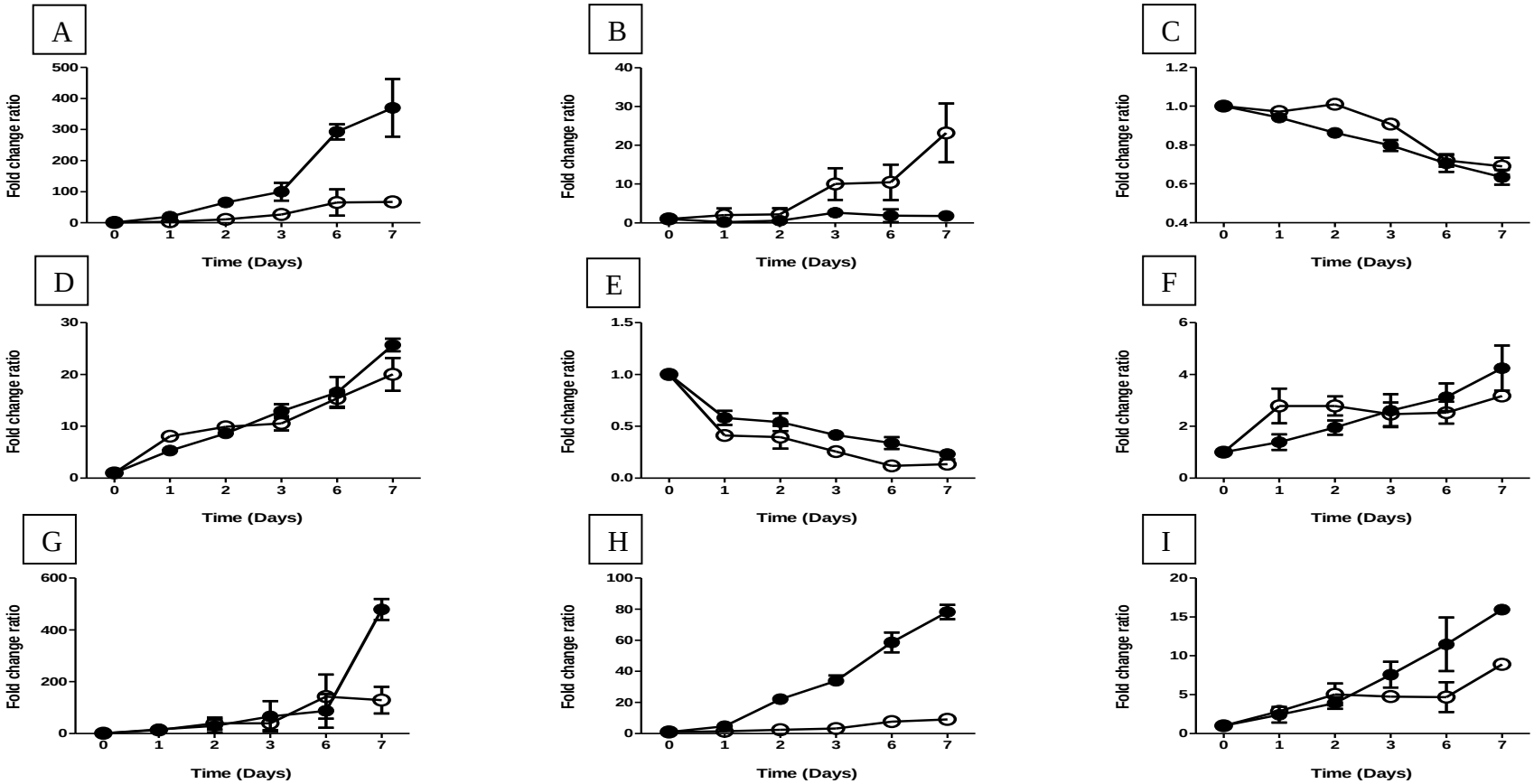

Figure 5.23: Time-dependent changes of Mtb H37Rv metabolites in CK-2-63-treated and untreated control cells

The following metabolite levels in untreated (closed circle) and CK-2-63-treated (open circle) cells were determined by LC-MS/MS, A) Alanine, B) Aspartate, C) Glutamate, D) Citrulline E) Ornithine, F) Glutamine, G) Proline, H) Hypoxanthine and I) Histidine. The final concentration of CK-2-63 was at IC_{90} (6.73 µM). The points represent the mean ± SEM of duplicate independent experiments. In CK-2-63-treated Mtb H37Rv, aspartate is noticeably increased while alanine, proline and hypoxanthine are at very low levels produced (GraphPad prism 5 Software Inc.).

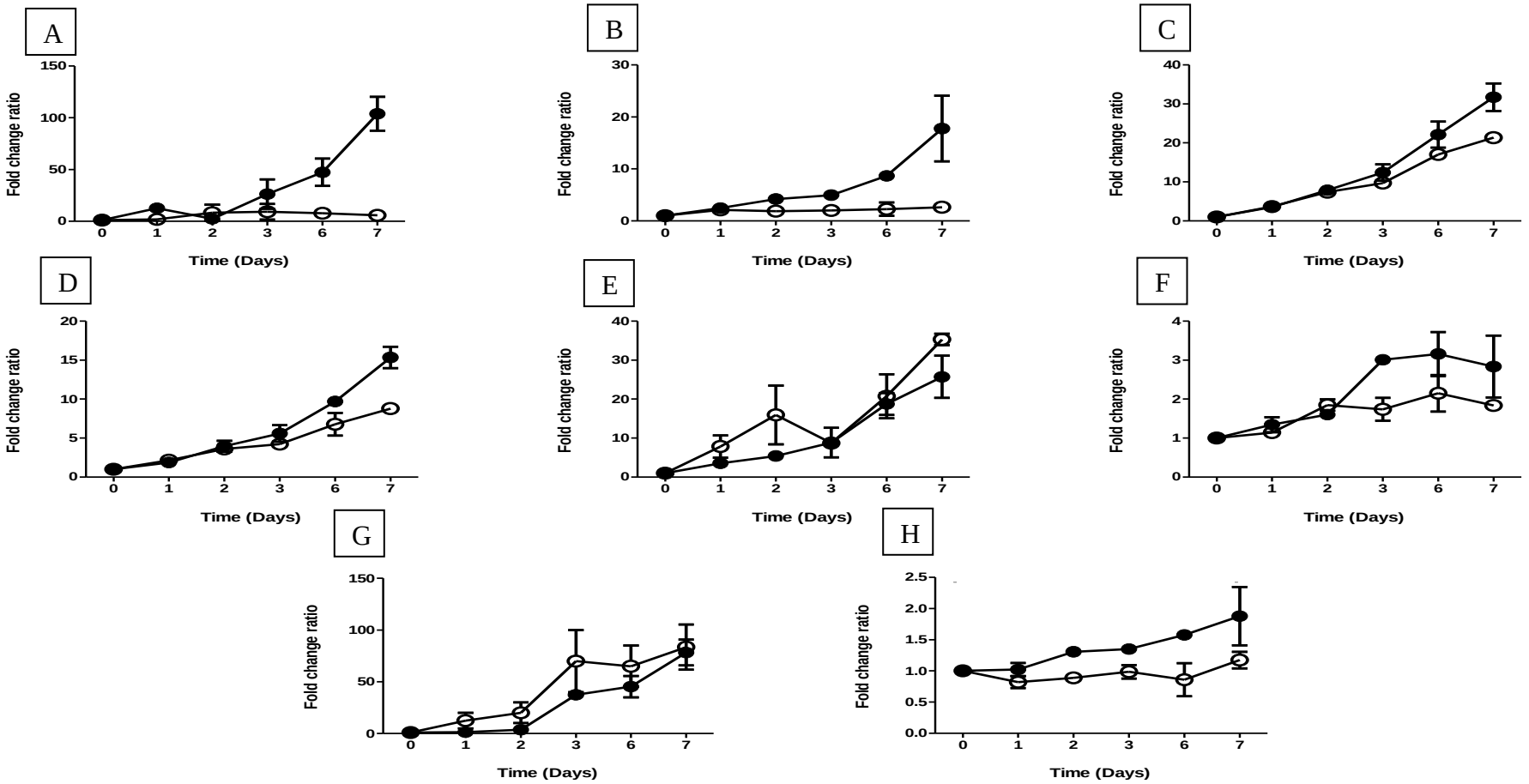

Figure 5.24: Time-dependent of changes Mtb H37Rv metabolites in CK-2-63-treated and untreated control cells

The following metabolite levels in untreated (closed circle) and CK-2-63-treated (open circle) cells were determined by LC-MS/MS, A) Valine, B) (iso)-leucine, C) Phenylalanine, D) Tryptophan E) Tyrosine, F) Lysine, G) Threonine and H) Methionine. The final concentration of CK-2-63 was at IC_{90} (6.73 µM). The points represent the mean ± SEM of duplicate independent experiments. In CK-2-63-treated Mtb H37Rv, (iso)-leucine, valine and methionine are produced at low levels (GraphPad prism 5 Software Inc.).

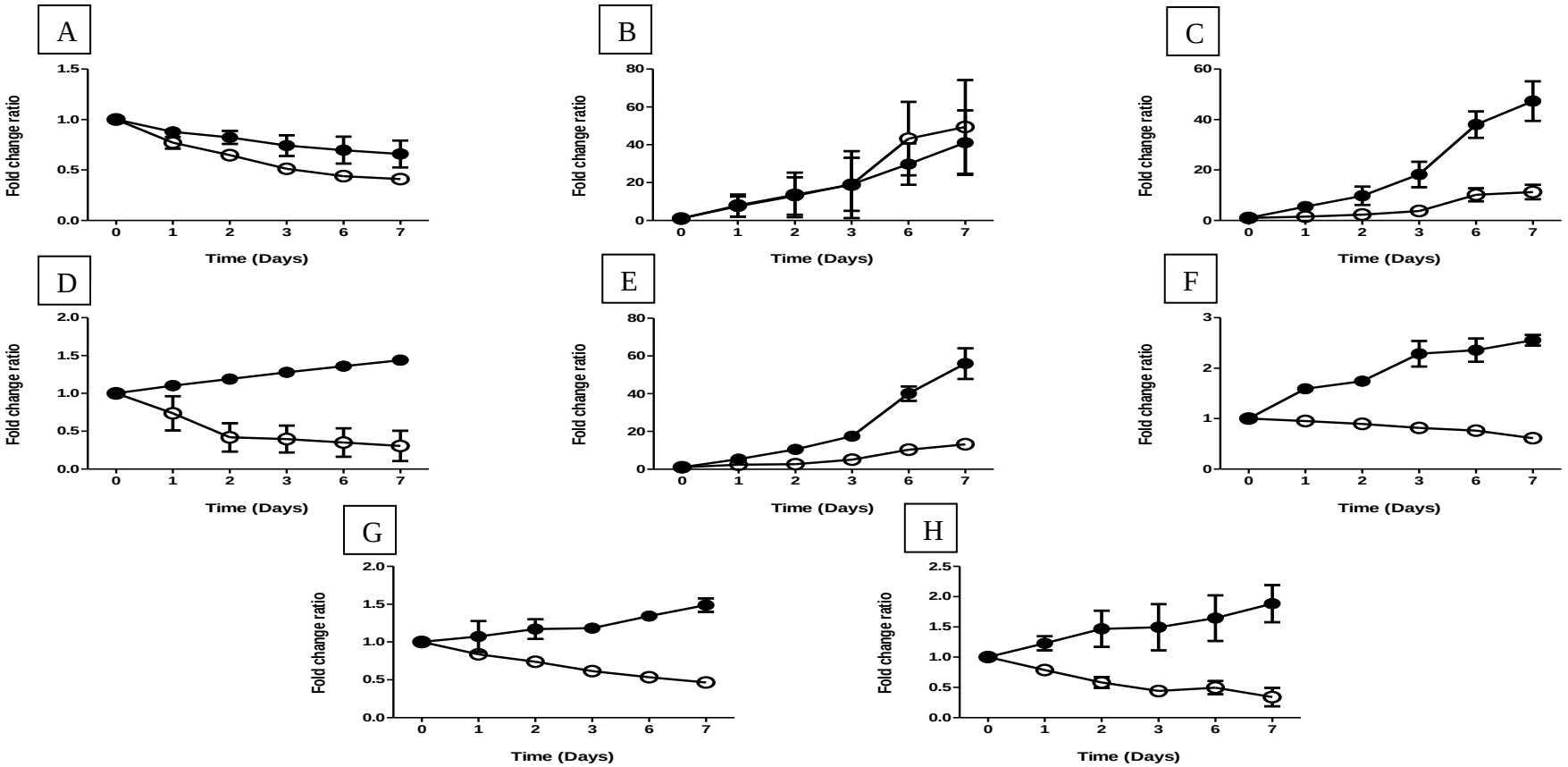

Figure 5.25: Time-dependent changes of Mtb H37Rv metabolites in RKA-307-treated and untreated control cells

The following metabolite levels in untreated (closed circle) and RKA-307-treated (open circle) cells were determined by LC-MS/MS, A) Glucose, B) Glycerol-3-phosphate (G-3-P), C) Succinate, D) Fumarate, E) Malate, F) Oxaloacetate, G) (iso)-Citrate and H) α-Ketoglutarate. The final concentration of RKA-307 was at IC_{90} (3.11 µM). The points represent the mean ± SEM of duplicate independent experiments. In RKA-307-treated Mtb H37Rv, succinate, malate, oxaloacetate are produced at low levels; fumarate, (iso)-citrate and α-Ketoglutarate levels are remarkably reduced (GraphPad prism 5 Software Inc.).

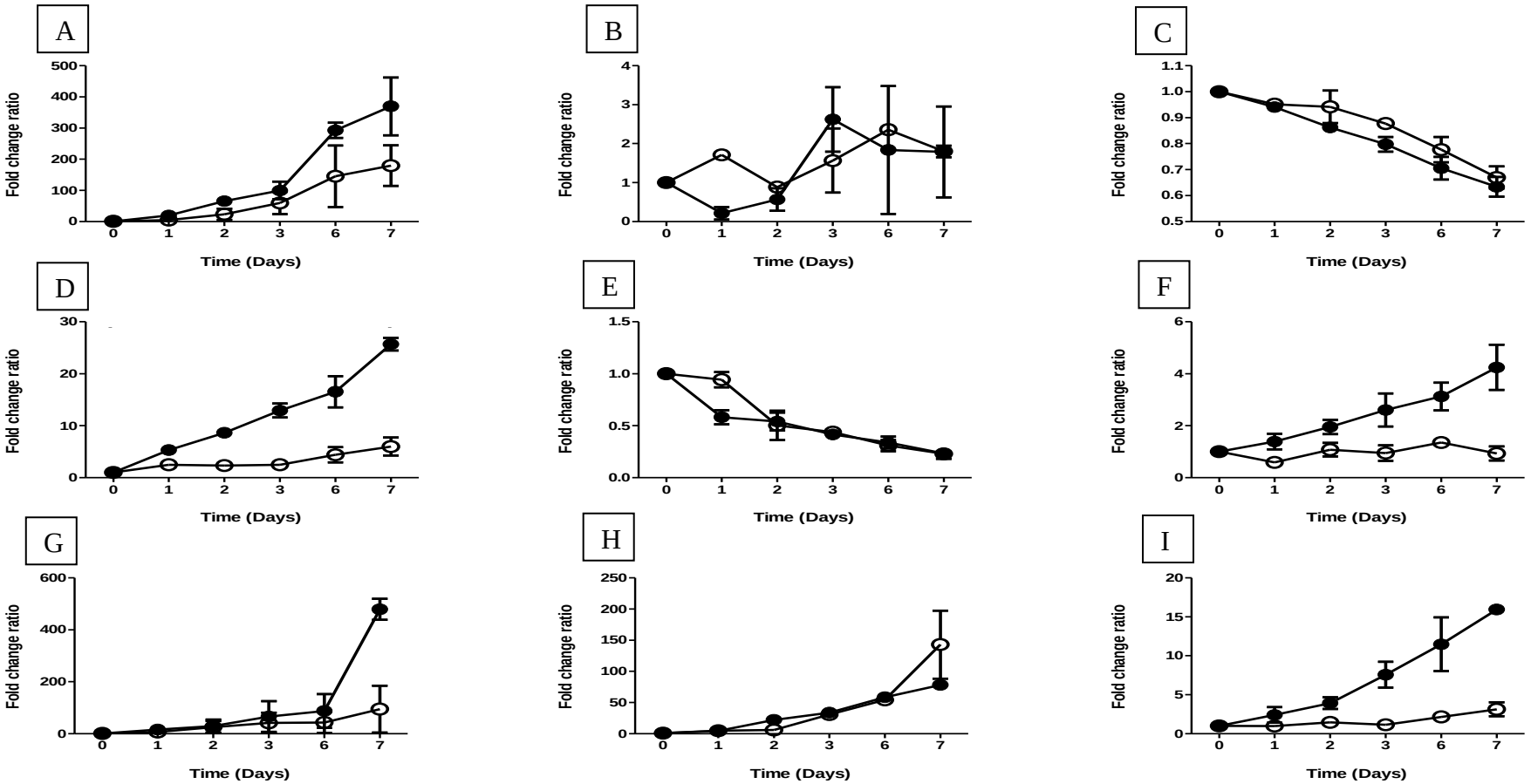

Figure 5.26: Time-dependent changes of Mtb H37Rv metabolites in RKA-307-treated and untreated control cells

The following metabolite levels in untreated (closed circle) and RKA-307-treated (open circle) cells were determined by LC-MS/MS, A) Alanine, B) Aspartate, C) Glutamate, D) Citrulline E) Ornithine, F) Glutamine, G) Proline, H) Hypoxanthine and I) Histidine. The final concentration of RKA-307 was at IC_{90} (3.11 µM). The points represent the mean ± SEM of duplicate independent experiments. In RKA-307-treated Mtb H37Rv, citrulline, histidine, proline and glutamine are produced at low levels (GraphPad prism 5 Software Inc.).

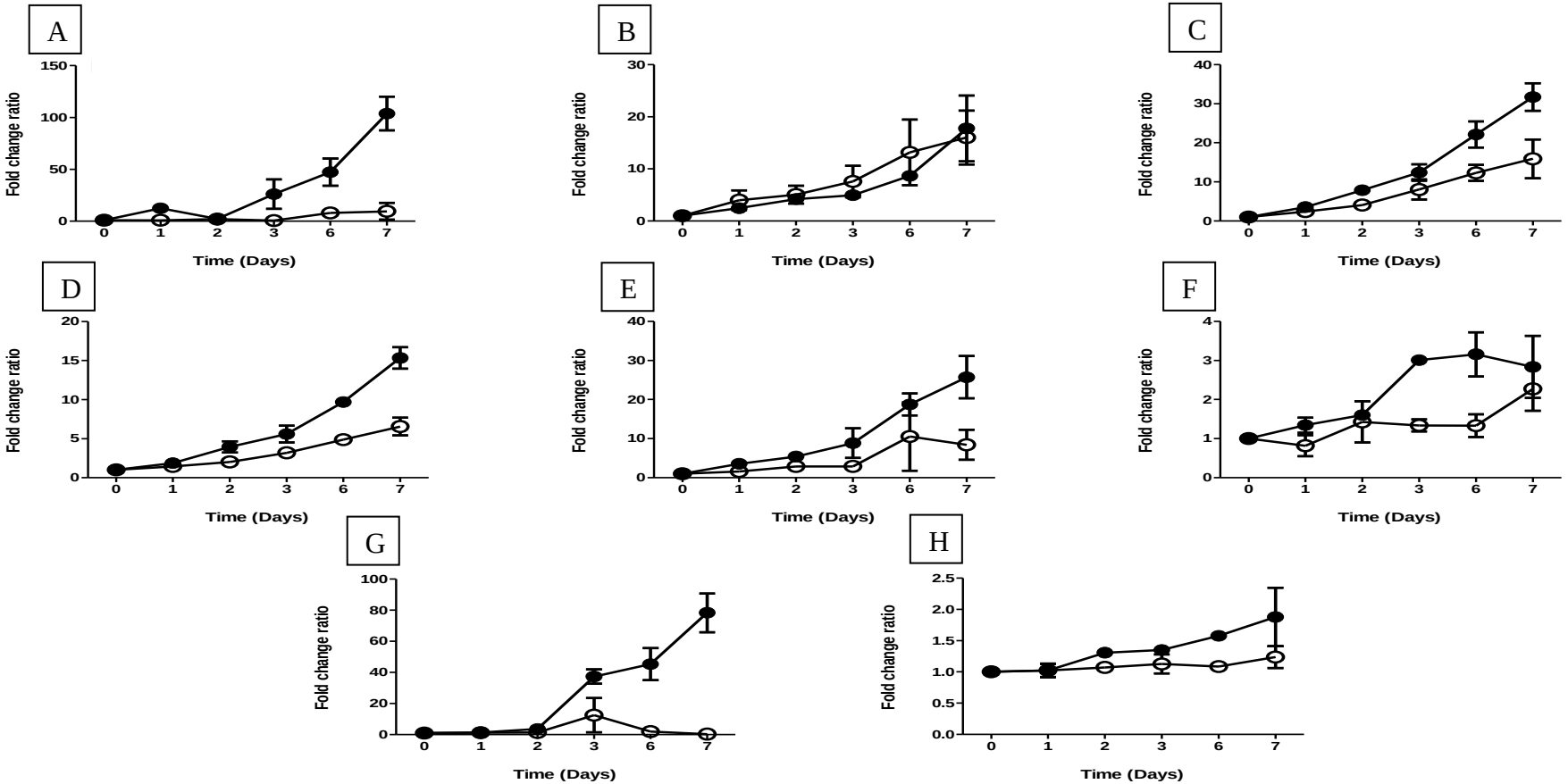

Figure 5.27: Time-dependent changes of Mtb H37Rv metabolites in RKA-307-treated and untreated control cells

The following metabolite levels in untreated (closed circle) and RKA-307-treated (open circle) cells were determined by LC-MS/MS, A) Valine, B) (iso)-Leucine, C) Phenylalanine, D) Tryptophan E) Tyrosine, F) Lysine, G) Threonine and H) Methionine. The final concentration of RKA-307 was at IC_{90} (3.11 µM). The points represent the mean ± SEM of duplicate independent experiments. In RKA-307-treated Mtb H37Rv, valine and threonine are at very low levels (GraphPad prism 5 Software Inc.).

5.4. Discussion

The greatest obstacles towards significant advances in TB drug development that target both replicating and non-replicating Mtb arise from the lack of the knowledge of mycobacterial physiology and the mechanisms associated with drug sensitivity. Pharmaco-genomics, -transcriptomics and -proteomics have been applied in *Mycobacterium tuberculosis* studies (241, 386, 390, 391). However, so far pharmaco-metabolomic studies of Mtb were limited to the Chakraborty *et al* (2013) study which explored the MoA of the antifolate para-aminosalicylic acid (PAS) (392).

Studies of the MoA of quinolone-type compounds used against Mtb *bd*-I and of current TB drugs were carried out to assess the potential of pharmaco-metabolomics to explore and/or validate the MoA of existing and new TB drugs. In this regard, the first-line TB drugs, INH-, EMB-, RIF- and STR-treated Mtb along with electron transport chain inhibitors, TPZ- and CK-2-63-treated Mtb were initially clustered in a 2-D PCA plot along with untreated Mtb H37Rv. Interestingly, however, RKA-307-treated Mtb had a distinct cluster. When PLS-DA analysis was applied. 2-D PLS-DA confirmed the discrete clustering of RKA-307-treated Mtb and furthermore, TPZ and CK-2-63-treated Mtb were observed to be closely associated with this cluster, consistent with overlapping MoA of respiratory chain inhibitors. In contrast, the first-line TB drugs-treated Mtb were clustered in close distance to the untreated Mtb H37Rv cluster. These observations could be credited to the general effect of the first-line TB drugs on the amino acids and common metabolic intermediates from which these amino acids are synthesized (Figure 1.14, Chapter I) or break down to (Figure 5.29). In contrast, ETC inhibitors, RKA-307-, TPZ- and CK-2-63-treated Mtb showed quite different effects of which RKA-307-treated Mtb revealed noticeable down-regulation effect on the most of TCA cycle intermediates and some of their related amino acids. Table 5.2 summarizes the metabolites that showed noticeable effects among treated Mtb H37Rv in comparison with that of untreated Mtb H37Rv. TPZ- and CK-2-63-treated Mtb displayed an additional effect which is a clear down-regulation of hypoxanthine, a purine synthesis intermediate (393). It is worth mentioning that although CK-2-63 and RKA-307 are Mtb *bd*-I inhibitors of the same class (quinolone-type compounds) and were found to cluster on the same side of

PLS-DA plots, they did exhibit different clustering directions. This might be explained by the structure variation between these compounds that, interestingly, also confirms the differences in the pharmacodynamics profiles that were found earlier (Chapter III).

Table 5.2: Metabolites showing notable fold change following drug exposure (Summarised from Figs. 5.7 – 5.27)

Drugs/inhibitors	Metabolites showed notable effect upon drug exposure
INH-treated Mtb	G-3-P, α-Ketoglutarate, malate, glutamate, ornithine, valine, alanine, hypoxanthine, lysine and threonine
EMB-treated Mtb	Fumarate, (iso)-citrate, alanine, proline and histidine
RIF-treated Mtb	Fumarate, (iso)-citrate, ornithine, (iso)-leucine, valine and threonine
STR-treated Mtb	Oxaloacetate, succinate, (iso)-citrate, ornithine, proline and histidine
TPZ-treated Mtb	(iso)-citrate, α-Ketoglutarate, malate, glutamate, ornithine, threonine, valine and hypoxanthine
CK-2-63-treated Mtb	Succinate, (iso)-citrate, alanine, aspartate, hypoxanthine, (iso)-leucine, proline, valine and methionine
RKA-307-treated Mtb	Succinate, fumarate, malate, oxaloacetate, (iso)-citrate, α-Ketoglutarate, Citrulline, glutamine, histidine, valine, proline and threonine

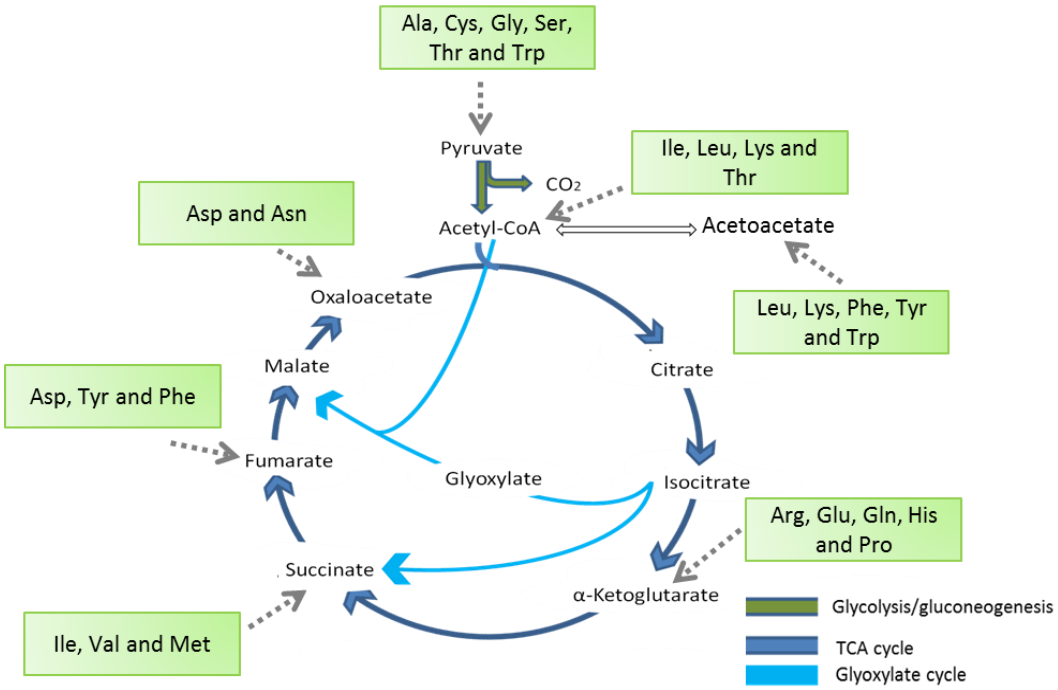

Figure 5.28: Degradation of amino acids to one of seven common metabolic intermediates (194)

Central carbon metabolic (CCM) pathways of Mtb, including the anabolic monomers (amino acids; green boxes) and the major catabolic intermediates that they breakdown to (dashed grey arrows) are shown. Arg, Arginine; Asn, Asparagine; Asp, Aspartic acid; Ala, Alanine; Cys, Cysteine; Gln, Glutamine; Glu, Glutamic acid; Gly, Glycine; Ile, Isoleucine; Leu, Leucine; Lys, Lysine; Pro, Proline; Ser, Serine; Thr, Threonine; Trp, Tryptophan; Tyr, Tyrosine; Val, Valine; Phe, Phenaylalanine; Met, Methionine.

The discrimination between the first-line TB drugs was further improved in the 3-D PLS-DA plot where INH- and STR-treated Mtb displayed closely related distance clusters, whereas the EMB-treated Mtb cluster was close to that of the untreated Mtb cluster. Moreover, RIF-treated Mtb was shown to have a distinctive cluster. This discrimination implied that each of the first-line TB drugs had different MoA although sharing a general effect on amino acids and common metabolic intermediates. Therefore, observations from other omics studies on the MoA of the first-line TB drugs will be highlighted in the following section in order to point out the expected effect of these drugs on Mtb metabolism and thus indirectly explain the clustering pattern of the first-line TB drugs.

INH-treated cells revealed substantial increases in G-3-P, α-Ketoglutarate, valine, alanine and lysine levels. Moreover, the level of malate and hypoxanthine notably increased by day 7. Glutamate and ornithine of INH-treated Mtb were found to be at very low levels. Threonine was also present in low amounts. Importantly, INH is known as a cell wall synthesis inhibitor. Pharmaco-proteomic studies on *Mycobacterium bovis* BCG (394) and on *Mycobacterium smegmatis* (395) along with a pharmaco-genomic study (396) and pharmaco-transcriptomic studies on Mtb (241, 386, 390) showed that INH-treated Mtb had a significant up-regulation in the FAS-II system. FAS-II is involved in the synthesis of mycolic acids, the primary target of INH. Upon exposure of Mtb to INH, Takayama *et al* (1972) found inhibition of mycolic acid synthesis components using thin-layer chromatography (85). Moreover, Argyrou *et al* (2006) detected nucleic acid biosynthesis suppression in proteomic profiling of INH-treated Mtb (397) and earlier biochemical analysis of INH-treated Mtb found depletion of NADH and NADPH pools (398). A pharmacoproteomic study of INH-treated Mtb showed up-regulation of proteins involved in cell wall processes such as the ESAT-6 family proteins, and down-regulation of 13 proteins including ATP-dependent DNA/RNA helicase (391). Unfortunately, FAS-II precursors such as acetyl-CoA, methylmalonyl-CoA and redox couples were below limits of detection in this study. Interestingly, an important perturbation of amino acid metabolism was observed in INH-treated Mtb. However, a previous study found that the total protein synthesis of Mtb treated with INH for 12 h remained unaffected using the Lowry *et al* (1951) conventional method for protein determination. These discrepancies might be because of the short drug incubation time in the study by Gangadharam *et al* (1963) (399, 400).

Regarding EMB that primarily targets arabinogalactan in the Mtb cell wall, EMB-treated Mtb showed a notable decrease in (iso)-citrate levels and low production of fumarate. Furthermore, the level of alanine, proline and histidine was notably decreased in EMB-treated Mtb. A pharmaco-proteomic study of EMB-treated *Mycobacterium smegmatis* found an up-regulation of FAS-II proteins (395). Similarly, Boshoff *et al* (2004) observed that the genes of FAS-II pathways were significantly affected, similarly to what has been seen with INH-treated Mtb, upon treating Mtb with EMB (241). Unfortunately in this study, for the EMB-treated Mtb group, the FAS-II precursors such as acetyl-CoA and methylmalonyl-CoA were not

determined (below LOD) as observed with INH-treated Mtb. Moreover, Jia *et al* (2005) found that Mtb treated with EMB had a similar effect to that of INH-treated Mtb in terms of up-regulating ESAT-6 family proteins. However, unlike INH-treated Mtb, up-regulation of ATP-dependent DNA/RNA helicase was also observed (391). It is worth mentioning that these differences between INH- and EMB-treated Mtb further explained the dissimilarities of those drugs in terms of 3D PLS-DA clustering, although both are cell wall synthesis inhibitiors.

RIF is a RNA synthesis inhibitor that acts by binding to RNA polymerase. Mtb treated with RIF revealed reduced levels of (iso)-citrate and fumarate and low production of and low utilization of threonine and ornithine, respectively. Moreover, RIF-treated Mtb showed a considerably increased level of (iso)-leucine and valine compared with drug-free control Mtb. A transcriptional study on *Haemophilus influenzae* protein synthesis patterns conducted by Evers *et al* (2001) found that RIF-treated *H. influenza* displayed up-regulation of RNA polymerase subunits and ribosomal protein along with the complete shutdown of RNA synthesis (401). Unfortunately, pyrimidine metabolism precursors such as carbamoyl-l-aspartate, orotate and dihydroorotate were below LOD. However, the obtained results of disruptions of some amino acids metabolism and TCA cycle metabolites could be regarded as a secondary effect of RIF on Mtb metabolome.

STR is a protein synthesis inhibitor that binds to a ribosomal subunit. STR-treated Mtb showed reduced levels of (iso)-citrate and low production of histidine, but substantial increases in ornithine, suucinate and oxaloacetate levels. Unlike RIF-treated *H. influenzae*, STR-treated *H. influenzae* exhibited no significant changes in RNA polymerase subunits, ribosomal protein and RNA synthesis (401). This observation supports 3-D PLS-DA data that showed a different pattern between RIF- and STR-treated Mtb. Moreover, Qiu *et al* (2005) wrote that the transcriptional study of STR-treated *Yersinia pestis* revealed a general repression of energy metabolism genes and retardation of metabolic process and RNA synthesis, but up-regulation of genes that relate to membrane proteins, lipoproteins and porins (402). Boshoff *et al* (2004) stated that RIF- and STR-treated Mtb resulted in global down-regulation of Mtb genes (241). Notably, these findings may explain this thesis finding of STR-treated Mtb.

TPZ-treated Mtb showed drastically decreased levels of (iso)-citrate, valine and malate but a noticeable increase in the levels of α-Ketoglutarate and ornithine. In addition, there was little or no utilization of glutamate and a low production of threonine and hypoxanthine. Boshoff *et al* (2004) found that the main effects of chlorpromazine (CPZ) and thioridazine (TRZ), phenothiazine-based compounds, were a reduction in ATP levels and a decreased intracellular $NADH/NAD^+$ ratio (241). Unfortunately, bioenergetic couples such as ATP and redox couples NADH and NAD were below LOD. However, the perturbations of amino acids metabolism and hypoxanthine could be related to the remote effect of TPZ on Mtb metabolome.

Concerning Mtb treated with RKA-307, a quinolone-type inhibitor, drastic reductions in levels of most TCA cycle intermediates were observed including succinate, malate, (iso)-citrate, fumarate, α-Ketoglutarate and oxaloacetate (compared with drug-free Mtb). RKA-307-treated Mtb also showed remarkable decreases in valine, threonine, citrulline, glutamine, proline and histidine levels. In contrast, CK-2-63, a compound of similar class to RKA-307, exhibited notable reduction in the level of succinate, (iso)-citrate, (iso)-leucine, hypoxanthine, alanine, valine, proline and methionine and a visible increase in aspartate level. RKA-307 and CK-2-63, as discussed earlier (Chapter 3.4), showed an inhibition effect against Mtb cytochrome *bd*-I oxidase. However, the difference between RKA-307 and CK-2-63 pharmaco-metabolomic profiling could be attributed to the differences in the compounds' structures, as discussed earlier (Chapter 3.4). The TCA cycle fluxes of a *Bacillus subtilis* mutant strain that lacked cytochrome aa_3 oxidase were quantitatively assessed using gas chromatography-mass spectrometry (GC-MS) and revealed a severe reduction of TCA cycle fluxes (403). Importantly, the reduction of some TCA cycle metabolites in RKA-307-treated Mtb might imply the concept of multiple targets (i.e it could show an inhibition effect on different respiratory components besides cytochrome *bd*-I oxidase).

Inside the cell, the level of metabolites is determined by complex regulatory processes, transcription and translation regulation, protein-protein interactions and enzymes-metabolites interactions (374, 377). The compensation of some metabolites by other pathways of a complex high connectivity metabolism network could explain

the absence of significant changes of drug/inhibitor-treated Mtb metabolites. Bhat *et al* (2010), who studied the metabolic adjustments in Mtb upon exposure to INH, wrote that, with regard to the disturbed metabolic pathways, the metabolic adjustment could be described as a distant effect within the metabolic network. This metabolic adjusment involves some important metabolites that are produced through alternate pathways to keep the biological reactions operational (404). For instance, although INH- and EMB-treated Mtb showed important changes that are involved in CCM metabolites but not in fatty acid or cell wall synthesis, they may still offer valuable information about the secondary effect of these drugs MoA.

This is the first study to investigate the metabolomic profiling of Mtb in response to first-line TB drugs as well as ETC inhibitors. Although no conclusive results regarding the MoA were generated, this study opens the door for future promising research towards the understanding not only of the specific responses of anti-TB drugs (primary MoA) but also the important secondary effects on Mtb metabolic network. In turn, new directions of anti-TB therapy development would consider developing co-drugs that target secondary responses on the Mtb metabolic network (376). The sensitivity of the LC-MS/MS used in this method showed some limitations, since metabolites of bioenergetic and redox couples such as ATP and NADH were below the limit of detection. Thus, using more sensitive analysis instrumentation (e.g. Orbitrap MS) and improved sample preparation methods would be advised for future studies. Moreover, for future work it is worth using different concentrations of drugs/inhibitors since drugs were found to induce gene expression only within a certain window of concentration (376, 405). This might be applied at the metabolic level as well, where low concentrations of drugs/inhibitors might not be adequate for affecting metabolite levels, whereas a high concentration might show death-related effects.

Chapter VI

General discussion

Mycobacterium tuberculosis, an organism discovered 130 years ago, remains a major health threat, claiming nearly 2 million individuals annually. After almost a century without the introduction of new vaccines, 11 candidates are currently in clinical trials (8). Likewise, after decades (nearly 50 years) with the current yet inadequate TB treatment and without novel classes of drugs to tackle today's TB pandemic, several candidates are currently in late development clinical phases (www.tballiance.org) (Chapter 1.7). On-going searches for new drug targets against Mtb are required in order to find the best multi-drug regimen that would overcome the current first- and second-line treatment drawbacks (Chapter 1.4). However, it is inevitable that the organism will develop resistance, even to new drugs. Therefore, a detailed understanding of the pathogenesis of Mtb (cross-talk with a human host) and the pathogen's response to drugs is vital. Mainly, there are three strategies that contribute in the enormous success of Mtb pathogenesis: first, macrophage reprogramming to impair organism degradation; second, formation of well-structured granulomas, creating a confined environment for the host-pathogen interfacing; and third, transition into a dormancy stage, rendering Mtb extremely resistant to host defence and drug action, which is characterised by slowing down of the metabolic machinery of Mtb, the carbon metabolic pathways and the membrane-embedded respiratory components (3, 16, 406).

Mtb has a heterogeneous, dynamic nature, and inter-conversion of diverse Mtb subpopulations does occur. This phenomenon, demonstrated through the Yin-Yang model (24) (Chapter 1.3.2.5), forms the basis of the current difficulties to eradicate Mtb, regardless of using the INH/RIF combination in the 4-month continuance phase of treatment to eliminate the possibility of dormant and/or persistent tubercle bacilli reverting. Therefore, the urgent medical need for new TB drugs will continuously present until efficient first-line and second-line regimens that have a bactericidal effect on active, latent and resistant forms of Mtb are established. Energy metabolism, including metabolic pathways and the ETC, have emerged as new target-pathways for the development of new anti-tubercular drugs, owing to the fact that active or dormant tubercle bacilli will need energy to keep them alive regardless of the level of this energy (i.e. high or low). Here, a review of this thesis is presented, conclusions are drawn and gaps in the work are highlighted so that they can be addressed in future research.

A key objective of the thesis (Chapter II) was the generation of a heterologous expression system for Mtb cytochrome *bd*-I oxidase in *E. coli* respiratory knockout mutant strains. A double-knockout ML16 strain, lacking two types of quinol:oxygen oxidoreductase (cytochrome bo_3 and cytochrome *bd*-I), and a triple-knockout MB44 strain, lacking all types of quinol:oxygen oxidoreductase (cytochrome bo_3, cytochrome *bd*-I and cytochrome *bd*-II), were used. Successfully, a heterologous expression system for Mtb cytochrome *bd*-I oxidase was established in both strains. However, some limitations of the triple-knockout strain were found, which will be discussed shortly. First of all, the generation and validation of a heterologous expression system for Mtb cytochrome *bd*-I oxidase in the ML16 strain (named as TML16) was successful in terms of biochemical characterisation by spectral analyses of TML16 strain and of microbiological characterisation by assessment of growth phenotypes and oxygen depletion in cultures during both aerobic and O_2-limited growth conditions. The spectral analyses of the TML16 stain confirmed the expression of recombinant Mtb cytochrome *bd*-I oxidase (Mtb *bd*-I) by restoration of its spectral signature, a peak at 631 nm. Importantly, an additional critical validation is that although the ML16 strain still harboured endogenous cytochrome *bd*-II genes, the haem-*d* absorbance peak that was expected to be present at about 628-632 nm (217, 218, 290, 292) was not recorded. Moreover, it was possible to correlate the spectrum profile with growth conditions. The ratios of the cytochrome *d* peak to the reference peak in TML16 and wild-type strains were higher in O_2-limited than in aerobic conditions. The microbiological assessment of TML16 growth phenotypes revealed the ability of Mtb *bd*-I to restore some of the important wild-type growth phenotypes, maintaining cell viability during the stationary phase, unlike the ML16 strain (4, 295) (Chapter 2.4).

Multidisciplinary approaches towards the characterisation of Mtb *bd*-I were implemented in Chapter III, revealing original and conclusive data of Mtb *bd*-I kinetics. Optimum conditions for enzyme activity were examined, revealing a pH of 7.5 to be for the highest Mtb *bd*-I activity. Moreover, for future biophysical characterisation, the effect of detergents on Mtb *bd*-I activity was assessed. Mtb cytochrome *bd*-I oxidase showed a substrate preference for dQH_2 over Q_1H_2 and Q_2H_2 (K_m = 19.25 μM, 51.5 μM and 65.2 μM). However, the physiological substrate of Mtb *bd*-I, MQH_2, could not be examined in this study due to solubility issues.

Importantly, Mtb *bd*-I was confirmed to conclusively catalyse the oxidation of quinol simultaneously with O_2 reduction resulting in a monophasic kinetic plot with dQH_2 and Q_1H_2 substrates. However, this reaction showed a biphasic kinetic plot with the substrate Q_2H_2, which acted as a non-competitive inhibitor at high substrate concentrations. The steady-state kinetics of Mtb *bd*-I were within the range of *bd*-I kinetics of previously studied organisms (211-213, 290, 321, 336, 345, 349, 354-357).

Targeting ETC components, as demonstrated by the discovery of TMC207, is one of the most promising areas toward the discovery of new anti-tubercular drugs (267). Therefore, characterising Mtb *bd*-I oxidase facilitated the study of its competency as a novel target for new TB chemotherapeutics. The goal was identifying a novel inhibitor that acts on the quinol oxidation site. Therefore, quinolone-type compounds (from in house libraries) were screened against Mtb *bd*-I and Mtb H37Rv, and the quinolone core of these compounds was found to be the key target for SAR development. A total of 23 quinolone-type inhibitors were examined, of which 9 inhibitors showed an acceptable inhibition profile with IC_{50} <4 μM against Mtb *bd*-I and with 50% or more inhibition against Mtb H37Rv (single-point screening at 5 μM inhibitor concentration). Interestingly, 5 compounds, RKA-307, RKA-310, MTD-403, SCR-8-12 and CK-3-23, showed significant correlation (*P* value < 0.01) between Mtb *bd*-I and Mtb H37Rv growth inhibition assays, suggesting that Mtb *bd*-I is a potential target for the quinolone-type inhibitors tested. This suggestion has been further confirmed by HepG2 assay, which showed that these compounds target the ETC. However, SCR-8-12 was shown to have a different mode of action, as it did not exhibit any differences between glucose and galactose HepG2 assays. This observation has been supported by time-kill kinetics, where SCR-8-12 was shown to have bactericidal activity, unlike the remaining quinolone-type compounds. Closer examination of the structure of SCR-8-12 (Dr G Nixon, Medicinal Chemists) indicates that this compound has a similar pharmacophore to fluoro-quinolones which may account for its distinct pharmacodynamic profile compared to other members of the series. The bacteriostatic activity of LT-9, RKA-307, RKA-310, CK-2-63 and MTD-403 showed a visible reduction by day 7. Importantly, TMC207 showed quite similar time-kill kinetics (365); thus, this observation strongly promotes increasing the drug incubation time for the quinolone-type compounds up

to at least 14 days in order to evaluate the full time-kill kinetics. Up to this point, MTD-403 was found to be the optimum compound against Mtb *bd*-I, although further improvements of the inhibitor DMPK are needed.

Although the generation and validation of a heterologous expression system for Mtb cytochrome *bd*-I oxidase in the ML16 strain (named as TML16) was successful and robust in all aspects, Chapter IV demonstrated the generation and validation of another heterologous expression system for Mtb cytochrome *bd*-I oxidase, but in a triple-knockout MB44 strain (named as TMB44). The reason for generating this system at the beginning was due to the absence of endogenous cytochrome *bd*-II, since the role of cytochrome *bd*-II in the ML16 strain was unknown. Therefore, we needed a backup plan for the study, due to the challenges faced during Mtb *bd*-I expression trials, which were countless in terms of obtaining a successful transformation, finding the ideal growth condition and preparing crude membranes. As demonstrated in chapter IV, this system represented an additional support system for TML16 data, which confirmed the basic Mtb *bd*-I kinetics that were obtained using the TML16 strain. However, TMB44 cannot replace TML16 because of the weakness of the MB44 strain and difficulties in preparing crude membranes.

Chapter V provided an introduction for future promising pharmaco-metabolomics works in Mtb. With the objective of contributing towards developing new therapeutics and obtaining a better picture of their MoA, two quinolone-type inhibitors that showed activity against Mtb *bd*-I were examined. Remarkably, RKA-307-treated Mtb revealed significant effects of the inhibitor on TCA cycle intermediates and some amino acid metabolites. Moreover, this study initially highlights the differences between two inhibitors of similar classes (i.e. RKA-307 and CK-2-63). The first-line TB drugs showed different significant fingerprints on Mtb metabolome; nevertheless, they were not conclusive. However, it confirmed the variation of MoA between these drugs and highlighted areas that require further detailed studies, such as the perturbation of amino acid metabolism.

With regards to the limitations of this study, qualitatively measuring O_2 saturation in the culture was one of the study limitations. Thus, growing cells in a chemostat model (253) was advised. Moreover, measuring the oxygen affinity of Mtb *bd*-I (a limitation of this study) which could be carried out following the protocol of D'mello *et al.* (1994) is needed for further enzyme characterisation (372).

Although MTD-403 was found to be the optimum inhibitor of Mtb *bd*-I and Mtb H37Rv, improving DMPK properties was necessary. Furthermore, extending the quinolone-type inhibitors incubation time in the time-kill assay was recommended in order to provide a conclusive view of the bactericidal/bacteriostatic nature of these inhibitors. This was owing to the TMC207 time-kill kinetic that showed a slow static effect in the first 7 days and a bactericidal action by 14 days (365).

For advanced studies of Mtb *bd*-I, enzyme purification would be the next step; however, unfortunately, Mtb *bd*-I was not His-tagged and thus different purification methods were required. Blue-Native polyacrylamide gel electrophoresis (BN-PAGE) was successfully used for isolating various respiratory components from mammalian and yeast mitochondria (407, 408). BN-PAGE is known to reduce the tendency of protein aggregation during analysis and to eliminate the need for using detergents, which in turn reduces the risk of detergent-sensitive protein denaturation (409). Applying this technique for Mtb *bd*-I purification is recommended since Mtb *bd*-I was found to be over-expressed.

The large diversity and complexity of the metabolites that exist in a living cell means that using only one method is unlikely to provide enough sensitivity to detect all metabolites. However, this is a predicted outcome, since many central metabolites are biosynthetic intermediates that are usually found at levels more than 10,000-fold lower than other metabolites (378, 410). Thus, due to the fact that such trace metabolites remain a challenge to measure, an instrument with increased sensitivity, such as the exactive Orbitrap MS is recommended (411). Moreover, this method is generic, as the column used in this method, Luna aminopropyl, detects most of the polar and few of the non-polar compounds. Therefore, fatty acid synthesis metabolites could not be included in this study. A variety of measurement tools exist

to obtain these diverse metabolites and using a single method makes it impossible to acquire them all (412). For instance, Kamphorst *et al.* (2011) successfully analysed fatty acid metabolism using a Luna C8 reversed-phase column (a column that is suitable for fatty acids metabolites) along with the exactive Orbitrap MS (413).

It is worth mentioning that the metabolome processing steps (cell growth, metabolism quenching, metabolite extraction, concentration and detection by LC-MS and data analysis) would be expected to have a major impact on the obtained results (378). Therefore, the experiment was applied following the metabolomics standard initiative (MSI) (http://msi-workgroups.sourceforge.net/). Some extraction methods could convey more or equivalent drawbacks when compared to others. For example, using centrifugation for harvesting cells carries the possibility of metabolites loss. Thus, using the filter culture method entails minimal risk of metabolome loss. This method is based on transferring a filter (cells grown on filter) from an agarose plate into a cold quenching solvent (380, 414). However, using the filter culture method for Mtb experiments bears high category 3 hazards and requires special advanced category 3 laboratory facilities that would not be found in standard category 3 Mtb laboratories.

Future work

Expressing Mtb *bd*-I allows the initial characterisation of the enzyme and would expedite future advanced characterisation, such as X-ray crystallographic studies and docking studies. The cutting-edge method used in this thesis and the findings necessitate the further application of metabolomics and exploration of the secrets of Mtb pathogenesis. The metabolic capability of an organism to adapt to diverse environments is considered a hallmark of microbial pathogenesis (378). Therefore, using the powerful technique of metabolomics to study Mtb opens doors for a wide range of applications and for global readouts of all 'omic' data. Revealing the mode of action of either current or future potential drugs and their relevance to the proposed primary target and on the secondary subsequent actions of these drugs would create a better strategy to improve and/or develop TB therapy (376). Furthermore, metabolomics would facilitate the study of the diverse dynamic nature of the Mtb subpopulations by using different latency models, from the simple *in*

vitro model (Wayne model) to the advanced *in vivo* model (Cornell model) in mice (20, 32, 33, 36). Watanabe *et al.* (2011) studied the metabolism of Mtb in response to hypoxia using a chemostat model. This study found a significant difference between Mtb aerobic and hypoxic cultures, in which succinate was found to be accumulated in the extracellular part of hypoxic cultures. Watanabe *et al.* (2011) concluded that Mtb sustained an energised membrane by coupling the secretion of succinate to the reductive branch of the TCA cycle (415). Moreover, targeted knockout techniques could be applied in order to reveal the function of Mtb *bd*-I and to assess its role during various stressful conditions, as well as during macrophage infection. Imaging techniques could be applied to examine the effect of Mtb *bd*-I absence on Mtb pathogenesis. This hypothesis is based on the high NO dissociation rate of cytochrome *bd*-I in *E. coli*, providing a strategy to evade the NO-mediated host immune attack (231, 416, 417). Remarkably, Jones *et al.* (2007) found that the *E. coli* mutant strain lacking *bd*-I failed to colonise the mouse intestine, which was in contrast to the *E. coli* mutant strain lacking cytochrome bo_3 (222). This finding emphasises the importance of cytochrome *bd*-I in organism pathogenicity. Such multidisciplinary approaches applied to expand our knowledge of Mtb would pinpoint the potential targets that could contribute to developing better interventions to tackle the problem of TB.

Appendixes

Appendix I: Growth curve of Mtb H37Rv

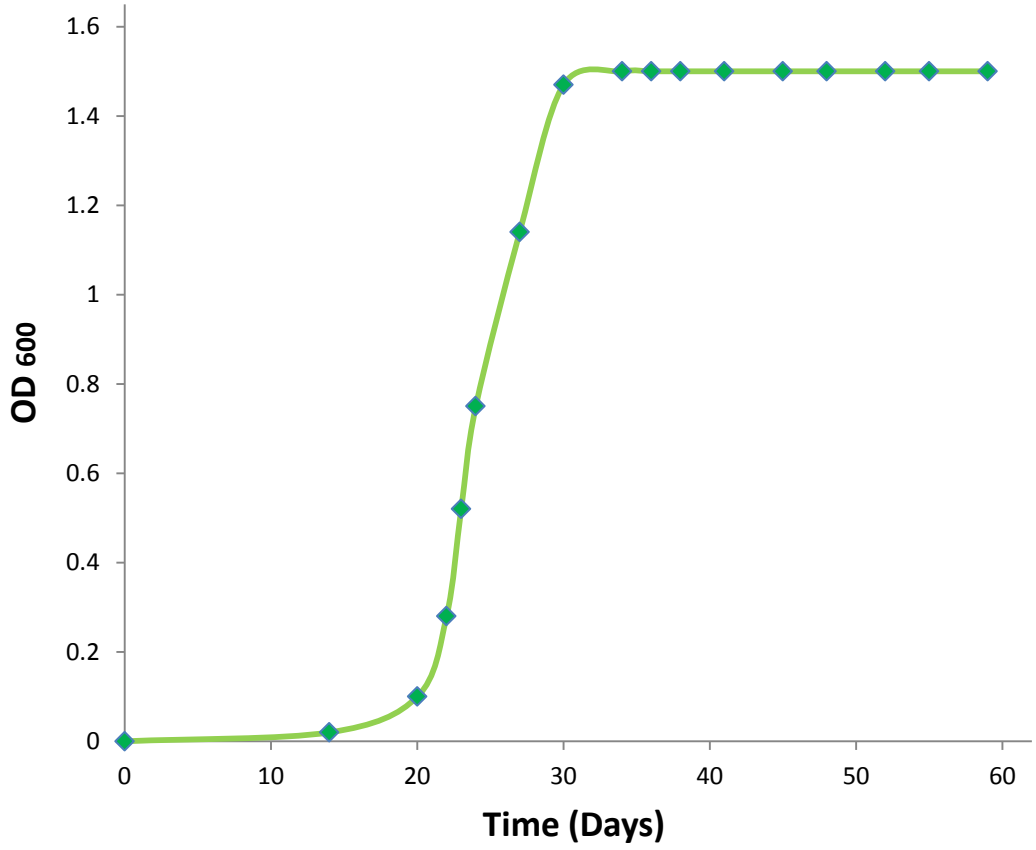

Figure A: Growth curve of aerobic culture of Mtb

Appendix I: (*Continued*)

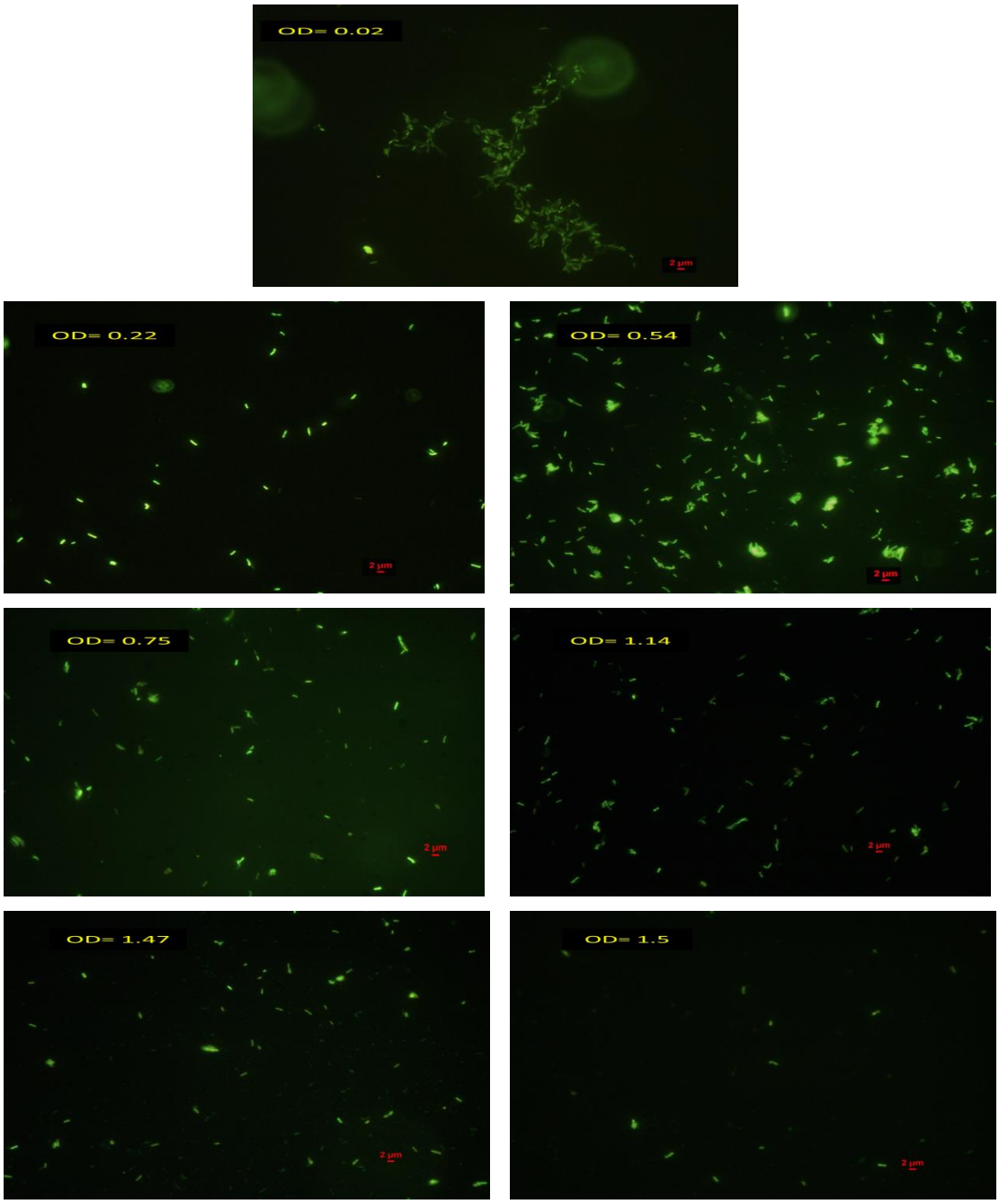

Figure B: Fluorescence microscopy images of Mtb H37Rv bacilli

Mtb H37Rv bacilli grown in aerobic culture was stained using Auramine Phenol. At the following OD values, 0.02, 0.22, 0.54, 0.75, 1.14, 1.47 and 1.5 which correspond to days of Mtb H37Rv culture that was shown in Figure A, Mtb H37Rv bacilli were stained and visualised under fluorescence microscopy. The images were viewed using 100 x amplification and the scale was at 2 µm.

Appendix I: (*Continued*)

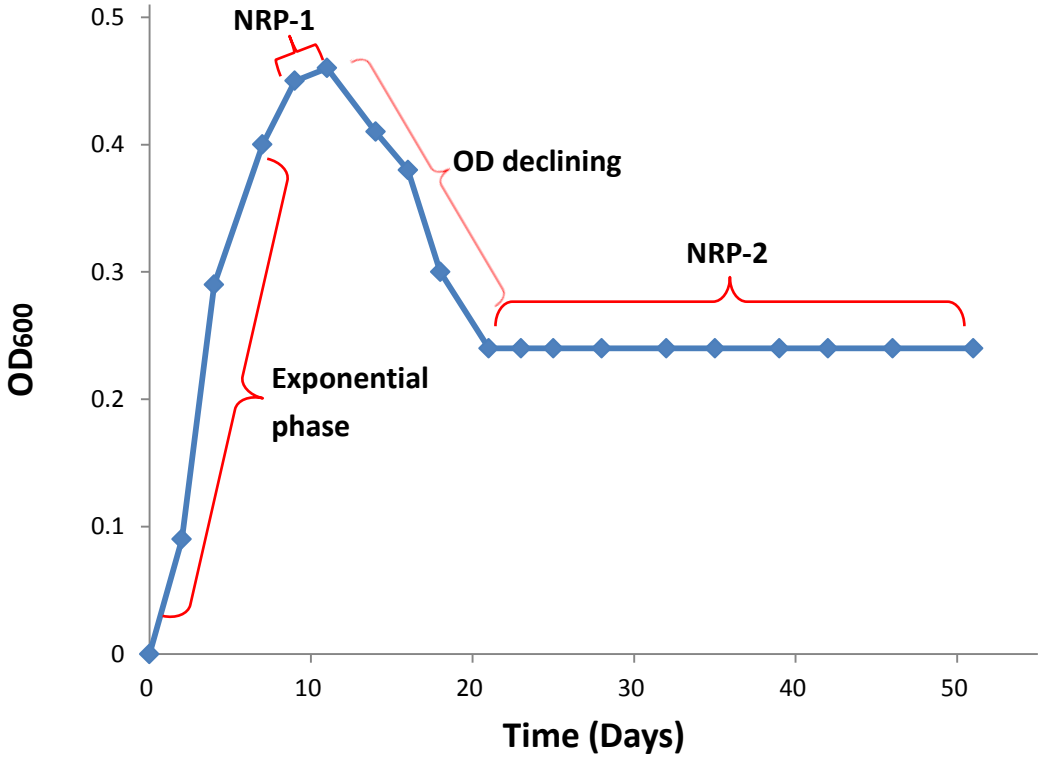

Figure C: Growth curve of anaerobic culture of Mtb (Wayne model)

There was a gradual depletion of oxygen from the Mtb culture, grown anaerobically. Mtb presents a distinct four-stage of growth, an initial exponential growth phase followed by non-replicating persistence (NRP) phase 1 (NRP-1) where a small increase in the optical densities presents. Subsequently, a phase of OD decreasing is shown which may represent the death of some cells that did not stand the stress of oxygen limitation. NRP-2 demonstrates the stabilisation of the numbers of the bacteria.

Appendix I: (*Continued*)

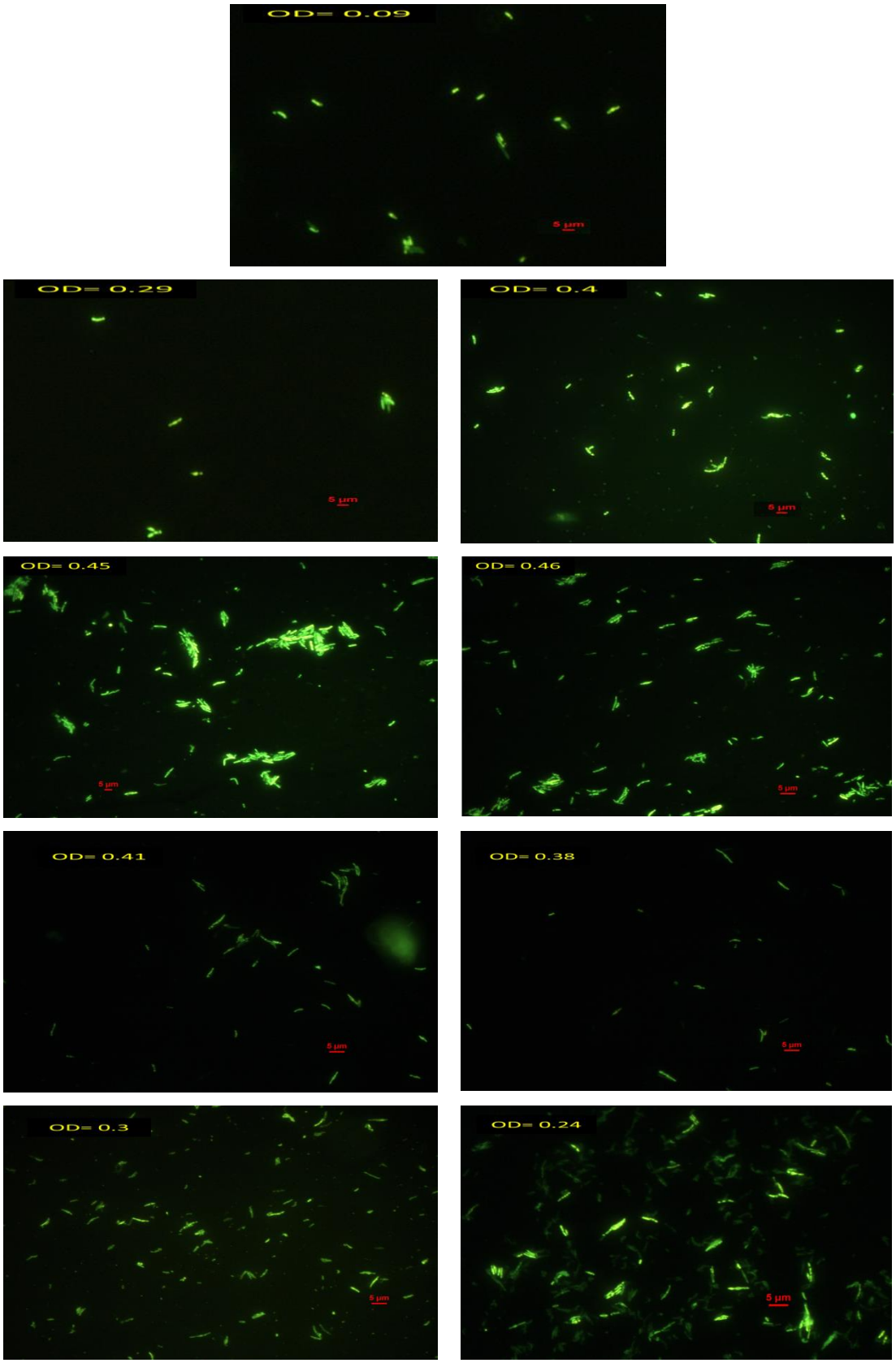

Figure D: Fluorescence microscopy images of Mtb H37Rv bacilli

Mtb H37Rv bacilli grown in anaerobic culture was stained using an Auramine Phenol staining. At the following OD values, 0.09, 0.29, 0.4, 0.45, 0.46, 0.41, 0.38, 0.3 and 0.24 which correspond days of Mtb H37Rv culture that was showed in Figure C, Mtb H37Rv bacilli were stained and visualised under fluorescence microscopy. Mtb H37Rv bacilli show visible increasing in length by OD = 0.45 (starts of NRP-1). The images were viewed using 100 x amplification and the scale was at 5 µm.

Appendix I: (*Continued*)

Auramine phenol staining method of Mtb

Auramine phenol and potassium permanganate (Pro-Lab Diagnostics, USA) were diluted 1 in 10 in dH_2O and stored at room temperature in the dark. Differentiator solution consisted of 1% (v/v) hydrochloric acid and 75% (v/v) absolute ethanol in dH2O.

A Mtb H37Rv culture was transferred to a 15 ml Falcon tube before being centrifuged at 3000 *g* for 10 min. Pelleted materials were resuspended in sterile phosphate buffer saline (PBS). A thin, uniform smear in a glass slide was prepared using 10 µl of suspension before being heat fixed on a heat block placed inside the safety cabinet for 5-10 min. Slides were flooded with the Auramine phenol stain, left to stand for 10 min and then rinsed with dH_2O. Slides were then flooded with differentiator solution (1% hydrochloric acid: ethanol: dH_2O) for 10 min, rinsed a second time with ddH_2O, flooded with 0.1% (w/v) potassium permanganate for 45-60 s and finally rinsed again with ddH_2O before being air dried. Subsequently, slides were mounted in 100µl of sterile PBS, a coverslip was placed on top of the smears and the slides sealed using nail polish. Slides were kept in darkness and examined immediately by fluorescence oil immersion microscopy using a wide blue (> 525 nm) long-pass filter at a magnification of 100x. Images were captured using a camera fitted to the fluorescence microscope.

Appendix II: Metabolomic technique tables

Table 1: LC-MS/MS parameters for metabolites detected in positive ESI mode (protonation, Molecule + H^+) Abbreviations: MW, Molecular Weight; CID, Collision Induced Dissociation; RT, retention time.

Metabolite	MW ($g.mol^{-1}$)	Precursor mass	CID	Product mass	RT (min)
Alanine	89.09	90.1	14	44.1	12.8
B-alanine	89.09	90.3	5	71.8	12.5
Serine	105.09	106	10	60	13.1
Proline	115.13	116	11	70	12.4
Valine	117.15	118	11	55	12.1
Threonine	119.12	120	11	74	13.3
Cysteine	121.16	122	21	59	26.1
(iso)-leucine	131.17	132	11	86	11.4
Asparagine	132.12	133	17	74	13.4
Ornithine	132.19	133	15	70	14.4
Aspartate	133.1	134	15	74	16.4
Glutamine	146.14	147	15	84	13.1
Lysine	146.19	147	16	84	14.4
Glutamate	147.13	148	15	84	16.5
Methionine	149.21	150	10	133	12
Histidine	155.15	156	12	110	13.6
Phenylalanine	165.19	166	28	103	11.6
Arginine	174.2	175	14	60	13.7
Citrulline	175.19	176	12	159	12.9
Carbamoyl-l-aspartate	176.12	177	17	74	21.5
Tyrosine	181.19	182	26	77	13
Tryptophan	204.23	205	16	146	11.9
GSH	307.32	308	19	162	19.7
UMP	324.18	325	12	97	22.3
AMP	347.22	348	21	136	22.8
UDP	404.16	405	19	97	23.1
ADP	427.20	428	31	136	23.5
TTP	482.16	483	25	81	27.3
CTP	483.15	484	21	112	25.1
UTP	484.14	485	30	97	27.7
ATP	507.18	508	37	136	25.5
GTP	523.18	524	37	152	27.8
GSSG	612.63	613	33	231	22
NAD	663.43	664	30	428	16.5
NADH	664.43	666	26	514	27.1
NADP	744.41	744	48	136	22.9
NADPH	745.41	746	16	729	31.9
FAD	785.55	786	24	348	22.9
Acetyl-CoA	809.57	810	28	303	24
Propionyl-CoA	823.60	824	33	317	24.2
Succinyl-CoA	867.60	868	38	361	25

Appendix II: (*Continued*)

Table 2: LC-MS/MS parameter for metabolites detected in negative ESI mode (deprotonation, Molecule – H^+) Abbreviations: MW, Molecular Weight; CID, Collision Induced Dissociation; RT, retention time.

Metabolite	MW ($g.mol^{-1}$)	Precursor mass	CID	Product mass	RT (min)
Lactate	90.08	89	11	43	14
Fumarate	116.07	115	11	71	25.5
Succinate	118.09	117	16	73	21.5
Oxaloacetate	132.07	131	12	87	24.2
Malate	134.09	133	12	115	21.6
Hypoxanthine	136.12	135	16	92	13.4
Methylmalonyl-CoA	867.61	866	20	821	25.0
Carbamyl phosphate	141.02	140	38	79	25.7
2-Oxoglutarate	146.11	145	11	101	26.6
DL-arabinose	150.13	149.1	7	130.6	10.8
Orotate	156.10	155	13	111	15.3
Dihydroorotate	158.11	157	14	113	14.1
PEP	168.04	167	20	79	23.3
DHAP	170.06	169	43	79	29
G-3-P	172.07	171	13	79	21.8
Glucose	180.16	179	18	59	11.7
(iso)-citrate	192.12	191	18	111	23.3

Appendix II: (*Continued*)

Table 3: Regression coefficients R^2, linearity range and limit of detection (LOD) for metabolites targeted in LC-MS/MS method

Metabolite	R^2	Linear Range (uM)	LOD (nM)	Metabolite	R^2	Linear Range (uM)	LOD (nM)
Propionyl-CoA	0.99	0.003 – 108.41	3	**AMP**	0.99	0.025 – 102.86	25
Tryptophan	0.98	0.005 – 174.87	5	**NAD**	0.99	0.026 – 53.83	26
Phenylalanine	0.99	0.006 – 216.2	6	**UMP**	0.98	0.026 – 110.17	26
Glucose	0.99	0.006 – 198.25	6	**GSH**	0.98	0.028 – 116.21	28
Citrulline	0.99	0.006 – 203.86	6	**GSSG**	0.98	0.028 – 58.3	28
Tyrosine	0.99	0.006 – 197.11	6	**2-Oxoglutarate**	0.99	0.029 – 244.45	29
G-3-P	0.99	0.006 – 207.55	6	**Valine**	0.99	0.037 – 304.86	37
(iso)-citrate	0.99	0.006 – 93	6	**UDP**	0.99	0.042 – 88.37	42
Methionine	0.99	0.007 – 239.36	7	**NADP**	0.99	0.047 – 48.04	47
Histidine	0.98	0.007 – 230.19	7	**Succinyl-CoA**	0.98	0.049 – 102.91	49
Dihydroorotate	0.99	0.007 – 56.47	7	**Hypoxanthine**	0.99	0.063 – 262.61	63
Lysine	0.99	0.007 – 244.3	7	**GTP**	0.99	0.066 – 68.26	66
Orotate	0.98	0.007 – 57.2	7	**CTP**	0.99	0.072 – 73.92	72
Glutamate	0.99	0.007 – 242.74	7	**UTP**	0.98	0.072 – 73.77	72
Acetyl-CoA	0.99	0.007 – 220.58	7	**Proline**	0.99	0.074 – 310.21	74
Ornithine	0.99	0.008 – 270.24	8	**Alanine**	0.99	0.096 – 400.87	96
Aspartate	0.99	0.008 – 268.32	8	**NADPH**	0.99	0.096 – 47.9	96
Malate	0.99	0.008 – 266.35	8	**Carbamoyl-l-aspartate**	0.99	0.097 – 202.78	97
Succinate	0.99	0.009 – 302.44	9	**NADH**	0.99	0.107 – 53.67	107
FAD	0.99	0.011 – 45.46	11	**PEP**	0.99	0.206 – 212.53	206
Glutamine	0.99	0.015 – 244.38	15	**TTP**	0.99	0.578 – 74.07	578
(iso)-leucine	0.98	0.016 – 272.27	16	**Fumarate**	0.98	0.615 – 307.69	615
Asparagine	0.98	0.016 – 270.32	16	**Serine**	0.99	0.68 – 339.84	680
ATP	0.98	0.017 – 70.42	17	**DHAP**	0.99	0.84 – 420.17	840
Threonine	0.99	0.018 – 299.82	18	**Cysteine**	0.98	1.179 – 589.73	1179
ADP	0.99	0.020 – 83.6	20	**Oxaloacetate**	0.98	5.4 – 2704.14	5400
Lactate	0.99	0.024 – 793.03	24	**Carbamoyl phosphate**	0.98	7.59 – 3799.39	7590
Arginine	0.99	0.025 – 205.02	25	**Methylmalonyl-CoA**	0.98	4.38 – 68.96	4380

Appendix III: Metabolites calibration curves

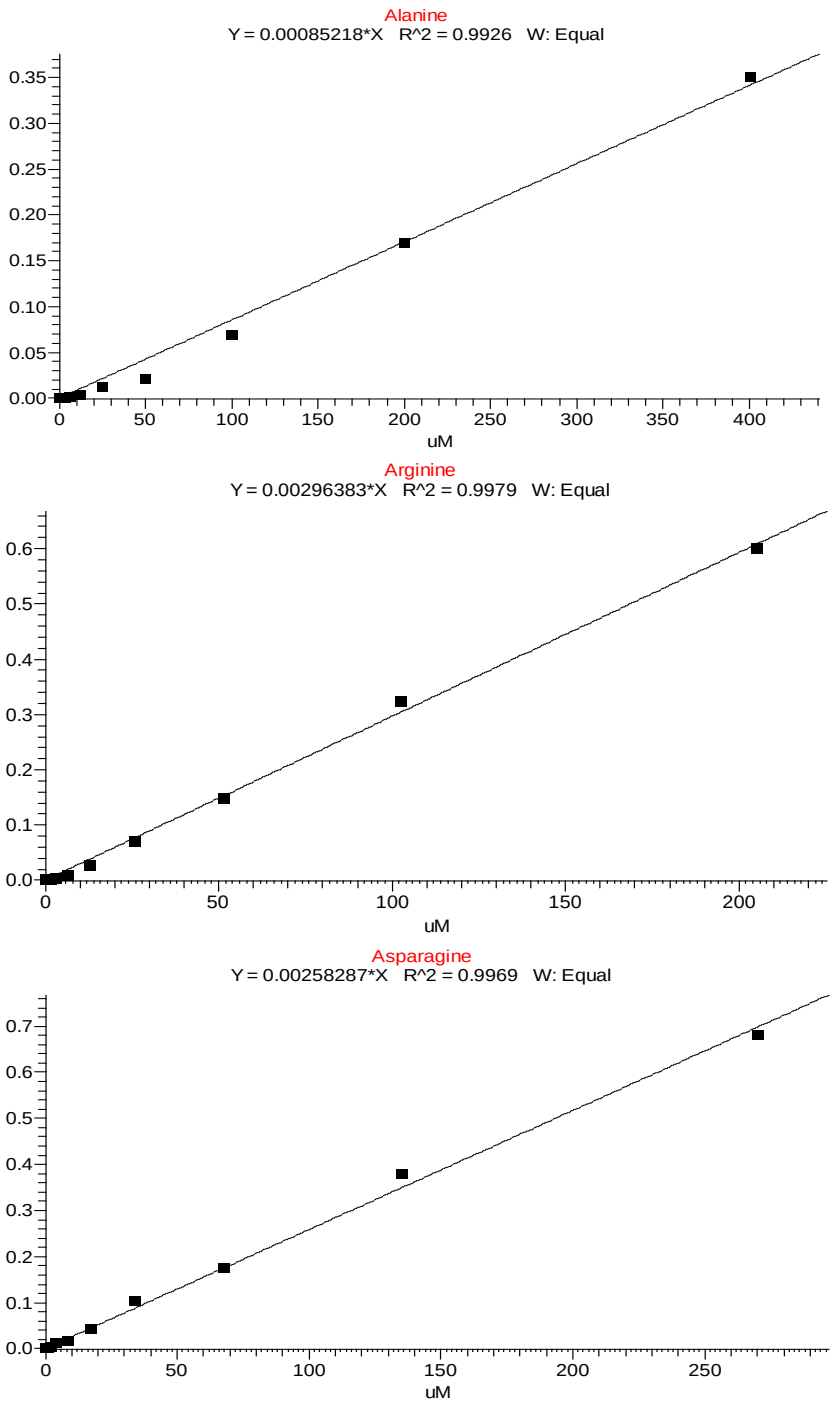

Figure 1. Standard calibration curves for alanine, arginine and asparagine show $R^2 \geq 0.99$.
The line of best fit for each calibration curve was generated using equal weighted linear regression as the mathematical model of best fit. Metabolites concentrations in samples were calculated from the resulting area ratio and the regression equation of the calibration curve.

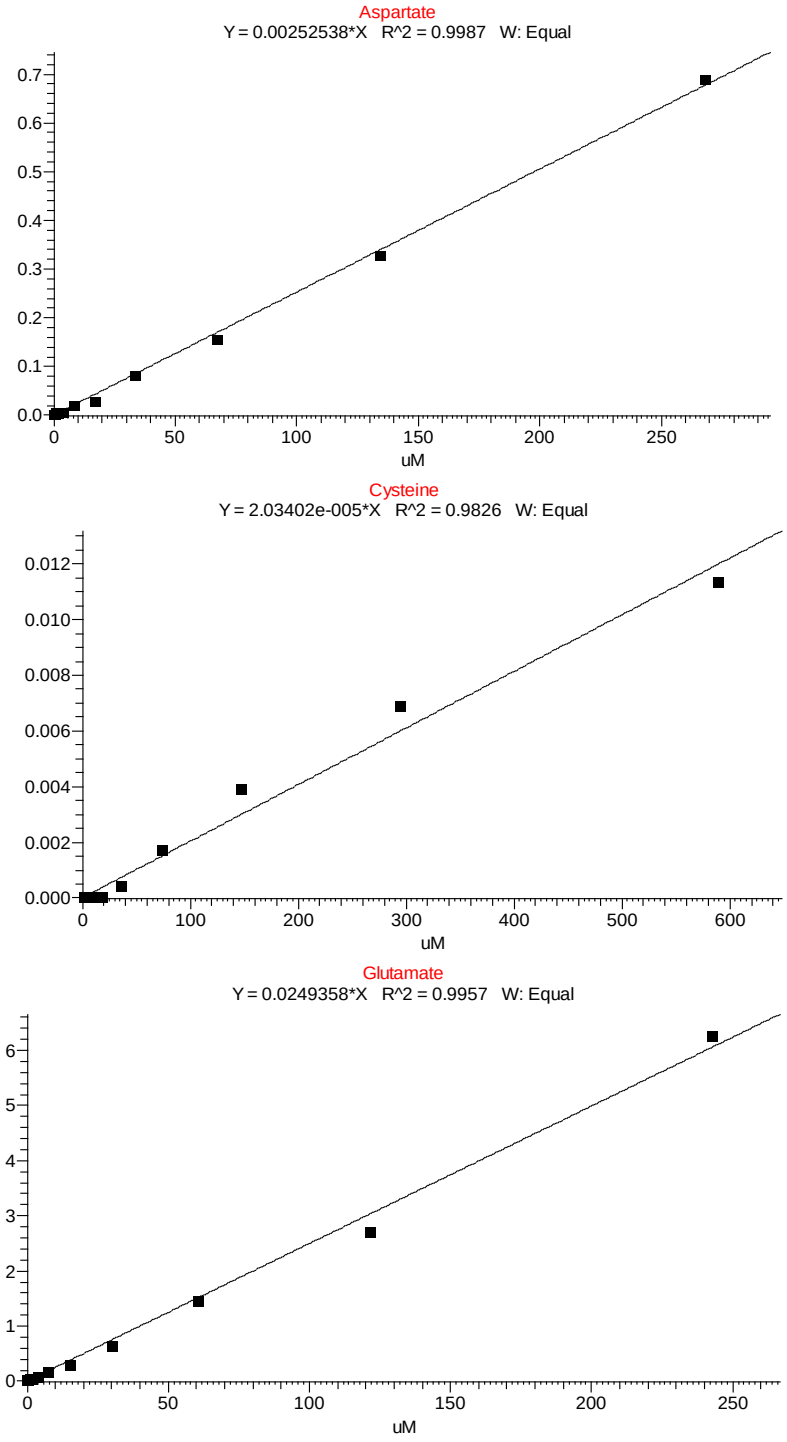

Figure 2. Standard calibration curves for aspartate, cysteine and glutamate show $R^2 \geq 0.98$.
The line of best fit for each calibration curve was generated using equal weighted linear regression as the mathematical model of best fit. Metabolites concentrations in samples were calculated from the resulting area ratio and the regression equation of the calibration curve.

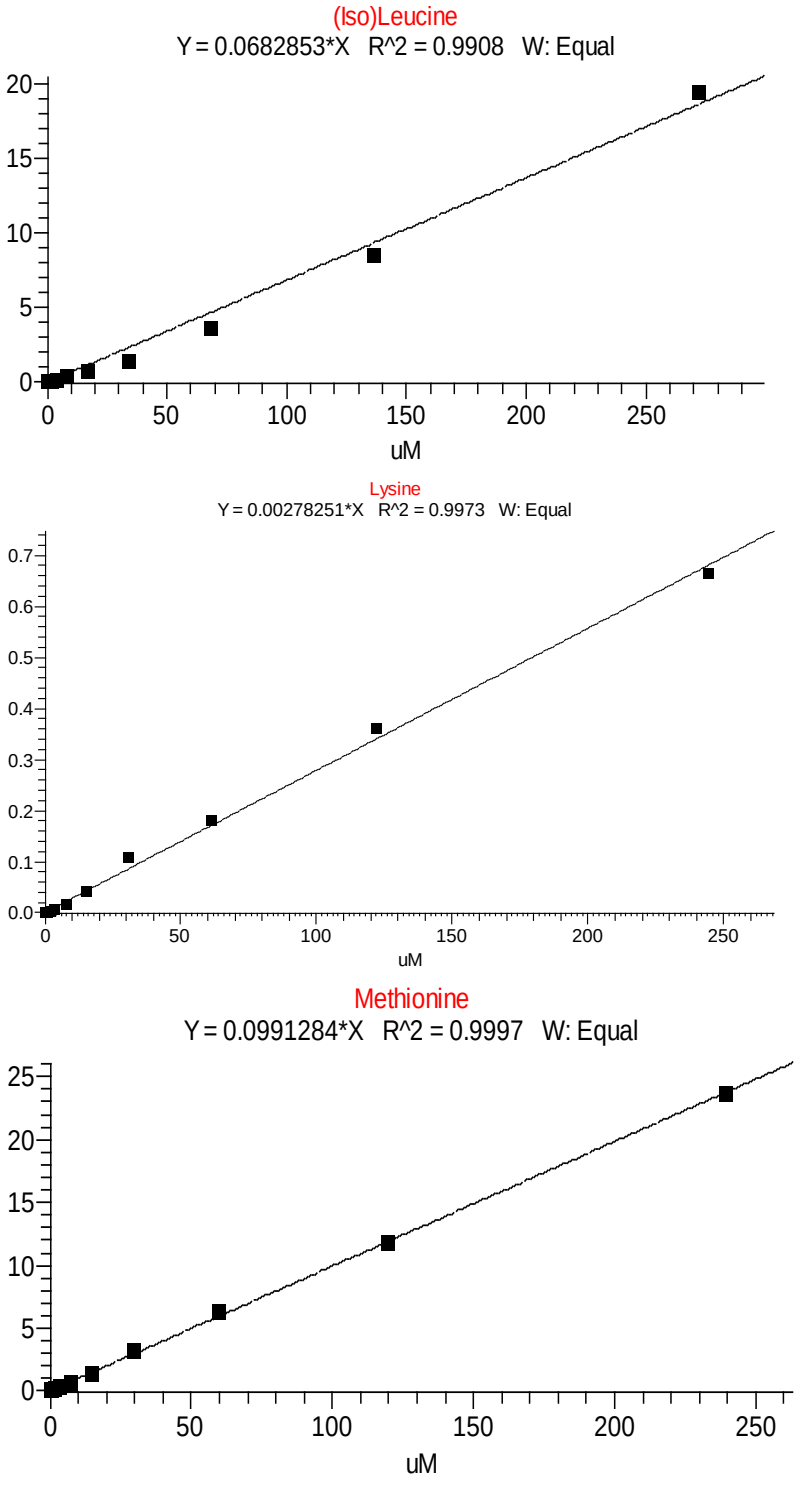

Figure 3. Standard calibration curves for (iso)-leucine, lysine and methionine show $R^2 \geq 0.99$. The line of best fit for each calibration curve was generated using equal weighted linear regression as the mathematical model of best fit. Metabolites concentrations in samples were calculated from the resulting area ratio and the regression equation of the calibration curve.

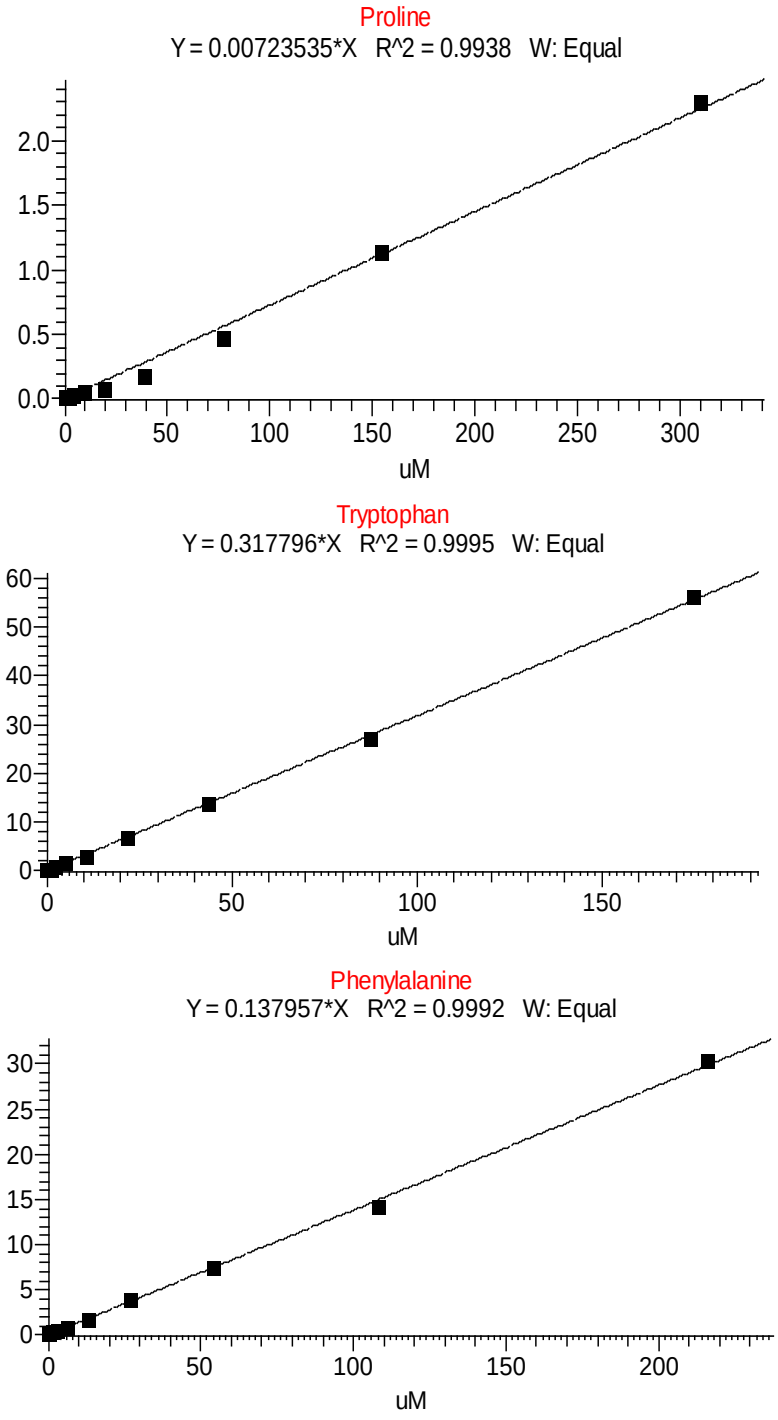

Figure 4. Standard calibration curves for proline, tryptophan and phenyalanine show $R^2 \geq 0.99$. The line of best fit for each calibration curve was generated using equal weighted linear regression as the mathematical model of best fit. Metabolites concentrations in samples were calculated from the resulting area ratio and the regression equation of the calibration curve.

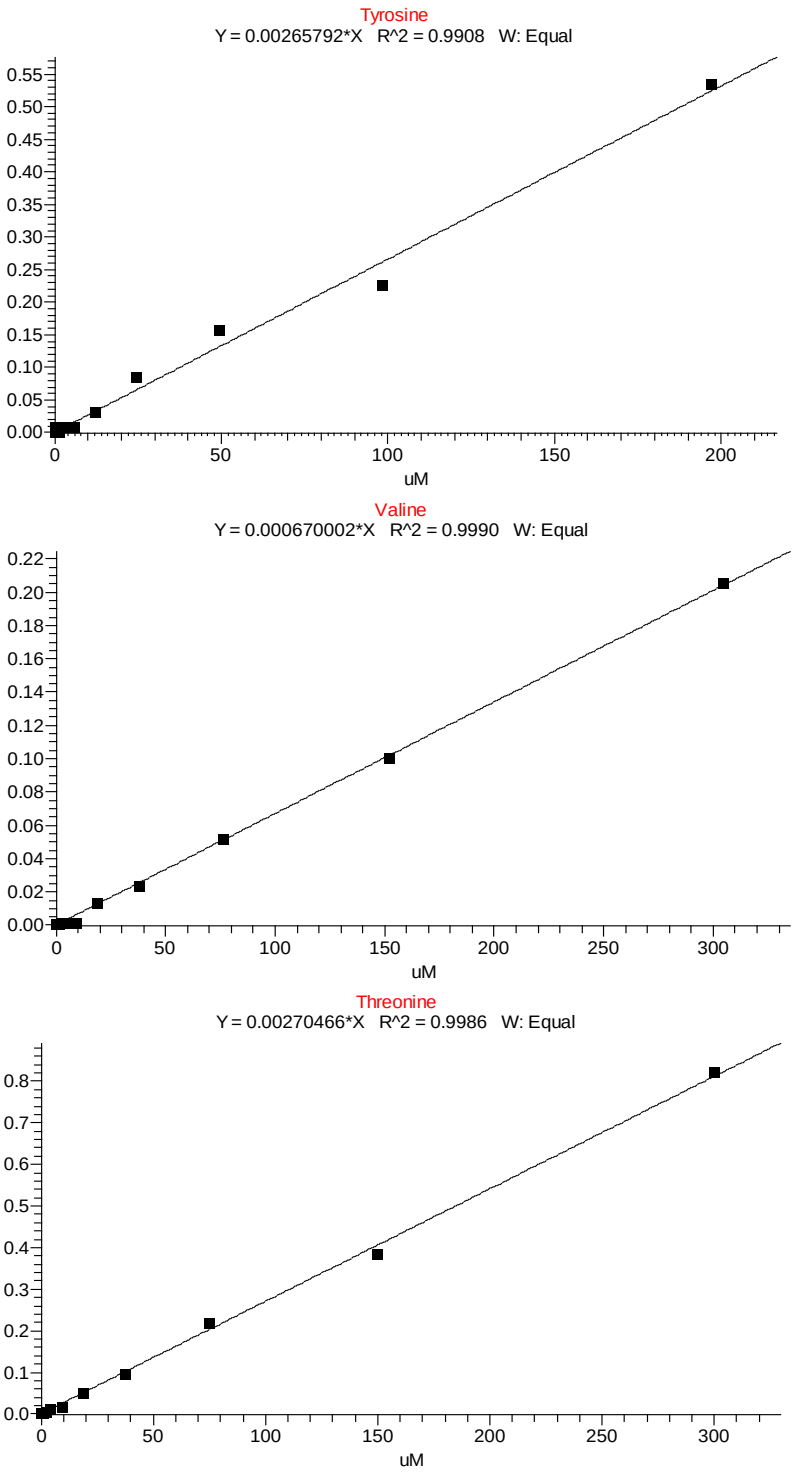

Figure 5. Standard calibration curves for tyrosine, valine and threonine show $R^2 \geq 0.99$.
The line of best fit for each calibration curve was generated using equal weighted linear regression as the mathematical model of best fit. Metabolites concentrations in samples were calculated from the resulting area ratio and the regression equation of the calibration curve.

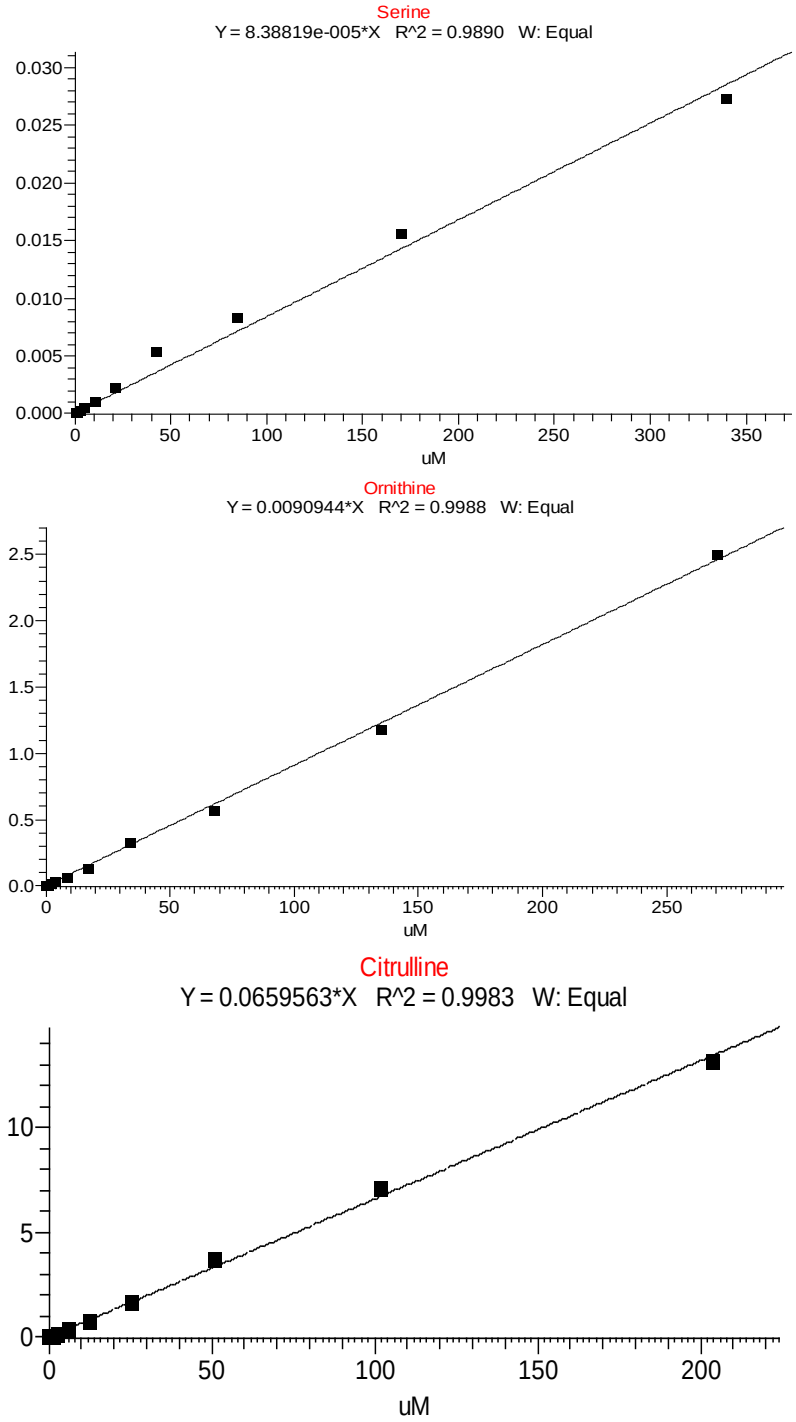

Figure 6. Standard calibration curves for serine, ornithine and citrulline show $R^2 \geq 0.98$.
The line of best fit for each calibration curve was generated using equal weighted linear regression as the mathematical model of best fit. Metabolites concentrations in samples were calculated from the resulting area ratio and the regression equation of the calibration curve.

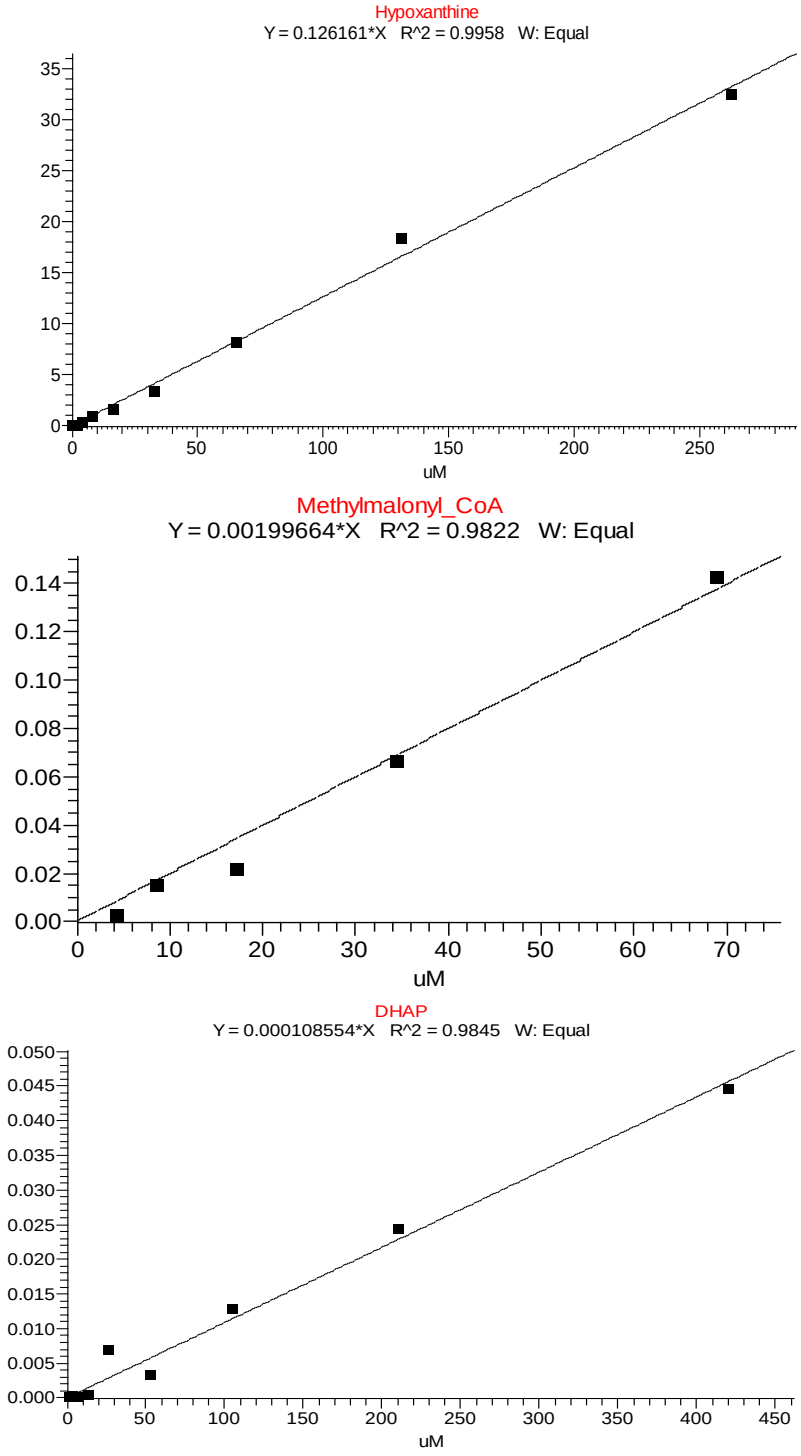

Figure 7. Standard calibration curves for hypoxanthine, methylmalonyl CoA and DHAP show $R^2 \geq 0.98$.

The line of best fit for each calibration curve was generated using equal weighted linear regression as the mathematical model of best fit. Metabolites concentrations in samples were calculated from the resulting area ratio and the regression equation of the calibration curve.

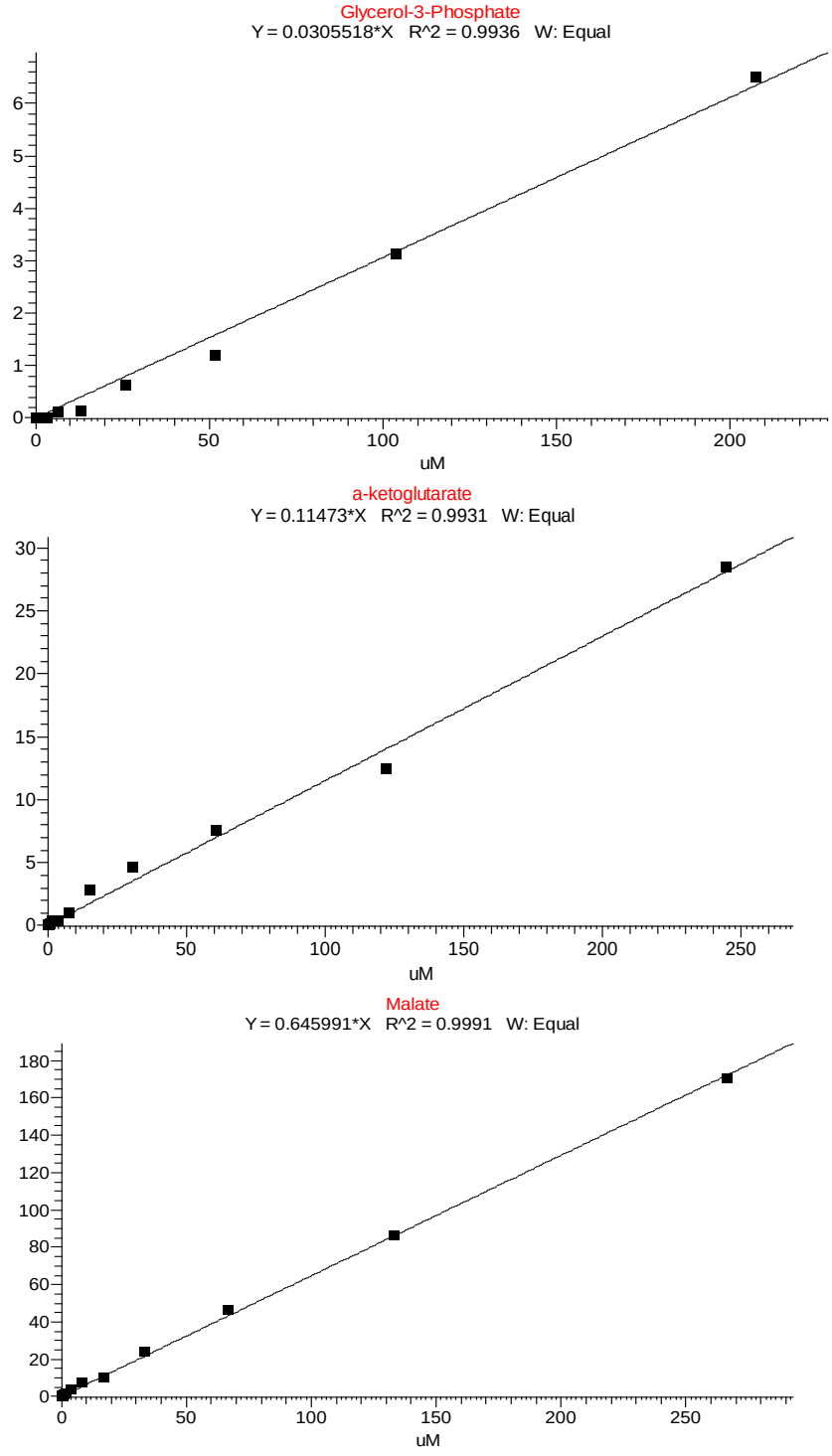

Figure 8. Standard calibration curves for glycerol-3-phosphate, 2-oxoglutarate and malate show $R^2 \geq 0.99$.

The line of best fit for each calibration curve was generated using equal weighted linear regression as the mathematical model of best fit. Metabolites concentrations in samples were calculated from the resulting area ratio and the regression equation of the calibration curve.

.

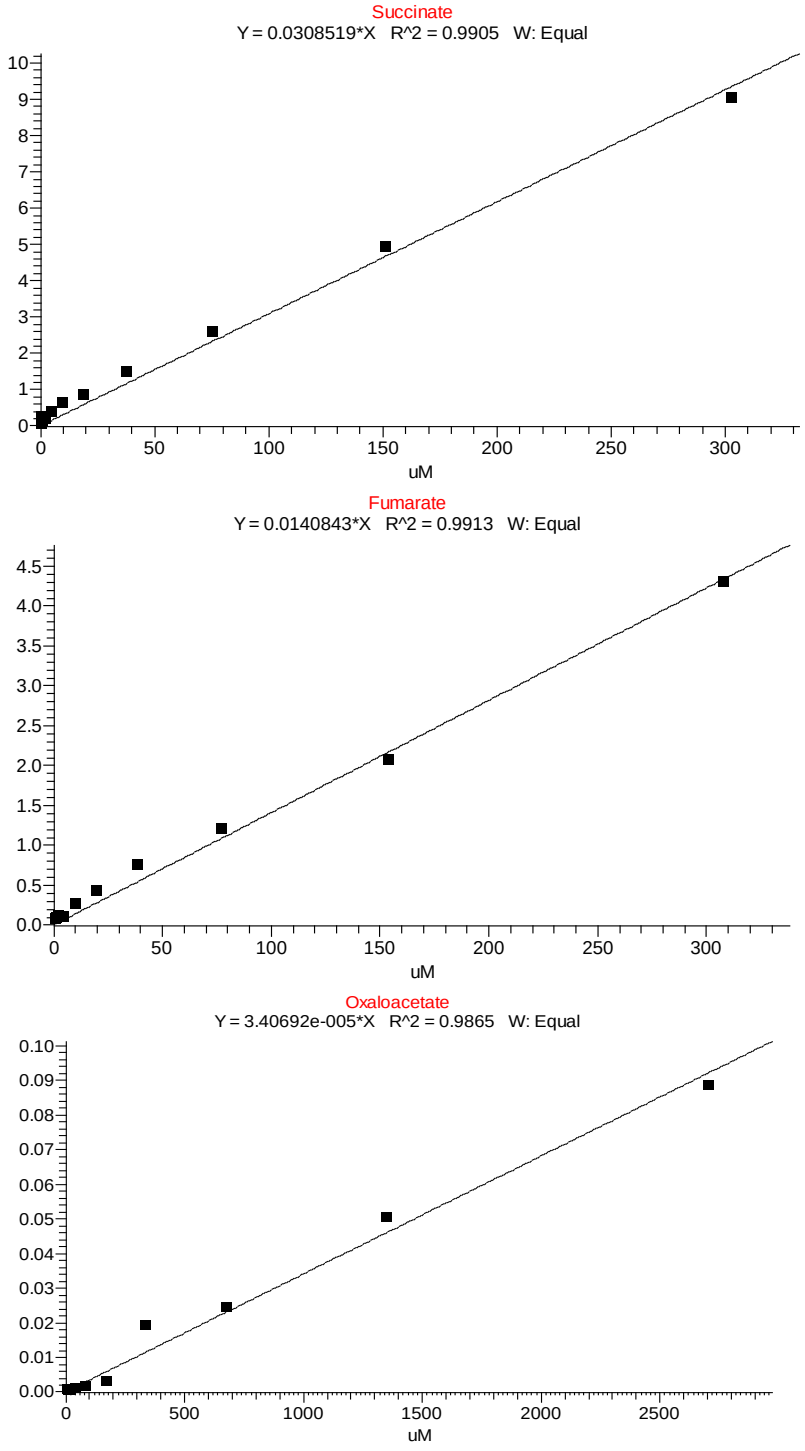

Figure 9. Standard calibration curves for succinate, fumarate and oxaloacetate show $R^2 \geq 0.99$. The line of best fit for each calibration curve was generated using equal weighted linear regression as the mathematical model of best fit. Metabolites concentrations in samples were calculated from the resulting area ratio and the regression equation of the calibration curve.

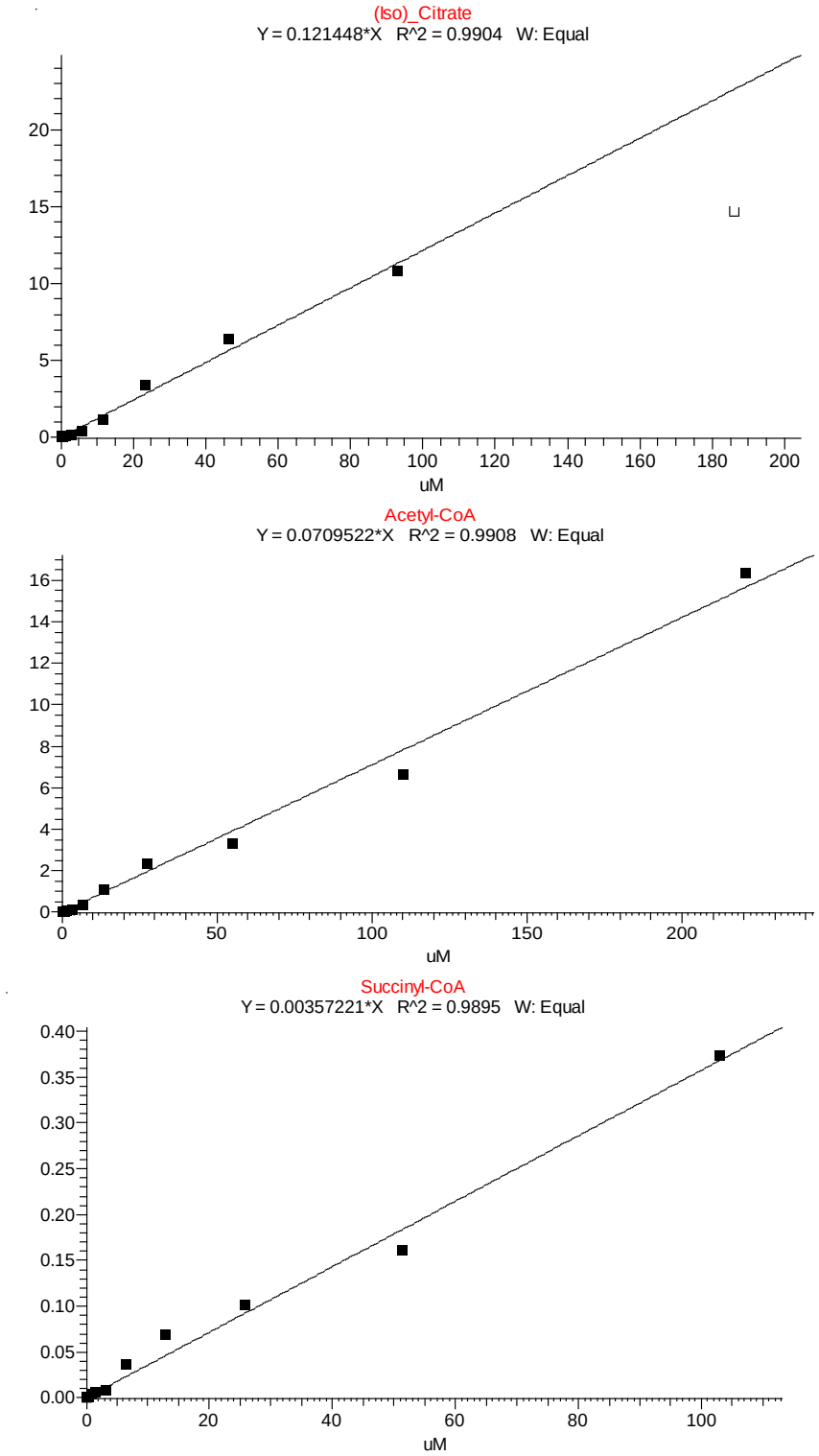

Figure 10. Standard calibration curves for (iso)-citrate, acetyl-CoA and succinyl-CoA show R^2 ≥0.99.

The line of best fit for each calibration curve was generated using equal weighted linear regression as the mathematical model of best fit. Metabolites concentrations in samples were calculated from the resulting area ratio and the regression equation of the calibration curve.

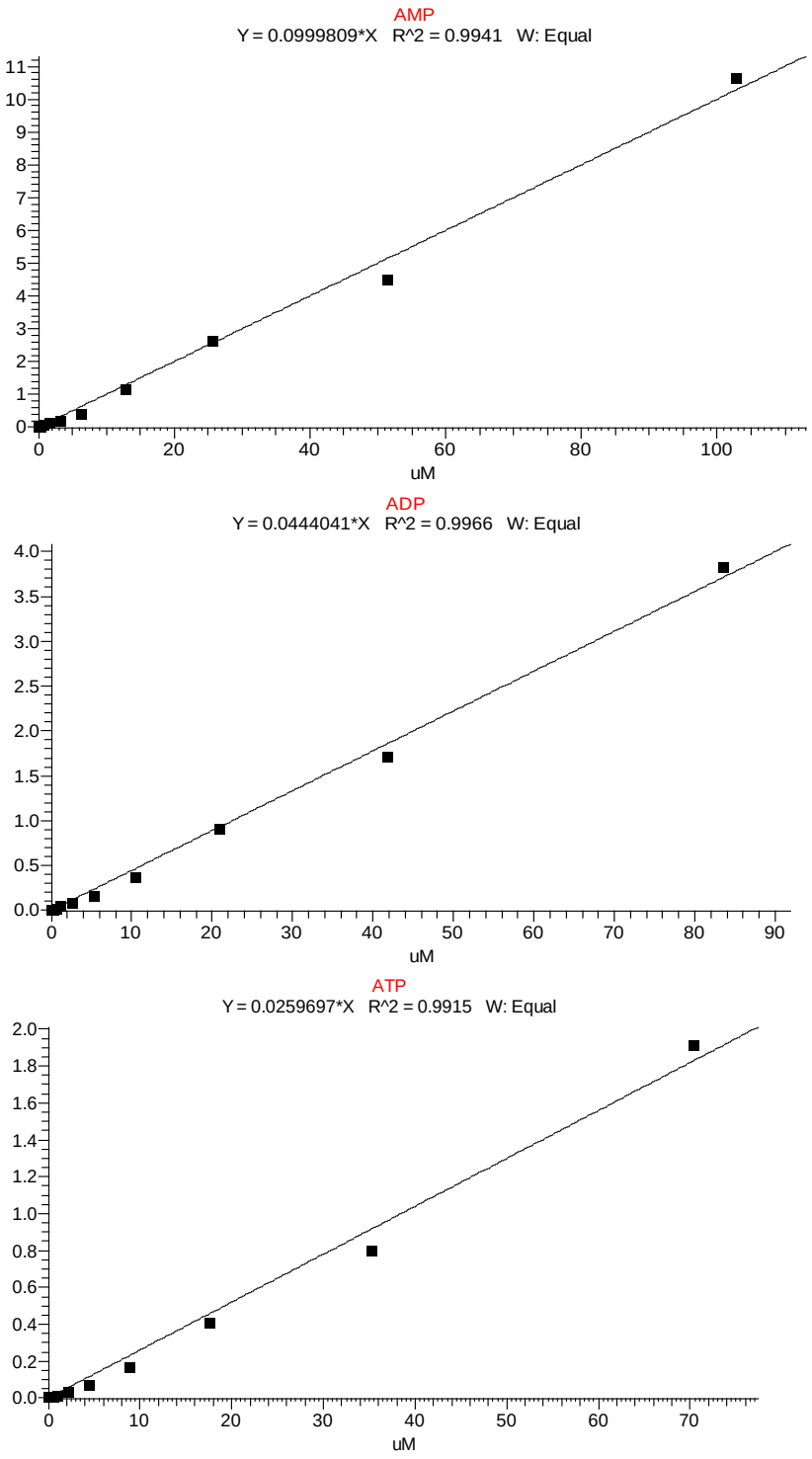

Figure 11. Standard calibration curves for AMP, ADP and ATP show $R^2 \geq 0.99$.
The line of best fit for each calibration curve was generated using equal weighted linear regression as the mathematical model of best fit. Metabolites concentrations in samples were calculated from the resulting area ratio and the regression equation of the calibration curve.

.

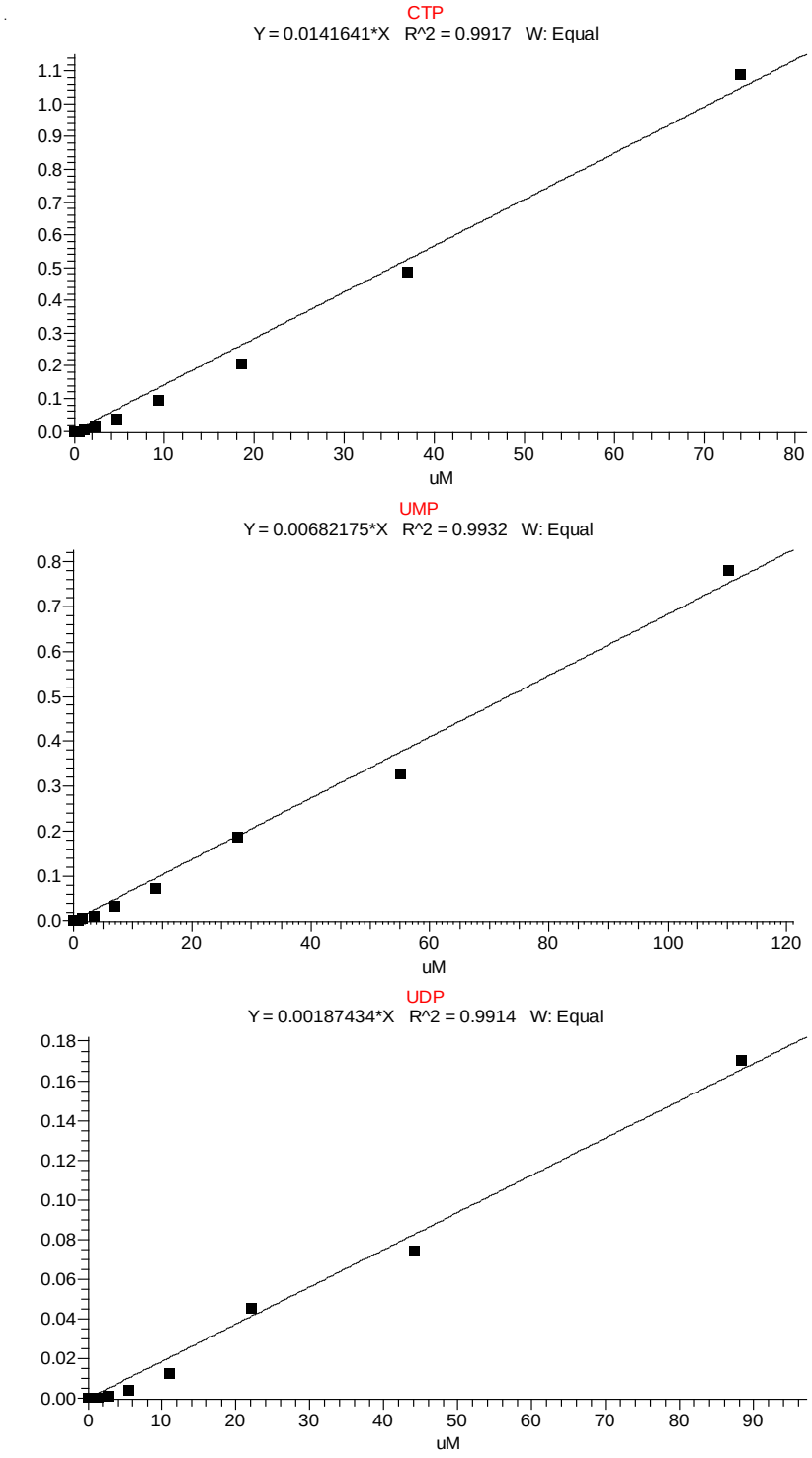

Figure 12. Standard calibration curves for CTP, UMP and UDP show $R^2 \geq 0.99$.
The line of best fit for each calibration curve was generated using equal weighted linear regression as the mathematical model of best fit. Metabolites concentrations in samples were calculated from the resulting area ratio and the regression equation of the calibration curve.

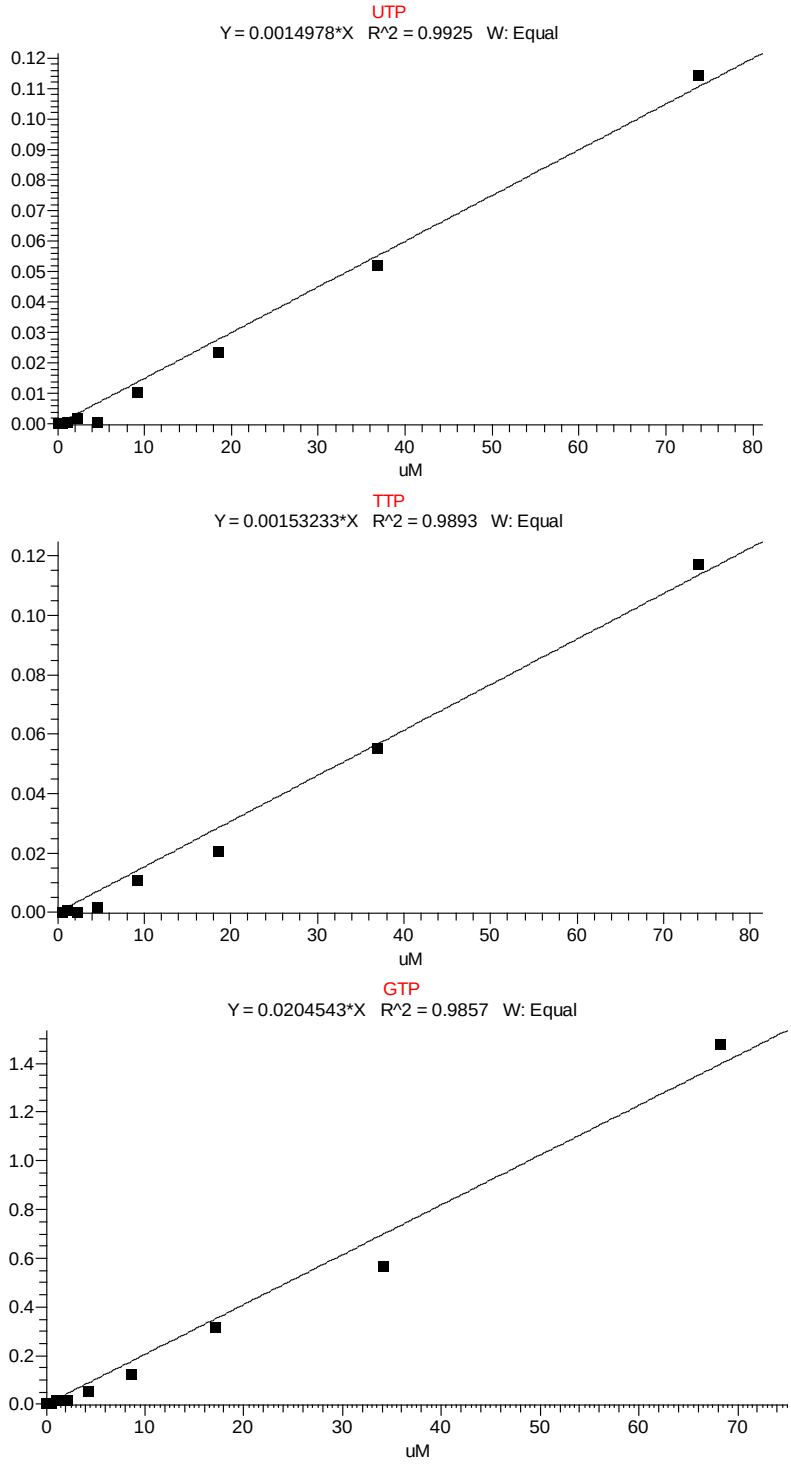

Figure 13. Standard calibration curves for UTP, TTP and GTP show $R^2 \geq 0.98$.
The line of best fit for each calibration curve was generated using equal weighted linear regression as the mathematical model of best fit. Metabolites concentrations in samples were calculated from the resulting area ratio and the regression equation of the calibration curve.

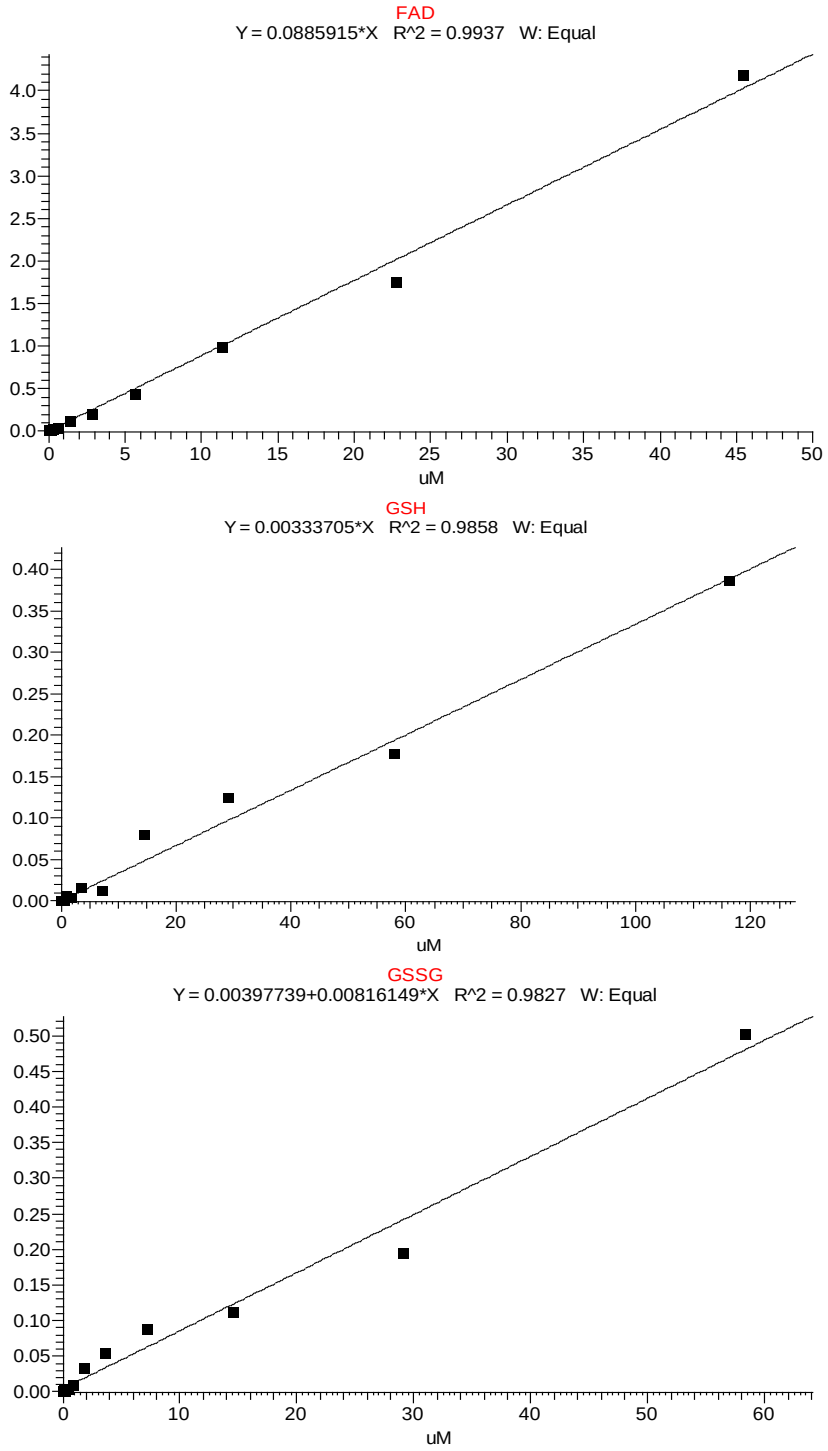

Figure 14. Standard calibration curves for FAD, GSH and GSSG show $R^2 \geq 0.98$.
The line of best fit for each calibration curve was generated using equal weighted linear regression as the mathematical model of best fit. Metabolites concentrations in samples were calculated from the resulting area ratio and the regression equation of the calibration curve.

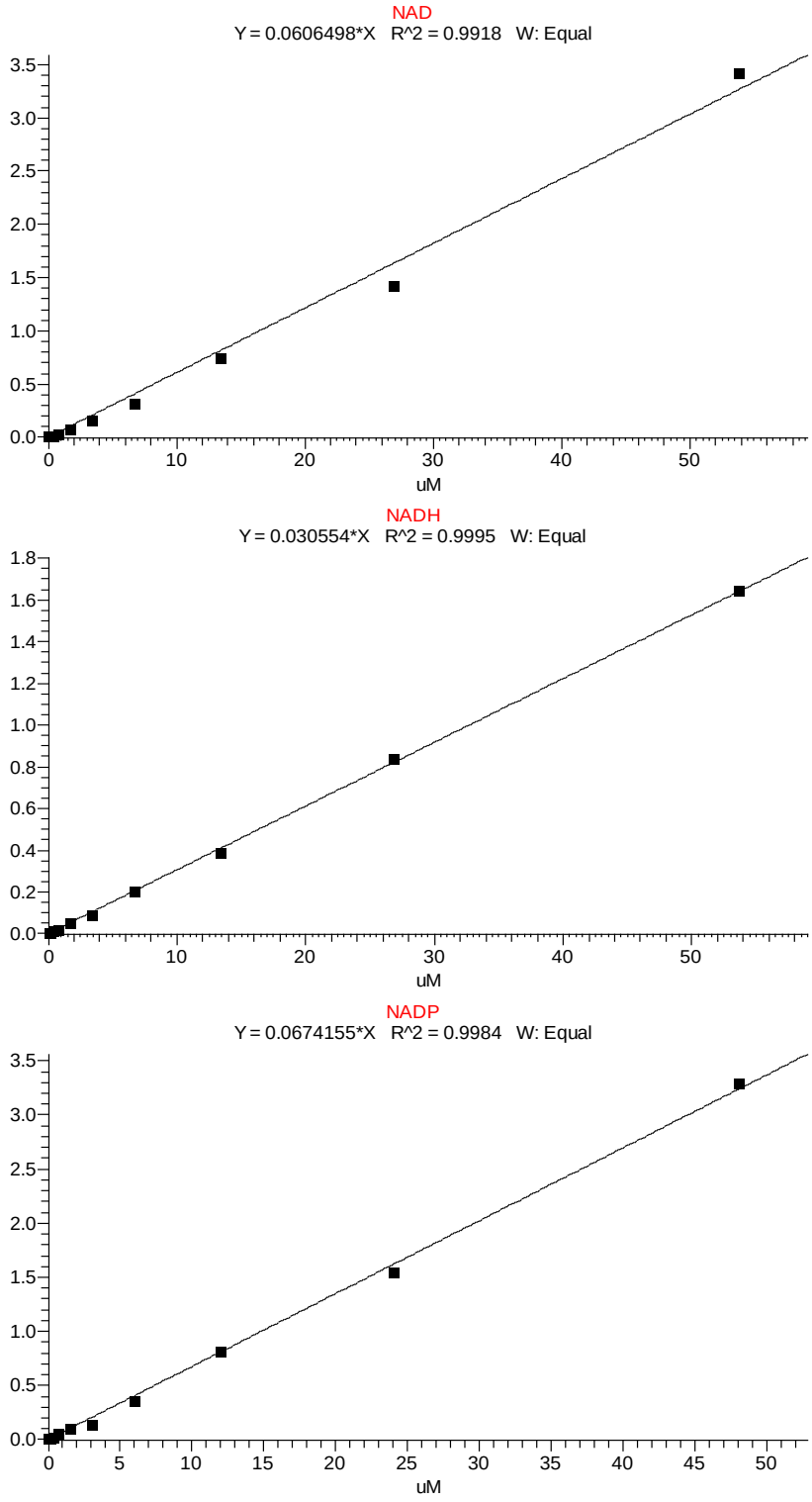

Figure 15. Standard calibration curves for NAD, NADH and NADP show $R^2 \geq 0.99$.
The line of best fit for each calibration curve was generated using equal weighted linear regression as the mathematical model of best fit. Metabolites concentrations in samples were calculated from the resulting area ratio and the regression equation of the calibration curve.

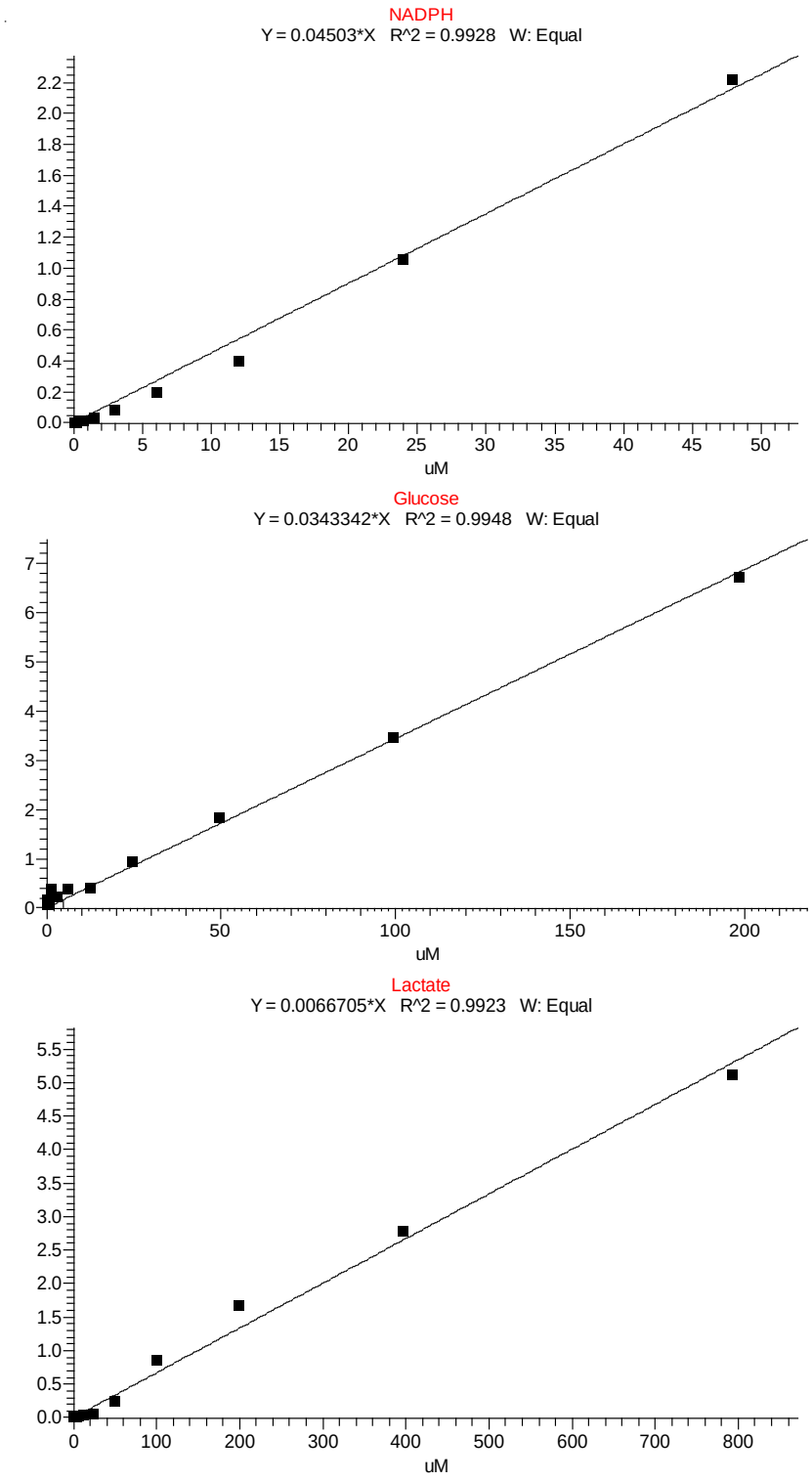

Figure 16. Standard calibration curves for NADPH, glucose and lactate show $R^2 \geq 0.99$.
The line of best fit for each calibration curve was generated using equal weighted linear regression as the mathematical model of best fit. Metabolites concentrations in samples were calculated from the resulting area ratio and the regression equation of the calibration curve.

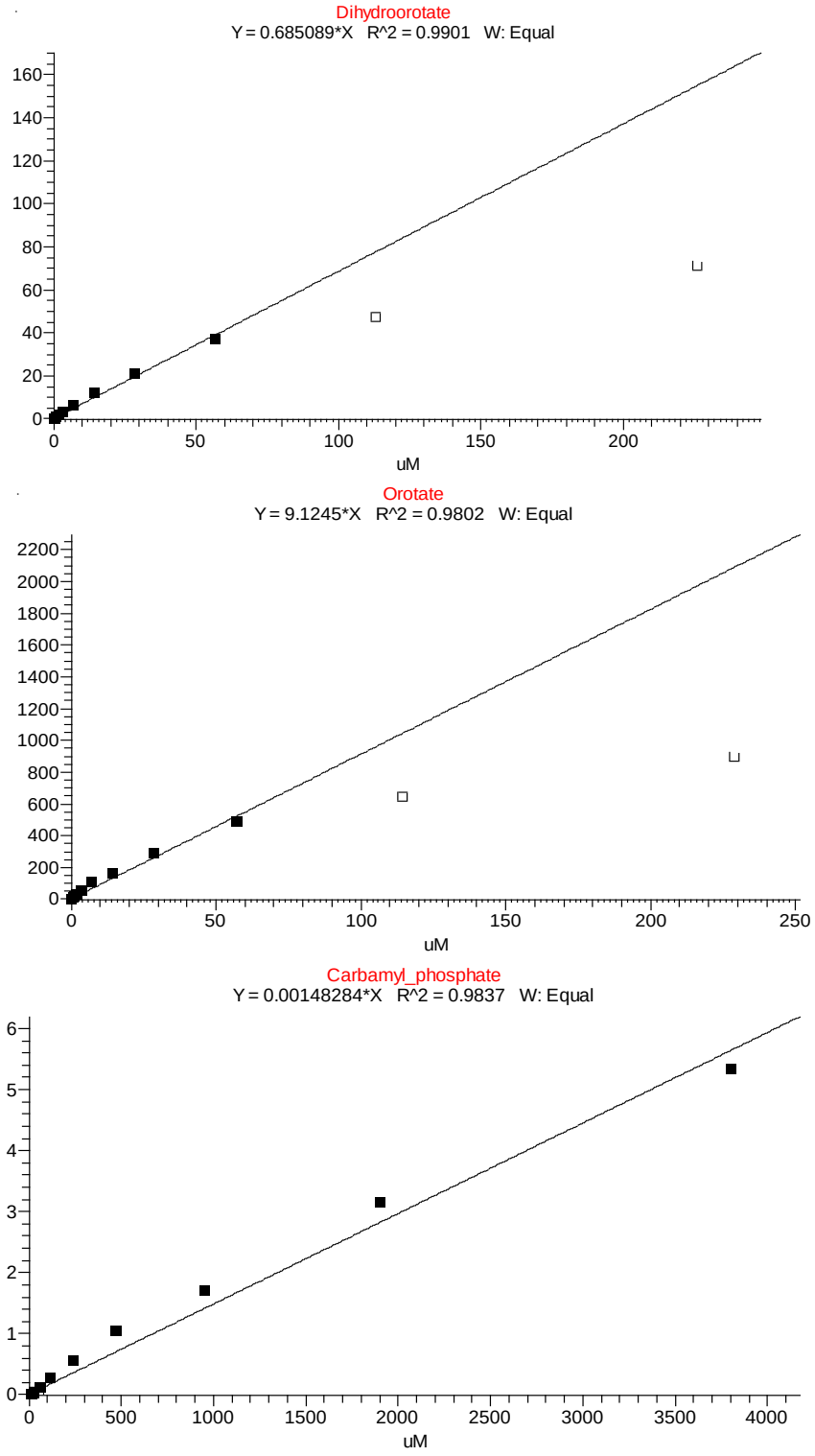

Figure 17. Standard calibration curves for dihydroorotate, orotate and carbamoyl-phosphate show $R^2 \geq 0.98$.

The line of best fit for each calibration curve was generated using equal weighted linear regression as the mathematical model of best fit. Metabolites concentrations in samples were calculated from the resulting area ratio and the regression equation of the calibration curve.

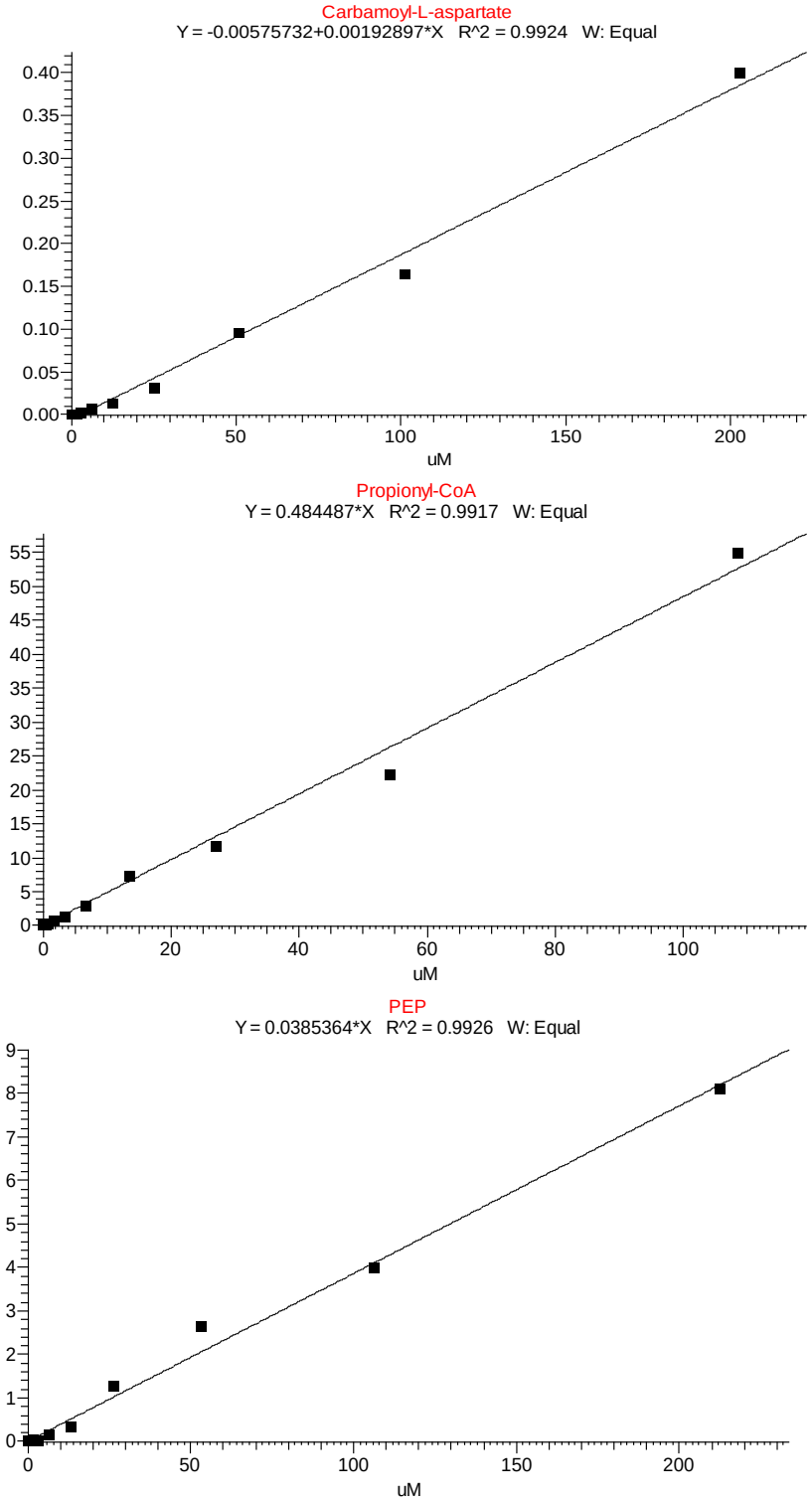

Figure 18. Standard calibration curves for carbamoyl-l-aspartate, propionyl-CoA and PEP show $R^2 \geq 0.99$.

The line of best fit for each calibration curve was generated using equal weighted linear regression as the mathematical model of best fit. Metabolites concentrations in samples were calculated from the resulting area ratio and the regression equation of the calibration curve.

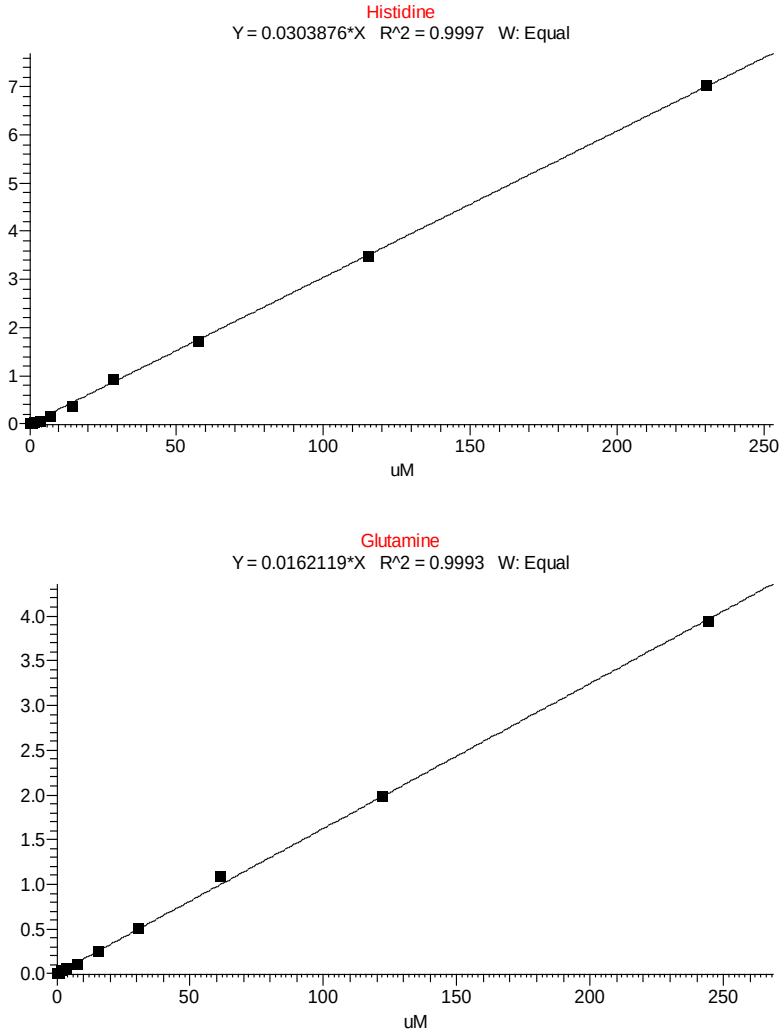

Figure 77. Standard calibration curves for histidine and glutamine show $R^2 \geq 0.99$.
The line of best fit for each calibration curve was generated using equal weighted linear regression as the mathematical model of best fit. Metabolites concentrations in samples were calculated from the resulting area ratio and the regression equation of the calibration curve.

References

1. **TB-Alliance.** 2012. Global Alliance for TB Drug Development-TB Alliance Pipeline. http://www.tballiance.org/downloads/Pipeline/TBA-Pipeline-May-2012.pdf.
2. **Griffin JE, Gawronski JD, DeJesus MA, Ioerger TR, Akerley BJ, Sassetti CM.** 2011. High-Resolution Phenotypic Profiling Defines Genes Essential for Mycobacterial Growth and Cholesterol Catabolism. Plos Pathogens **7**.
3. **WHO.** 2011. Global tuberculosis control: WHO report 2011. http://www.who.int/tb/publications/global_report/2011/en/index.html.
4. **Hurdle JG, O'Neill AJ, Chopra I, Lee RE.** 2011. Targeting bacterial membrane function: an underexploited mechanism for treating persistent infections. Nature Reviews Microbiology **9:**62-75.
5. **WHO.** 2010. Multidrug and extensively drug-resistant TB (M/XDR-TB): 2010 global report on surveillance and response. http://whqlibdoc.who.int/publications/2010/9789241599191_eng.pdf.
6. **Sharma SK, Mohan A.** 2006. Multidrug-resistant tuberculosis - A menace that threatens to destabilize tuberculosis control. Chest **130:**261-272.
7. **Ottenhoff THM, Kaufmann SHE.** 2012. Vaccines against Tuberculosis: Where Are We and Where Do We Need to Go? Plos Pathogens **8**.
8. **Kaufmann SHE.** 2011. Fact and fiction in tuberculosis vaccine research: 10 years later. Lancet Infectious Diseases **11:**633-640.
9. **Chatterjee D, Khoo KH.** 1998. Mycobacterial lipoarabinomannan: an extraordinary lipoheteroglycan with profound physiological effects. Glycobiology **8:**113-120.
10. **Niederweis M, Danilchanka O, Huff J, Hoffmann C, Engelhardt H.** 2010. Mycobacterial outer membranes: in search of proteins. Trends in Microbiology **18:**109-116.
11. **Glickman MS, Jacobs WR.** 2001. Microbial pathogenesis of Mycobacterium tuberculosis: Dawn of a discipline. Cell **104:**477-485.
12. **Vergne I, Chua J, Singh SB, Deretic V.** 2004. Cell biology of Mycobacterium tuberculosis phagosome. Annual Review of Cell and Developmental Biology **20:**367-394.
13. **Ehlers S.** 2009. Lazy, Dynamic or Minimally Recrudescent? On the Elusive Nature and Location of the Mycobacterium Responsible for Latent Tuberculosis. Infection **37:**87-95.
14. **Barry CE, Boshoff HI, Dartois V, Dick T, Ehrt S, Flynn J, Schnappinger D, Wilkinson RJ, Young D.** 2009. The spectrum of latent tuberculosis: rethinking the biology and intervention strategies. Nature Reviews Microbiology **7:**845-855.
15. **Kaplan G, Post FA, Moreira AL, Wainwright H, Kreiswirth BN, Tanverdi M, Mathema B, Ramaswamy SV, Walther G, Steyn LM, Barry CE, III, Bekker L-G.** 2003. Mycobacterium tuberculosis growth at the cavity surface: A microenvironment with failed immunity. Infection and Immunity **71:**7099-7108.
16. **Gengenbacher M, Kaufmann SHE.** 2012. Mycobacterium tuberculosis: success through dormancy. Fems Microbiology Reviews **36:**514-532.
17. **Ulrichs T, Kaufmann SHE.** 2006. New insights into the function of granulomas in human tuberculosis. J. Pathol. **208:**261-269.
18. **Gupta A, Kaul A, Tsolaki AG, Kishore U, Bhakta S.** 2012. Mycobacterium tuberculosis: Immune evasion, latency and reactivation. Immunobiology **217:**363-374.
19. **Tufariello JM, Chan J, Flynn JL.** 2003. Latent tuberculosis: mechanisms of host and bacillus that contribute to persistent infection. Lancet Infectious Diseases **3:**578-590.

20. **Boshoff HIM, Barry CE.** 2005. Tuberculosis - Metabolism and respiration in the absence of growth. Nature Reviews Microbiology **3:**70-80.
21. **Peyron P, Vaubourgeix J, Poquet Y, Levillain F, Botanch C, Bardou F, Daffe M, Emile J-F, Marchou B, Cardona P-J, de Chastellier C, Altare F.** 2008. Foamy Macrophages from Tuberculous Patients' Granulomas Constitute a Nutrient-Rich Reservoir for M-tuberculosis Persistence. Plos Pathogens **4**.
22. **Via LE, Lin L, Ray SM, Carrillo J, Allen SS, Eum SY, Taylor K, Klein E, Manjunatha U, Gonzales J, Lee EG, Park SK, Raleigh JA, Cho SN, McMurray DN, Flynn JL, Barry CE.** 2008. Tuberculous granulomas are hypoxic in guinea pigs, rabbits, and nonhuman primates. Infection and Immunity **76:**2333-2340.
23. **Puissegur MP, Botanch C, Duteyrat JL, Delsol G, Caratero C, Altare F.** 2004. An in vitro dual model of mycobacterial granulomas to investigate the molecular interactions between mycobacteria and human host cells. Cellular Microbiology **6:**423-433.
24. **Zhang Y, Yew WW, Barer MR.** 2012. Targeting Persisters for Tuberculosis Control. Antimicrobial Agents and Chemotherapy **56:**2223-2230.
25. **Gomez JE, McKinney JD.** 2004. M-tuberculosis persistence, latency, and drug tolerance. Tuberculosis **84:**29-44.
26. **Barer MR.** 1997. Viable but non-culturable and dormant bacteria: Time to resolve an oxymoron and a misnomer? Journal of Medical Microbiology **46:**629-631.
27. **Leung AN.** 1999. Pulmonary tuberculosis: The essentials. Radiology **210:**307-322.
28. **Zumla A, Atun R, Maeurer M, Mwaba P, Ma Z, O'Grady J, Bates M, Dheda K, Hoelscher M, Grange J.** 2011. Viewpoint: Scientific dogmas, paradoxes and mysteries of latent Mycobacterium tuberculosis infection. Tropical Medicine & International Health **16:**79-83.
29. **Yang Z, Rosenthal M, Rosenberg NA, Talarico S, Zhang L, Marrs C, Thomsen VO, Lillebaek T, Andersen AB.** 2011. How dormant is Mycobacterium tuberculosis during latency? A study integrating genomics and molecular epidemiology. Infection Genetics and Evolution **11:**1164-1167.
30. **Henderson B, Lund PA, Coates ARM.** 2010. Multiple moonlighting functions of mycobacterial molecular chaperones. Tuberculosis **90:**119-124.
31. **Gill WP, Harik NS, Whiddon MR, Liao RP, Mittler JE, Sherman DR.** 2009. A replication clock for Mycobacterium tuberculosis. Nature Medicine **15:**211-214.
32. **Wayne LG.** 1994. DORMANCY OF MYCOBACTERIUM-TUBERCULOSIS AND LATENCY OF DISEASE. European Journal of Clinical Microbiology & Infectious Diseases **13:**908-914.
33. **Wayne LG, Hayes LG.** 1996. An in vitro model for sequential study of shiftdown of Mycobacterium tuberculosis through two stages of nonreplicating persistence. Infection and Immunity **64:**2062-2069.
34. **Wayne LG, Sohaskey CD.** 2001. Nonreplicating persistence of Mycobacterium tuberculosis. Annual Review of Microbiology **55:**139-163.
35. **Zhang Y.** 2012. Metronidazole validates drugs targeting hypoxic bacteria for improved treatment of tuberculosis. Proceedings of the National Academy of Sciences of the United States of America **109**.
36. **McCune RM, Tompsett R, McDermott W.** 1956. THE FATE OF MYCOBACTERIUM TUBERCULOSIS IN MOUSE TISSUES AS DETERMINED BY THE MICROBIAL ENUMERATION TECHNIQUE .2. THE CONVERSION OF TUBERCULOUS INFECTION TO THE LATENT STATE BY THE ADMINISTRATION OF PYRAZINAMIDE AND A COMPANION DRUG. Journal of Experimental Medicine **104:**763-802.
37. **McCune RM, Tompsett R.** 1956. FATE OF MYCOBACTERIUM TUBERCULOSIS IN MOUSE TISSUES AS DETERMINED BY THE MICROBIAL ENUMERATION TECHNIQUE .1.

THE PERSISTENCE OF DRUG-SUSCEPTIBLE TUBERCLE BACILLI IN THE TISSUES DESPITE PROLONGED ANTIMICROBIAL THERAPY. Journal of Experimental Medicine **104:**737-&.

38. **Parrish NM, Dick JD, Bishai WR.** 1998. Mechanisms of latency in Mycobacterium tuberculosis. Trends in Microbiology **6:**107-112.
39. **Loebel RO, Shorr E, Richardson HB.** 1933. The influence of foodstuffs upon the respiratory metabolism and growth of human tubercle bacilli. Journal of Bacteriology **26:**139-166.
40. **Gengenbacher M, Rao SPS, Pethe K, Dick T.** 2010. Nutrient-starved, non-replicating Mycobacterium tuberculosis requires respiration, ATP synthase and isocitrate lyase for maintenance of ATP homeostasis and viability. Microbiology-Sgm **156:**81-87.
41. **Rifat D, Bishai WR, Karakousis PC.** 2009. Phosphate Depletion: A Novel Trigger for Mycobacterium tuberculosis Persistence. Journal of Infectious Diseases **200:**1126-1135.
42. **Hampshire T, Soneji S, Bacon J, James BW, Hinds J, Laing K, Stabler RA, Marsh PD, Butcher PD.** 2004. Stationary phase gene expression of Mycobacterium tuberculosis following a progressive nutrient depletion: a model for persistent organisms? Tuberculosis **84:**228-238.
43. **Voskuil MI, Visconti KC, Schoolnik GK.** 2004. Mycobacterium tuberculosis gene expression during adaptation to stationary phase and low-oxygen dormancy. Tuberculosis **84:**218-227.
44. **Deb C, Lee CM, Dubey VS, Daniel J, Abomoelak B, Sirakova TD, Pawar S, Rogers L, Kolattukudy PE.** 2009. A Novel In Vitro Multiple-Stress Dormancy Model for Mycobacterium tuberculosis Generates a Lipid-Loaded, Drug-Tolerant, Dormant Pathogen. Plos One **4**.
45. **Zhang Y.** 2007. Advances in the treatment of tuberculosis. Clinical Pharmacology & Therapeutics **82:**595-600.
46. **Neyrolles O, Hernandez-Pando R, Pietri-Rouxel F, Fornes P, Tailleux L, Barrios Payan JA, Pivert E, Bordat Y, Aguilar D, Prevost M-C, Petit C, Gicquel B.** 2006. Is Adipose Tissue a Place for Mycobacterium tuberculosis Persistence? Plos One **1**.
47. **Garton NJ, Waddell SJ, Sherratt AL, Lee SM, Smith RJ, Senner C, Hinds J, Rajakumar K, Adegbola RA, Besra GS, Butcher PD, Barer MR.** 2008. Cytological and transcript analyses reveal fat and lazy persister-like bacilli in tuberculous sputum. Plos Medicine **5:**634-645.
48. **Zhang Y.** 2004. Persistent and dormant tubercle bacilli and latent tuberculosis. Frontiers in Bioscience **9:**1136-1156.
49. **Bigger JW.** 1944. Treatment of staphylococcal infections with penicillin - By intermittent sterilisation. Lancet **2:**497-500.
50. **Li Y, Zhang Y.** 2007. PhoU is a persistence switch involved in persister formation and tolerance to multiple antibiotics and stresses in Escherichia coli. Antimicrobial Agents and Chemotherapy **51:**2092-2099.
51. **Ma C, Sim S, Shi W, Du L, Xing D, Zhang Y.** 2010. Energy production genes sucB and ubiF are involved in persister survival and tolerance to multiple antibiotics and stresses in Escherichia coli. Fems Microbiology Letters **303:**33-40.
52. **Dhar N, McKinney JD.** 2010. Mycobacterium tuberculosis persistence mutants identified by screening in isoniazid-treated mice. Proceedings of the National Academy of Sciences of the United States of America **107:**12275-12280.
53. **Junemann S.** 1997. Cytochrome bd terminal oxidase. Biochimica Et Biophysica Acta-Bioenergetics **1321:**107-127.

54. **Bernstein J, Lott WA, Steinberg BA, Yale HL.** 1952. CHEMOTHERAPY OF EXPERIMENTAL TUBERCULOSIS .5. ISONICOTINIC ACID HYDRAZIDE (NYDRAZID) AND RELATED COMPOUNDS. American Review of Tuberculosis **65:**357-364.
55. **Fox HH.** 1952. THE CHEMICAL APPROACH TO THE CONTROL OF TUBERCULOSIS. Science **116:**129-134.
56. **Solotorovsky M, Gregory FJ, Ironson EJ, Bugie EJ, Oneill RC, Pfister K.** 1952. PYRAZINOIC ACID AMIDE - AN AGENT ACTIVE AGAINST EXPERIMENTAL MURINE TUBERCULOSIS. Proceedings of the Society for Experimental Biology and Medicine **79:**563-565.
57. **Yeager RL, Munroe WGC, Dessau FI.** 1952. PYRAZINAMIDE (ALDINAMIDE) IN THE TREATMENT OF PULMONARY TUBERCULOSIS. American Review of Tuberculosis **65:**523-546.
58. **Thomas JP, Baughn CO, Shepherd RG, Wilkinson RG.** 1961. A NEW SYNTHETIC COMPOUND WITH ANTITUBERCULOUS ACTIVITY IN MICE - ETHAMBUTOL (DEXTRO-2,2'-(ETHYLENEDIIMINO)-DI-1-BUTANOL). American Review of Respiratory Disease **83:**891-&.
59. **Clark J, Wallace A.** 1967. The susceptibility of mycobacteria to rifamide and rifampicin. Tubercle **48:**144-148.
60. **Grumbach F, Rist N.** 1967. Experimental antitubercular activity of rifampicin, a derivative of rifamycin SV. Rev Tuberc Pneumol (Paris) **31:**749-762.
61. **Nitti V, Catena E, Ninni A, Difilipp.A.** 1967. ACTIVITY OF RIFAMPICIN IN EXPERIMENTAL TUBERCULOSIS OF GUINEA PIG. Chemotherapy **12:**369-&.
62. **Pallanza R, Arioli V, Furesz S, Bolzoni G.** 1967. RIFAMPICIN - A NEW RIFAMYCIN .2. LABORATORY STUDIES ON ANTITUBERCULOUS ACTIVITY AND PRELIMINARY CLINICAL OBSERVATIONS. Arzneimittel-Forschung **17:**529-&.
63. **WHO.** 2011. THE GLOBAL PLAN TO STOP TB 2011–2015. http://www.stoptb.org/assets/documents/global/plan/TB_GlobalPlanToStopTB2011-2015.pdf.
64. **WHO.** 2009. Treatment of tuberculosis: guidelines – 4th ed. http://whqlibdoc.who.int/publications/2010/9789241547833_eng.pdf.
65. **Lienhardt C, Glaziou P, Uplekar M, Loennroth K, Getahun H, Raviglione M.** 2012. Global tuberculosis control: lessons learnt and future prospects. Nature Reviews Microbiology **10:**407-416.
66. **Michel J-B, Yeh PJ, Chait R, Moellering RC, Jr., Kishony R.** 2008. Drug interactions modulate the potential for evolution of resistance. Proceedings of the National Academy of Sciences of the United States of America **105:**14918-14923.
67. **du Toit LC, Pillay V, Danckwerts MP.** 2006. Tuberculosis chemotherapy: current drug delivery approaches. Respiratory Research **7**.
68. **Mitchison DA, Coates ARM.** 2004. Predictive in vitro models of the sterilizing activity of anti-tuberculosis drugs. Current Pharmaceutical Design **10:**3285-3295.
69. **Johnson R, Streicher EM, Louw GE, Warren RM, van Helden PD, Victor TC.** 2006. Drug resistance in Mycobacterium tuberculosis. Current Issues in Molecular Biology **8:**97-111.
70. **De Cock KM, Chaisson RE.** 1999. Will DOTS do it? A reappraisal of tuberculosis control in countries with high rates of HIV infection. International Journal of Tuberculosis and Lung Disease **3:**457-465.
71. **Kimerling ME, Kluge H, Vezhnina N, Iacovazzi T, Demeulenaere T, Portaels F, Matthys F.** 1999. Inadequacy of the current WHO re-treatment regimen in a central Siberian prison: treatment failure and MDR-TB. International Journal of Tuberculosis and Lung Disease **3**.

72. **Long R.** 2007. The Canadian lung Association/Canadian Thoracic Society and tuberculosis prevention and control. Canadian Respiratory Journal **14**.
73. **Nuermberger EL, Spigelman MK, Yew WW.** 2010. Current development and future prospects in chemotherapy of tuberculosis. Respirology **15:**764-778.
74. **Holland DP, Sanders GD, Hamilton CD, Stout JE.** 2009. Costs and Cost-effectiveness of Four Treatment Regimens for Latent Tuberculosis Infection. American Journal of Respiratory and Critical Care Medicine **179:**1055-1060.
75. **Spyridis NP, Spyridis PG, Gelesme A, Sypsa V, Valianatou M, Metsou F, Gourgiotis D, Tsolia MN.** 2007. The effectiveness of a 9-month regimen of isoniazid alone versus 3-and 4-month regimens of isoniazid plus rifampin for treatment of latent tuberculosis infection in children: Results of an 11-year Randomized study. Clinical Infectious Diseases **45:**715-722.
76. **Lin PL, Dartois V, Johnston PJ, Janssen C, Via L, Goodwin MB, Klein E, Barry CE, III, Flynn JL.** 2012. Metronidazole prevents reactivation of latent Mycobacterium tuberculosis infection in macaques. Proceedings of the National Academy of Sciences of the United States of America **109**.
77. **Lambert PA.** 2002. Cellular impermeability and uptake of biocides and antibiotics in Gram-positive bacteria and mycobacteria. Journal of Applied Microbiology **92:**46S-54S.
78. **Viveiros M, Portugal I, Bettencourt R, Victor TC, Jordaan AM, Leandro C, Ordway D, Amaral L.** 2002. Isoniazid-induced transient high-level resistance in Mycobacterium tuberculosis. Antimicrobial Agents and Chemotherapy **46:**2804-2810.
79. **De Rossi E, Ainsa JA, Riccardi G.** 2006. Role of mycobacterial efflux transporters in drug resistance: an unresolved question. Fems Microbiology Reviews **30:**36-52.
80. **Choudhuri BS, Sen S, Chakrabarti P.** 1999. Isoniazid accumulation in Mycobacterium smegmatis is modulated by proton motive force-driven and ATP-dependent extrusion systems. Biochemical and Biophysical Research Communications **256:**682-684.
81. **Zhang Y, Heym B, Allen B, Young D, Cole S.** 1992. THE CATALASE PEROXIDASE GENE AND ISONIAZID RESISTANCE OF MYCOBACTERIUM-TUBERCULOSIS. Nature **358:**591-593.
82. **Wengenack NL, Lopes H, Kennedy MJ, Tavares P, Pereira AS, Moura I, Moura JJG, Rusnak F.** 2000. Redox potential measurements of the Mycobacterium tuberculosis heme protein KatG and the isoniazid-resistant enzyme KatG(S315T): Insights into isoniazid activation. Biochemistry **39:**11508-11513.
83. **Johnsson K, Schultz PG.** 1994. MECHANISTIC STUDIES OF THE OXIDATION OF ISONIAZID BY THE CATALASE PEROXIDASE FROM MYCOBACTERIUM-TUBERCULOSIS. Journal of the American Chemical Society **116:**7425-7426.
84. **Rozwarski DA, Grant GA, Barton DHR, Jacobs WR, Sacchettini JC.** 1998. Modification of the NADH of the isoniazid target (InhA) from Mycobacterium tuberculosis. Science **279:**98-102.
85. **Takayama K, Wang L, David HL.** 1972. EFFECT ON ISONIAZID ON IN-VIVO MYCOLIC ACID SYNTHESIS, CELL-GROWTH, AND VIABILITY OF MYCOBACTERIUM-TUBERCULOSIS. Antimicrobial Agents and Chemotherapy **2:**29-&.
86. **Zhang Y, Amzel LM.** 2002. Tuberculosis drug targets. Current Drug Targets **3:**131-154.
87. **Nguyen M, Claparols C, Bernadou J, Meunier B.** 2001. A fast and efficient metal-mediated oxidation of isoniazid and identification of isoniazid - NAD(H) adducts. Chembiochem **2:**877-883.
88. **Ducasse-Cabanot S, Cohen-Gonsaud M, Marrakchi H, Nguyen M, Zerbib D, Bernadou J, Daffe M, Labesse G, Quemard A.** 2004. In vitro inhibition of the

Mycobacterium tuberculosis beta-ketoacyl-acyl carrier protein reductase MabA by isoniazid. Antimicrobial Agents and Chemotherapy **48:**242-249.

89. **Thiemer-Kruger E.** 1958. Isonicotinic acid hypothesis of the antituberculous action of isoniazid. Am Rev Tuberc **77:**364-367.
90. **Scior T, Meneses Morales I, Garces Eisele SJ, Domeyer D, Laufer S.** 2002. Antitubercular isoniazid and drug resistance of Mycobacterium tuberculosis: A review. Archiv der Pharmazie (Weinheim) **335:**511-525.
91. **Banerjee A, Dubnau E, Quemard A, Balasubramanian V, Um KS, Wilson T, Collins D, Delisle G, Jacobs WR.** 1994. INHA, A GENE ENCODING A TARGET FOR ISONIAZID AND ETHIONAMIDE IN MYCOBACTERIUM-TUBERCULOSIS. Science **263:**227-230.
92. **Wade MM, Zhang Y.** 2004. Mechanisms of drug resistance in mycobacterium tuberculosis. Frontiers in Bioscience **9:**975-994.
93. **Vilcheze C, Weisbrod TR, Chen B, Kremer L, Hazbon MH, Wang F, Alland D, Sacchettini JC, Jacobs WR, Jr.** 2005. Altered NADH/NAD(+) ratio mediates coresistance to isoniazid and ethionamide in mycobacteria. Antimicrobial Agents and Chemotherapy **49:**708-720.
94. **Miesel L, Weisbrod TR, Marcinkeviciene JA, Bittman R, Jacobs WR, Jr.** 1998. NADH dehydrogenase defects confer isoniazid resistance and conditional lethality in Mycobacterium smegmatis. Journal of Bacteriology **180:**2459-2467.
95. **Payton M, Auty R, Delgoda R, Everett M, Sim E.** 1999. Cloning and characterization of arylamine N-acetyltransferase genes from Mycobacterium smegmatis and Mycobacterium tuberculosis: Increased expression results in isoniazid resistance. Journal of Bacteriology **181:**1343-1347.
96. **Chen P, Bishai WR.** 1998. Novel selection for isoniazid (INH) resistance genes supports a role for NAD(+)-binding proteins in mycobacterial INH resistance. Infection and Immunity **66:**5099-5106.
97. **Lee ASG, Teo ASM, Wong SY.** 2001. Novel mutations in ndh in isoniazid-resistant Mycobacterium tuberculosis isolates. Antimicrobial Agents and Chemotherapy **45:**2157-2159.
98. **Hillas PJ, del Alba FS, Oyarzabal J, Wilks A, de Montellano PRO.** 2000. The AhpC and AhpD antioxidant defense system of Mycobacterium tuberculosis. Journal of Biological Chemistry **275:**18801-18809.
99. **Sarich TC, Zhou T, Adams SP, Bain AI, Wall RA, Wright JM.** 1995. A MODEL OF ISONIAZID-INDUCED HEPATOTOXICITY IN RABBITS. J. Pharmacol. Toxicol. Methods **34:**109-116.
100. **Singh N, Golani A, Patel Z, Maitra A.** 2008. Transfer of isoniazid from circulation to breast milk in lactating women on chronic therapy for tuberculosis. British Journal of Clinical Pharmacology **65:**418-422.
101. **Obrien RJ, Long MW, Cross FS, Lyle MA, Snider DE.** 1983. HEPATOTOXICITY FROM ISONIAZID AND RIFAMPIN AMONG CHILDREN TREATED FOR TUBERCULOSIS. Pediatrics **72:**491-499.
102. **Ellard GA, Humphries MJ, Allen BW.** 1993. CEREBROSPINAL-FLUID DRUG CONCENTRATIONS AND THE TREATMENT OF TUBERCULOUS MENINGITIS. American Review of Respiratory Disease **148:**650-655.
103. **Vinnard C, Winston CA, Wileyto EP, MacGregor RR, Bisson GP.** 2010. Isoniazid resistance and death in patients with tuberculous meningitis: retrospective cohort study. British Medical Journal **341**.
104. **Blumberg HM, Leonard MK, Jasmer RM.** 2005. Update on the treatment of tuberculosis and latent tuberculosis infection (vol 293, pg 2776, 2005). Jama-Journal of the American Medical Association **294:**182-182.

105. **Somoskovi A, Parsons LM, Salfinger M.** 2001. The molecular basis of resistance to isoniazid, rifampin, and pyrazinamide in Mycobacterium tuberculosis. Respiratory Research **2:**164-168.
106. **Telenti A, Imboden P, Marchesi F, Lowrie D, Cole S, Colston MJ, Matter L, Schopfer K, Bodmer T.** 1993. DETECTION OF RIFAMPICIN-RESISTANCE MUTATIONS IN MYCOBACTERIUM-TUBERCULOSIS. Lancet **341:**647-650.
107. **Levin ME, Hatfull GF.** 1993. MYCOBACTERIUM-SMEGMATIS RNA-POLYMERASE - DNA SUPERCOILING, ACTION OF RIFAMPICIN AND MECHANISM OF RIFAMPICIN RESISTANCE. Molecular Microbiology **8:**277-285.
108. **Mitchison DA, Nunn AJ.** 1986. INFLUENCE OF INITIAL-DRUG RESISTANCE ON THE RESPONSE TO SHORT-COURSE CHEMOTHERAPY OF PULMONARY TUBERCULOSIS. American Review of Respiratory Disease **133:**423-430.
109. **Niemi M, Backman JT, Fromm MF, Neuvonen PJ, Kivisto KT.** 2003. Pharmacokinetic interactions with rifampicin - Clinical relevance. Clinical Pharmacokinetics **42:**819-850.
110. **Girling DJ.** 1978. HEPATIC TOXICITY OF ANTI-TUBERCULOSIS REGIMENS CONTAINING ISONIAZID, RIFAMPICIN AND PYRAZINAMIDE. Tubercle **59:**13-32.
111. **Villarino ME, Ridzon R, Weismuller PC, Elcock M, Maxwell RM, Meador J, Smith PJ, Carson ML, Geiter LJ.** 1997. Rifampin preventive therapy for tuberculosis infection - Experience with 157 adolescents. American Journal of Respiratory and Critical Care Medicine **155:**1735-1738.
112. **Martinez E, Collazos J, Mayo J.** 1999. Hypersensitivity reactions to rifampin - Pathogenetic mechanisms, clinical manifestations, management strategies, and review of the anaphylactic-like reactions. Medicine **78:**361-369.
113. **Takayama K, Kilburn JO.** 1989. INHIBITION OF SYNTHESIS OF ARABINOGALACTAN BY ETHAMBUTOL IN MYCOBACTERIUM-SMEGMATIS. Antimicrobial Agents and Chemotherapy **33:**1493-1499.
114. **Deng LY, Mikusova K, Robuck KG, Scherman M, Brennan PJ, McNeil MR.** 1995. RECOGNITION OF MULTIPLE EFFECTS OF ETHAMBUTOL ON METABOLISM OF MYCOBACTERIAL CELL-ENVELOPE. Antimicrobial Agents and Chemotherapy **39:**694-701.
115. **Mikusova K, Slayden RA, Besra GS, Brennan PJ.** 1995. BIOGENESIS OF THE MYCOBACTERIAL CELL-WALL AND THE SITE OF ACTION OF ETHAMBUTOL. Antimicrobial Agents and Chemotherapy **39:**2484-2489.
116. **Sassetti CM, Boyd DH, Rubin EJ.** 2003. Genes required for mycobacterial growth defined by high density mutagenesis. Molecular Microbiology **48:**77-84.
117. **Amin AG, Goude R, Shi L, Zhang J, Chatterjee D, Parish T.** 2008. EmbA is an essential arabinosyltransferase in Mycobacterium tuberculosis. Microbiology-Sgm **154:**240-248.
118. **Goude R, Amin AG, Chatterjee D, Parish T.** 2008. The critical role of embC in Mycobacterium tuberculosis. Journal of Bacteriology **190:**4335-4341.
119. **Goude R, Amin AG, Chatterjee D, Parish T.** 2009. The Arabinosyltransferase EmbC Is Inhibited by Ethambutol in Mycobacterium tuberculosis. Antimicrobial Agents and Chemotherapy **53:**4138-4146.
120. **Telenti A, Philipp WJ, Sreevatsan S, Bernasconi C, Stockbauer KE, Wieles B, Musser JM, Jacobs WR.** 1997. The emb operon, a gene cluster of Mycobacterium tuberculosis involved in resistance to ethambutol. Nature Medicine **3:**567-570.
121. **Jadaun GPS, Das R, Upadhyay P, Chauhan DS, Sharma VD, Katoch VM.** 2009. Role of embCAB gene mutations in ethambutol resistance in Mycobacterium tuberculosis isolates from India. International Journal of Antimicrobial Agents **33:**483-486.

122. **Griffith DE, Brown-Elliott BA, Shepherd S, McLarty J, Griffith L, Wallace RJ.** 2005. Ethambutol ocular toxicity in treatment regimens for Mycobacterium avium complex lung disease. American Journal of Respiratory and Critical Care Medicine **172:**250-253.
123. **Handbook-of-anti-tuberculosis-agents.** 2008. Handbook of anti-tuberculosis agents. Tuberculosis **88:**85-169.
124. **Zhang Y.** 2005. The magic bullets and tuberculosis drug targets. Annual review of pharmacology and toxicology **45:**529-564.
125. **Zhang Y, Permar S, Sun ZH.** 2002. Conditions that may affect the results of susceptibility testing of Mycobacterium tuberculosis to pyrazinamide. Journal of Medical Microbiology **51:**42-49.
126. **Wade MM, Zhang Y.** 2004. Anaerobic incubation conditions enhance pyrazinamide activity against Mycobacterium tuberculosis. Journal of Medical Microbiology **53:**769-773.
127. **Tarshis MS, Weed WA.** 1953. LACK OF SIGNIFICANT INVITRO SENSITIVITY OF MYCOBACTERIUM TUBERCULOSIS TO PYRAZINAMIDE ON 3 DIFFERENT SOLID MEDIA. American Review of Tuberculosis **67:**391-395.
128. **McDermott W, Tompsett R.** 1954. ACTIVATION OF PYRAZINAMIDE AND NICOTINAMIDE IN ACIDIC ENVIRONMENTS INVITRO. American Review of Tuberculosis **70:**748-754.
129. **Zhang Y, Scorpio A, Nikaido H, Sun ZH.** 1999. Role of acid pH and deficient efflux of pyrazinoic acid in unique susceptibility of Mycobacterium tuberculosis to pyrazinamide. Journal of Bacteriology **181:**2044-2049.
130. **Zhang Y, Mitchison D.** 2003. The curious characteristics of pyrazinamide: a review. International Journal of Tuberculosis and Lung Disease **7:**6-21.
131. **Heifets L, Higgins M, Simon B.** 2000. Pyrazinamide is not active against Mycobacterium tuberculosis residing in cultured human monocyte-derived macrophages. International Journal of Tuberculosis and Lung Disease **4:**491-495.
132. **Zhang Y, Wade MM, Scorpio A, Zhang H, Sun ZH.** 2003. Mode of action of pyrazinamide: disruption of Mycobacterium tuberculosis membrane transport and energetics by pyrazinoic acid. Journal of Antimicrobial Chemotherapy **52:**790-795.
133. **Zimhony O, Cox JS, Welch JT, Vilcheze C, Jacobs WR.** 2000. Pyrazinamide inhibits the eukaryotic-like fatty acid synthetase I (FASI) of Mycobacterium tuberculosis. Nature Medicine **6:**1043-1047.
134. **Raynaud C, Laneelle MA, Senaratne RH, Draper P, Laneelle G, Daffe M.** 1999. Mechanisms of pyrazinamide resistance in mycobacteria: importance of lack of uptake in addition to lack of pyrazinamidase activity. Microbiology-Sgm **145:**1359-1367.
135. **Corbella X, Vadillo M, Cabellos C, Fernandezviladrich P, Rufi G.** 1995. HYPERSENSITIVITY HEPATITIS DUE TO PYRAZINAMIDE. Scandinavian Journal of Infectious Diseases **27:**93-94.
136. **Blumberg HM, Burman WJ, Chaisson RE, Daley CL, Etkind SC, Friedman LN, Fujiwara P, Grzemska M, Hopewell PC, Iseman MD, Jasmer RM, Koppaka V, Menzies RI, O'Brien RJ, Reves RR, Reichman LB, Simone PM, Starke JR, Vernon AA.** 2003. American Thoracic Society/Centers for Disease Control and Prevention/Infectious Diseases Society of America: treatment of tuberculosis. Am J Respir Crit Care Med **167:**603-662.
137. **Peloquin CA, Berning SE, Nitta AT, Simone PM, Goble M, Huitt GA, Iseman MD, Cook JL, Curran-Everett D.** 2004. Aminoglycoside toxicity: Daily versus thrice-weekly dosing for treatment of mycobacterial diseases. Clinical Infectious Diseases **38:**1538-1544.

138. **Sacchettini JC, Rubin EJ, Freundlich JS.** 2008. Drugs versus bugs: in pursuit of the persistent predator Mycobacterium tuberculosis. Nature Reviews Microbiology **6:**41-52.
139. **Wayne LG, Sramek HA.** 1994. METRONIDAZOLE IS BACTERICIDAL TO DORMANT CELLS OF MYCOBACTERIUM-TUBERCULOSIS. Antimicrobial Agents and Chemotherapy **38:**2054-2058.
140. **Zhang Y, Yew WW.** 2009. Mechanisms of drug resistance in Mycobacterium tuberculosis. International Journal of Tuberculosis and Lung Disease **13:**1320-1330.
141. **Migliori GB, De Iaco G, Besozzi G, Centis R, Cirillo DM.** 2007. First tuberculosis cases in Italy resistant to all tested drugs. Euro surveillance : bulletin europeen sur les maladies transmissibles = European communicable disease bulletin **12:**E070517.070511.
142. **Velayati AA, Masjedi MR, Farnia P, Tabarsi P, Ghanavi J, ZiaZarifi AH, Hoffner SE.** 2009. Emergence of New Forms of Totally Drug-Resistant Tuberculosis BacilliSuper Extensively Drug-Resistant Tuberculosis or Totally Drug-Resistant Strains in Iran. CHEST Journal **136:**420-425.
143. **WHO.** 2010. Indicators of diagnosis, notification and treatment of multidrug-resistant TB, by country and year. http://www.who.int/tb/challenges/mdr/en/.
144. **WHO.** 2010. Multidrug and extensively drug-resistant TB (M/XDR-TB): 2010 global report on surveillance and response, Geneva, Switzerland.
145. **WHO.** 2001. GUIDELINES FOR DRUG SUSCEPTIBILITY TESTING FOR SECOND-LINE ANTI-TUBERCULOSIS DRUGS FOR DOTS-PLUS. http://www.who.int/docstore/gtb/publications/mdrtb/tb_2001_288/guidelines.pdf.
146. **Park SK, Kim CT, Song SD.** 1998. Outcome of chemotherapy in 107 patients with pulmonary tuberculosis resistant to isoniazid and rifampin. International Journal of Tuberculosis and Lung Disease **2:**877-884.
147. **WHO.** 2011. Guidelines for the programmatic management of drug-resistant tuberculosis. http://whqlibdoc.who.int/publications/2011/9789241501583_eng.pdf.
148. **Cole ST, Brosch R, Parkhill J, Garnier T, Churcher C, Harris D, Gordon SV, Eiglmeier K, Gas S, Barry CE, Tekaia F, Badcock K, Basham D, Brown D, Chillingworth T, Connor R, Davies R, Devlin K, Feltwell T, Gentles S, Hamlin N, Holroyd S, Hornby T, Jagels K, Krogh A, McLean J, Moule S, Murphy L, Oliver K, Osborne J, Quail MA, Rajandream MA, Rogers J, Rutter S, Seeger K, Skelton J, Squares R, Squares S, Sulston JE, Taylor K, Whitehead S, Barrell BG.** 1998. Deciphering the biology of Mycobacterium tuberculosis from the complete genome sequence. Nature **393:**537-+.
149. **Mathema B, Kurepina NE, Bifani PJ, Kreiswirth BN.** 2006. Molecular epidemiology of tuberculosis: Current insights. Clinical Microbiology Reviews **19:**658-+.
150. **Blattner FR, Plunkett G, Bloch CA, Perna NT, Burland V, Riley M, ColladoVides J, Glasner JD, Rode CK, Mayhew GF, Gregor J, Davis NW, Kirkpatrick HA, Goeden MA, Rose DJ, Mau B, Shao Y.** 1997. The complete genome sequence of Escherichia coli K-12. Science **277:**1453-&.
151. **Anand P, Sankaran S, Mukherjee S, Yeturu K, Laskowski R, Bhardwaj A, Bhagavat R, Brahmachari SK, Chandra N, Consortium O.** 2011. Structural Annotation of Mycobacterium tuberculosis Proteome. Plos One **6**.
152. **Camus JC, Pryor MJ, Medigue C, Cole ST.** 2002. Re-annotation of the genome sequence of Mycobacterium tuberculosis H37Rv. Microbiology-Sgm **148:**2967-2973.
153. **Domenech P, Barry CE, Cole ST.** 2001. Mycobacterium tuberculosis in the post-genomic age. Current Opinion in Microbiology **4**.

154. **Schnappinger D, Ehrt S, Voskuil MI, Liu Y, Mangan JA, Monahan IM, Dolganov G, Efron B, Butcher PD, Nathan C, Schoolnik GK.** 2003. Transcriptional adaptation of Mycobacterium tuberculosis within macrophages: Insights into the phagosomal environment. Journal of Experimental Medicine **198:**693-704.
155. **Rachman H, Strong M, Schaible U, Schuchhardt J, Hagens K, Mollenkopf H, Eisenberg D, Kaufmann SHE.** 2006. Mycobacterium tuberculosis gene expression profiling within the context of protein networks. Microbes and Infection **8:**747-757.
156. **Rohde KH, Abramovitch RB, Russell DG.** 2007. Mycobacterium tuberculosis invasion of macrophages: Linking bacterial gene expression to environmental cues. Cell Host & Microbe **2:**352-364.
157. **Cappelli G, Volpe E, Grassi M, Liseo B, Colizzi V, Mariani F.** 2006. Profiling of Mycobacterium tuberculosis gene expression during human macrophage infection: Upregulation of the alternative sigma factor G, a group of transcriptional regulators, and proteins with unknown function. Research in Microbiology **157**.
158. **Rachman H, Strong M, Ulrichs T, Grode L, Schuchhardt J, Mollenkopf H, Kosmiadi GA, Eisenberg D, Kaufmann SHE.** 2006. Unique transcriptome signature of Mycobacterium tuberculosis in pulmonary tuberculosis. Infection and Immunity **74:**1233-1242.
159. **Starck J, Kallenius G, Marklund BI, Andersson DI, Akerlund T.** 2004. Comparative proteome analysis of Mycobacterium tuberculosis grown under aerobic and anaerobic conditions. Microbiology-Sgm **150**.
160. **de Carvalho LPS, Fischer SM, Marrero J, Nathan C, Ehrt S, Rhee KY.** 2010. Metabolomics of Mycobacterium tuberculosis Reveals Compartmentalized Co-Catabolism of Carbon Substrates. Chemistry & Biology **17**.
161. **Somashekar BS, Amin AG, Rithner CD, Troudt J, Basaraba R, Izzo A, Crick DC, Chatterjee D.** 2011. Metabolic Profiling of Lung Granuloma in Mycobacterium tuberculosis Infected Guinea Pigs: Ex vivo (1)H Magic Angle Spinning NMR Studies. Journal of Proteome Research **10:**4186-4195.
162. **Lamichhane G, Zignol M, Blades NJ, Geiman DE, Dougherty A, Grosset J, Broman KW, Bishai WR.** 2003. A postgenomic method for predicting essential genes at subsaturation levels of mutagenesis: Application to Mycobacterium tuberculosis. Proceedings of the National Academy of Sciences of the United States of America **100:**7213-7218.
163. **Hutchison CA, Peterson SN, Gill SR, Cline RT, White O, Fraser CM, Smith HO, Venter JC.** 1999. Global transposon mutagenesis and a minimal mycoplasma genome. Science **286:**2165-2169.
164. **Jacobs MA, Alwood A, Thaipisuttikul I, Spencer D, Haugen E, Ernst S, Will O, Kaul R, Raymond C, Levy R, Liu CR, Guenthner D, Bovee D, Olson MV, Manoil C.** 2003. Comprehensive transposon mutant library of Pseudomonas aeruginosa. Proceedings of the National Academy of Sciences of the United States of America **100:**14339-14344.
165. **Sassetti CM, Boyd DH, Rubin EJ.** 2001. Comprehensive identification of conditionally essential genes in mycobacteria. Proceedings of the National Academy of Sciences of the United States of America **98:**12712-12717.
166. **Zhang YJ, Ioerger TR, Huttenhower C, Long JE, Sassetti CM, Sacchettini JC, Rubin EJ.** 2012. Global Assessment of Genomic Regions Required for Growth in Mycobacterium tuberculosis. Plos Pathogens **8**.
167. **Sharma P, Hellingwerf KJ, de Mattos MJT, Bekker M.** 2012. Uncoupling of Substrate-Level Phosphorylation in Escherichia coli during Glucose-Limited Growth. Applied and Environmental Microbiology **78**.

168. **Munoz-Elias EJ, McKinney JD.** 2006. Carbon metabolism of intracellular bacteria. Cellular Microbiology **8:**10-22.
169. **Tian J, Bryk R, Itoh M, Suematsu M, Nathan C.** 2005. Variant tricarboxylic acid cycle in Mycobacterium tuberculosis: Identification of alpha-ketoglutarate decarboxylase. Proceedings of the National Academy of Sciences of the United States of America **102:**10670-10675.
170. **Wagner T, Bellinzoni M, Wehenkel A, O'Hare HM, Alzari PM.** 2011. Functional Plasticity and Allosteric Regulation of alpha-Ketoglutarate Decarboxylase in Central Mycobacterial Metabolism. Chemistry & Biology **18**.
171. **Baughn AD, Garforth SJ, Vilcheze C, Jacobs WR.** 2009. An Anaerobic-Type alpha-Ketoglutarate Ferredoxin Oxidoreductase Completes the Oxidative Tricarboxylic Acid Cycle of Mycobacterium tuberculosis. Plos Pathogens **5**.
172. **McKinney JD, zu Bentrup KH, Munoz-Elias EJ, Miczak A, Chen B, Chan WT, Swenson D, Sacchettini JC, Jacobs WR, Russell DG.** 2000. Persistence of Mycobacterium tuberculosis in macrophages and mice requires the glyoxylate shunt enzyme isocitrate lyase. Nature **406:**735-738.
173. **Talaat AM, Lyons R, Howard ST, Johnston SA.** 2004. The temporal expression profile of Mycobacterium tuberculosis infection in mice. Proceedings of the National Academy of Sciences of the United States of America **101:**4602-4607.
174. **Timm J, Post FA, Bekker LG, Walther GB, Wainwright HC, Manganelli R, Chan WT, Tsenova L, Gold B, Smith I, Kaplan G, McKinney JD.** 2003. Differential expression of iron-, carbon-, and oxygen-responsive mycobacterial genes in the lungs of chronically infected mice and tuberculosis patients. Proceedings of the National Academy of Sciences of the United States of America **100**.
175. **Munoz-Elias EJ, Upton AM, Cherian J, McKinney JD.** 2006. Role of the methylcitrate cycle in Mycobacterium tuberculosis metabolism, intracellular growth, and virulence. Molecular Microbiology **60:**1109-1122.
176. **Anishetty S, Pulimi M, Pennathur G.** 2005. Potential drug targets in Mycobacterium tuberculosis through metabolic pathway analysis. Computational Biology and Chemistry **29**.
177. **Yang XX, Nesbitt NM, Dubnau E, Smith I, Sampson NS.** 2009. Cholesterol Metabolism Increases the Metabolic Pool of Propionate in Mycobacterium tuberculosis. Biochemistry **48:**3819-3821.
178. **Savvi S, Warner DF, Kana BD, McKinney JD, Mizrahi V, Dawes SS.** 2008. Functional characterization of a vitamin B(12)-dependent methylmalonyl pathway in Mycobacterium tuberculosis: Implications for propionate metabolism during growth on fatty acids. Journal of Bacteriology **190:**3886-3895.
179. **Munoz-Elias EJ, McKinney JD.** 2005. Mycobacterium tuberculosis isocitrate lyases 1 and 2 are jointly required for in vivo growth and virulence. Nature Medicine **11:**638-644.
180. **Beste DJV, Bonde B, Hawkins N, Ward JL, Beale MH, Noack S, Noeh K, Kruger NJ, Ratcliffe RG, McFadden J.** 2011. C-13 Metabolic Flux Analysis Identifies an Unusual Route for Pyruvate Dissimilation in Mycobacteria which Requires Isocitrate Lyase and Carbon Dioxide Fixation. Plos Pathogens **7**.
181. **Gould TA, de Langemheen HV, Munoz-Elias EJ, McKinney JD, Sacchettini JC.** 2006. Dual role of isocitrate lyase 1 in the glyoxylate and methylcitrate cycles in Mycobacterium tuberculosis. Molecular Microbiology **61:**940-947.
182. **Textor S, Wendisch VF, DeGraaf A, Muller U, Linder MI, Linder D, Buckel W.** 1997. Propionate oxidation in Escherichia coli: evidence for operation of a methylcitrate cycle in bacteria. Archives of Microbiology **168**.

183. **Pandey AK, Sassetti CM.** 2008. Mycobacterial persistance requires the utilization of host cholesterol. Proceedings of the National Academy of Sciences of the United States of America **105**.
184. **Griffin JE, Pandey AK, Gilmore SA, Mizrahi V, McKinney JD, Bertozzi CR, Sassetti CM.** 2012. Cholesterol Catabolism by Mycobacterium tuberculosis Requires Transcriptional and Metabolic Adaptations. Chemistry & Biology **19**.
185. **Asselineau J, Lederer E.** 1950. STRUCTURE OF THE MYCOLIC ACIDS OF MYCOBACTERIA. Nature **166**.
186. **Smith S, Witkowski A, Joshi AK.** 2003. Structural and functional organization of the animal fatty acid synthase. Progress in Lipid Research **42**.
187. **Bhatt A, Molle V, Besra GS, Jacobs WR, Jr., Kremer L.** 2007. The Mycobacterium tuberculosis FAS-II condensing enzymes: their role in mycolic acid biosynthesis, acid-fastness, pathogenesis and in future drug development. Molecular Microbiology **64**.
188. **Kumar A, Farhana A, Guidry L, Saini V, Hondalus M, Steyn AJC.** 2011. Redox homeostasis in mycobacteria: the key to tuberculosis control? Expert Reviews in Molecular Medicine **13**.
189. **Farhana A, Guidry L, Srivastava A, Singh A, Hondalus MK, Steyn AJC.** 2010. Reductive Stress in Microbes: Implications for Understanding Mycobacterium tuberculosis Disease and Persistence, p. 43-117. *In* Poole RK (ed.), Advances in Microbial Physiology, Vol 57, vol. 57.
190. **Masood R, Sharma YK, Venkitasubramanian TA.** 1985. METABOLISM OF MYCOBACTERIA. Journal of Biosciences **7**.
191. **Shin J-H, Yang J-Y, Jeon B-Y, Yoon YJ, Cho S-N, Kang Y-H, Ryu DH, Hwang G-S.** 2011. H-1 NMR-based Metabolomic Profiling in Mice Infected with Mycobacterium tuberculosis. Journal of Proteome Research **10:**2238-2247.
192. **Eisenreich W, Dandekar T, Heesemann J, Goebel W.** 2010. Carbon metabolism of intracellular bacterial pathogens and possible links to virulence. Nature Reviews Microbiology **8**.
193. **Rhee KY, de Carvalho LPS, Bryk R, Ehrt S, Marrero J, Park SW, Schnappinger D, Venugopal A, Nathan C.** 2011. Central carbon metabolism in Mycobacterium tuberculosis: an unexpected frontier. Trends in Microbiology **19:**307-314.
194. **Voet DJ, Voet JG, Pratt CW.** 2008. Principles of Biochemistry, 3rd ed. John Wiley & Sons, Inc., Hoboken.
195. **Kana BD, Machowski EE, Schechter N, Teh J-S, Rubin H, Mizrahi V.** 2009. Electron Transport and Respiration in Mycobacteria. Mycobacterium: Genomics and Molecular Biology**:**35-64.
196. **McAdam RA, Quan S, Smith DA, Bardarov S, Betts JC, Cook FC, Hooker EU, Lewis AP, Woollard P, Everett MJ, Lukey PT, Bancroft GJ, Jacobs WR, Duncan K.** 2002. Characterization of a Mycobacterium tuberculosis H37Rv transposon library reveals insertions in 351 ORFs and mutants with altered virulence. Microbiology-Sgm **148:**2975-2986.
197. **Weinstein EA, Yano T, Li LS, Avarbock D, Avarbock A, Helm D, McColm AA, Duncan K, Lonsdale JT, Rubin H.** 2005. Inhibitors of type IINADH :-menaquinone oxidoreductase represent a class of antitubercular drugs. Proceedings of the National Academy of Sciences of the United States of America **102:**4548-4553.
198. **Velmurugan K, Chen B, Miller JL, Azogue S, Gurses S, Hsu T, Glickman M, Jacobs WR, Jr., Porcelli SA, Briken V.** 2007. Mycobacterium tuberculosis nuoG is a virulence gene that inhibits apoptosis of infected host cells. Plos Pathogens **3:**972-980.
199. **Cecchini G, Maklashina E, Yankovskaya V, Iverson TM, Iwata S.** 2003. Variation in proton donor/acceptor pathways in succinate:quinone oxidoreductases. FEBS Letters **545:**31-38.

200. **Van Hellemond JJ, Tielens AGM.** 1994. Expression and functional properties of fumarate reductase. Biochemical Journal **304:**321-331.
201. **Farrand SK, Taber HW.** 1974. CHANGES IN MENAQUINONE CONCENTRATION DURING GROWTH AND EARLY SPORULATION IN BACILLUS-SUBTILIS. Journal of Bacteriology **117:**324-326.
202. **Collins MD, Goodfellow M, Minnikin DE, Alderson G.** 1985. MENAQUINONE COMPOSITION OF MYCOLIC-ACID-CONTAINING ACTINOMYCETES AND SOME SPOROACTINOMYCETES. Journal of Applied Bacteriology **58:**77-86.
203. **Teh JS, Yano T, Rubin H.** 2007. Type IINADM : menaquinone oxidoreductase of Mycobacterium tuberculosis. Infectious Disorders - Drug Targets **7:**169-181.
204. **Roehm K-H.** 2001. Electron carriers: proteins and cofactors in oxidative phosphorylation. . Encyclopedia of Life Sciences. .
205. **Jasaitis A, Borisov VB, Belevich NP, Morgan JE, Konstantinov AA, Verkhovsky MI.** 2000. Electrogenic reactions of cytochrome bd. Biochemistry **39:**13800-13809.
206. **Belevich I, Borisov VB, Zhang J, Yang K, Konstantinov AA, Gennis RB, Verkhovsky MI.** 2005. Time-resolved electrometric and optical studies on cytochrome bd suggest a mechanism of electron-proton coupling in the di-heme active site. Proceedings of the National Academy of Sciences of the United States of America **102:**3657-3662.
207. **Lenaerts AJ, Hoff D, Aly S, Ehlers S, Andries K, Cantarero L, Orme IM, Basaraba RJ.** 2007. Location of persisting mycobacteria in a guinea pig model of tuberculosis revealed by R207910. Antimicrobial Agents and Chemotherapy **51:**3338-3345.
208. **Haagsma AC, Driessen NN, Hahn M-M, Lill H, Bald D.** 2010. ATP synthase in slow- and fast-growing mycobacteria is active in ATP synthesis and blocked in ATP hydrolysis direction. Fems Microbiology Letters **313:**68-74.
209. **Fisher N, Warman AJ, Ward SA, Biagini GA.** 2009. TYPE II NADH: QUINONE OXIDOREDUCTASES OF PLASMODIUM FALCIPARUM AND MYCOBACTERIUM TUBERCULOSIS: KINETIC AND HIGH-THROUGHPUT ASSAYS. Methods in Enzymology, Vol 456: Mitochondrial Function, Part a: Mitochondrial Electron Transport Complexes and Reactive Oxygen Species **456:**303-320.
210. **Lamrabet O, Pieulle L, Aubert C, Mouhamar F, Stocker P, Dolla A, Brasseur G.** 2011. Oxygen reduction in the strict anaerobe Desulfovibrio vulgaris Hildenborough: characterization of two membrane-bound oxygen reductases. Microbiology-Sgm **157**.
211. **Borisov VB, Gennis RB, Hemp J, Verkhovsky MI.** 2011. The cytochrome bd respiratory oxygen reductases. Biochimica Et Biophysica Acta-Bioenergetics **1807:**1398-1413.
212. **Miller MJ, Gennis RB.** 1983. THE PURIFICATION AND CHARACTERIZATION OF THE CYTOCHROME-D TERMINAL OXIDASE COMPLEX OF THE ESCHERICHIA-COLI AEROBIC RESPIRATORY-CHAIN. Journal of Biological Chemistry **258:**9159-9165.
213. **Kita K, Konishi K, Anraku Y.** 1984. TERMINAL OXIDASES OF ESCHERICHIA-COLI AEROBIC RESPIRATORY-CHAIN .2. PURIFICATION AND PROPERTIES OF CYTOCHROME-B558-D COMPLEX FROM CELLS GROWN WITH LIMITED OXYGEN AND EVIDENCE OF BRANCHED ELECTRON-CARRYING SYSTEMS. Journal of Biological Chemistry **259:**3375-3381.
214. **Green GN, Fang H, Lin RJ, Newton G, Mather M, Georgiou CD, Gennis RB.** 1988. THE NUCLEOTIDE-SEQUENCE OF THE CYD LOCUS ENCODING THE 2 SUBUNITS OF THE CYTOCHROME-D TERMINAL OXIDASE COMPLEX OF ESCHERICHIA-COLI. Journal of Biological Chemistry **263:**13138-13143.
215. **Osborne JP, Gennis RB.** 1999. Sequence analysis of cytochrome bd oxidase suggests a revised topology for subunit I. Biochimica Et Biophysica Acta-Bioenergetics **1410:**32-50.

216. **Cunningham L, Williams HD.** 1995. ISOLATION AND CHARACTERIZATION OF MUTANTS DEFECTIVE IN THE CYANIDE-INSENSITIVE RESPIRATORY PATHWAY OF PSEUDOMONAS-AERUGINOSA. Journal of Bacteriology **177:**432-438.
217. **Sturr MG, Krulwich TA, Hicks DB.** 1996. Purification of a cytochrome bd terminal oxidase encoded by the Escherichia coli app locus from a Delta cyo Delta cyd strain complemented by genes from Bacillus firmus OF4. Journal of Bacteriology **178:**1742-1749.
218. **Shepherd M, Sanguinetti G, Cook GM, Poole RK.** 2010. Compensations for Diminished Terminal Oxidase Activity in Escherichia coli CYTOCHROME bd-II-MEDIATED RESPIRATION AND GLUTAMATE METABOLISM. Journal of Biological Chemistry **285:**18464-18472.
219. **Heidelberg JF, Eisen JA, Nelson WC, Clayton RA, Gwinn ML, Dodson RJ, Haft DH, Hickey EK, Peterson JD, Umayam L, Gill SR, Nelson KE, Read TD, Tettelin H, Richardson D, Ermolaeva MD, Vamathevan J, Bass S, Qin HY, Dragoi I, Sellers P, McDonald L, Utterback T, Fleishmann RD, Nierman WC, White O, Salzberg SL, Smith HO, Colwell RR, Mekalanos JJ, Venter JC, Fraser CM.** 2000. DNA sequence of both chromosomes of the cholera pathogen Vibrio cholerae. Nature **406:**477-483.
220. **Trumpower BL, Gennis RB.** 1994. ENERGY TRANSDUCTION BY CYTOCHROME COMPLEXES IN MITOCHONDRIAL AND BACTERIAL RESPIRATION - THE ENZYMOLOGY OF COUPLING ELECTRON-TRANSFER REACTIONS TO TRANSMEMBRANE PROTON TRANSLOCATION. Annual Review of Biochemistry **63:**675-716.
221. **Shi LB, Sohaskey CD, Kana BD, Dawes S, North RJ, Mizrahi V, Gennaro ML.** 2005. Changes in energy metabolism of Mycobacterium tuberculosis in mouse lung and under in vitro conditions affecting aerobic respiration. Proceedings of the National Academy of Sciences of the United States of America **102:**15629-15634.
222. **Jones SA, Chowdhury FZ, Fabich AJ, Anderson A, Schreiner DM, House AL, Autieri SM, Leatham MP, Lins JJ, Jorgensen M, Cohen PS, Conway T.** 2007. Respiration of Escherichia coli in the mouse intestine. Infection and Immunity **75:**4891-4899.
223. **Dincturk HB, Demir V, Aykanat T.** 2011. Bd oxidase homologue of photosynthetic purple sulfur bacterium Allochromatium vinosum is co-transcribed with a nitrogen fixation related gene. Antonie Van Leeuwenhoek **99:**211-220.
224. **Hassani BK, Steunou AS, Liotenberg S, Reiss-Husson F, Astier C, Ouchane S.** 2010. Adaptation to Oxygen ROLE OF TERMINAL OXIDASES IN PHOTOSYNTHESIS INITIATION IN THE PURPLE PHOTOSYNTHETIC BACTERIUM, RUBRIVIVAX GELATINOSUS. Journal of Biological Chemistry **285:**19891-19899.
225. **Yamamoto Y, Poyart C, Trieu-Cuot P, Lamberet G, Gruss A, Gaudu P.** 2005. Respiration metabolism of Group B Streptococcus is activated by environmental haem and quinone and contributes to virulence. Molecular Microbiology **56:**525-534.
226. **Borisov VB, Forte E, Giuffre A, Konstantinov A, Sarti P.** 2009. Reaction of nitric oxide with the oxidized di-heme and heme-copper oxygen-reducing centers of terminal oxidases: Different reaction pathways and end-products. J. Inorg. Biochem. **103:**1185-1187.
227. **Forte E, Borisov VB, Konstantinov AA, Brunori M, Giuffre A, Sarti P.** 2007. Cytochrome bd, a key oxidase in bacterial survival and tolerance to nitrosative stress. Ital J Biochem **56:**265-269.
228. **Borisov VB, Davletshin AI, Konstantinov AA.** 2010. Peroxidase activity of cytochrome bd from Escherichia coli. Biochemistry-Moscow **75:**428-436.
229. **Huycke MM, Moore D, Joyce W, Wise P, Shepard L, Kotake Y, Gilmore MS.** 2001. Extracellular superoxide production by Enterococcus faecalis requires

demethylmenaquinone and is attenuated by functional terminal quinol oxidases. Molecular Microbiology **42:**729-740.

230. **Heintz D, Gallien S, Wischgoll S, Ullmann AK, Schaeffer C, Kretzschmar AK, van Dorsselaer A, Boll M.** 2009. Differential Membrane Proteome Analysis Reveals Novel Proteins Involved in the Degradation of Aromatic Compounds in Geobacter metallireducens. Mol. Cell. Proteomics **8:**2159-2169.
231. **Mason MG, Shepherd M, Nicholls P, Dobbin PS, Dodsworth KS, Poole RK, Cooper CE.** 2009. Cytochrome bd confers nitric oxide resistance to Escherichia coli. Nature Chemical Biology **5:**94-96.
232. **Parish T, Brown A.** 2009. Mycobacterium: Genomics and Molecular Biology. Mycobacterium: Genomics and Molecular Biology.
233. **Shi L, Sohaskey CD, North RJ, Gennaro ML.** 2008. Transcriptional characterization of the antioxidant response of Mycobacterium tuberculosis in vivo and during adaptation to hypoxia in vitro. Tuberculosis **88:**1-6.
234. **Fu HA, Iuchi S, Lin ECC.** 1991. THE REQUIREMENT OF ARCA AND FNR FOR PEAK EXPRESSION OF THE CYD OPERON IN ESCHERICHIA-COLI UNDER MICROAEROBIC CONDITIONS. Molecular & General Genetics **226:**209-213.
235. **Avetisyan AV, Bogachev AV, Murtasina RA, Skulachev VP.** 1992. INVOLVEMENT OF A D-TYPE OXIDASE IN THE NA+-MOTIVE RESPIRATORY-CHAIN OF ESCHERICHIA-COLI GROWING UNDER LOW DELTA(MU)BARH+ CONDITIONS. Febs Letters **306:**199-202.
236. **Wall D, Delaney JM, Fayet O, Lipinska B, Yamamoto T, Georgopoulos C.** 1992. ARC-DEPENDENT THERMAL REGULATION AND EXTRAGENIC SUPPRESSION OF THE ESCHERICHIA-COLI CYTOCHROME-D OPERON. Journal of Bacteriology **174:**6554-6562.
237. **Ashcroft JR, Haddock BA.** 1975. SYNTHESIS OF ALTERNATIVE MEMBRANE-BOUND REDOX CARRIERS DURING AEROBIC GROWTH OF ESCHERICHIA-COLI IN PRESENCE OF POTASSIUM CYANIDE. Biochemical Journal **148:**349-352.
238. **Bogachev AV, Murtazina RA, Shestopalov AI, Skulachev VP.** 1995. INDUCTION OF THE ESCHERICHIA-COLI CYTOCHROME-D BY LOW DELTA(MU)OVER-BAR(H+) AND BY SODIUM-IONS. Eur. J. Biochem. **232:**304-308.
239. **Tamegai H, Kawano H, Ishii A, Chikuma S, Nakasone K, Kato C.** 2005. Pressure-regulated biosynthesis of cytochrome bd in piezo- and psychrophilic deep-sea bacterium Shewanella violacea DSS12. Extremophiles **9:**247-253.
240. **Walters SB, Dubnau E, Kolesnikova I, Laval F, Daffe M, Smith I.** 2006. The Mycobacterium tuberculosis PhoPR two-component system regulates genes essential for virulence and complex lipid biosynthesis. Molecular Microbiology **60:**312-330.
241. **Boshoff HIM, Myers TG, Copp BR, McNeil MR, Wilson MA, Barry CE.** 2004. The transcriptional responses of Mycobacterium tuberculosis to inhibitors of metabolism - Novel insights into drug mechanisms of action. Journal of Biological Chemistry **279:**40174-40184.
242. **Matsoso LG, Kana BD, Crellin PK, Lea-Smith DJ, Pelosi A, Powell D, Dawes SS, Rubin H, Coppel RL, Mizrahi V.** 2005. Function of the cytochrome bc(1)-aa(3) branch of the respiratory network in mycobacteria and network adaptation occurring in response to its disruption. Journal of Bacteriology **187:**6300-6308.
243. **Siegele DA, Imlay KR, Imlay JA.** 1996. The stationary-phase-exit defect of cydC (surB) mutants is due to the lack of a functional terminal cytochrome oxidase. Journal of Bacteriology **178:**6091-6096.
244. **Poole RK, Hatch L, Cleeter MWJ, Gibson F, Cox GB, Wu GH.** 1993. CYTOCHROME BD BIOSYNTHESIS IN ESCHERICHIA-COLI - THE SEQUENCES OF THE CYDC AND CYDD

GENES SUGGEST THAT THEY ENCODE THE COMPONENTS OF AN ABC MEMBRANE TRANSPORTER. Molecular Microbiology **10:**421-430.

245. **Poole RK, Gibson F, Wu GH.** 1994. THE CYDD GENE-PRODUCT, COMPONENT OF A HETERODIMERIC ABC TRANSPORTER, IS REQUIRED FOR ASSEMBLY OF PERIPLASMIC CYTOCHROME-C AND OF CYTOCHROME-BD IN ESCHERICHIA-COLI. Fems Microbiology Letters **117:**217-224.
246. **Tseng CP, Albrecht J, Gunsalus RP.** 1996. Effect of microaerophilic cell growth conditions on expression of the aerobic (cyoABCDE and cydAB) and anaerobic (narGHJI, frdABCD, and dmsABC) respiratory pathway genes in Escherichia coli. Journal of Bacteriology **178:**1094-1098.
247. **Braibant M, Gilot P, Content J.** 2000. The ATP binding cassette (ABC) transport systems of Mycobacterium tuberculosis. Fems Microbiology Reviews **24:**449-467.
248. **Pittman MS, Corker H, Wu GH, Binet MB, Moir AJG, Poole RK.** 2002. Cysteine is exported from the Escherichia coli cytoplasm by CydDC, an ATP-binding cassette-type transporter required for cytochrome assembly. Journal of Biological Chemistry **277:**49841-49849.
249. **Pittman MS, Robinson HC, Poole RK.** 2005. A bacterial glutathione transporter (Escherichia coli CydDC) exports reductant to the periplasm. Journal of Biological Chemistry **280:**32254-32261.
250. **Cotter PA, Melville SB, Albrecht JA, Gunsalus RP.** 1997. Aerobic regulation of cytochrome d oxidase (cydAB) operon expression in Escherichia coli: Roles of Fnr and ArcA in repression and activation. Molecular Microbiology **25:**605-615.
251. **Georgellis D, Kwon O, Lin ECC.** 2001. Quinones as the redox signal for the Arc two-component system of bacteria. Science **292:**2314-2316.
252. **Alexeeva S, Hellingwerf KJ, de Mattos MJT.** 2003. Requirement of ArcA for redox regulation in Escherichia coli under microaerobic but not anaerobic or aerobic conditions. Journal of Bacteriology **185:**204-209.
253. **Kana BD, Weinstein EA, Avarbock D, Dawes SS, Rubin H, Mizrahi V.** 2001. Characterization of the cydAB-encoded cytochrome bd oxidase from Mycobacterium smegmatis. Journal of Bacteriology **183:**7076-7086.
254. **Becker S, Vlad D, Schuster S, Pfeiffer P, Unden G.** 1997. Regulatory O-2 tensions for the synthesis of fermentation products in Escherichia coli and relation to aerobic respiration. Archives of Microbiology **168:**290-296.
255. **Zhang J, Oettmeier W, Gennis RB, Hellwig P.** 2002. FTIR spectroscopic evidence for the involvement of an acidic residue in quinone binding in cytochrome bd from Escherichia coli. Biochemistry **41:**4612-4617.
256. **Yang K, Zhang J, Vakkasoglu AS, Hielscher R, Osborne JP, Hemp J, Miyoshi H, Hellwig P, Gennis RB.** 2007. Glutamate 107 in subunit I of the cytochrome bd quinol oxidase from Escherichia coli is protonated and near the heme d/heme b(595) binuclear center. Biochemistry **46:**3270-3278.
257. **Spinner F, Cheesman MR, Thomson AJ, Kaysser T, Gennis RB, Peng QY, Peterson J.** 1995. THE HEME B(558) COMPONENT OF THE CYTOCHROME BD QUINOL OXIDASE COMPLEX FROM ESCHERICHIA-COLI HAS HISTIDINE METHIONINE AXIAL LIGATION. Biochemical Journal **308:**641-644.
258. **Kranz RG, Barassi CA, Miller MJ, Green GN, Gennis RB.** 1983. IMMUNOLOGICAL CHARACTERIZATION OF AN ESCHERICHIA-COLI STRAIN WHICH IS LACKING CYTOCHROME-D. Journal of Bacteriology **156:**115-121.
259. **Newton G, Gennis RB.** 1991. INVIVO ASSEMBLY OF THE CYTOCHROME-D TERMINAL OXIDASE COMPLEX OF ESCHERICHIA-COLI FROM GENES ENCODING THE 2 SUBUNITS EXPRESSED ON SEPARATE PLASMIDS. Biochimica Et Biophysica Acta **1089:**8-12.

260. **Green GN, Lorence RM, Gennis RB.** 1986. SPECIFIC OVERPRODUCTION AND PURIFICATION OF THE CYTOCHROME-B558 COMPONENT OF THE CYTOCHROME-D COMPLEX FROM ESCHERICHIA-COLI. Biochemistry **25:**2309-2314.
261. **Zhang J, Barquera B, Gennis RB.** 2004. Gene fusions with beta-lactamase show that subunit I of the cytochrome bd quinol oxidase from E-coli has nine transmembrane helices with the O-2 reactive site near the periplasmic surface. Febs Letters **561:**58-62.
262. **Bloch DA, Borisov VB, Mogi T, Verkhovsky MI.** 2009. Heme/heme redox interaction and resolution of individual optical absorption spectra of the hemes in cytochrome bd from Escherichia coli. Biochimica Et Biophysica Acta-Bioenergetics **1787:**1246-1253.
263. **Lorence RM, Koland JG, Gennis RB.** 1986. COULOMETRIC AND SPECTROSCOPIC ANALYSIS OF THE PURIFIED CYTOCHROME-D COMPLEX OF ESCHERICHIA-COLI - EVIDENCE FOR THE IDENTIFICATION OF CYTOCHROME-A1 AS CYTOCHROME-B595. Biochemistry **25:**2314-2321.
264. **Meunier B, Madgwick SA, Reil E, Oettmeier W, Rich PR.** 1995. NEW INHIBITORS OF THE QUINOL OXIDATION SITES OF BACTERIAL CYTOCHROMES BO AND BD. Biochemistry **34:**1076-1083.
265. **Mogi T, Ui H, Shiomi K, Omura S, Kita K.** 2008. Gramicidin S identified as a potent inhibitor for cytochrome bd-type quinol oxidase. Febs Letters **582:**2299-2302.
266. **Cho SH, Warit S, Wan BJ, Hwang CH, Pauli GF, Franzblau SG.** 2007. Low-oxygen-recovery assay for high-throughput screening of compounds against nonreplicating Mycobacterium tuberculosis. Antimicrobial Agents and Chemotherapy **51:**1380-1385.
267. **Koul A, Dendouga N, Vergauwen K, Molenberghs B, Vranckx L, Willebrords R, Ristic Z, Lill H, Dorange I, Guillemont J, Bald D, Andries K.** 2007. Diarylquinolines target subunit c of mycobacterial ATP synthase. Nature Chemical Biology **3**.
268. **Sawada K, Kato Y, Imai K, Li L, Wada M, Matsushita K, Yokota A.** 2012. Mechanism of increased respiration in an H+-ATPase-defective mutant of Corynebacterium glutamicum. Journal of Bioscience and Bioengineering **113:**467-473.
269. **Noda S, Takezawa Y, Mizutani T, Asakura T, Nishiumi E, Onoe K, Wada M, Tomita F, Matsushita K, Yokota A.** 2006. Alterations of cellular physiology in Escherichia coli in response to oxidative phosphorylation impaired by defective F-1-ATPase. Journal of Bacteriology **188:**6869-6876.
270. **Betts JC, Lukey PT, Robb LC, McAdam RA, Duncan K.** 2002. Evaluation of a nutrient starvation model of Mycobacterium tuberculosis persistence by gene and protein expression profiling. Molecular Microbiology **43:**717-731.
271. **Voskuil MI, Schnappinger D, Visconti KC, Harrell MI, Dolganov GM, Sherman DR, Schoolnik GK.** 2003. Inhibition of respiration by nitric oxide induces a Mycobacterium tuberculosis dormancy program. Journal of Experimental Medicine **198:**705-713.
272. **Bacon J, James BW, Wernisch L, Williams A, Morley KA, Hatch GJ, Mangan JA, Hinds J, Stoker NG, Butcher PD, Marsh PD.** 2004. The influence of reduced oxygen availability on pathogenicity and gene expression in Mycobacterium tuberculosis. Tuberculosis (Amsterdam) **84:**205-217.
273. **Rao SPS, Alonso S, Rand L, Dick T, Pethe K.** 2008. The protonmotive force is required for maintaining ATP homeostasis and viability of hypoxic, nonreplicating Mycobacterium tuberculosis. Proceedings of the National Academy of Sciences of the United States of America **105:**11945-11950.
274. **Koul A, Vranckx L, Dendouga N, Balemans W, Van den Wyngaert I, Vergauwen K, Goehlmann HWH, Willebrords R, Poncelet A, Guillemont J, Bald D, Andries K.** 2008.

Diarylquinolines are bactericidal for dormant mycobacteria as a result of disturbed ATP homeostasis. Journal of Biological Chemistry **283:**25273-25280.

275. **Rengarajan J, Bloom BR, Rubin EJ.** 2005. Genome-wide requirements for Mycobacterium tuberculosis adaptation and survival in macrophages. Proceedings of the National Academy of Sciences of the United States of America **102:**8327-8332.
276. **Brown GC.** 2001. Regulation of mitochondrial respiration by nitric oxide inhibition of cytochrome c oxidase. Biochimica Et Biophysica Acta-Bioenergetics **1504:**46-57.
277. **Brunori M, Giuffre A, Forte E, Mastronicola D, Barone MC, Sarti P.** 2004. Control of cytochrorne c oxidase activity by nitric oxide. Biochimica Et Biophysica Acta-Bioenergetics **1655:**365-371.
278. **Fenhalls G, Stevens L, Moses L, Bezuidenhout J, Betts JC, van Helden P, Lukey PT, Duncan K.** 2002. In situ detection of Mycobacterium tuberculosis transcripts in human lung granulomas reveals differential gene expression in necrotic lesions. Infection and Immunity **70:**6330-6338.
279. **Koul A, Arnoult E, Lounis N, Guillemont J, Andries K.** 2011. The challenge of new drug discovery for tuberculosis. Nature **469:**483-490.
280. **Andries K, Verhasselt P, Guillemont J, Gohlmann HWH, Neefs JM, Winkler H, Van Gestel J, Timmerman P, Zhu M, Lee E, Williams P, de Chaffoy D, Huitric E, Hoffner S, Cambau E, Truffot-Pernot C, Lounis N, Jarlier V.** 2005. A diarylquinoline drug active on the ATP synthase of Mycobacterium tuberculosis. Science **307:**223-227.
281. **Villemagne B, Crauste C, Flipo M, Baulard AR, Deprez B, Willand N.** 2012. Tuberculosis: The drug development pipeline at a glance. European Journal of Medicinal Chemistry **51**.
282. **Warman AJ, Rito TS, Fisher NE, Moss DM, Berry NG, O'Neill PM, Ward SA, Biagini GA.** 2012. Antitubercular pharmacodynamics of phenothiazines. Journal of Antimicrobial Chemotherapy.
283. **Cynamon M, Sklaney MR, Shoen C.** 2007. Gatiffoxacin in combination with rifampicin in a murine tuberculosis model. Journal of Antimicrobial Chemotherapy **60**.
284. **Spigelman MK.** 2007. New tuberculosis therapeutics: A growing pipeline. Journal of Infectious Diseases **196**.
285. **Chen P, Gearhart J, Protopopova M, Einck L, Nacy CA.** 2006. Synergistic interactions of SQ109, a new ethylene diamine, with front-line antitubercular drugs in vitro. Journal of Antimicrobial Chemotherapy **58**.
286. **Sacksteder KA, Protopopova M, Barry CE, Andries K, Nacy CA.** 2012. Discovery and development of SQ109: a new antitubercular drug with a novel mechanism of action. Future Microbiology **7**.
287. **Cole ST.** 1999. Learning from the genome sequence of Mycobacterium tuberculosis H37Rv. Febs Letters **452:**7-10.
288. **Reddy TBK, Riley R, Wymore F, Montgomery P, DeCaprio D, Engels R, Gellesch M, Hubble J, Jen D, Jin H, Koehrsen M, Larson L, Mao M, Nitzberg M, Sisk P, Stolte C, Weiner B, White J, Zachariah ZK, Sherlock G, Galagan JE, Ball CA, Schoolnik GK.** 2009. TB database: an integrated platform for tuberculosis research. Nucleic Acids Research **37:**D499-D508.
289. **Berney M, Cook GM.** 2010. Unique Flexibility in Energy Metabolism Allows Mycobacteria to Combat Starvation and Hypoxia. Plos One **5**.
290. **Bekker M, de Vries S, Ter Beek A, Hellingwerf KJ, de Mattos MJT.** 2009. Respiration of Escherichia coli Can Be Fully Uncoupled via the Nonelectrogenic Terminal Cytochrome bd-II Oxidase. Journal of Bacteriology **191:**5510-5517.
291. **Dassa J, Fsihi H, Marck C, Dion M, Kiefferbontemps M, Boquet PL.** 1991. A NEW OXYGEN-REGULATED OPERON IN ESCHERICHIA-COLI COMPRISES THE GENES FOR A

PUTATIVE 3RD CYTOCHROME-OXIDASE AND FOR PH 2.5 ACID-PHOSPHATASE (APPA). Molecular & General Genetics **229:**341-352.

292. **Atlung T, Knudsen K, Heerfordt L, Brondsted L.** 1997. Effects of sigma(S) and the transcriptional activator AppY on induction of the Escherichia coli hya and cbdAB-appA operons in response to carbon and phosphate starvation. Journal of Bacteriology **179:**2141-2146.
293. **Brondsted L, Atlung T.** 1996. Effect of growth conditions on expression of the acid phosphatase (cyx-appA) operon and the appY gene, which encodes a transcriptional activator of Escherichia coli. Journal of Bacteriology **178:**1556-1564.
294. **Cohen GN.** 2011. Bacterial Growth.
295. **Siegele DA, Kolter R.** 1993. ISOLATION AND CHARACTERIZATION OF AN ESCHERICHIA-COLI MUTANT DEFECTIVE IN RESUMING GROWTH AFTER STARVATION. Genes & Development **7:**2629-2640.
296. **Kolter R, Siegele DA, Tormo A.** 1993. THE STATIONARY-PHASE OF THE BACTERIAL LIFE-CYCLE. Annual Review of Microbiology **47**.
297. **Sambrook J, Russell DW.** 2001. Molecular cloning: A laboratory manual. Molecular cloning: A laboratory manual.
298. **Frey B, Suppmann B.** 1995. Biochemica **2:**34-35.
299. **NEB.** 2011. NEB UK Expressions. http://www.neb.uk.com/latest/documents/neb_uk_expressions_oct11.pdf.
300. **Datsenko KA, Wanner BL.** 2000. One-step inactivation of chromosomal genes in Escherichia coli K-12 using PCR products. Proceedings of the National Academy of Sciences of the United States of America **97:**6640-6645.
301. **Miroux B, Walker JE.** 1996. Over-production of proteins in Escherichia coli: Mutant hosts that allow synthesis of some membrane proteins and globular proteins at high levels. Journal of Molecular Biology **260:**289-298.
302. **Wagner S, Klepsch MM, Schlegel S, Appel A, Draheim R, Tarry M, Hogbom M, van Wijk KJ, Slotboom DJ, Persson JO, de Gier J-W.** 2008. Tuning Escherichia coli for membrane protein overexpression. Proceedings of the National Academy of Sciences of the United States of America **105:**14371-14376.
303. **Novagen®.** 2003. pET system manual, p. 68. *In* Novagen® aboEB (ed.), the pET Manual, 10 ed.
304. **Bradford MM.** 1976. RAPID AND SENSITIVE METHOD FOR QUANTITATION OF MICROGRAM QUANTITIES OF PROTEIN UTILIZING PRINCIPLE OF PROTEIN-DYE BINDING. Analytical Biochemistry **72**.
305. **Karakashev D, Galabova D, Simeonov I.** 2003. A simple and rapid test for differentiation of aerobic from anaerobic bacteria. World Journal of Microbiology & Biotechnology **19:**233-238.
306. **O'Brien J, Wilson I, Orton T, Pognan F.** 2000. Investigation of the Alamar Blue (resazurin) fluorescent dye for the assessment of mammalian cell cytotoxicity. European Journal of Biochemistry **267**.
307. **Winstedt L, Yoshida KI, Fujita Y, von Wachenfeldt C.** 1998. Cytochrome bd biosynthesis in Bacillus subtilis: Characterization of the cydABCD operon. Journal of Bacteriology **180:**6571-6580.
308. **Green GN, Kranz JE, Gennis RB.** 1984. CLONING THE CYD GENE LOCUS CODING FOR THE CYTOCHROME-D COMPLEX OF ESCHERICHIA-COLI. Gene **32:**99-106.
309. **Arutyunyan AM, Sakamoto J, Inadome M, Kabashima Y, Borisov VB.** 2012. Optical and magneto-optical activity of cytochrome bd from Geobacillus thermodenitrificans. Biochimica Et Biophysica Acta-Bioenergetics **1817**.

310. **Kabashima Y, Kishikawa J, Kurokawa T, Sakamoto J.** 2009. Correlation Between Proton Translocation and Growth: Genetic Analysis of the Respiratory Chain of Corynebacterium glutamicum. Journal of Biochemistry **146:**845-855.
311. **Cotter PA, Chepuri V, Gennis RB, Gunsalus RP.** 1990. CYTOCHROME-O (CYOABCDE) AND D (CYDAB) OXIDASE GENE-EXPRESSION IN ESCHERICHIA-COLI IS REGULATED BY OXYGEN, PH, AND THE FNR GENE-PRODUCT. Journal of Bacteriology **172:**6333-6338.
312. **Ye RW, Tao W, Bedzyk L, Young T, Chen M, Li L.** 2000. Global gene expression profiles of Bacillus subtilis grown under anaerobic conditions. Journal of Bacteriology **182:**4458-4465.
313. **Ingledew WJ, Poole RK.** 1984. THE RESPIRATORY CHAINS OF ESCHERICHIA-COLI. Microbiological Reviews **48:**222-271.
314. **Green GN, Kranz RG, Lorence RM, Gennis RB.** 1984. IDENTIFICATION OF SUBUNIT-I AS THE CYTOCHROME-B558 COMPONENT OF THE CYTOCHROME-D TERMINAL OXIDASE COMPLEX OF ESCHERICHIA-COLI. Journal of Biological Chemistry **259:**7994-7997.
315. **Yamanaka T, Fujii K.** 1980. CYTOCHROME A-TYPE TERMINAL OXIDASE DERIVED FROM THIOBACILLUS-NOVELLUS - MOLECULAR AND ENZYMATIC-PROPERTIES. Biochimica Et Biophysica Acta **591:**53-62.
316. **Delgado MJ, Yeoman KH, Wu GH, Vargas C, Davies AE, Poole RK, Johnston AWB, Downie JA.** 1995. CHARACTERIZATION OF THE CYCHJKL GENES INVOLVED IN CYTOCHROME-C BIOGENESIS AND SYMBIOTIC NITROGEN-FIXATION IN RHIZOBIUM-LEGUMINOSARUM. Journal of Bacteriology **177:**4927-4934.
317. **Obrian MR, Kirshbom PM, Maier RJ.** 1987. TN5-INDUCED CYTOCHROME MUTANTS OF BRADYRHIZOBIUM-JAPONICUM - EFFECTS OF THE MUTATIONS ON CELLS GROWN SYMBIOTICALLY AND IN CULTURE. Journal of Bacteriology **169:**1089-1094.
318. **Santana M, Kunst F, Hullo MF, Rapoport G, Danchin A, Glaser P.** 1992. MOLECULAR-CLONING, SEQUENCING, AND PHYSIOLOGICAL CHARACTERIZATION OF THE QOX OPERON FROM BACILLUS-SUBTILIS ENCODING THE AA3-600 QUINOL OXIDASE. Journal of Biological Chemistry **267:**10225-10231.
319. **Siegel LM, Murphy MJ, Kamin H.** 1973. REDUCED NICOTINAMIDE ADENINE-DINUCLEOTIDE PHOSPHATE-SULFITE REDUCTASE OF ENTEROBACTERIA .1. ESCHERICHIA-COLI HEMOFLAVOPROTEIN - MOLECULAR PARAMETERS AND PROSTHETIC GROUPS. Journal of Biological Chemistry **248:**251-264.
320. **Azarkina N, Siletsky S, Borisov V, von Wachenfeldt C, Hederstedt L, Konstantinov AA.** 1999. A cytochrome bb '-type quinol oxidase in Bacillus subtilis strain 168. Journal of Biological Chemistry **274:**32810-32817.
321. **Kolonay JF, Moshiri F, Gennis RB, Kaysser TM, Maier RJ.** 1994. PURIFICATION AND CHARACTERIZATION OF THE CYTOCHROME BD COMPLEX FROM AZOTOBACTER-VINELANDII - COMPARISON TO THE COMPLEX FROM ESCHERICHIA-COLI. Journal of Bacteriology **176:**4177-4181.
322. **Ratledge C.** 1999. Iron metabolism, p. 260-286 pp. *In* Ratledge C, Dale, J.W., (ed.), Mycobacteria: Molecular Biology and Virulence, 1st ed. Wiley-Blackwell, Oxford.
323. **Gonzalez-Pinzon R, Haggerty R, Myrold DD.** 2012. Measuring aerobic respiration in stream ecosystems using the resazurin-resorufin system. Journal of Geophysical Research-Biogeosciences **117**.
324. **Zhang HX, Du GH, Zhang JT.** 2004. Assay of mitochondrial functions by resazurin in vitro. Acta Pharmacologica Sinica **25**.
325. **Geckil H, Stark BC, Webster DA.** 2001. Cell growth and oxygen uptake of Escherichia coli and Pseudomonas aeruginosa are differently effected by the genetically engineered Vitreoscilla hemoglobin gene. Journal of Biotechnology **85:**57-66.

326. **Khosravi M, Ryan W, Webster DA, Stark BC.** 1990. VARIATION OF OXYGEN REQUIREMENT WITH PLASMID SIZE IN RECOMBINANT ESCHERICHIA-COLI. Plasmid **23**.
327. **Haggerty R, Argerich A, Marti E.** 2008. Development of a ''smart'' tracer for the assessment of microbiological activity and sediment-water interaction in natural waters: The resazurin-resorufin system. Water Resources Research **44:**10.
328. **Edwards SE, Loder CS, Wu GH, Corker H, Bainbridge BW, Hill S, Poole RK.** 2000. Mutation of cytochrome bd quinol oxidase results in reduced stationary phase survival, iron deprivation, metal toxicity and oxidative stress in Azotobacter vinelandii. Fems Microbiology Letters **185:**71-77.
329. **Simon J, van Spanning RJM, Richardson DJ.** 2008. The organisation of proton motive and non-proton motive redox loops in prokaryotic respiratory systems. Biochimica Et Biophysica Acta-Bioenergetics **1777:**1480-1490.
330. **Unden G, Bongaerts J.** 1997. Alternative respiratory pathways of Escherichia coli: Energetics and transcriptional regulation in response to electron acceptors. Biochimica Et Biophysica Acta-Bioenergetics **1320:**217-234.
331. **Hastings SF, Kaysser TM, Jiang FS, Salerno JC, Gennis RB, Ingledew WJ.** 1998. Identification of a stable semiquinone intermediate in the purified and membrane bound ubiquinol oxidase cytochrome bd from Escherichia coli. European Journal of Biochemistry **255**.
332. **Gennis RB.** 1998. How does cytochrome oxidase pump protons? Proceedings of the National Academy of Sciences of the United States of America **95**.
333. **Borisov VB.** 2008. Interaction of bd-type quinol oxidase from Escherichia coli and carbon monoxide: Heme d binds CO with high affinity. Biochemistry-Moscow **73:**14-22.
334. **Copeland R.** 2005. Evaluation of enzyme inhibitors in drug discovery: a guide Medicinal Chemists and Pharmacologists. John Wiley & Sons, Inc., Hoboken, NJ, USA.
335. **Wilson K.** 2010. Enzymes. *In* Wilson KaW, John. (ed.), Principle and Techniques of Biochemistry and Molecular Biology, vol. seven. Cambridge University Press, Cambridge.
336. **Lorence RM, Miller MJ, Borochov A, Faimanweinberg R, Gennis RB.** 1984. EFFECTS OF PH AND DETERGENT ON THE KINETIC AND ELECTROCHEMICAL PROPERTIES OF THE PURIFIED CYTOCHROME-D TERMINAL OXIDASE COMPLEX OF ESCHERICHIA-COLI. Biochimica Et Biophysica Acta **790:**148-153.
337. **Mogi T, Akimoto S, Endou S, Watanabe-Nakayama T, Mizuochi-Asai E, Miyoshi H.** 2006. Probing the ubiquinol-binding site in cytochrome bd by site-directed mutagenesis. Biochemistry **45:**7924-7930.
338. **Diacon AH, Pym A, Grobusch M, Patientia R, Rustomjee R, Page-Shipp L, Pistorius C, Krause R, Bogoshi M, Churchyard G, Venter A, Allen J, Palomino JC, De Marez T, van Heeswijk RPG, Lounis N, Meyvisch P, Verbeeck J, Parys W, de Beule K, Andries K, Mc Neeley DF.** 2009. The Diarylquinoline TMC207 for Multidrug-Resistant Tuberculosis. New England Journal of Medicine **360:**2397-2405.
339. **Haagsma AC, Podasca I, Koul A, Andries K, Guillemont J, Lill H, Bald D.** 2011. Probing the Interaction of the Diarylquinoline TMC207 with Its Target Mycobacterial ATP Synthase. Plos One **6**.
340. **Pidathala C, Amewu R, Pacorel B, Nixon GL, Gibbons P, Hong WD, Leung SC, Berry NG, Sharma R, Stocks PA, Srivastava A, Shone AE, Charoensutthivarakul S, Taylor L, Berger O, Mbekeani A, Hill A, Fisher NE, Warman AJ, Biagini GA, Ward SA, O'Neill PM.** 2012. Identification, Design and Biological Evaluation of Bisaryl Quinolones Targeting Plasmodium falciparum Type II NADH:Quinone Oxidoreductase (PfNDH2). Journal of Medicinal Chemistry **55:**1831-1843.

341. **Leung SC, Gibbons P, Amewu R, Nixon GL, Pidathala C, Hong WD, Pacorel B, Berry NG, Sharma R, Stocks PA, Srivastava A, Shone AE, Charoensutthivarakul S, Taylor L, Berger O, Mbekeani A, Hill A, Fisher NE, Warman AJ, Biagini GA, Ward SA, O'Neill PM.** 2012. Identification, Design and Biological Evaluation of Heterocyclic Quinolones Targeting Plasmodium falciparum Type II NADH:Quinone Oxidoreductase (PfNDH2). Journal of Medicinal Chemistry **55:**1844-1857.

342. **Sharma R, Lawrenson AS, Fisher NE, Warman AJ, Shone AE, Hill A, Mbekeani A, Pidathala C, Amewu RK, Leung S, Gibbons P, Hong DW, Stocks P, Nixon GL, Chadwick J, Shearer J, Gowers I, Cronk D, Parel SP, O'Neill PM, Ward SA, Biagini GA, Berry NG.** 2012. Identification of Novel Antimalarial Chemotypes via Chemoinformatic Compound Selection Methods for a High-Throughput Screening Program against the Novel Malarial Target, PfNDH2: Increasing Hit Rate via Virtual Screening Methods. Journal of Medicinal Chemistry **55:**3144-3154.

343. **Fisher N, Castleden CK, Bourges I, Brasseur G, Dujardin G, Meunier B.** 2004. Human disease-related mutations in cytochrome b studied in yeast. Journal of Biological Chemistry **279:**12951-12958.

344. **Kihira C, Hayashi Y, Azuma N, Noda S, Maeda S, Fukiya S, Wada M, Matsushita K, Yokota A.** 2012. Alterations of glucose metabolism in Escherichia coli mutants defective in respiratory-chain enzymes. Journal of Biotechnology **158:**215-223.

345. **Matsumoto Y, Muneyuki E, Fujita D, Sakamoto K, Miyoshi H, Yoshida M, Mogi T.** 2006. Kinetic mechanism of quinol oxidation by cytochrome bd studied with ubiquinone-2 analogs. Journal of Biochemistry **139:**779-788.

346. **David HL.** 1970. Probability distribution of drug-resistant mutants in unselected populations of *Mycobacterium tuberculosis*. Applied Microbiology **20:**810-814.

347. **Wayne LG, Hayes LG.** 1996. An in vitro model for sequential study of shiftdown of Mycobacterium tuberculosis through two stages of nonreplicating persistence. Infection and Immunity **64:**2062-2069.

348. **Hartkoorn RC, Chandler B, Owen A, Ward SA, Squire SB, Back DJ, Khoo SH.** 2007. Differential drug susceptibility of intracellular and extracellular tuberculosis, and the impact of P-glycoprotein. Tuberculosis **87:**248-255.

349. **Mogi T, Miyoshi H.** 2009. Properties of Cytochrome bd Plastoquinol Oxidase from the Cyanobacterium Synechocystis sp PCC 6803. Journal of Biochemistry **145:**395-401.

350. **Collins LA, Franzblau SG.** 1997. Microplate Alamar blue assay versus BACTEC 460 system for high-throughput screening of compounds against Mycobacterium tuberculosis and Mycobacterium avium. Antimicrobial Agents and Chemotherapy **41**.

351. **Torres E, Moreno E, Ancizu S, Barea C, Galiano S, Aldana I, Monge A, Perez-Silanes S.** 2011. New 1,4-di-N-oxide-quinoxaline-2-ylmethylene isonicotinic acid hydrazide derivatives as anti-Mycobacterium tuberculosis agents. Bioorganic & Medicinal Chemistry Letters **21**.

352. **Vladimir L.** 2003. comprehensive enzyme kinetics. Plenum publishers, New York.

353. **Copeland R.** 2005. Chapter 3: Reversible mode of inhibitor interactions with enzymes, Evaluation of enzyme inhibitors in drug discovery: a guide Medicinal Chemists and Pharmacologists. John Wiley & Sons, Inc., Hoboken, NJ, USA.

354. **Junemann S, Butterworth PJ, Wrigglesworth JM.** 1995. A SUGGESTED MECHANISM FOR THE CATALYTIC CYCLE OF CYTOCHROME BD TERMINAL OXIDASE BASED ON KINETIC-ANALYSIS. Biochemistry **34:**14861-14867.

355. **Konishi K, Ouchi M, Kita K, Horikoshi I.** 1986. PURIFICATION AND PROPERTIES OF A CYTOCHROME B560-D COMPLEX, A TERMINAL OXIDASE OF THE AEROBIC

RESPIRATORY-CHAIN OF PHOTOBACTERIUM-PHOSPHOREUM. Journal of Biochemistry **99:**1227-1236.

356. **Yang FD, Yu L, Yu CA, Lorence RM, Gennis RB.** 1986. USE OF AN AZIDO-UBIQUINONE DERIVATIVE TO IDENTIFY SUBUNIT-I AS THE UBIQUINOL BINDING-SITE OF THE CYTOCHROME-D TERMINAL OXIDASE COMPLEX OF ESCHERICHIA-COLI. Journal of Biological Chemistry **261:**4987-4990.
357. **Smith A, Hill S, Anthony C.** 1990. THE PURIFICATION, CHARACTERIZATION AND ROLE OF THE D-TYPE CYTOCHROME-OXIDASE OF KLEBSIELLA-PNEUMONIAE DURING NITROGEN-FIXATION. Journal of General Microbiology **136:**171-180.
358. **Sakamoto K, Miyoshi H, Takegami K, Mogi T, Anraku Y, Iwamura H.** 1996. Probing substrate binding site of the Escherichia coli quinol oxidases using synthetic ubiquinol analogues. Journal of Biological Chemistry **271**.
359. **Sakamoto K, Miyoshi H, Ohshima M, Kuwabara K, Kano K, Akagi T, Mogi T, Iwamura H.** 1998. Role of the isoprenyl tail of ubiquinone in reaction with respiratory enzymes: Studies with bovine heart mitochondrial complex I and Escherichia coli bo-type ubiquinol oxidase. Biochemistry **37:**15106-15113.
360. **Sakamoto J, Koga E, Mizuta T, Sato C, Noguchi S, Sone N.** 1999. Gene structure and quinol oxidase activity of a cytochrome bd-type oxidase from Bacillus stearothermophilus. Biochimica Et Biophysica Acta-Bioenergetics **1411:**147-158.
361. **Leroux FR, Manteau B, Vors J-P, Pazenok S.** 2008. Trifluoromethyl ethers - synthesis and properties of an unusual substituent. Beilstein Journal of Organic Chemistry **4**.
362. **Jeschke P, Baston E, Leroux FR.** 2007. alpha-fluorinated ethers as "exotic" entity in medicinal chemistry. Mini-Reviews in Medicinal Chemistry **7**.
363. **Swiss R, Will Y.** 2011. Assessment of mitochondrial toxicity in HepG2 cells cultured in high-glucose- or galactose-containing media. Current protocols in toxicology / editorial board, Mahin D. Maines (editor-in-chief) ... [et al.] **Chapter 2**.
364. **Pankey GA, Sabath LD.** 2004. Clinical relevance of bacteriostatic versus bactericidal mechanisms of action in the treatment of gram-positive bacterial infections. Clinical Infectious Diseases **38**.
365. **Dhillon J, Andries K, Phillips PPJ, Mitchison DA.** 2010. Bactericidal activity of the diarylquinoline TMC207 against Mycobacterium tuberculosis outside and within cells. Tuberculosis **90**.
366. **de Steenwinkel JEM, de Knegt GJ, ten Kate MT, van Belkum A, Verbrugh HA, Kremer K, van Soolingen D, Bakker-Woudenberg I.** 2010. Time-kill kinetics of anti-tuberculosis drugs, and emergence of resistance, in relation to metabolic activity of Mycobacterium tuberculosis. Journal of Antimicrobial Chemotherapy **65:**2582-2589.
367. **Donald PR, Diacon AH.** 2008. The early bactericidal activity of anti-tuberculosis drugs: a literature review. Tuberculosis **88**.
368. **Jindani A, Aber VR, Edwards EA, Mitchison DA.** 1980. THE EARLY BACTERICIDAL ACTIVITY OF DRUGS IN PATIENTS WITH PULMONARY TUBERCULOSIS. American Review of Respiratory Disease **121**.
369. **Jindani A, Dore CJ, Mitchison DA.** 2003. Bactericidal and sterilizing activities of antituberculosis drugs during the first 14 days. American Journal of Respiratory and Critical Care Medicine **167:**1348-1354.
370. **Dmello R, Hill S, Poole RK.** 1996. The cytochrome bd quinol oxidase in Escherichia coli has an extremely high oxygen affinity and two oxygen-binding haems: Implications for regulation of activity in vivo by oxygen inhibition. Microbiology-Uk **142:**755-763.
371. **Belevich I, Borisov VB, Konstantinov AA, Verkhovsky MI.** 2005. Oxygenated complex of cytochrome bd from Escherichia coli: Stability and photolability. Febs Letters **579:**4567-4570.

372. **Dmello R, Hill S, Poole RK.** 1994. DETERMINATION OF THE OXYGEN AFFINITIES OF TERMINAL OXIDASES IN AZOTOBACTER-VINELANDII USING THE DEOXYGENATION OF OXYLEGHEMOGLOBIN AND OXYMYOGLOBIN - CYTOCHROME BD IS A LOW-AFFINITY OXIDASE. Microbiology-Uk **140:**1395-1402.
373. **Portnoy VA, Herrgard MJ, Palsson BO.** 2008. Aerobic Fermentation of D-Glucose by an Evolved Cytochrome Oxidase-Deficient Escherichia coli Strain. Applied and Environmental Microbiology **74:**7561-7569.
374. **Bajad S, Shulaev V.** 2011. LC-MS-based metabolomics. *In* Metz TO (ed.), Metabolic Profiling Methods In Molecular Biology, vol. 708. Humana Press Inc., Totowa, NJ.
375. **Goodacre R, Vaidyanathan S, Dunn WB, Harrigan GG, Kell DB.** 2004. Metabolomics by numbers: acquiring and understanding global metabolite data. Trends in Biotechnology **22:**245-252.
376. **Wecke T, Mascher T.** 2011. Antibiotic research in the age of omics: from expression profiles to interspecies communication. Journal of Antimicrobial Chemotherapy **66:**2689-2704.
377. **Villas-Boas SG, Mas S, Akesson M, Smedsgaard J, Nielsen J.** 2005. Mass spectrometry in metabolome analysis. Mass Spectrometry Reviews **24:**613-646.
378. **Reaves ML, Rabinowitz JD.** 2011. Metabolomics in systems microbiology. Current Opinion in Biotechnology **22:**17-25.
379. **Merlo ME, Jankevics A, Takano E, Breitling R.** 2011. Exploring the metabolic state of microorganisms using metabolomics. Bioanalysis **3**.
380. **Rabinowitz JD.** 2007. Cellular metabolomics of Escherchia coli. Expert Review of Proteomics **4:**187-198.
381. **Maharjan RP, Ferenci T.** 2003. Global metabolite analysis: the influence of extraction methodology on metabolome profiles of Escherichia coli. Analytical Biochemistry **313:**145-154.
382. **Crutchfield CA, Lu WY, Melamud E, Rabinowitz JD.** 2010. MASS SPECTROMETRY-BASED METABOLOMICS OF YEAST, p. 393-426, Methods in Enzymology, Vol 470: Guide to Yeast Genetics:, vol. 470.
383. **Rabinowitz JD, Kimball E.** 2007. Acidic acetonitrile for cellular metabolome extraction from Escherichia coli. Analytical Chemistry **79:**6167-6173.
384. **Bajad SU, Lu W, Kimball EH, Yuan J, Peterson C, Rabinowitz JD.** 2006. Separation and quantitation of water soluble cellular metabolites by hydrophilic interaction chromatography-tandem mass spectrometry. Journal of Chromatography A **1125:**76-88.
385. **Kimball E, Rabinowitz JD.** 2006. Identifying decomposition products in extracts of cellular metabolites. Analytical Biochemistry **358:**273-280.
386. **Wilson M, DeRisi J, Kristensen H-H, Imboden P, Rane S, Brown PO, Schoolnik GK.** 1999. Exploring drug-induced alterations in gene expression in Mycobacterium tuberculosis by microarray hybridization. Proceedings of the National Academy of Sciences of the United States of America **96:**12833-12838.
387. **Biagini GA, Fisher N, Shone AE, Mubaraki MA, Srivastava A, Hill A, Antoine T, Warman AJ, Davies J, Pidathala C, Amewu RK, Leung SC, Sharma R, Gibbons P, Hong DW, Pacorel B, Lawrenson AS, Charoensutthivarakul S, Taylor L, Berger O, Mbekeani A, Stocks PA, Nixon GL, Chadwick J, Hemingway J, Delves MJ, Sinden RE, Zeeman A-M, Kocken CHM, Berry NG, O'Neill PM, Ward SA.** 2012. Generation of quinolone antimalarials targeting the Plasmodium falciparum mitochondrial respiratory chain for the treatment and prophylaxis of malaria. Proceedings of the National Academy of Sciences **109:**8298-8303.
388. **Xia J, Mandal R, Sinelnikov IV, Broadhurst D, Wishart DS.** 2012. MetaboAnalyst 2.0—a comprehensive server for metabolomic data analysis. Nucleic Acids Research.

389. **Jolliffe IT.** 2002. Principal Component Analysis. Springer, Secaucus, NJ, USA.
390. **Betts JC, McLaren A, Lennon MG, Kelly FM, Lukey PT, Blakemore SJ, Duncan K.** 2003. Signature gene expression profiles discriminate between isoniazid-, thiolactomycin-, and triclosan-treated Mycobacterium tuberculosis. Antimicrobial Agents and Chemotherapy **47:**2903-2913.
391. **Jia L, Coward L, Gorman GS, Noker PE, Tomaszewski JE.** 2005. Pharmacoproteomic effects of isoniazid, ethambutol, and N-geranyl-N '-(2-adamantyl)ethane-1,2-diamine (SQ109) on Mycobacterium tuberculosis H37Rv. Journal of Pharmacology and Experimental Therapeutics **315:**905-911.
392. **Chakraborty S, Gruber T, Barry CE, III, Boshoff HI, Rhee KY.** 2013. Para-Aminosalicylic Acid Acts as an Alternative Substrate of Folate Metabolism in Mycobacterium tuberculosis. Science **339:**88-91.
393. **Biazus G, Schneider CZ, Palma MS, Basso LA, Santos DS.** 2009. Hypoxanthine-guanine phosphoribosyltransferase from Mycobacterium tuberculosis H37Rv: Cloning, expression, and biochemical characterization. Protein Expression and Purification **66:**185-190.
394. **Hughes MA, Silva JC, Geromanos SJ, Townsend CA.** 2006. Quantitative proteomic analysis of drug-induced changes in mycobacteria. Journal of Proteome Research **5:**54-63.
395. **Wang R, Marcotte EM.** 2008. The proteomic response of Mycobacterium smegmatis to anti-tuberculosis drugs suggests targeted pathways. Journal of Proteome Research **7:**855-865.
396. **Fu LM.** 2006. Exploring drug action on Mycobacterium tuberculosis using affymetrix oligonucleotide genechips. Tuberculosis **86:**134-143.
397. **Argyrou A, Jin L, Siconilfi-Baez L, Angeletti RH, Blanchard JS.** 2006. Proteome-wide profiling of isoniazid targets in mycobacterium tuberculosis. Biochemistry **45:**13947-13953.
398. **Awaness AM, Mitchison DA.** 1973. CUMULATIVE EFFECTS OF PULSED EXPOSURES OF MYCOBACTERIUM-TUBERCULOSIS TO ISONIAZID. Tubercle **54:**153-158.
399. **Gangadharam PRJ, Schaefer WB, Harold FM.** 1963. SELECTIVE INHIBITION OF NUCLEIC ACID SYNTHESIS IN MYCOBACTERIUM TUBERCULOSIS BY ISONIAZID. Nature **198:**712-&.
400. **Lowry OH, Rosebrough NJ, Farr AL, Randall RJ.** 1951. PROTEIN MEASUREMENT WITH THE FOLIN PHENOL REAGENT. Journal of Biological Chemistry **193:**265-275.
401. **Evers S, Di Padova K, Meyer M, Langen H, Fountoulakis M, Keck W, Gray CP.** 2001. Mechanism-related changes in the gene transcription and protein synthesis patterns of Haemophilus influenzae after treatment with transcriptional and translational inhibitors. Proteomics **1:**522-544.
402. **Qiu JF, Zhou DS, Han YP, Zhang L, Tong ZZ, Song YJ, Dai EH, Li B, Wang J, Guo ZB, Zhai JH, Du ZM, Wang XY, Yang RF.** 2005. Global gene expression profile of Yersinia pestis induced by streptomycin. Fems Microbiology Letters **243:**489-496.
403. **Zamboni N, Sauer U.** 2003. Knockout of the high-coupling cytochrome aa(3) oxidase reduces TCA cycle fluxes in Bacillus subtilis. Fems Microbiology Letters **226:**121-126.
404. **Bhat AG, Vashisht R, Chandra N.** 2010. Modeling metabolic adjustment in Mycobacterium tuberculosis upon treatment with isoniazid. Systems and synthetic biology **4:**299-309.
405. **Urban A, Eckermann S, Fast B, Metzger S, Gehling M, Ziegelbauer K, Ruebsamen-Waigmann H, Freiberg C.** 2007. Novel whole-cell antibiotic biosensors for compound discovery. Applied and Environmental Microbiology **73:**6436-6443.
406. **Zumla A, Raviglione M, Hafner R, von Reyn CF.** 2013. CURRENT CONCEPTS Tuberculosis. New England Journal of Medicine **368:**745-755.

407. **Schagger H, Pfeiffer K.** 2000. Supercomplexes in the respiratory chains of yeast and mammalian mitochondria. Embo Journal **19:**1777-1783.
408. **Arnold I, Pfeiffer K, Neupert W, Stuart RA, Schagger H.** 1998. Yeast mitochondrial F1F0-ATP synthase exists as a dimer: identification of three dimer-specific subunits. Embo Journal **17:**7170-7178.
409. **Schagger H.** 2001. Blue-Native gel to isolate protein cpmplexes from mitochondria, p. 231-244. *In* Pon L, Schon, EA., (ed.), Mitochondria. Academic press, California, USA.
410. **Bennett BD, Kimball EH, Gao M, Osterhout R, Van Dien SJ, Rabinowitz JD.** 2009. Absolute metabolite concentrations and implied enzyme active site occupancy in Escherichia coli. Nature Chemical Biology **5:**593-599.
411. **Lu W, Clasquin MF, Melamud E, Amador-Noguez D, Caudy AA, Rabinowitz JD.** 2010. Metabolomic Analysis via Reversed-Phase Ion-Pairing Liquid Chromatography Coupled to a Stand Alone Orbitrap Mass Spectrometer. Analytical Chemistry **82:**3212-3221.
412. **Azizan KA, Baharum SN, Ressom HW, Noor NM.** 2012. GC-MS Analysis and PLS-DA Validation of the Trimethyl Silyl-Derivatization Techniques. American Journal of Applied Sciences **9:**1124-1136.
413. **Kamphorst JJ, Fan J, Lu W, White E, Rabinowitz JD.** 2011. Liquid Chromatography-High Resolution Mass Spectrometry Analysis of Fatty Acid Metabolism. Analytical Chemistry **83:**9114-9122.
414. **Brauer MJ, Yuan J, Bennett BD, Lu W, Kimball E, Botstein D, Rabinowitz JD.** 2006. Conservation of the metabolomic response to starvation across two divergent microbes. Proceedings of the National Academy of Sciences of the United States of America **103:**19302-19307.
415. **Watanabe S, Zimmermann M, Goodwin MB, Sauer U, Barry CE, III, Boshoff HI.** 2011. Fumarate Reductase Activity Maintains an Energized Membrane in Anaerobic Mycobacterium tuberculosis. Plos Pathogens **7**.
416. **Borisov VB, Forte E, Sarti P, Brunori M, Konstantinov AA, Giuffre A.** 2007. Redox control of fast ligand dissociation from Escherichia coli cytochrome bd. Biochemical and Biophysical Research Communications **355:**97-102.
417. **Giuffrè A, Borisov VB, Mastronicola D, Sarti P, Forte E.** 2012. Cytochrome bd oxidase and nitric oxide: From reaction mechanisms to bacterial physiology. FEBS Letters **586:**622-629.